



City Research Online

City, University of London Institutional Repository

Citation: Tsang, Yik Chong (2013). The effect of aberrations and light scatter on visual performance at photopic and mesopic light levels. (Unpublished Doctoral thesis, City University London)

This is the unspecified version of the paper.

This version of the publication may differ from the final published version.

Permanent repository link: <https://openaccess.city.ac.uk/id/eprint/2476/>

Link to published version:

Copyright: City Research Online aims to make research outputs of City, University of London available to a wider audience. Copyright and Moral Rights remain with the author(s) and/or copyright holders. URLs from City Research Online may be freely distributed and linked to.

Reuse: Copies of full items can be used for personal research or study, educational, or not-for-profit purposes without prior permission or charge. Provided that the authors, title and full bibliographic details are credited, a hyperlink and/or URL is given for the original metadata page and the content is not changed in any way.

City Research Online:

<http://openaccess.city.ac.uk/>

publications@city.ac.uk

THE EFFECT OF ABERRATIONS AND LIGHT SCATTER ON VISUAL PERFORMANCE AT PHOTOPIC AND MESOPIC LIGHT LEVELS

A Thesis submitted by

Yik Chong Tsang

for the degree of

Doctor of Philosophy

ADVISORS

Professor C C Hull, Head of Department, Department of
Optometry and Visual Science, City University, London UK.

Professor John Barbur, Professor of Optics and Visual Science,
Department of Optometry and Visual Science, City University,
London UK.

Applied Vision Research Centre, City University, London UK.

July 2013

TABLE OF CONTENTS

TABLE OF CONTENTS	2
LIST OF TABLES	11
LIST OF FIGURES	12
ACKNOWLEDGEMENTS	21
DECLARATION	22
ABSTRACT	23
Chapter One - Background	25
1.1 Background	25
1.1.1 The CAA Test	25
1.1.2 The City University Scatter Test	26
1.2 Synopsis	27
1.3 Aims of the Project:	28
Chapter Two – Changes in the Optics of the Eye caused by Corneal Refractive Surgery	30
2.1 The main Laser Refractive Procedures:	30
2.1.1 Photorefractive Keratectomy (PRK)	30
2.1.2 Laser Assisted Keratomileusis (LASIK)	30
2.1.3 Laser Epithelial Keratomileusis (LASEK)	31
2.1.4 Epi-Lasik.	31
2.2 Complications of Refractive Surgery:	31
2.3 Recent Changes in Refractive Surgery	32
2.3.1 Wavefront sensing	33
2.3.2 Femtosecond LASIK	33
2.3.3 Improvements to Lasers:	34
2.3.4 Antimetabolites	34
2.4 Factors that Limit Visual Performance	35
2.4.1 Aberrations	35

2.4.2 Monochromatic Aberrations	35
2.4.3 Spherical Aberration	37
2.4.4 Coma	37
2.4.5 Zernike Representation of Wavefront Aberration	39
2.4.5.1 Optical Society of America notation	39
2.4.5.2 1st & higher order terms	41
2.4.5.3 6th order & higher	41
2.4.5.4 Individual Zernike Terms	42
2.4.5.5 A Spherical Aberration Zernike Polynomial	42
2.4.5.6 A Coma Zernike Polynomial	42
2.5 Wavefront Aberration Measurement	42
2.5.1 Contour Maps	43
2.5.2 The Hartmann- Shack sensor	43
2.5.3 Wavelength correction	44
2.6 Effect of Ocular Aberrations on Visual Performance	44
2.6.1 Aberrations over Large Ranges	44
2.6.2 Aberrations and Normal Subjects	45
2.6.3 Aberrations and Supernormal Vision	46
2.6.4 Zernike Modes and Visual Performance	47
2.6.5 Aberrations and the Search for Metrics	49
2.6.6 Aberrations and Refractions:	49
2.7 Scattered Light	51
2.7.1 Visibility glare:	52
2.7.2 The Scatter Equation	52
2.7.3 Integrated Straylight parameter k'	53
2.7.4 The causes of straylight in a Normal Eye.	54
2.7.5 Additional Causes of increased retinal straylight	55
2.7.6 Straylight and Vision Tests	55
2.7.6.1 Straylight and visual acuity	56
2.7.6.2 Straylight and glare sensitivity	56

2.7.6.3 Straylight and slitlamp based examination.	56
2.7.7 Methods of Measuring Scatter	57
2.7.7.1 The Halometer	57
2.7.7.2 The Brightness Acuity Tester (BAT)	57
2.7.6.3 The van den Berg Straylightmeter	57
2.7.7.4 Hartmann Shack:	58
2.8 Contrast Sensitivity	59
2.8.1 Straylight and contrast sensitivity	60
2.8.2 Crowding and Contrast	60
2.9 Optical Changes Induced by Refractive Surgery	61
2.9.1 Increased Aberrations:	61
2.9.2 Corneal Topography Data	61
2.9.3 Aberrations of the Whole Eye	61
2.9.4 Objective Measurements of Aberrations	62
2.9.5 Spherical Aberrations	62
2.9.6 Internal Optical Aberration Changes and spherical aberration	63
2.9.7 Coma	64
2.9.8 Role of Pupil Centration on Aberration Measurement	64
2.9.9 5th and Higher Order Aberrations	65
2.9.10 Increased Scattered Light / Glare /Haze.	65
2.9.11 Refractive Instability	66
2.9.12 Q Value & Refractive Surgery	67
2.9.13 Studies Assessing Visual Performance.	67
2.9.13.1 Contrast Sensitivity	67
2.9.13.3 Visual Acuity:	68
2.9.14 Pupil Size Effects	70
Chapter Three - The Visual Pathway and the Decline of Visual Acuity with Eccentricity	71
3.1 Anatomy & Physiology of the Visual Pathway	71

3.1.1 Basic Retinal Anatomy	71
3.1.2 Post retinal Pathways	71
3.1.3 Photoreceptors	72
3.1.4 Spatial resolution and spatial summation - Photopic Vs Scotopic Conditions.	73
3.1.5 Horizontal Cells	76
3.1.6 Bipolar Cells	76
3.1.7 Amacrine Cells	77
3.1.8 Ganglion Cells and Receptive Fields	77
3.1.9 The dLGN	81
3.1.10 Parvo and Magno cells	81
3.1.11 The Cortex	83
3.1.12 The Striate Cortex	83
3.1.13 Simple and Complex Cells	84
3.1.14 The Extrastriate Cortex	86
3.1.15 Cortical Modularity	87
3.1.16 Visual Area 4 and Inferotemporal Cortex	87
3.1.17 Visual Area 5	88
3.1.18 Bottom Up and Top Down Attention	89
3.2. The Decline in Acuity with Eccentricity	89
3.2.1 Introduction	89
3.2.2 Straight – Line Relationship between Visual Acuity & Eccentricity	90
3.2.3 Cortical Magnification Factor	91
3.2.4 Experiments with Landolt Rings	92
3.2.5 Cone and Ganglion Cell Density	93
3.2.6 Ganglion Cell Receptive Field Density	95
3.2.7 Ganglion Cell Receptive Field Size	96
3.2.8 Stimulus Presentation Time	97
3.2.9 Neural Factors	99

3.2.10 Optical Factors	101
3.2.11 Multiple Factors	103
3.2.12 Equations describing the variation of acuity with eccentricity.	104
3.2.13 Mesopic Levels	105
Chapter Four – Initial Investigations of Parameters affecting the CAA Test	110
4.1 The CAA Test	110
4.2 CAA Test Apparatus - Equipment and Set-up	111
4.3 General Test Parameters	114
4.4 Mesopic Testing	114
4.5 Previous CAA Test Results	115
4.6 Patient selection and characteristics	119
4.7. Investigation 1 Contrast Sensitivity Effects and Artificial Pupils	119
4.7.1 Introduction	119
4.7.2 Hypothesis	120
4.7.3 Methods	120
4.7.4 The City University contrast sensitivity test apparatus:	120
4.7.5 Subjects	121
4.7.6 Results	122
4.7.7 Discussion	124
4.7.8 Conclusion	126
4.8 Investigations with the CAA Test Parameters:	126
4.8.1. Investigation 2: High Contrast versus Low contrast CAA Tests	126
4.8.2 Hypothesis	126
4.8.3 Methods	126
4.8.4 Subjects	127

4.8.5 Results	128
4.8.6 Discussion	130
4.8.7 Conclusion	131
4.9 Investigation 3: Crowding Effects	131
4.9.1 Introduction	131
4.9.2 Hypothesis	132
4.9.3 Methods	132
4.9.4 Subjects	132
4.9.5 Guide Contrast Effects Results	132
4.9.6 Discussion	134
4.9.7 Conclusion	136
4.10 Initial Investigation 4: Timing Effects	136
4.10.1 Introduction	136
4.10.2 Hypothesis	136
4.10.3 Method	136
4.10.4 Subjects	136
4.10.5 Results	137
4.10.6 Discussion	138
4.11 Conclusions	139
Chapter Five – The Effect of Natural Aberrations on the CAA Test	140
5.1 Overall Aim	140
5.2 Apparatus and Procedures: Hartmann Shack	140
5.3 Examining the Foveal Dip	142
5.3.1 Hypothesis	143
5.3.2 Method	143
5.3.3 Subjects	143
5.3.4 Results	145

5.3.5 Discussion	148
5.4 Conclusions	151
Chapter Six – The Effect of increased Spherical Aberration on the CAA Test	152
6.1 Introduction	152
6.2. Initial Study	154
6.2.1 Hypothesis	154
6.2.2 Subjects	154
6.2.3 Apparatus	154
6.2.3.1 Q Value Contact Lenses	154
6.2.3.2 WASCA Aberrations and Pupil Size Measurement	155
6.2.3.3 WASCA Procedure	156
6.2.4 Methods	156
6.2.5 Results	157
6.2.6 Discussion	159
6.3 Main Study	159
6.3.1 Hypothesis	159
6.3.2 Main Study Subjects	160
6.3.3 Main Study methods	161
6.3.4 Results	161
6.3.4.4 Analysis of results using Quadratic Regressions	164
6.3.4.5 Regressions Against other Variables	167
6.3.4.6 Q Value lenses vs CAA Test Performance	169
6.4 Discussion	173
6.4.1 Q Value vs Spherical Aberration and Defocus.	173
6.4.2 CAA Test Results: Q value vs Visual Performance	173
6.4.3 Spherical Aberration and Visual Performance.	176
6.4.4 Coma and CAA Test results.	181
6.4.6 Contact Lens advantages for aberration generation:	183

6.5 Limitations of the study with Aberration Controlled contact lenses	184
6.5.1 Movement and Centration	184
6.5.2 Adaptation	184
6.5.3 Binocularity	184
6.5.4 Corneal Modelling	184
6.6 Conclusion	185
Chapter Seven – Scatter and Visual Performance	187
7.1.1 Introduction	187
7.2 Subjects	187
7.3 Methods	190
7.4 Subject's instructions	194
7.5 Results	194
7.5.1 Scatter and the CAA Test	194
7.5.2 Scatter and Pupil Sizes	195
7.5.3 Scatter and Q value	196
7.5.4 Scatter and two case study subjects:	197
7.6 Discussion	201
Chapter Eight – Summary & Conclusions	205
8.1 Summary of Results	205
8.2 Conclusions	206
8.2.1 Chapter 4 – Experimental investigations on Visual performance. Changes with Eccentricity.	206
8.2.2 Chapter 5 – Effect of Natural Aberrations on the CAA Test	207
8.2.3 Chapter 6 – The effect of Q value and Spherical Aberration on the CAA Test.	207
8.2.4 Chapter 7 – Scatter and Visual Performance	208
8.5 Achievements of the Project	208

8.6 Concluding Remarks	209
Appendix 1	210
A1.1 CAA Artificial Pupil Results	210
A1.2 Further Guide Contrast Results	216
A1.3 Further Stimulus Onset Time Results	220
A1.4 Effect of High Contrast on Mesopic Results	225
Appendix 2	229
A2 Other Significant Regressions	229
Appendix 3	233
A3.1 Scatter and Spherical Aberration	233
A3.2 Scatter and Pupil Sizes	245
References	249

List of Tables

Table 4.1 The parameters used to conduct the City University CS test	121
Table 4.2 Subjects used for the artificial 6 mm, 3 mm Pupil Contrast Sensitivity Study.	122
Table 4.3 Contrast Sensitivity for Each Subject.	123
Table 4.4 Subjects examined for the artificial 6 mm, 3 mm Pupil High & Low Contrast CAA Test Study.	127
Table 4.5 Subjects examined for the decreased guide contrast and increased stimulus onset time experiments.	132
Table 5.1 Subjects used for the natural aberrations versus CAA Test Study.	144
Table 5.2 Photopic & Mesopic Gap Acuties, Foveal Dips & Higher Order Aberrations.	146
Table 6.1 Q values of the aberration controlled Contact Lenses	154
Table 6.2 Pilot Study Differences in photopic gap acuties generated by Q = -2 and Q = +1.5 contact lenses.	157
Table 6.3 Pilot Study Differences in mesopic gap acuties generated by Q = -2 and Q = +1.5 contact lenses.	157
Table 6.4 Patients used for the Aberration controlled contact lens study.	160
Table 7.1 Subjects used for the Scatter versus CAA Test Study.	188
Table 7.2 Subjects used for the Scatter versus Pupil Size Study.	189
Table 7.3 Subjects used for the Scatter versus Q Value Study.	189
Table 7.4 Subjects used for the Scatter Study concerning abnormal conditions.	190

List of Figures

Figure 2.1 Spherical Aberration: (a) The refracted ray (b) a contour map of the wavefront (perpendicular to rays) aberration in primary spherical aberration: the pupil is shown as being square (c) isometric view of the shape of the wavefront aberration (Charman (2003).	37
Figure 2.2 (a) Ray Paths in a system with negative coma and the associated point image (b) wavefront map for coma (c) isometric view of map (arbitrary scales) (Charman, 2005)	38
Figure 2.3 The forms of the wavefront deformations associated with each of the first few orders of polynomials. Isometric projections are shown (Charman, 2003).	41
Figure 2.4. A spherical IOL producing positive spherical aberration (Dietze & Cox, 2003).	50
Figure 3.1 The Visual Pathway (taken from Schwartz, 2004 figure 2-10, p16)	72
Figure 3.2 Retinal Distribution of rods and M- and L- cones (Osterberg, 1935, taken from Schwartz, 2004 figure 3-7, p34)	73
Figure 3.3. Schematic showing the organization of the primate retina. (taken from Schwartz, 2004, figure 12-11, p274)	77
Figure 3.4. Intracellular recordings from the various neural elements in the mudpuppy retina (taken from Schwartz, 2004, figure 12-7, p269)	79
Figure 3.5 Mean minimal angle of resolution, one standard deviation above and one standard deviation below, as functions of retinal eccentricity. Data from 20 observers, one eye only, Weymouth (1958).	91

Figure 3.6 MAR as a function of eccentricity on the horizontal meridian in five visual acuity tasks: grating acuity (filled circles) Snellen (E 's) Landolt (O 's), dot direction (squares), dot separation (dots) Open symbols refer to measurement from the middle of dots in the dot tests. Filled symbols refer to measurements from the nearest edges of the dots, Virsu et al (1987).	93
Figure 3.7 A Retinal and External Line Spread Functions for Subject WNC B The variation of Cone Separation and visual Acuity (in minutes of arc) with Peripheral Angle, and the variation in Retinal Ganglion cell interval with Peripheral Angle, Jennings and Charman (1981).	95
Figure 3.8 Plots of the spatial frequency -1 for the CSF peak value, against eccentric visual angle for counterphasing and static stimuli Drasdo, Thompson and Deeley (1990).	98
Figure 3.9 Photoreceptor Densities as Functions of Eccentricity along the Horizontal Meridian (Oyster 1999).	106
Figure 3.10 Minimal angle of resolution of the light and dark adapted eye as functions of retinal eccentricity. Data from Fick (1898), (Weymouth (1958)).	107
Figure 3.11 Visual acuity using Landolt rings along the horizontal meridian of the temporal retina at five different intensity levels ranging from 4.9 to 9.0 log micromcrolamberts, Mandelbaum and Sloan (1947).	108
Figure 3.12 Change of acuity with retinal location for different background luminances, Subject L.S. (Sloan,1968)	109

Figure 4.1 CAA Test Fixation spot and Fixation flankers, and Landolt Ring (with gap of diameter/5 ($D/5$)).	110
Figure 4.2 CAA Test Apparatus Setup	111
Figure 4.3 Averaged Photopic and Mesopic CAA test results. Target Size versus Eccentricity. The error bars represent 2 standard errors.	116
Figure 4.4 Illustration of Foveal Dips under photopic and mesopic conditions. Error bars are two standard errors.	117
Figure 4.5 Contrast Sensitivity Differences for 8 subjects with 6 mm and 3 mm pupils. Error bars are 2 standard errors.	123
Figure 4.6. Photopic Gap Acuity results at high and low contrast for 5 subjects. Error bars are 2 standard errors.	128
Figure 4.7: Mesopic Gap Acuity results at high and low contrast for 3 subjects. Error bars are 2 standard errors.	129
Figure 4.8 Guide Contrast reduced, Photopic CAA Test Differences for three Subjects. Error bars are two standard errors	133
Figure 4.9 Guide Contrast reduced, Mesopic CAA Test Differences for three Subjects. Error bars are two standard errors	134
Figure 4.10 Stimulus Onset Time increased, Photopic CAA Test Differences for three Subjects. Error bars are two standard errors	137
Figure 4.11 Stimulus Onset Time increased, Mesopic CAA Test Differences for three Subjects. Error bars are two standard errors.	138
Figure 5.1. Optical layout of wavefront sensor.	141
Figure 5.2 Calculation of Foveal Dip	145

Figure 5.3 Photopic Foveal Dip vs Higher Order Aberrations: Pupil size 6 mm	147
Figure 5.4: Mesopic Foveal Dip vs Higher Order Aberrations: Pupil size 6 mm	148
Figure 6.1 Initial Study Photopic & Mesopic Gap Size Differences generated by $Q = -2$ and $Q = +1.5$ contact lenses.	158
Figure 6.2 Q Value vs Z (4,0) Spherical Aberration over a 4.5 mm Pupil, for 6 subjects.	162
Figure 6.3 Q Value vs Z (2,0) Defocus over a 4.5 mm Pupil, for 6 subjects.	163
Figure 6.4: Z (4,0) Spherical Aberration (for a 4.5mm pupil) vs Photopic Gap Acuity Quadratic Regression.	164
Figure 6.5: Z (4,0) Spherical Aberration vs Mesopic Gap Acuity Quadratic Regression.	165
Figure 6.6 Z (4,0) Spherical Aberration Differences generated by the $Q = -2$ and $Q = -1$ Contact Lenses compared to the $Q = +1.5$ and $Q = +1$ differences. Error bars are two standard errors. (Differences are shown in absolute values).	166
Figure 6.7 Seidel Coma for a 4.5 mm pupil vs Central Photopic Gap Acuity for six Subjects	167
Figure 6.8 Seidel Coma vs Central Mesopic Gap Acuity for 6 Subjects	168
Figure 6.9 Main Study Photopic Gap Size Differences Error bars are 2 standard errors.	169

Figure 6.10 . Photopic Gap acuities for the Q = -2, -1, 0,. +1, +1.5 lenses for Seven Subjects. Error bars are 2 standard errors.	170
Figure 6.11 Main Study Mesopic Gap Size Differences Error bars are 2 standard errors.	171
Figure 6.12 Mesopic Gap acuities for the Q = -2,-1, 0,. +1, +1.5 lenses for Seven Subjects. Error bars are 2 standard errors.	172
Figure 7.1. Schematic diagram showing the stimulus arrangement for the light scatter test.	191
Figure 7.2. Illustration of the sinusoidal modulation of retinal illuminance over the central test target caused by light scattered from the modulated annulus and its compensation, achieved by counterphase modulation of the screen luminance.	192
Figure 7.3 Mesopic Foveal Dip vs Scatter k'	195
Figure 7.4 Scatter k' versus Pupil Size. Means are in red. Medians are shown by the horizontal lines. 95% confidence intervals are denoted by the box plots boundaries.	196
Figure 7.5 Scatter k' vs Q value Quadratic regression.	197
Figure 7.6. Scatter Function for subject LH suffering from photophobia.	198
Figure 7.7 Scatter Function for subject suffering from dry eye and photophobia – Subject PG.	199
Figure 7.8 Scatter k' Differences generated by changes in Q values. Error bars are two standard errors.	200

Figure 7.9 Scatter k' Differences generated by Pupil Size, & pathology. Error bars are two standard errors.	201
Figure A1.1: Differences in Photopic Gap Acuities due to 6 mm and 3 mm pupil sizes at 24% and 125% contrast. Error bars are 2 standard errors.	210
Figure A1.2: Photopic Gap Acuity results at high and low contrast for subject MS	211
Figure A.1.3: Photopic Gap Acuity results at high and low contrast for subject AnP Error bars are 2 standard errors.	212
Figure A1.4: Photopic Gap Acuity results at high and low contrast for subject AP. Error bars are 2 standard errors.	212
Figure A1.5: Photopic Gap Acuity results at high and low contrast for subject CO. Error bars are 2 standard errors.	213
Figure A1.6: Photopic Gap Acuity results at high and low contrast for subject SL. Error bars are 2 standard errors.	214
Figure A1.7 Photopic Gap Acuity results at high and low contrast for subject MS – a repeat run. Error bars are 2 standard errors.	215
Figure A1.8. CAA Guide contrast changed - Photopic Tests - subject DT. Error bars are 2 standard errors.	216
Figure A1.9 Guide Contrast reduced Mesopic Gap Acuity Tests - subject DT. Error bars are 2 standard errors.	216
Figure A1.10 Guide Contrast reduced Photopic CAA Tests - subject JK. Error bars are 2 standard errors.	217

Figure A1.11 Guide Contrast reduced Mesopic CAA Tests - subject JK. Error bars are 2 standard errors.	218
Figure A1.12: Stimulus Onset Time increased, Photopic Gap Acuity Tests for subject LD. Error bars are 2 standard errors.	218
Figure A1.13: Stimulus Onset Time increased, mesopic Gap Acuity Tests - subject LD. Error bars are 2 standard errors.	219
Figure A1.14: Stimulus Onset Time increased, Photopic Gap Acuity Tests for subject LD. Error bars are 2 standard errors.	220
Figure A1.15: Stimulus Onset Time increased, mesopic Gap Acuity Tests - subject LD. Error bars are 2 standard errors.	221
Figure A1.16 Stimulus Onset Time increased, photopic Gap Acuity Tests - subject JK Error bars are 2 standard errors.	222
Figure A1.17: Stimulus Onset Time increased, mesopic Gap Acuity Tests - subject JK. Error bars are 2 standard errors.	223
Figure A1.18 Stimulus Onset Time increased, photopic Gap Acuity Tests - subject DT. Error bars are 2 standard errors.	224
Figure A1.19: Stimulus Onset Time increased, mesopic Gap Acuity Tests - subject DT. Error bars are 2 standard errors.	224
Figure A1.20: Mesopic Gap Acuity results at high and low contrast for subject GB Error bars are 2 standard errors	225
Figure A1.21: Photopic and Mesopic Gap Acuity results at high and low contrast for subject PM. Error bars are 2 standard errors.	226

Figure A1.22: Effect of artificial 3 mm pupil on high contrast Mesopic Gap Acuity for subject HW. Error bars are 2 standard errors	227
Figure A1.23: Photopic and Mesopic Gap Acuity results at high and low contrast for subject LW. Error bars are 2 standard errors.	228
Figure A2.1 Linear regression between photopic central gap acuity and Seidel Coma	229
Figure A2.2: Seidel Coma Differences generated by the Q value lenses. Error bars are 2 standard errors.	230
Figure A2.3 Linear regression between photopic central gap acuity and Seidel Astigmatism.	231
Figure A2.4: Seidel Astigmatism Differences generated by the Q value lenses. Error bars are 2 standard errors.	232
Figure A3.1: Scatter function of the eye. Subject CG Right eye tests. Q value plano and +1.00 Contact Lenses compared. Error bars represent two standard errors.	233
Figure A3.2: Scatter function of the eye. Subject CG Right eye tests, Q value plano and +1.50 Contact Lenses compared.	234
Figure A3.3: Scatter function of the eye. Subject CG Right eye tests, Q value plano and -1.00 Contact Lenses compared.	235
Figure A3.4: Scatter function of the eye. Subject CG, Right Eye, Q value plano and -2.00 Contact Lenses compared.	236
Figure A3.5: Scatter function of the eye. Subject CT, Left Eye, Q value plano and +1.00 Contact Lenses compared.	237

Figure A3.6: Scatter function of the eye. Subject CT, Left Eye, Q value plano and +1.50 Contact Lenses compared.	238
Figure A3.7: Scatter function of the eye. Subject CT, left eye, Q value plano and -1.00 Contact Lenses compared.	239
Figure A3.8: Scatter function of the eye. Subject CT, left eye, Q value plano and -2.00 Contact Lenses compared.	240
Figure A3.9: Scatter function of the eye. Subject KP, right eye, Q value plano and +1.00 Contact Lenses compared.	241
Figure A3.10: Scatter function of the eye. Subject KP, right eye, Q value plano and +1.50 Contact Lenses compared.	242
Figure A3.11: Scatter function of the eye. Subject KP, right eye, Q value plano and -1.00 Contact Lenses compared.	243
Figure A3.12: Scatter function of the eye. Subject KP, right eye, Q value plano and -2.00 Contact Lenses compared.	244
Figure A3.13 Scatter Function for 6 and 3mm pupils for Subject MS	245
Figure A3.14. Scatter Function for 6 and 3mm pupils for Subject SL	246
Figure A3.15. Scatter Function for 6 and 3mm pupils for Subject JLB	247
Figure A3.16. Scatter Function for 6 and 3mm pupils for Subject LD	248

Acknowledgements

I gratefully acknowledge my advisors Professor Chris Hull and John Barbur. I would particularly like to thank Chris for his continuous assistance, enthusiasm, and expertise in various aspects of computer vision without which this project would never have seen the light. Also, Professor John Barbur for his advice and vast knowledge particularly in vision science aspects which without this project would not be complete.

I also wish to thank all members of the academic and technical staff within the Optometry Department of City University.

I am very grateful to both Dr Catherine Chisholm, Professor David Edgar and Professor David Thomson for their clinical support. I also wish to thank Dr Luis Diaz-Santana, Professor Chris Dainty and David Lara-Saucedo for the use of equipment at Imperial College.

This research was sponsored by the College of Optometrists, England, United Kingdom, to whom I am very grateful.

Finally, I would like to thank my parents for their endless love, care and encouragement. I would also like to thank all my family members for their support all the time.

Declaration

I grant the power of discretion to the University Librarian to allow this thesis to be copied in whole in part without further to me. This permission covers only single copies made for study purposes, subject to normal conditions of acknowledgement.

Abstract

The Contrast Acuity Assessment (CAA) test was developed to assess the minimum spatial vision requirements for commercial pilots. The goal of the CAA test was for it to be sensitive to retinal image degradation in subjects who had undergone excimer laser refractive surgery. Increased aberrations and scattered light or abnormal processing of visual information in the retina and/or the visual pathway are the main causes of retinal image degradation. The purpose of this study was to further investigate the effect of aberrations, scatter and other parameters on the CAA test under photopic and mesopic conditions. This could help to provide explanations for previous CAA test results.

The effect of contrast, stimulus onset time, pupil size and crowding on the CAA test was examined. This was in order to try to provide explanations for the decline in Landolt ring gap acuity over the central 5 degrees, as observed in previous CAA test results, which had shown a foveal dip to occur under photopic and mesopic conditions. Contrast Sensitivity was measured on eight subjects using 6 and 3 mm artificial pupils using the City University Contrast Sensitivity Test. A significant trend of decreasing contrast sensitivity with increased pupil size occurred for the middle and lower spatial frequencies (1.2 and 6.1 cpd), but not for the highest 19.1 cpd spatial frequency.

The effects of using high contrast (125%) rather than low contrast (24%) CAA test targets were investigated, in combination with the use of artificial pupils of 6 mm and 3 mm. We concluded that low contrast could play a role in producing a foveal dip under photopic and mesopic conditions.

The effect of crowding and stimulus onset time on the CAA Test was examined on 3 subjects, by reducing the contrast of the fixation guides under mesopic and photopic conditions and increasing stimulus onset time. This gave inconclusive results. No significant conclusions were drawn concerning the effect of crowding or stimulus onset time on the CAA foveal dip.

The effect of aberrations on normal subjects on the photopic and mesopic CAA test was examined, to determine whether they may have influenced the foveal dip. 14

subjects were tested with natural pupils, under photopic conditions and 10 subjects, were tested under mesopic conditions. A Shack Hartmann aberrometer was used to take wavefront aberration measurements. No significant regressions were found between aberrations and foveal dip. We concluded that aberrations were probably not the cause of the foveal dip.

Q value lenses consisting of $Q = -2$, $Q = -1$, $Q = 0$, $Q = +1$ and $Q = +1.5$ contact lenses were tested on subjects with natural pupils, to determine whether the CAA test could pick up larger non-physiological changes in aberrations. Large changes in visual performance were observed. Z (4,0) spherical aberration versus central CAA gap acuity was found to produce a significant quadratic regression under mesopic conditions. Seidel coma and Seidel astigmatism were also found to produce significant linear regressions. under photopic conditions.

Scatter was measured in 4 subjects, using 6 mm and 3 mm artificial pupils, to determine whether scatter would increase with the larger pupil size. Linear regressions of scatter k' versus foveal dip gave results which were not statistically significant. Scatter was measured for 3 subjects using the 5 different Q value contact lenses, to see if the Q values affected the scatter. The results were not statistically significant. The differences in scatter produced were found to be far less than the increase of scatter found in two subjects with pathological conditions. We concluded that scatter played an insignificant role in producing the foveal dip or changing visual performance with the use of Q value contact lenses.

The project produced a systematic investigation of the parameters affecting the CAA test. A statistically significant association, described by a quadratic regression curve, exists between CAA mesopic gap acuity and Z (4,0) spherical aberration.

Chapter One.

1.1 Background

Laser refractive surgery and particularly wavefront guided ablation together with Shack-Hartmann aberrometry have done much to create a massive interest in the effects of aberrations and light scatter on visual performance. All forms of corneal refractive surgery can sometimes cause an increase in optical aberrations and scattered light (Ondatwgui, 2012), both of which lead to a reduction in retinal image contrast.

Irregular aberrations tend to increase following corneal refractive surgery, particularly positive spherical-like and coma-like aberrations (Kamiya et al., 2012). As with forward light scatter, the result is to reduce the contrast of the retinal image, particularly when the effect of the aberrations is increased under low illumination (e.g., mesopic conditions) as a result of pupil dilation (Queiros et al., 2010).

1.1.1 The CAA Test

The Contrast Acuity Assessment (CAA) test was developed to be sensitive to retinal image degradation in subjects who had undergone excimer laser refractive surgery, as well as being relevant to visual demands in commercial aviation. Assessment of the visual environment and the tasks involved in piloting a commercial aircraft formed the basis for the selection of the CAA test parameters. This test covers a functional visual field of $\pm 5^\circ$. An important part of the test was performed under low ambient illumination involving mesopic levels of light adaptation when the pupil size is large and the effects of aberrations and scattered light are therefore more pronounced. Decreased performance on the CAA test is thought to be a result of either significant degradation of retinal image quality, caused by increased aberrations and scattered light, or abnormal processing of visual information in the retina and/or the visual pathway (Chisholm et al., 2003).

The functional visual field corresponds to the angular subtense of a single flight deck display screen ($\pm 5^\circ$) since the information on adjacent screens cannot be resolved during a single fixation due to the rapid drop in retinal spatial resolution with eccentricity (Mandelbaum & Sloan, 1947, Millodot, 1966). A background light level

of 12 cd/m² was selected for photopic laboratory measurements, while at night the measured background light levels on the flight deck were approximately 0.05 cd/m², so this level was selected for mesopic testing. The CAA test was designed to assess orientation discrimination based on contrast acuity. A Landolt ring was selected as the target due to its similarity to many of the alphanumeric characters and the fact that it provides a simple target for inexperienced subjects. The CAA test has numerous advantages over other techniques that can be employed to assess a loss of visual performance. Unlike commonly available letter charts, it allows performance to be assessed across the functional visual field and employs target sizes known to be sensitive to a loss of visual performance following refractive surgery (Montes-Mico & Charman, 2001).

The CAA test has not been specifically assessed for whether it could actually pick up changes in visual performance due to specific amounts of spherical aberration. Spherical aberration has been shown to be produced by corneal refractive surgery. Therefore the effects of spherical aberration were of great interest in relation to the CAA test.

Decreases in CAA test visual performance have been found with refractive surgery subjects (Chisholm et al., 2003). However it was not known whether this was due to aberrations or scatter. Our study sought to investigate these issues.

1.1.2 The City University Scatter Test

There are five major sources that contribute to the total amount of ocular straylight: the cornea, the iris, the sclera, the retina and the lens (de Waard et al., 1992). It is assumed that for young healthy eyes the total amount of straylight is given 1/3 by the cornea, 1/3 by the lens and 1/3 by the iris, sclera and retina, but these ratios change with age, pigmentation and specific pathologies. Corneal light scatter is constant with age (Ijspeert et al., 1990; van den Berg, 1995) while retinal straylight may also increase with lens opacities (i.e. cataracts) (Ijspeert et al., 1990) or after corneal refractive surgery (Rocha et al., 2009).

Haze can be visible after corneal refractive surgery, since light is scattered toward the observer (back scatter) by large numbers of activated keratocytes within the corneal

tissue and disruption is caused to the lamellae of the corneal stroma (Yulish et al., 2012, Tanabe et al., 2004). High contrast acuity may be impaired in the presence of intense haze but the correlation between haze and visual performance is relatively poor (Tanabe et al., 2004).

The City University light scatter program was used to measure light scatter (Hennelly, 2000). It uses extended scatter sources that can be generated on a visual display and employs a flicker cancellation technique similar to that described by van den Berg and colleagues (van den Berg & Spekreijse, 1987). The dimensions of the scattering source are adjusted for five eccentricities so as to maintain a constant illuminance level in the plane of the pupil (see pages 192-196). The luminance of the dark disc at the centre of the annulus is modulated sinusoidally in counter-phase with the scatter source so as to null out the modulation of retinal illuminance caused by scattered light. The nulling display target luminance is what is needed to balance the retinal illuminance caused by the scattered light (see figure 7.1 Chapter 7). This was measured for each of the five annuli that formed the scatter source. The output of the scatter program produced three parameters n , k , and k' .

The scatter index, n , describes the angular distribution of scattered light in a given eye, while k , the straylight parameter, is proportional to the overall level of scatter in the eye (Barbur et al., 1993). The empirical scatter function based on n and k was then used to compute k' (Barbur et al., 1993; Hennelly et al., 1998). This procedure generates an index k' , the integrated straylight parameter, that shows less variability and therefore provides a more sensitive measure of changes in scattered light.

The City University test can be compared to the compensation comparison method as used by the C-Quant apparatus. The C-Quant determines retinal straylight but assumes constant angular dependence, (Cervino, Gonzales-Mejome et al., 2008). This may be contrasted to the City University Scatter program which uses five different scatter angles, by using different annulus sizes. This allows the integrated straylight parameter, k' to be obtained.

1.2 Synopsis

Chapter 1: The background, synopsis and aims of the project are given.

Chapter 2: The main refractive surgery procedures are outlined. The optics of the limitations of vision are described. The complications of refractive surgery are described. Recent developments in refractive surgery are described.

Chapter 3: The visual pathway is described. The variation of visual acuity with eccentricity is examined in the literature in relation to the central 5 degrees of the CAA test.

Chapter 4: Previous CAA test results are examined, in which the presence of a foveal dip is observed. To try to find explanations for the CAA test results, parameters such as guide contrast, stimulus onset time, and the effect of pupil size were examined.

Chapter 5: The effect of natural aberrations on the CAA test was examined, to determine their role in the formation of the foveal dip and their effect on the CAA test..

Chapter 6: Spherical aberration was induced with Q value contact lenses. The effect of spherical aberration on the CAA test was investigated. This was to determine whether the CAA test could pick up changes due to spherical aberration.

Chapter 7 The effect of pupil size, Q value lenses and pathology on the scatter test was investigated, to determine whether it was aberrations or scatter that had been influencing the CAA test results.

Chapter 8 The conclusions for the project are given.

.

1.3 Aims of the Project:

The aims of the project were:

1) To examine the decrease in acuity with eccentricity around the central five degrees and relate this change to aberrations, scatter, crowding or retinal factors, in relation to the City University CAA test.

2) To simulate the aberrations induced by refractive surgery and relate these changes to changes in performance of the City University CAA test.

Chapter Two

2. Changes in the Optics of the Eye caused by Corneal Refractive Surgery

This chapter examines the changes in the optics of the eye caused by corneal refractive surgery. Methods of assessing the resulting visual performance changes are also discussed.

2.1 The main Laser Refractive Procedures:

The excimer laser refractive surgery procedures most commonly employed are laser assisted keratomileusis (LASIK) and laser epithelial keratomileusis (LASEK) (Ewbank, 2010). EpiLasik and photorefractive keratectomy (PRK) are also quite commonly offered in the UK.

2.1.1 Photorefractive Keratectomy (PRK)

This is usually recommended for low myopes and hyperopes. The Royal College of Ophthalmologists (2011) define 'low' = 0 – 3 D (dioptres), 'moderate' = 3 to 6 D, 'high' = 6 to 10 D, and 'extreme' = more than 10 D.

In this procedure, the corneal epithelial layer is removed manually, mechanically or by alcohol debridement to expose the Bowman's membrane after instillation of topical anaesthetic drops. The excimer laser is then directly applied to ablate the underlying bare corneal stroma. The epithelium grows back, usually within a week over the stromal tissue (Shah, 2007).

2.1.2 Laser Assisted Keratomileusis (LASIK)

LASIK can be performed for the treatment of myopia, hyperopia and astigmatism. This procedure is a combination of lamellar corneal surgery and laser. A corneal stromal flap is created by a microkeratome (an automated fixed depth blade). The stromal flap is lifted and the laser ablation of the stroma is carried out, then the flap is replaced. In many centres in the UK, LASIK is being used as an alternative to PRK for corrections up to –12 D (Royal College of Ophthalmologists, 2011). The surgeon

must be sure that the cornea is thick enough to allow a good outcome and avoid side effects.

2.1.3 Laser Epithelial Keratomileusis (LASEK)

This is usually recommended for low to moderate degrees of myopia, hyperopia and astigmatism. Typically, a 9 mm corneal ring is applied and filled with a weak alcohol solution for about 30 seconds. This creates a split at the epithelial basement membrane level allowing the epithelium to become detached as an intact sheet. The epithelial flap created is lifted to bare the corneal stroma. The laser ablation is performed on the stromal bed, and the flap is replaced after the laser ablation. This procedure is more suitable than LASIK for deep-set eyes, small palpebral apertures and particularly flat or steep corneas (Shah, 2007). In thin corneas, it may be more suitable than LASIK for higher levels of myopia. No incision into the stroma is required. This technique is relatively new compared to PRK and LASIK.

2.1.4 Epi-Lasik.

Epi-Lasik is a relatively new version of surface ablation like PRK that is more similar to LASEK with some distinct advantages over LASIK. A microkeratome with a blunt blade is utilized to mechanically cleave the epithelium from the Bowman's membrane, leaving an exposed area for excimer laser ablation. Epi-Lasik preserves the structural integrity of the stroma and is heralded as minimizing patient discomfort when compared to PRK and LASEK. Some researchers suggest it may shorten the length of time before visual recovery, and reduce the incidence of corneal haze associated with other surface ablation procedures, such as PRK and LASEK (Gamaly et al., 2007).

The Royal College of Ophthalmologists (2011) has classified PRK, LASEK and Epi-LASIK as surface treatment procedures, in contrast to LASIK which is an intrastromal procedure.

2.2 Complications of Refractive Surgery:

Refractive complications, for all laser procedures, include overcorrection, under correction, decentred ablation, increased aberrations and irregular astigmatism. Other complications include haze, glare and haloes, dry eye, reduced corneal sensitivity and

ectasia (Oliveira-Soto & Charman, 2002). Intra-operative complications of PRK include haze, haloes, and infectious keratitis. The complications of LASEK are also similar to those of PRK but are of lesser magnitude (Anderson, Beran, & Schneider, 2002).

For LASIK, intra-operative complications include flap complications, irregular flaps, incomplete flap, lost flap and a free flap etc. Published flap complications are low (0.3%) (Jacobs & Taravella, 2002) but the newer microkeratomes have rates that are probably a lot lower. Post-operative complications include diffuse lamellar keratitis, epithelial ingrowth (the epithelium growing within the stromal interface), flap dislocation and infection (Farah et al., 1998 Sachdev et al., 2002).

2.3 Recent Changes in Refractive Surgery

Ewbank (2010)'s Laser Clinic Survey revealed that LASEK and LASIK were the most commonly offered treatments. In recent years there has been a growing trend towards more invasive procedures, traditionally the preserve of hospital-based clinics, as new treatments emerged and more clinics have expanded the range they offer. Among other treatments listed by the Ewbank (2010)'s sample were cataract surgery, clear lens extraction, phakic IOLs, Conductive keratoplasty, Epilasik and PRK.

For most clinics responding to the survey, the adoption of new and improved treatments was considered the most significant development for the industry as a whole, including corneal collagen cross-linking (CCL) and corneal relaxing incisions. More implants and intraocular surgery, increased interest in presbyopia treatments including monovision, more wavefront IntraLase and a move away from LASIK towards LASEK were among trends that had been noticed by the clinics. New lasers and diagnostic equipment, such as OCT and topographers, were the main areas of recent investment.

A trend towards non-laser and intraocular techniques, and more private clinics and hospitals offering refractive treatments alongside cataract and other procedures, has led to the distinction between refractive surgery providers and general ophthalmic clinics becoming increasingly blurred.

2.3.1 Wavefront sensing

Wavefront sensing assesses the optical properties of the eye beyond sphere and cylinder and measures irregular astigmatism as a higher-order wavefront aberration (Levy et al., 2005). Measurement of the eye's wavefront has been recently used for customized corneal ablation, that is, wavefront-guided refractive surgery, which may be used to correct or at least minimize optical aberrations and consequently improve or preserve visual performance (e.g. Bababeyev et al., 2008).

Wavefront technology has enabled postoperative levels of higher order aberrations to be maintained at pre operation levels. However it does not allow supernormal vision to be easily achieved, as there are too many underlying variations, such as wound healing and biomechanical factors.

2.3.2 Femtosecond LASIK

In this procedure, a stromal flap is created using femtosecond laser ablation i.e. without a mechanical cut using a microkeratome. The flap is then lifted, the laser ablation is carried out and then the flap is replaced in a similar fashion to traditional LASIK.

An advantage of using a femtosecond laser to create the flap in LASIK is the reduced risk of major flap complications. Also, the system enables better flexibility in the parameters of the flap and better control of its depth. Edge designs can be employed to improve the stability of the flap after repositioning, which in turn may reduce the risk of postoperative astigmatism and asymmetric higher order aberrations, flap folds and dislocation, and epithelial ingrowth. Femtosecond lasers enable the safer cutting of thinner flaps of less than 100 microns, which leaves more stromal tissue that can be ablated, enabling LASIK to be performed on patients with moderately thin corneas or high myopia who would otherwise not be suitable. The greater reproducibility of femtosecond laser created flaps may facilitate more reliable prediction of flap-induced aberrations, and so aid the correction of HOAs with customised wavefront ablations (Netto et al., 2007; Johnson, 2007).

A disadvantage of femtosecond cut flaps is that the duration of the surgical procedure is prolonged by a few minutes, because the cornea takes a few minutes to regain its

transparency, which is necessary prior to excimer ablation. Another drawback of the technique is the high cost of the technology.

2.3.3 Improvements to Lasers:

In recent years, development of new technology in refractive surgery has been rapid. These include laser eye tracking systems with iris registration, to ensure treatments are well centred. Faster, more efficient excimer lasers have been developed. Improved optimization of algorithms has occurred, to minimize spherical and other higher-order aberrations (HOAs). Wavefront-guided (WFG) customized ablations, improvements in mechanical microkeratome technology and safety, with the advantages of the femtosecond laser in creation of the flap have all occurred, (Sutton & Kim, 2010).

The use of larger flap diameters, smoother ablations, larger optical zones, and the capacity to blend ablations to 8 mm or more, has allowed surgeons to address the issue of optical zone/mesopic pupil size mismatch, which is a potential source for night vision disturbances (Periman, 2003).

2.3.4 Antimetabolites

Owing to the limited success of corticosteroids to treat stromal haze and their tendency to increase intraocular pressure, especially in highly myopic populations, other topically applied agents such as mitomycin C (MMC) have been trialled. The predominant effect in inhibiting or treating haze appears to be at the level of blocked replication of keratocytes or other progenitor cells of myofibroblasts (Goldsberry et al., 2007, Johnson, 2007). This antimetabolite has been shown to be effective at treating established haze and, through intraoperative application use shortly after surgery, prevents its formation in high-risk groups in PRK and LASEK (Kim et al., 2010; Nasaralla et al., 2007; Nakano et al., 2007). An added virtue of MMC is that, because it inhibits the normal corneal response, less tissue needs to be ablated to obtain a given refractive result.

Recent investigations on the pharmacological treatment of haze have concentrated on inhibiting the differentiation of keratocytes into myofibroblasts, a manifestation of the corneal wound healing response. Myofibroblasts are cells with reduced transparency

that are largely responsible for clinically observable haze. The generation and maintenance of myofibroblasts can be limited by targeting transforming growth factor β (TGF- β). Anti-TGF- β antibody has been shown to reduce haze incidence after PRK (Moller-Pedersen et al., (1998), Johnson, 2007).

2.4 Factors that Limit Visual Performance

2.4.1 Aberrations

All optical systems suffer from two types of aberration. Chromatic aberration arises from the fact that the refractive index of optical materials changes with the wavelength of the light. Monochromatic aberration occurs since the paraxial formulae which predict that a point object will give a point image in a defined position are only valid when the light rays make small angles with the normals to the optical surfaces.

This thesis is mainly concerned with monochromatic aberrations.

2.4.2 Monochromatic Aberrations

The classical theory of monochromatic aberrations was developed by von Seidel and others to describe the image defects observed with optical systems in which the centres of curvature of all the optical surfaces lie on a common optical axis, there being rotational symmetry about the optical axis. In the eye, this condition is rarely fulfilled, since surfaces may lack rotational symmetry about an axis, may be tilted or have their centres of curvature laterally displaced. However, the basic Seidel description is still useful (Charman, 2003).

Monochromatic aberrations occur due to the small-angle, paraxial approximation breaking down. The fundamental formula from which many lens equations are derived is Snell's law, i.e. $n \cdot \sin i = n' \cdot \sin i'$

where n and n' are the refractive indices on either side of the refractive boundary and i and i' are the angles of incidence and refraction respectively.

The sine and cosine of any angle θ can be approximated by their series expansions:

$$\sin \theta = \theta - \frac{\theta^3}{3!} + \frac{\theta^5}{5!} - \frac{\theta^7}{7!} \quad (1)$$

$$\cos \theta = 1 - \frac{\theta^2}{2!} + \frac{\theta^4}{4!} - \frac{\theta^6}{6!} \quad (2)$$

If the angle is small (e.g. <0.05 radians or 3°), the higher power terms after the first can reasonably be ignored. This is the situation for which paraxial theory is valid and leads to ideal image formation where each object point is represented by a single image point, and the overall image is simply a magnified version of the object.

As the ray angles increase, due to the object point moving off the axis or the aperture of the lens system increasing, the higher order terms start to become progressively more important. The result is that the small-angle, paraxial approximation breaks down, and significant monochromatic aberrations result.

Aberrations can either blur the image of a point or result in the point image being in the 'wrong' longitudinal or transverse position, as compared to that expected on the basis of simple paraxial theory. The symmetrical properties of centred optical systems result in five 3rd order or Seidel aberrations. Spherical aberration and coma are the ones mainly caused by refractive surgery.

There are two alternative ways of visualising the characteristics of aberration: the ray aberration and the wavefront aberration. In the ray description, if a lens is 'perfect', all the rays from any object point, are focused by the lens to a unique image point. If diffraction is allowed for, the image 'point' is, in fact, an Airy diffraction pattern. The alternative 'wave' picture is that spherical waves diverge from the object point to be transformed by the lens system into spherical waves, which converge onto the image point.

In the 'ideal' case of an emmetropic eye, the exiting wavefronts consist of parallel rays and plane wavefronts leaving the eye. If aberration is present, the exiting wavefronts will be deformed. Thus, the wavefront aberration or error is determined by comparing these deformed wavefronts with ideal plane (i.e. spheres with infinite radius) wavefronts in the exit pupil of the eye (which is the entrance pupil when light enters the eye).

2.4.3 Spherical Aberration

Spherical aberration is the only Seidel aberration which occurs when the object and image points lie on the optical axis of a centred system (although it is also found off-axis). Spherical aberration arises because the power of the system is not constant across its aperture but varies for each annular zone in the lens.

Figure 2.1 shows the commonly found ocular case of undercorrected (positive) primary spherical aberration. The marginal rays are focused closer to the lens than the paraxial rays. There is no unique point image and the light distribution differs on either side of the 'best' focus.

The corresponding wavefront aberration is shown as a contour map in Figure 2.1b and is represented isometrically in Figure 2.1c. The amount of wavefront aberration varies with the fourth power of the zonal radius in the pupil. The contours of wavefront aberration are always circular for pure spherical aberration of any type.

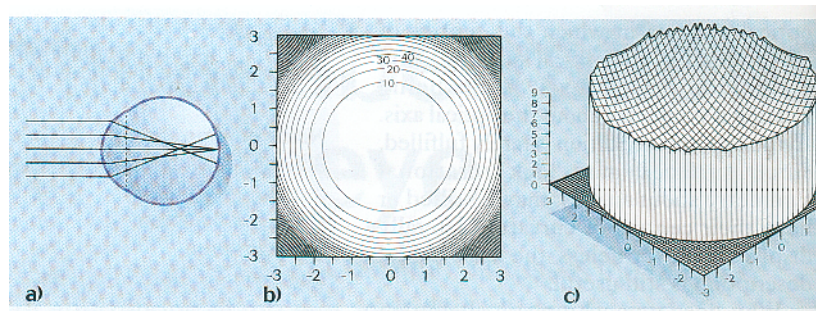


Figure 2.1 Spherical Aberration: (a) The refracted ray (b) a contour map of the wavefront (perpendicular to rays) aberration in primary spherical aberration: the pupil is shown as being square (c) isometric view of the shape of the wavefront aberration (Charman, 2003).

2.4.4 Coma

This is an off-axis aberration. In coma, each off-axis image point is drawn out into a 'comet' shape. The tail of the comet always points either towards (negative coma) or away from (positive coma) the axis of the centred optical system. The length of the tail of the comet increases as the object and image points move further away from the lens axis.

Coma occurs because whereas the rays which pass through the centre of the aperture

stop and exit pupil form an image at the expected Gaussian image position, rays passing through any annular zone in the pupil form an annular or ring image which is slightly displaced from the Gaussian image.

These 'rings' get larger and more displaced as the zonal radius increases, the overall effect being to produce the 'comet' form of the image. A map of the wavefront aberration shows that the wavefront is basically tilted about the sagittal section, one half of the overall wavefront showing progressively greater amounts of positive aberration as one moves away from the sagittal section, while the other becomes increasingly negative. The aberration in the sagittal section is always zero. The angle of tilt increases as one goes further from the sagittal section, as is shown by the contour lines getting closer together (figure 2.2(b)).

Since coma is an off-axis aberration, it would not be expected for coma to occur on the axis of the eye. However, the eye is not a true centred system and the visual axis does not coincide with the approximate optical axis. Much evidence shows that coma-like aberration occurs on the visual axis of many eyes and may affect visual acuity.

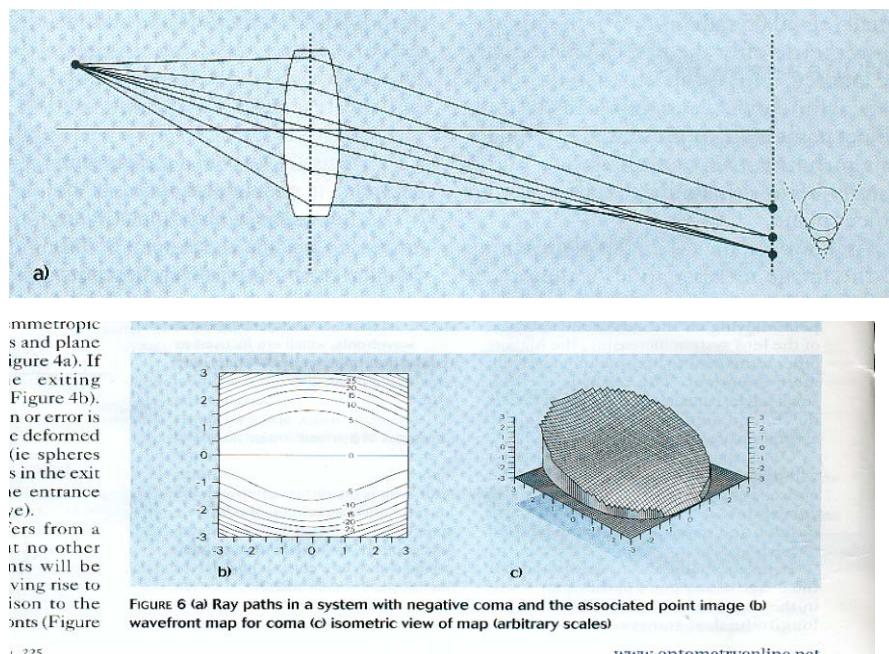


Figure 2.2 (a) Ray Paths in a system with negative coma and the associated point image (b) wavefront map for coma (c) isometric view of map (arbitrary scales) (Charman, 2005)

2.4.5 Zernike Representation of Wavefront Aberration

Currently, the most common method for describing the wavefront error of the eye is the normalized Zernike expansion (Thibos et al., 2000). This approach involves representing the wavefront aberration as the sum of a series of individual Zernike polynomial terms. The relative importance of each one of these is quantified in terms of its coefficient, which gives the contribution of the term to the overall root-mean-square (RMS) wavefront aberration.

The Zernike expansion is in common use for several reasons. It provides an efficient way to specify an entire wavefront aberration map with a relatively small set of Zernike coefficients. Individual Zernike basic functions (i.e., modes) are related to classical optical aberrations, such as defocus, astigmatism, coma, and spherical aberration. Also, when normalized by the recommended Optical Society of America (OSA) system, the Zernike functions are mutually orthogonal (i.e. independent of one another, over a unit pupil) and the root mean squared (RMS) wavefront error of each function is given by its coefficient. Consequently, a Zernike expansion provides a convenient accounting scheme in which the total RMS wavefront error is equal to the square root of the sum of the squares of the individual coefficients in the Zernike spectrum of a wavefront aberration map (Marsack et al., 2004, Charman, 2005).

A disadvantage is that coefficients calculated for one pupil diameter are not valid for smaller pupil diameters and have to be recalculated either by fitting new polynomials to wavefront data over the required pupil diameter or by mathematical conversion (Schwiegerling (2002), Campbell (2003)). Also, the Zernike analysis cannot be directly applied when the pupil is not circular.

2.4.5.1 Optical Society of America notation

Various notations can be used to represent the Zernike polynomials but most workers and manufacturers of aberrometer equipment are now using the standard system devised by a committee of the Optical Society of America (Thibos, Applegate et al., 2002). This system uses polar coordinates. Since the Zernike polynomials are only orthogonal over a unit circle, the normalised radial distance in the pupil $\rho = r/r_{max}$ is used as one polar coordinate, where r_{max} is the maximum pupil diameter for the measured wavefront aberration. The other coordinate is the azimuthal angle θ . The

wavefront aberration $W(\rho,\theta)$ is broken down as the sum of the Zernike polynomials, as follows:

$$W(\rho,\theta) = \sum_n^m C_n^m Z_n^m(\rho,\theta) = C_0^0 Z_0^0(\rho,\theta) + C_1^{-1} Z_1^{-1}(\rho,\theta) + C_2^{-2} Z_2^{-2}(\rho,\theta) + C_2^0 Z_2^0(\rho,\theta) + C_2^2 Z_2^2(\rho,\theta) + C_3^{-3} Z_3^{-3}(\rho,\theta) + C_3^{-1} Z_3^{-1}(\rho,\theta) + C_3^1 Z_3^1(\rho,\theta) + C_3^3 Z_3^3(\rho,\theta) + \text{terms of fourth order and above}$$

where C_n^m is the coefficient for each of the Zernike polynomials $Z_n^m(\rho,\theta)$ and the coefficients will vary with the aberration of the particular eye. The subscript n represents the highest order (power) of the radial term ρ contained in the particular polynomial, which also contains a cosine or sine term of a multiple, $m\theta$, of the azimuthal angle, so that m is often termed the azimuthal frequency. The numbers n and m are either both odd or even. Each Zernike polynomial $Z_n^m(\rho,\theta)$ is the product of three components: a normalization term, a polynomial in ρ of order n , and an azimuthal component of the form $\sin(m\theta)$ or $\cos(m\theta)$. The magnitude of the coefficient C_n^m gives the amount of deformation of that type, expressed as an RMS wavefront deviation.

Any wavefront aberration which varies smoothly across a circular pupil can be described in Zernike terms. The coefficient of each polynomial is chosen to minimise the variance between the actual wavefront W' and the analytical wavefront W represented by the polynomial.

The polynomials can be arranged in a pyramidal manner, with higher-order Zernike modes representing increasingly complex patterns of deformation.

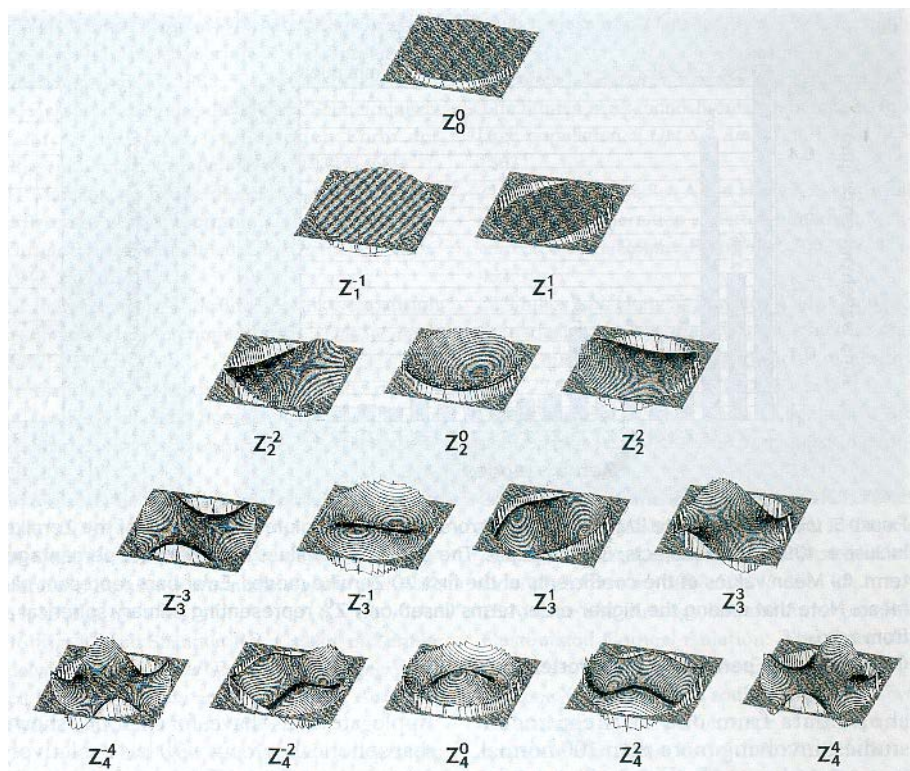


Figure 2.3 The forms of the wavefront deformations associated with each of the first few orders of polynomials. Isometric projections are shown (Charman, 2003).

2.4.5.2 1st & higher order terms

The Zernike terms can be related to traditional concepts of refractive error and aberration according to the order, n , of their radial components. The zero-order (piston) term is not significant; first-order terms represent prismatic effects; second order terms relate to spherical and astigmatic defocus; third- and fifth-order terms, coma-like aberrations; and the fourth and sixth-order terms spherical-like aberration.

2.4.5.3 6th order & higher

Although theoretically the Zernike terms continue to higher and higher orders, it is rarely of interest to go further than the sixth-order in the case of the eye since the corresponding coefficients are very small, resulting in these terms contributing little to the overall aberration. The very high order polynomials represent wavefronts with aberrations which change rapidly with position in the pupil, whereas under most circumstances the wavefront from the natural eye or after laser surgery is normally relatively smooth. Also, many instruments for measuring aberration only sample the wavefront at a limited number of points across the pupil and are incapable of detecting the rapid variations in error that are associated with, e.g. sixth-order and higher aberrations.

2.4.5.4 Individual Zernike Terms

The essential feature of the individual Zernike terms is that each higher-order Zernike polynomial includes balancing lower-order terms to minimise the root-mean square wavefront aberration contributed by that particular polynomial.

2.4.5.5 A Spherical Aberration Zernike Polynomial

For the Z_4^0 polynomial, $5^{1/2} (6\rho^4 - 6\rho^2 + 1)$, the ρ^4 term corresponds to rotationally symmetric, primary spherical aberration, with zero wavefront aberration (corresponding to the paraxial focus) at the centre of the pupil. However, if the ray intersection pattern for spherical aberration near the aberrated point image is examined, it can be shown that the 'best' focus, giving the most concentrated point image, is not at the paraxial focus but somewhere between the marginal and paraxial foci. This focal shift corresponds to the ρ^2 defocus term in the polynomial. Finally, the mean wavefront error is made zero by adding the constant piston term '1'. The $5^{1/2}$ multiplier is a normalisation factor selected to give the polynomial unit variance.

2.4.5.6 A Coma Zernike Polynomial

In the case of the horizontal and vertical third-order coma terms Z_3^{-1} , $(8^{1/2} (3\rho^3 - 2\rho)\sin\theta)$, and Z_3^1 , $(8^{1/2} (3\rho^3 - 2\rho)\cos\theta)$, the 'tilt' aberration associated with the ρ^3 term is balanced with first-order (ρ) tilt to minimise the RMS contribution. There is no need for a piston term to make the mean aberration zero since the aberration for both these coma terms is antisymmetrical about either a horizontal or vertical axis. In fact the form of the polynomials is such that the mean wavefront aberration is zero for all the Zernike terms, with the exception of the piston term.

2.5 Wavefront Aberration Measurement

To assess the wavefront aberration, the aberrated wavefront in the exit pupil of the system is normally compared with an ideal spherical or reference wavefront, centred on the Gaussian image point. The two wavefronts are selected to coincide in the centre of the exit pupil. The wavefront aberration or error is the distance between the actual and reference wavefronts, as a function of position in the pupil and is usually taken as positive if the actual wavefront is in advance of the reference sphere and negative if it is behind (Charman, 2003).

In the case of the eye, the image is inaccessible because it lies on the retina. Many objective aberrometers, therefore, measure the aberrations in object space, in front of the eye. A point source is generated on the retina, often by sending a laser beam into the eye (Charman, 2003).

2.5.1 Contour Maps

The wavefront aberration is typically shown as a contour map. The contours join points in the exit pupil where the wavefront aberration has the same value. In general, closely packed contours will indicate large amounts of aberration and a poor image. An 'ideal' system will have a wavefront aberration that is everywhere zero and hence have no contours in its wavefront map. In commercial aberrometers, the contour map is often presented in colour, with 'hot' colours like red indicating positive values of aberration and cooler, bluer colours, negative values. In general, the wavefront aberration will vary from point to point across the object and image fields.

2.5.2. The Hartmann- Shack sensor

Most commercial aberrometers are of this type. A narrow beam (for example, 1 mm wide) from a point radiation source is imaged by the eye. The light reflected from the fundus travels through a Hartmann-Shack wave-front sensor (Liang et al., 1994, Liang & Williams, 1997), consisting of an array of micro-lenses (typically of the order of 0.5 mm diameter) and onto the array of a CCD camera. The Hartmann-Shack sensor is conjugate with the pupil and its focal plane is at the camera array. For a perfect eye, the wavefront at the sensor would be a plane wave. Each microlens isolates a small bundle of radiation passing through a small region of the pupil. The transverse ray aberration (slope of the wavefront) associated with each microlens can be determined from the departure of the centroid of its corresponding image from the ideal image position.

Fluctuations in aberrations over the order of seconds can be followed. The method can be used as part of an adaptive optics system to correct aberrations of the eye (Liang, Williams & Miller, 1997). Another advantage of this technique is that it is robust to eye position, as the software algorithm can be used to determine the pupil centre accurately, particularly if there is high sampling in the pupil ($\gg 100$ positions).

Spot overlapping due to high aberrations or defocus is a major concern, which means that the instrument may have a limited dynamic range. Auxiliary optics is needed on the outgoing path to correct most of the defocus of the eye.

2.5.3 Wavelength correction

The Hartmann-Shack sensor and most other objective aberrometers use infrared radiation in the approximate range of 780 to 900 nm. There are several advantages in using near infrared instead of visible radiation. It is comfortable because the eye is not sensitive to infrared radiation. The source cannot influence accommodation. Pupil dilation is usually not required because pupillary responses are not sensitive to infrared, and fundus reflectance is higher than in visible radiation (Atchison & Smith, 2000).

The aberrations and in particular the second-order defocus must relate to visible wavelengths to be relevant to vision. Infrared radiations penetrate deeper into the fundus than do visible wavelengths, which would give a small myopic shift in refraction but there is a much stronger hypermetropic shift because of the longitudinal chromatic aberration of the eye.

Using Hartmann-Shack and laser ray tracing methods, Llorente and colleagues (2003) found that aberrations changed little from the infrared (787 nm) to the visible (543 nm) radiation, except for the defocus term. Other studies found small changes only in aberrations other than defocus (Lopez-Gil & Howland., 1999; Marcos et al., 1999; Fernandez et al., 2004).

2.6 Effect of Ocular Aberrations on Visual Performance

The effect of aberrations on visual performance has been studied in various ways. This has included the effect of aberrations over small and large ranges, the effect of different Zernike modes, the influence of aberrations on refraction, and the search for the best metric to predict visual performance.

2.6.1 Aberrations over Large Ranges

Over a large range of RMS errors (an equivalent dioptric range of around 3 dioptres), it has been found that visual acuity decreases with increasing RMS error of the

anterior corneal surface. Applegate et al., (2000) examined 13 normals and 78 patients with a variety of corneal conditions including surgically removed pterygia, penetrating keratoplasty, keratoconus, radial keratotomy and laser in situ keratomileusis. Videokeratographs were taken for all patients and used to calculate corneal first surface wavefront variance. Visual performance was quantified by measurements of contrast sensitivity at high and low contrast. Corneas with increased wavefront variance showed a quantifiable decrease in visual performance that was pupil size dependent. Hence, it was suggested that minimizing higher order aberrations by wavefront-guided refractive surgery would improve visual performance. However, this inverse correlation between ocular aberrations and visual performance had been found only in data sets with abnormally increased aberrations.

2.6.2 Aberrations and Normal Subjects

Over a more normal range of subjects, researchers have found differing results. A few researchers have found a relationship between visual performance and aberrations in specific areas (e.g. Oshika, 2006) and other researchers have found little relation (e.g. Joslin and associates, 2003). Researchers have investigated how measures other than high contrast VA under photopic conditions may be affected by aberrations.

Oshika et al., (2006) examined the higher-order aberrations, for a 4 mm pupil, of three hundred and seven eyes of 161 normal subjects using the Hartmann-Shack wavefront analyzer. The root-mean-square of the third- and fourth-order Zernike coefficients were used to represent coma-like and spherical-like aberrations, respectively. They found that in normal human eyes, coma-like aberrations of the eye significantly influenced the contrast sensitivity function. Multiple linear regression analysis revealed that coma-like aberration was significantly associated with the area under the low contrast sensitivity function (AULCSF), low-contrast VA and letter contrast sensitivity but spherical-like aberration, age, and photopic pupil diameter were not.

Some studies have found that tasks with lower contrast and lower luminance than the task of photopic high contrast acuity correlate better with retinal image quality in a large population. For instance, Pesudovs et al., (2004) examined 148 subjects who were undergoing or had undergone cataract surgery. It was found that their wave aberration metrics correlated better with mesopic low contrast visual acuity, making this their visual performance test of choice. This may have occurred because

decreasing the luminance to mesopic levels allows the pupil to dilate, which, in the typical normal eye, decreases retinal image quality (Levy et al., 2005; Charman, 1991) and acuity (Haegerstrom-Portnoy et al., 1997).

Other studies however have not found a strong relation between aberrations and visual performance. For instance, Joslin and associates (2003) examined eighteen eyes of nine myopic subjects fitted with CRT (corneal refractive therapy) contact lenses. CRT with contact lenses for myopia was found to have significantly increased higher order aberrations, whereas it had no significant effect on visual acuity. Similarly, modification in the overall aberration pattern of the eye induced by accommodation was not associated with any significant effect on image quality (Artal et al., 2002).

2.6.3 Aberrations and Supernormal Vision

Researchers have also examined subjects with supernormal vision. A mixture of results have been found. For instance, Applegate et al., (2006) measured the aberrations, and high and low contrast acuity at photopic and mesopic light levels of 49 normal subjects with 20/17 or better monocular high-contrast logarithm of the minimum angle of resolution (logMAR) acuity. The correlation between image quality and visual acuity was concluded to be higher for letters of low contrast on a dim background because of the greater individual variation in log performance under these conditions in the normal population with 20/17 or better acuity.

In contrast to this, some researchers have not found aberrations to be lower in subjects with supernormal vision. For instance, Levy et al., (2005) investigated the higher order aberrations from the third to the eighth orders in a selected sample of 70 eyes with supernormal vision, (taken as natural UCVA of $\geq 20/15$). The amount of ocular aberrations in these eyes was found to be considerable and the magnitudes were comparable to those of myopic eyes, including those before refractive surgery.

Applegate, Marsack et al., (2003) put forward reasons for why at lower levels of aberrations, the RMS wavefront error is not a good predictor of visual acuity. This low correlation was attributed to the variation in the neural transfer function between the subjects, the low sensitivity of common clinical measures to low levels of aberration, and the fact that a combination of aberrations may interact to improve or

reduce visual performance, depending on their radial orders, sign, and angular frequency. These findings have led to researchers investigating how aberrations interact to optimise visual performance. A search for new metrics of optical and neural performance that will better correlate with clinical measures of visual performance has also taken place.

2.6.4 Zernike Modes and Visual Performance

Researchers have found that the Zernike mode can influence visual performance. For instance, Young et al., (2011) assessed reading performance on 19 subjects, using text with a simulated monochromatic aberration (defocus, coma, or secondary astigmatism). It was found that the rate of decline in reading performance with increasing aberration amplitude was smaller for coma than for secondary astigmatism or defocus. This led Young et al., (2011) to suggest that these differences may mean that the nature of the visual task is important when determining which aberrations have the greatest impact. It was found that the rate of decline in reading performance with increasing aberration amplitude was smaller for coma than for secondary astigmatism or defocus. Defocus and secondary astigmatism had an impact on word identification. Reading impairment caused by coma was attributed to effects on saccade targeting, possibly due to changes in the spacings between letters.

Fang et al., (2009) evaluated optical quality in white light for a myopic population using metrics such as the area under the modulation transfer function and the visual Strehl ratio. The aberrations of one hundred and thirteen myopic eyes of 113 subjects were examined. They concluded that fourth radial order aberrations had the largest impact on the magnitude of the modulation transfer function (MTF) of myopic eyes. A greater percentage of third-order aberrations produced better optical quality compared with fourth to sixth-order aberrations, assuming the RMS was constant.

Ravikumar et al., (2010) studied the effects of spatial phase shifts on object recognition, by simulating image blur computationally for defocus, astigmatism, coma, and spherical aberration. It was shown that 180° phase shifts reduce visual acuity, whereas those with a phase shift of less than 180° (coma, for example) do not. Computed images served as the visual stimuli to determine the effects of phase errors

on visual acuity for single letters, letter clusters, and faces. In the presence of positive spherical aberration, acuity loss due to phase errors was more for hyperopic defocus than for myopic defocus, because the contrast of phase-reversed components was much higher for hyperopic defocus. Phase shifts introduced by coma were less than 180° and consequently had a smaller impact on acuity.

Applegate et al., (2002) examined three subjects for a fixed RMS error of $0.25 \mu\text{m}$ over a 6 mm pupil, to find out how each mode of the normalized Zernike polynomial (second through the fourth radial order) affected high and low contrast logMAR visual acuity. Optically aberrated logMAR charts were used. Wavefront error concentrated near the centre of the pupil was found to adversely affect visual acuity more than modes near the edge of the pupil. Large changes in chart appearance were also not reflected in equally large decreases in visual performance (i.e., subjects could correctly identify highly aberrated letters). Interactions between modes complicated the weighting of each Zernike mode for visual impact.

Charman (2003) commented that this variation in effect was comparable to the effect of a given cylindrical refractive error on visual acuity (i.e. a constant magnitude of second-order wavefront aberration), varying with the orientation of the cylinder axis.

Similarly, Applegate, Marsack et al., (2003) investigated how pairs of Zernike modes interacted to increase or decrease visual acuity, while keeping total RMS wavefront error constant at $0.25 \mu\text{m}$ over a 6 mm pupil. Acuity varied significantly depending on which modes were mixed and the relative contribution of each mode. Modes 2 radial orders apart, and having the same sign and angular frequency tended to combine to increase visual acuity. Modes within the same radial order tended to combine to decrease acuity.

This experimental result revealed a variation in high contrast visual acuity of nearly two lines on a log MAR chart, despite the fact that the total RMS error was held constant. This finding demonstrated that the manner in which the Zernike modes were combined significantly impacted measured acuity in a way that RMS wave-front error and equivalent dioptric error could not predict. The likely reason suggested for

this was that RMS wavefront error specified only the standard deviation of the wavefront error over the pupil. It does not contain any information as to how this wavefront error is distributed within the pupil.

It should be noted though, that it would be unlikely for a real eye to exhibit an error in only two modes because real eyes tend to have some error across many modes (Howland & Howland, 1977 ; Thibos et al., 2002).

2.6.5 Aberrations and the Search for Metrics

Due to the RMS not being a good predictor of visual quality, researchers have searched for better metrics of visual quality, with varying results. For instance, Bühren et al., (2009), compared four wavefront-error representations on 56 eyes one month after LASIK for myopia, under 3 lighting conditions - photopic, high mesopic & low mesopic. The visual Strehl ratio based on optical transfer function (VSOTF) showed the highest predictability. This was found to be better than the root-mean-square (RMS) value of Zernike orders 2 to 5 (total RMS), the higher-order aberration (HOA) RMS, and a wavefront-error breakdown into the RMS of lower-order aberrations, coma, spherical aberration, and remaining HOA.

Lombardo & Lombardo (2010) suggested that it may be unrealistic to suppose that only a single metric can capture all aspects of image and optical quality. A group of image-quality metrics that appreciates the importance of the range of spatial frequencies used in daily vision - between 1 cpd and 40 cpd was suggested as being the best choice.

Marshack et al., (2004), on the other hand, used the data set of Applegate, Marsack et al., (2003) to investigate the ability of 31 scalar metrics derived from wave aberration maps to predict changes in high-contrast logMAR acuity. The best metric was found to be the visual Strehl ratio, which accounted for 81% of the variance in high-contrast logMAR acuity.

2.6.6 Aberrations and Refractions

The measurement and influence of aberrations on subjective refractions has also been examined, resulting in various conclusions. Eliminating second-order Zernike

aberrations is equivalent to minimizing the root mean squared (RMS) wavefront error, but this minimization does not necessarily optimise the quality of the retinal image (King, 1968; Mahajan, 1991).

Iskander et al., (2007) investigated the applicability of four different measures for objective refraction assessment that were derived from a set of estimated Zernike wavefront coefficients. Data from 120 eyes from 60 normal subjects were used to assess the correlation between the subjective and objective refractions. Their results suggested that the objective spherocylindrical refraction calculated from the estimated refractive power map via the Zernike power polynomials was superior to the other considered representations.

A straightforward way by which spherical aberration could influence defocus has been mentioned by Dietze & Cox (2005), who performed ray tracing through a model eye with an equi-biconvex spherical IOL and with a spherical aberration-correcting aspheric IOL. They pointed out that the circle of least confusion can be shifted by spherical aberration, since spherical aberration produces non-paraxial defocus (figure 2.4).

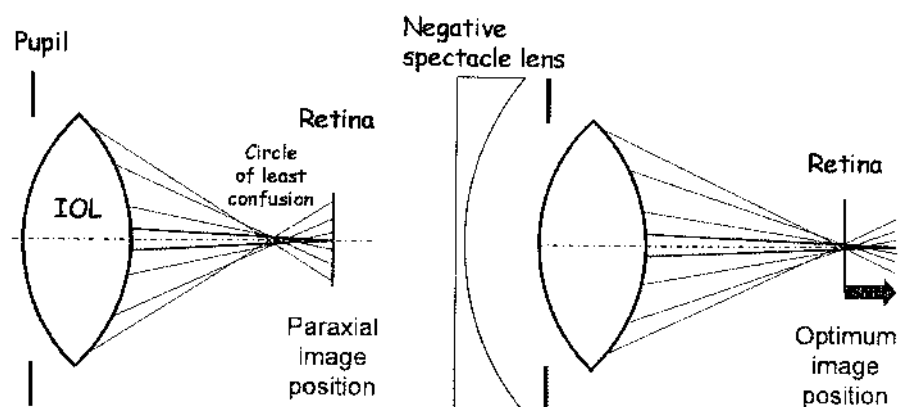


Figure 2.4. A spherical IOL producing positive spherical aberration (Dietze & Cox, 2005).

In figure 2.4 on the left, after correction of paraxial defocus, the rays form a circle of least confusion, which lies in front of the image plane. In figure 2.4 on the right, after correction of non paraxial defocus, a negatively powered lens shifts the circle of least confusion onto the retina.

This suggests positive spherical aberration should produce negative defocus. However Dietze & Cox (2005) also suggested that in terms of producing refraction results from aberration maps, other factors such as other aberrations may also alter the position of the circle of least confusion and the final refractive result. Each change in pupil size will produce different levels of spherical aberration, and hence different levels of nonparaxial defocus. Also, the Stiles Crawford effect may influence the circle of least confusion so that it may not lie on the retina after a subjective refraction.

Previous studies have indicated that subjective refractions in aberrated eyes did not minimize RMS, and probably did not achieve paraxial focus. For instance, Thibos, Hong et al., (2002) showed that carefully refracted subjects still had significant amounts of residual Zernike defocus (Z^0_2), which means that the RMS wavefront error was not minimized by a subjective refraction. Similar results were found by Guirao et al., (2003), who reported that refractions based on minimum RMS wavefront error made the eye myopic, while refractions based on paraxial focus made the eye hyperopic. In addition, Cheng et al., (2003) found that, in the presence of spherical aberration, visual acuity was better with paraxial focus than with the defocus that minimized RMS.

2.7 Scattered Light

Since scattered light in the eye can affect visual performance, its measurement is of great interest. Numerous studies have attempted to quantify the amount of scattered light in the human eye and in particular its angular dependence (Holladay, 1926; Stiles, 1929; Stiles and Crawford, 1937).

The term, scattered light, is used commonly to describe the random change in direction caused by the irregularity of the distribution of the small particles within a medium. The scattering of electromagnetic waves results in the transfer of energy from an incident beam to a collection of scattering centres and the subsequent re-emission of all or some of this energy in directions other than that of the incident beam. Such effects are also encountered in reflection, refraction and diffraction

phenomena, where the change in direction is more orderly and is not random. Its measurement with the City University Scatter test is described on pages 192-196.

When the scattering centres are of equal or larger dimension than the wavelength of the incident beam, the angular distribution of the scattered beam tends to follow more closely the direction of the incident beam. This type of scattering process is referred to as coherent or elastic, since no change of photon energy is involved. Incoherent scattering involves a change of direction as well as wavelength and is observed less frequently and is also less relevant to the human eye.

2.7.1 Visibility glare: When the amount of scattered light in the eye is large, either as a result of changes in the structure of the eye or the presence of intense sources of light, a significant impairment of vision occurs, and this is sometimes described as visibility glare (Vos & Bouman, 1959).

2.7.2 The Scatter Equation

The image of a point source of light on the retina can in the best case be described by a point spread function caused by diffraction in the eye. The effect of scattered light is to increase significantly the proportion of light distributed outside the region of the point spread function. The annular dependence of scattered light at an eccentricity, θ , away from a point source, can be described by a power law relationship of the form

$$L_s(\theta) = kE\theta^{-n} \quad \text{Eq. 1}$$

where E represents the illuminance level generated by the scattering source in the plane of the pupil and k and n are constants for a given eye (Stiles, 1929). A logarithmic transformation of equation 1 shows that $\log(L_s)$ relates linearly to $\log(\theta)$. i.e.,

$$\log(L_s) = \log(kE) - n \log(\theta) \quad \text{Eq. 2}$$

The gradient of the straight-line relationship given by equation 2 yields the scatter index, n. The intercept, $\log(kE)$, and knowledge of E the illuminance level in the plane of the pupil can be used to calculate the constant, k.

These constants provide information regarding the amount (parameter k) and the angular dependence (parameter n) of the scattered light and relate to the number and the size of particles or molecules, which cause scattered light. The constants k and n are also known as the straylight parameter and the scatter index, respectively. The amount of scattered light and hence the straylight parameter, k , increase as a result of increases in the density of the scattering particles, provided that the absorption of light is either negligible or remains constant. The constant k takes into account the number of particles involved as well as their absorption properties. Large k values and/or small n values can result in degraded visual performance. Scattered light as described by equation 1 is distributed mostly around the direction of the incident beam (e.g. it is very directional).

2.7.3 Integrated Straylight parameter k' :

The integrated scatter parameter, k' , also gives useful information about scatter (Barbur et al., 1995). This is the integral of the scatter function of the eye from 2° - 90° (per unit incident flux in the plane of the pupil). It is proportional to the amount of light scatter in the eye, independent of its angular distribution. This parameter shows significantly less variation from eye to eye or in repeated measurements in the same eye (Barbur et al., 1995). The 2° limit was selected arbitrarily simply because the empirical scatter function, $L_s = kE\theta^{-n}$ fails to predict accurately small angle scatter and becomes infinitely large as the scatter angle approaches zero degrees.

$$k' = \int_2^{90} k \theta^{-n} d\theta \quad (3)$$

This can be simplified to

$$k' = k \left[\frac{90^{1-n} - 2^{1-n}}{1-n} \right] \quad (4)$$

The advantage of using k' is that measurements of k' do not inherently change with angle and so may offer a better parameter to estimate the amount of scattered light in

the eye. When used in conjunction with measurements at different angles, the value of n can be estimated also to give further information about the scatter function of the eye and a more accurate estimate of the amount of scatter.

Kvansakul (2005) suggested that in order to estimate the forward scatter in the eye, a range of scatter angles should be tested. Ideally the values of n and k' should be calculated so that the whole scatter function is investigated with both the amount and distribution of scattered light in the eye measured.

2.7.4 The causes of straylight in a Normal Eye.

Eye media disturbance can cause light scattering, resulting in a veil of straylight over the retinal image. The patient may complain of hazy vision, increased glare hindrance, loss of contrast and colour, etc. In an ideal eye there would be no light scattering at all, but because the eye media are not optically ideal, there will always be some light scattering. The amount of retinal straylight depends on age and pigmentation.

Within the normal eye, there are five major sources that contribute to the total amount of straylight: the cornea, the iris, the sclera, the lens, and the fundus (Weale, 1986, Vos & Bouman, 1964). For a young, healthy, Caucasian eye, the total amount of straylight is, roughly speaking, 1/3 caused by the cornea, 1/3 by the lens, and 1/3 by the iris, sclera, and fundus (Vos & Bougard, 1963, Hemenger, 1992). These ratios change with age and pigmentation. Corneal light scatter is more or less constant with age, but may increase as an unwanted side effect of refractive surgery. The iris and sclera are not completely opaque. Depending on the level of pigmentation, some of the light falling on the iris and sclera will be transmitted and contribute to the light that reaches the retina. This contribution will be low for pigmented non-Caucasians (with brown eyes), but might be considerable for lightly pigmented blond Caucasians with blue eyes (van den Berg et al., 1991). Light scattering by the crystalline lens increases with age, especially when people develop a cataract, which in terms of straylight can be seen as an accelerated ageing of the lens. The fundus does not absorb all the light, so part of the light that reaches the retina will be reflected backwards and scattered to different locations on the retina, thus contributing to the total amount of straylight.

The eye also has features which reduce scatter. For instance, the pigmented RPE is darkly pigmented, enabling it to absorb light photons that are not absorbed by the photoreceptors, which reduces light scatter within the eye. Also, a vascular network covers the retina, except in the fovea, which is avascular. This adaptation prevents the scattering of light by retinal vessels and maximizes the visual resolution provided by the fovea. Metabolic nourishment for foveal (and nonfoveal) cones is provided by the choroid. Additionally, surrounding the fovea is a region of the retina referred to as the macula lutea, which contains a non-photosensitive yellow pigment that is located in the inner retina. This pigment absorbs blue light (maximal absorption is in the region of 460 nm) and may aid vision by reducing light scatter or minimizing the effects of chromatic aberration (Wald, 1945).

2.7.5 Additional Causes of increased retinal straylight

Pathologies such as cataract and external factors such as refractive surgery may also caused increased retinal straylight. If a cataract starts to develop the earliest complaints often are from increased straylight, such as increased glare hindrance when driving at night. Other complaints may include hazy vision, loss of contrast and colour, halos around bright lights, and difficulties with against the light face recognition. Most corneal disturbances such as corneal dystrophies cause strong increases in straylight. In some cases, visual acuity can be maintained despite large increases in straylight, such as in corneal oedema.

In refractive surgery wound healing can cause haze in the cornea. Visual acuity hardly suffers, but complaints from straylight may cause glare. Contact lenses also often cause straylight to increase. Deposits or scratches can often be identified as a major cause of increased straylight, but if the cornea reacts to improper use of contact lenses, straylight may increase substantially. Turbidity in the vitreous can also cause large increases in straylight, often again without much effect on visual acuity.

2.7.6 Straylight and Vision Tests

Straylight can affect other tests, such as contrast sensitivity, visual acuity and slit lamp examination. Reduced Snellen acuity with low contrast letters, and poorer chromatic

discrimination correlates well with increased levels of scattered light, although the most drastic effects are observed in measurements of contrast sensitivity, which exhibits a large decrease, with the high frequency range being the most affected.

2.7.6.1 Straylight and visual acuity

Van den Berg (1986) and Beckman et al., (1991) have suggested that there is only a weak relation between straylight and high contrast visual acuity. This is because straylight is determined by light scattering over larger angles (1 to 90 degrees), whereas visual acuity is determined by light deflections over small angles (< 0.1 degree, more commonly known as aberrations). For example, +2.00 diopter trial lens in front of a subject's eye will definitely change the subject's visual acuity, whereas the straylight value will stay mostly the same. On the other hand, putting a fog filter in front of the subject's eye will show a dramatically increased straylight value, whereas visual acuity may hardly decrease (van den Berg, 2008).

2.7.6.2 Straylight and glare sensitivity

A better correlation between straylight and contrast sensitivity may be found when contrast sensitivity is measured with a glare source next to the measurement chart (Vos 1984). But in that case differences between subjects will also depend on differences in contrast sensitivity that already exist without the glare source. So the parameter that best relates to the straylight value is the *decrease* in contrast sensitivity caused by the glare source.

There have been attempts to measure glare sensitivity in this way with glare testers. For instance, the BAT consists of a plain contrast sensitivity measurement with a glare source at the side.

2.7.6.3 Straylight and slitlamp based examination.

Slit lamp examination can give an indication that scatter is occurring in the eye, by assessing opacities of the optical media. Objective measurements using backward light scatter, such as those based on the slitlamp examination principle (e.g. the digital slitlamp, Scheimpflug system, Lens Opacity Meter, LOCS) can be used. These opacities are partly responsible for the amount of light scattering in the eye, but they account for only a part of the total light scattering. The transparency of the iris and

sclera, as well as the amount of light reflected from the fundus, are not assessed by the slitlamp examination. Also, with the slitlamp only the light that is scattered back from the optical media is examined (Weale, 1986). This is not the light that reaches the retina, which is the light that is scattered in the forward direction. Studies show that no direct relation exists between the forward and backward scatter. To assess the effect of straylight on the eye, it is better to measure the amount of forward scatter.

2.7.7 Methods of Measuring Scatter

There are various methods of measuring scatter.

2.7.7.1 The Halometer

The halometer test, is a form of disability glare test. The technique utilises a self-illuminating optotype target, which can be seen in either red or green light from a working distance of 30 cm (Babizhayev et al., 2003). A single dot glare source is used and the patient's task is to move the optotype closer to the glare source until it disappears due to the veiling glare from that source. A halometer score is determined from the angle of the glare source. A glare sensitivity (glare radius) score is gained using both red and green optotypes, so that the effects of light absorption can be separated from those of light scatter.

2.7.7.2 The Brightness Acuity Tester (BAT)

The BAT is a hand-held instrument that consists of a hemispheric bowl with an internally illuminated surface (Holladay et al., 1987). The subject holds the device to their eye and views the chart through a central 12 mm aperture. Different intensity settings can be used. However the high intensity setting has been reported to give inappropriately high predictions of disability glare (Neumann et al., 1988; Prager et al., 1989) and can reduce contrast beyond a chart's limits with some early cataract patients (Regan, 1991; Elliott & Hurst, 1990). The BAT can be used with the Pelli-Robson CS and Regan VA charts.

2.7.7.3 The van den Berg Straylightmeter

A 1° circular target is viewed, surrounded by an annulus with an outer radius of 2° of steady luminance of 30 cd/m² (van den Berg & Spekreijse, 1987). Concentric with this target and positioned along the inside of the viewing tube are three rings of

yellow (λ_{max} 570 nm) light-emitting diodes. They are positioned at angular distances of 3.5°, 10°, and 28° from the subject's eye. The LED sources flicker sinusoidally at 8 Hz. The three rings are illuminated separately to allow measurement of light scatter at each of the three angular positions. The subject is instructed to observe the central target, and one of the three glare rings is switched on. Forward light scatter within the eye causes a visible flicker to be seen on the central target.

The luminance modulation of the central target is increased, which flickers in counterphase to the LED sources. The depth of modulation of this counterphase light which produces zero perceived flicker corresponds directly to the amount of forward light scatter (van den Berg, 1986; Ijspeert et al., 1990).

For a given scattering angle, the luminance modulation of the central target is increased and the point at which the central flicker ceases is recorded. The modulation is then increased further until the flicker reappears, corresponding to where the target modulation overwhelms that caused by straylight. Refractive blur has virtually no effect on the measurements, because the central target is large and the task is to perceive a flickering stimulus, (van den Berg, 1986, Ijspeert et al., 1990).

Elliott & Bullimore (1993) suggested that forward light scatter measured using the van den Berg Straylightmeter has several advantages. It provides a direct measure of forward light scatter, i.e. not one estimated from contrast or resolution loss resulting from a glare source. It also provides measures of light scatter at different glare angles, and therefore it can be used to compare disability glare tests using various types of glare geometry. Additionally, the results are free from neuronal interference and the scores are repeatable and sensitive. For example, the test has been able to show differences in forward light scatter between normal subjects with different eye pigmentation. The amount of contrast loss caused by the light scatter can also be calculated.

2.7.7.4 Hartmann Shack:

A newer method of measuring scatter involves the use of the Hartmann-Shack aberrometer. For instance, Cervino et al., (2008) used image-analysis software to quantify scatter from centroid patterns obtained using the WASCA Hartmann-Shack

analyzer. Three scatter values were obtained in 6 model eyes and 10 human eyes. Measurements were made in the human eyes with the C-Quant straylight meter (Oculus) to obtain psychometric and objective measures of retinal straylight. A good correlation was achieved between psychometric and objective scatter measurements.

Thibos & Hong (1999) showed that the Shack-Hartmann aberrometer provides additional information about the eye's imperfections on a very fine spatial scale, which scatter light and further degrade the quality of the retinal image. They suggested that, spatial maps of the variation of optical aberrations and scatter across the eye's entrance pupil could represent an improved description of the optical imperfections of the abnormal eye.

More recently, metrics involving scatter have been assessed for their effect on visual performance. Donnelly et al., (2004) obtained Shack Hartman Wavefront-Sensor (SHWS) images from 148 patients with cataracts. Scattering was described in a scatter map and by five single-value metrics characterizing SHWS lenslet point spread functions. Visual acuities (assessed by low and high contrast VA under mesopic and photopic conditions) were found to have decreased proportionately to the scatter metrics. The resulting metrics explained the significant variance in visual acuity, especially in the aging eye. Together with a backscatter metric they explained approximately 50% of the variance in VA. This new technique can be contrasted with the view that scatter hardly affects VA (van den Berg, 2008). The Shack Hartman Wavefront-Sensor may allow finer measurements to be made to allow a link between scatter and VA to be made.

2.8 Contrast Sensitivity

Haymes et al., (2006) pointed out that contrast sensitivity (CS) is a fundamental aspect of vision. Its measurement provides useful independent information in relation to a patient's visual function, which may not be revealed by visual acuity (Haegerstrom-Portnoy, 2005; Haymes et al., 2006).

Studies have shown a significant relationship between contrast sensitivity and many activities such as driving performance (Owsley et al., 1998). There is also evidence to

suggest that contrast sensitivity measurement may have some value in the detection and progression of ocular diseases, such as cataract (Elliott & Hurst, 1990) and glaucoma (Ansari et al., 2002). Contrast sensitivity tests have also been useful for evaluating ophthalmic treatments such as cataract surgery (McGwin et al., 2003) and laser refractive surgery (Yamane et al., 2004).

2.8.1 Straylight and contrast sensitivity

Increased straylight leads to lower contrast sensitivity (Koch & Lie, 1990; Irving & Woo, 1993) but the decrease in contrast sensitivity is much smaller than the increase in straylight. Five times increased light scattering lowers the contrast sensitivity function by only 20%. Therefore, contrast sensitivity cannot be used as a valid means to assess the amount of straylight, even though it is influenced by it.

Elliot & Bullimore (1993) evaluated various glare tests, including the van den Berg Straylightmeter and the Brightness Acuity Tester used with the Pelli-Robson and Regan charts. Their data indicated that contrast sensitivity or low contrast acuity measured in the presence of glare was superior to disability glare scores in assessing cataract patients with a normal neural function. Under glare conditions, contrast sensitivity and low contrast acuity scores from the Pelli-Robson, Regan, and Berkeley tests provided similarly reliable, discriminative, and valid measures of visual assessment in cataract.

2.8.2 Crowding and Contrast

Crowding has been described as a situation where the presence of flankers disrupts the observers' ability to identify a visual target. In particular, crowding refers to a phenomenon that is observed when the target and flankers are positioned within some critical distance in the visual field (Livne & Sagi, 2007).

Crowding is thought to affect mainly identification and fine discrimination (He, Cavanagh, & Intriligator, 1997; Pelli et al., 2004). Felisberti et al., (2005) tested the role of target saliency in crowding and concluded that the target's saliency can attenuate the effect. They manipulated saliency by several means (eg. contrast and orientation). Livne & Sagi (2007) also tested the effect that relative target contrast

has and found similar results, with an abolishment of crowding when the target's contrast is exceeded by approximately four times that of the flankers.

2.9 Optical Changes Induced by Refractive Surgery

2.9.1 Increased Aberrations:

Aberrations have been examined in post refractive surgery subjects in various ways, which have included the use of corneal topography and laser ray-tracing techniques.

2.9.2 Corneal Topography Data

Optical changes induced by refractive surgery occur on the cornea and the anterior corneal surface provides the main contribution to refraction. Therefore a large part of the analysis reported in the literature has been based on corneal topography data (Marcos et al., 2001). Corneal aberrations have been computed from corneal height maps, which provide information on the imaging-forming capability of the cornea alone. Results from different authors indicate that, in the past, corneal aberrations increased substantially after refractive surgery (Oshika et al., 1999, Schwiegerling & Snyder, 2000).

2.9.3 Aberrations of the Whole Eye

Marcos et al., (2001) however pointed out that pupil centration and internal optical aberrations are not accounted for in studies based on corneal topography measurements, but they also played an important role in evaluating individual surgical outcomes. Therefore they suggested that corneal aberrations were not sufficient to describe the overall optical quality of the eye, because other parameters (such as position, thickness, and refractive index of the lens, axial length, or pupil centration) also play an important role in image formation.

Marcos et al., (2001) therefore measured total and corneal aberrations in a group of 14 eyes before and after LASIK surgery. Total aberrations were measured using a laser ray-tracing technique. Corneal aberrations were obtained from corneal elevation maps. They found that LASIK induced a round central area (with various amounts of decentration, depending on the eye) of positive aberration, surrounded by an area of negative aberration.

Moreno-Barriuso et al., (2001) measured the ocular aberrations of 22 myopic eyes, which were treated with LASIK refractive surgery using a laser ray tracing technique. RMS wavefront error was found to have increased significantly in all eyes but two after surgery. On average, LASIK induced a significant 1.9-fold increase in the RMS error for a 6.5 mm pupil. The main contribution was due to the increase of spherical aberration. It was confirmed that standard refractive surgery procedures may induce considerable amounts of 3rd and higher order overall aberrations. Their impact increased notably for large pupil sizes, which explained reported experiences of night vision problems, such as halos.

2.9.4 Objective Measurements of Aberrations

Objective techniques, used for the measurement of ocular aberrations, have also been used to measure the effect of refractive surgery on image quality.

Thibos and Hong (1999) presented data on one eye measured with a Hartmann-Shack aberrometer both before and on the day after LASIK refractive surgery to demonstrate the applicability of the technique and reported the limits to the technique for highly aberrated eyes. They showed that it was possible to obtain at least a partial topographic map of the refractive aberrations of the patient's eyes, but severe losses of data integrity could occur.

2.9.5 Spherical Aberrations

Various studies in the past have found an increase in spherical aberration after refractive surgery. Increased spherical aberration was particularly common after the correction of myopia, since ablation merely flattens the central regions of the cornea, while the periphery remains steep. This changes the asphericity of the cornea from a prolate to an oblate shape or from negative to positive asphericity. This is reflected in a change of spherical aberration towards more positive values. For instance, Benito et al., (2011) studied 22 eyes which had undergone standard LASIK to correct myopia. Standard myopic LASIK was found to produce a significant increase of ocular high-order aberrations at 1 month after surgery. During the next 8 months, a small increase of ocular and corneal positive spherical aberration was also found. They concluded that standard myopic LASIK decreased ocular optical quality.

Yoon et al., (2005) developed a non-toric eye model to explain how spherical aberration is induced after myopic and hyperopic laser refractive surgery. Their clinical data showed that positive spherical aberration was induced after myopic correction and negative spherical aberration increased after hyperopic correction. More recently with wavefront technology, spherical aberration has become less of a problem after refractive surgery.

2.9.6 Internal Optical Aberration Changes and spherical aberration

Marcos et al., (2001) found that in their LASIK patients, the anterior corneal spherical aberration increased more than the total spherical aberration. It was suggested that this was due to spherical aberration of negative sign being induced on the posterior corneal surface. The effect was larger as the preoperative spherical refractive error increased and did not depend on the preoperative internal aberrations. The same analysis for post-LASIK third-order aberrations showed no statistically significant difference between corneal and total aberrations. Therefore, Marcos et al., (2001) concluded that third-order aberrations did not seem to be induced on the posterior corneal surface.

In respect of hyperopia, Llorente et al., (2004) evaluated changes induced by standard laser in situ keratomileusis (LASIK) for hyperopia on total and corneal optical quality on 13 eyes. Spherical aberration was found to have changed to negative values. Hyperopic LASIK was found to have induced larger changes than myopic LASIK, compared to an equivalent group of myopic eyes from a previous study. Induced corneal spherical aberration was six times larger after hyperopic LASIK, for a similar range of correction, and of opposite sign. As with myopic LASIK, changes in internal spherical aberration were of opposite sign to those induced on the corneal anterior surface.

Durrie et al., (2010) compared differences in visual outcomes and induced spherical aberration after conventional and wavefront-optimized LASIK for the treatment of hyperopia in 51 eyes. Induced spherical aberration was negative for the conventional and wavefront-optimized treatment groups. Although not statistically significant, a

trend towards less induced negative spherical aberrations was noted with the wavefront-optimized treatment

2.9.7 Coma

Studies have often found an increase in coma. For instance, Serrao et al., (2011) investigated 98 eyes and examined the optical quality of the anterior cornea during a 6-year follow-up after photorefractive keratectomy (PRK) for myopia. They found a statistically significant postoperative increase of coma in the high-myopia group.

Lihua et al., (2010) studied the influence of treatment decentration on induced wavefront aberrations by considering oblique incidence in a mathematical model of the anterior corneal surface. The results revealed that significant coma was induced from the treatment translation, and it was nearly proportional to the translation or corrected refraction of vision correction. Oblique incidence played an important role in the impact of treatment decentration on the induced aberrations in refractive surgery. It was concluded that treatment decentration should be minimized by all means, particularly for high myopia.

This view agreed with the study of Tsai et al., (2000). Tsai et al., (2000) examined 16 eyes, which had been treated with PRK, and 161, which had undergone, LASIK. All treatments had used an eye tracker. The amount of decentration was analyzed by corneal topography. Patient-related factors were found to influence centration. Centration was better in the second eye (due to the effect of learning) and decentration was more severe in eyes with high myopia. They concluded that an eye tracker, which makes the laser beam follow the eye's movements, helps to avoid severe decentration. However, it could not alone ensure good centration, as patient cooperation and fixation were also important.

2.9.8 Role of Pupil Centration on Aberration Measurement

Artal et al., (1996) has pointed out that the position of the pupil is important for a correct estimation of retinal image quality and should be taken into account when predicting visual performance from corneal aberration data. Therefore, the processing algorithms of Marcos et al., (2001) aligned the corneal aberration pattern with the

total aberration pattern, which was referred to the pupil centre. Although spherical aberration was not changed significantly by recentration (3% on average), third-order aberrations changed by 22%. Although direct corneal data showed no coma, when the actual pupil position was taken into account it was observed that coma became predominant along with spherical aberration.

2.9.9 5th and Higher Order Aberrations

Moreno-Barriuso et al., (2001) found a slight increase of 5th and higher order aberrations, which was not statistically significant. It was suggested the main impact of surgery occurred on 3rd and 4th order aberrations, whereas 5th and higher remained almost unaffected. Moreno-Barriuso et al., (2001) suggested that it could be because PRK and LASIK do not induce micro-irregularities in the cornea, at least of sizes larger than the measurement beam size, which was 0.5 mm in their study.

2.9.10 Increased Scattered Light / Glare /Haze.

Corneal haze can be caused by refractive surgery, due to wound healing and the induced presence of stromal opacities. Researchers have often found increased scatter due to refractive surgery. For instance, Ondategui et al., (2012) evaluated 34 eyes that had PRK and 55 eyes that had LASIK. PRK and LASIK were found to have increased the objective scatter index by factors of 1.48 and 1.57, respectively. The 3 month postoperative objective scatter index was higher in both eyes as a direct consequence of the increase in intensity at broader angles measured postoperatively, which means that the intraocular scattered light was higher after both procedures. The intraocular scattering worsened in proportion to the preoperative refraction.

Increased reflectivity can occur due to anterior stromal wound healing and the presence of keratocytes, producing a loss of corneal transparency, due to increased scattering (Moller-Pedersen (2000). Corneal haze can develop over the first few weeks and often subsides by one year (Shah, 2007).

After PRK, increased light-scattering from reflective myofibroblasts and other wound-healing phenotypes is a major cause of stromal haze, (Moller-Pedersen, 2003). By contrast, it has been found that the central cornea generally remains clear after LASIK, although haze due to fibrosis and myofibroblast transformation can develop

next to the flap margin, at the basement membrane incision, in LASIK-treated rabbits, (Ivarsen et al., 2004).

2.9.11 Refractive Instability

Histological experiments have shown that wound healing is a major cause of refractive instability and intersubject variability outcomes. Moller-Pedersen (2003) suggested that refractive outcomes of both PRK and LASIK have shown an exceedingly wide variation, due to there being no precise control of the actual photoablation depth during surgery in each individual patient (i.e. the exact amount of stromal tissue removed). Also there is no precise control of the postoperative wound-healing response that tends to distort the induced refractive correction by the addition of variable amounts of new repair tissue.

Immediately following excimer laser photoablation treatment for myopia, the patient is left with an intentional (hyperopic) over-correction to account for the subsequent myopic regression of treatment effect. However, the subsequent refractive regression varies considerably among individuals, and so the procedure may leave the patient emmetropic, hyperopic, or myopic.

Longer term studies of both PRK (2-5 year follow-up) and LASIK (2-year follow-up) have revealed a continued potential for ongoing myopic regression with time (Han et al., 2000), suggesting that corneal wound healing is considerably delayed in humans and may require decades to be completed. This may be contrasted to the 14 year PRK follow up study of Bricola et al., (2009), who suggested that the postoperative refraction continues to be stable for up to 14 years. Zalentein et al., (2009), on the other hand, in their 7 year follow up of LASIK patients commented that although refractive results after LASIK were relatively good in the short term, they tended to decline over time. Higher refractive errors and younger patient age tended to decrease refractive stability.

Corneal ectasia can also lead to refractive instability. Corneal ectasia is a progressive steepening and thinning of the cornea after excimer laser corneal refractive surgery that reduces uncorrected and often best spectacle-corrected visual acuity (Randleman et al., 2008). Risk factors that have been established for corneal ectasia after corneal

refractive surgery include: topographic abnormalities, low preoperative corneal thickness, young age, and high myopia. Other factors, such as a history of eye rubbing, unstable refractions, a family history of ectatic corneal disease, and an underlying increase in corneal elasticity, also may make corneal ectasia after refractive surgery more likely . A 2010 survey of LASIK surgeons found that 52% have had a documented case of post-LASIK ectasia in their surgical patients (Duffey & Leaming, 2010)

2.9.12 Q Value & Refractive Surgery

Refractive surgery has often been found to change the corneal asphericity (Q), For instance, Bottos et al., (2011) evaluated changes in corneal asphericity (Q) and spherical aberrations after refractive surgery using Scheimpflug imaging. 177 myopic eyes and 32 hyperopic eyes were examined. It was found that there was a tendency for Q values and spherical aberrations to become more positive after myopic ablation and more negative after hyperopic ablation. The changes depended on the magnitude of the refractive correction.

Refractive surgery can also lead to unexpected changes in Q value. Alio et al., (2008) pointed out that, factors such as biomechanical changes, the wound-healing process, and the effects of the flap are sources of variations of the planned corneal surface. Pallikaris et al., (2002) have shown that the creation of the flap induces unexpected changes in corneal asphericity and corneal aberrations.

2.9.13 Studies Assessing Visual Performance.

Studies have indicated that most changes in visual performance occur in contrast sensitivity (CSF), low contrast visual acuity, and visual acuity measured under low illumination (i.e., with large pupils).

2.9.13.1 Contrast Sensitivity

Reports have demonstrated that the contrast sensitivity function can be compromised by keratorefractive surgery. For instance, Nassiri et al., (2011) examined the contrast sensitivity of 132 eyes after wavefront-optimized or conventional photorefractive keratectomy (PRK) in myopic patients with or without astigmatism. In both groups, the postoperative mesopic and photopic contrast sensitivity decreased significantly at

most spatial frequencies.

Varying contrast sensitivity results have been found more recently with LASIK. Alarcon et al., (2011) evaluated visual quality in 50 eyes after laser in situ keratomileusis (LASIK) performed to achieve monovision in 25 presbyopic patients. Contrast sensitivity function was found to have diminished, especially in the nondominant eye and with binocular vision. In contrast to this, Keir et al., (2011) examined 31 patients who had been treated with wavefront-guided LASIK for hyperopia. Unlike Alarcon et al., (2011) no significant changes in contrast sensitivity were found. This may have been due to wavefront-guided LASIK being a better technique.

Similarly, Mirafteb et al., (2011) examined 41 patients who had undergone wavefront-guided LASIK in one eye and wavefront-optimized LASIK in the fellow eye for myopic astigmatism. Contrast sensitivity did not decrease in either group and no statistically significant differences between groups were noted. Arbelaez et al., (2010) found similar results using the nonwavefront-guided aspheric algorithm of the SCHWIND AMARIS excimer laser.

Earlier studies have found decreases in contrast sensitivity after refractive surgery. For instance, Yamane et al., (2004) examined the contrast sensitivity and low contrast visual acuity of 110 patients undergoing LASIK. LASIK was found to have significantly improved logMAR best corrected visual acuity, but it was found to have significantly reduced the area under the log contrast sensitivity function (AULCSF) and low-contrast visual acuity. It was found that the greater the amount of achieved myopia correction was, the greater were the changes in the contrast sensitivity function. The induced changes in AULCSF by LASIK showed significant correlations with changes in total higher-order, coma-like, and spherical-like aberrations.

Induced corneal irregular astigmatism has also been found to influence contrast sensitivity. Tomidokoro et al., (2001) examined seventy-nine eyes without corneal haze, which had been treated with PRK. Corneal irregular astigmatism was calculated using Fourier series harmonic analysis of the videokeratography data. After PRK,

AULCSFs were found to be significantly smaller for day vision and night vision, compared with normal controls. AULCSFs for day and night vision were significantly and negatively correlated with asymmetry and higher order irregular components, but not with the regular astigmatism component.

2.9.13.3 Visual Acuity:

A classic but not the only test of visual performance is high-contrast visual acuity (Marsack et al., (2004). However, despite many reports of increased higher-order aberrations after keratorefractive surgery, fewer studies have reported a decline of best-spectacle corrected visual acuity (BSCVA) after successful refractive surgery. This may be due to high contrast visual acuity charts being less sensitive at detecting changes in visual performance.

Arbelaez et al., (2010) assessed 358 eyes that had undergone non wavefront-guided LASIK for moderate myopia with astigmatism. No eyes lost 2 or more lines of best spectacle-corrected visual acuity. One line is the day-to-day variability in measuring visual acuity. The two eyes losing one line of best spectacle corrected VA were eyes with preoperative super vision (20/16) that resulted in normal vision (20/20) postoperatively.

Manche & Haw (2011) compared LASIK and PRK in a study of 68 eyes. At 1 month, best spectacle-corrected visual acuity (BSCVA) was worse in the PRK group. By 3 months, this difference had resolved. In both LASIK and PRK groups, no eyes lost 2 or more lines of BSCVA. In the PRK group, 2 eyes lost 1 line, 21 eyes had no change, 9 eyes gained 1 line, and 1 eye gained 1 or more lines of BSCVA at 12 months.

Earlier research has sometimes found decreases in low contrast VA. For instance Verdon, Bullimore, & Maloney (1996) examined the effect of PRK on best-corrected visual performance on 18 subjects with myopia. It was found that low-contrast visual acuity losses after PRK were notably greater than high-contrast visual acuity losses, and that low-contrast visual acuity was a sensitive measure for gauging the outcome and safety of refractive surgery. One year after PRK, the mean best-corrected high-contrast visual acuity was reduced by half a line, and the mean best-corrected low-contrast visual acuity was reduced by 1 1/2 lines. The losses were greater when the

subject's pupils were dilated and a glare source was used. The reduction in dilated low-contrast visual acuity was found to be positively correlated with decentration of the ablation zone.

2.9.14 Pupil Size Effects

Disturbance of vision and optical glare phenomena are produced when pupil diameter increases, especially at night. Reasons for these phenomena can be small ablation zones, optical distortion within the corneal ablation area, decentred ablation zones, and residual stromal scarring. Researchers have investigated the effects of ablation zone size. For instance Mok et al., (2005) studied the monochromatic wavefront aberrations of 96 eyes of patients with normal myopic astigmatism before and after conventional LASIK. Patients were divided into three groups according to optical zone diameter. They concluded that a larger surgical optical zone diameter significantly decreased higher order aberrations after LASIK. One disadvantage of increasing the optical zone diameter is that it would also significantly increase the amount of corneal tissue removal.

O'Brart et al., (1995) examined eighty patients who were treated with PRK. They found that treatment with 6 mm ablation diameters precipitated less initial overcorrection, and greatly improved the predictability of PRK, compared to treatment with 5 mm ablation diameters. This 6 mm diameter was associated with a reduction in complications impairing postoperative visual performance, such as corneal and stromal haze, night vision problems, regression of the correction and loss of visual acuity. A large scotopic pupil size was put forward as a possible explanation for this finding.

Chapter Three

3. The Visual Pathway and the Decline of Visual Acuity with Eccentricity

3.1 Anatomy & Physiology of the Visual Pathway

3.1.1 Basic Retinal Anatomy

The retina is a complex neural structure that actively analyses the image that is focused on it. The photoreceptors on the retina consist of rods and cones. They respond to light, transforming radiant energy into electrical activity, which is transmitted to retinal bipolar cells and then onto retinal ganglion cells. The long axons of the retinal ganglion cells leave the eye, to form the second cranial nerve (the optic nerve).

3.1.2 Post retinal Pathways

At the optic chiasm, ganglion cell fibres from the nasal retina of each eye cross over to join the temporal fibres of the fellow eye to form the optic tract. As a result, the fibres constituting the left optic tract carry information regarding the right visual field, and fibres in the right optic tract encode the left visual field.

The primary target of the optic tract is the dorsal lateral geniculate nucleus (dLGN), a thalamic nucleus. Most, but not all, retinal ganglion cells synapse in this six-layered structure. Layers 2, 3, and 5 receive input from the ipsilateral eye, whereas layers 1, 4, and 6 receive input from the contralateral eye.

The cells of the dLGN send most of their axons to the cerebral cortex, the most highly evolved portion of the brain. This structure consists of two hemispheres, connected by the corpus callosum (Pestranta et al., 2012). The cortical area in which most dLGN axons synapse is the striate visual cortex (Figure 3.1).

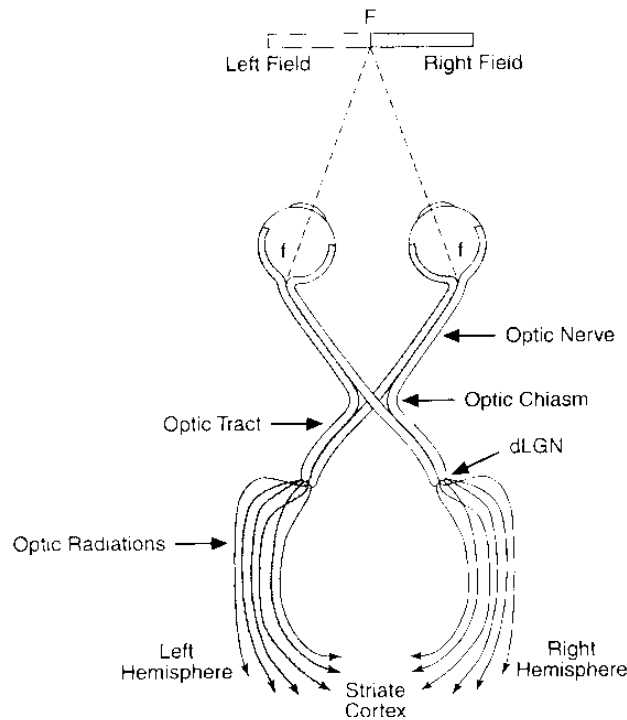


Figure 3.1 The Visual Pathway (taken from Schwartz, 2004 figure 2-10, p16)

The individual parts of the visual pathway are now described in more detail.

3.1.3 Photoreceptors

Photoreceptors are specialized sensory receptors containing a photosensitive pigment that absorbs light quanta, converting this radiant energy into electrical activity. Both rods and cones are slightly depolarised relative to a typical neuron. They have a resting membrane potential of about -50 mV. When exposed to light, photoreceptors hyperpolarize - their potential goes from -50 mV to a value closer to -70 mV (Tomita, 1970). This is noteworthy because stimulation is typically thought to cause depolarisation rather than hyperpolarisation.

The degree of photoreceptor hyperpolarization is related to the intensity of the stimulus, with an intense stimulus causing greater hyperpolarization than a less intense stimulus. This is one reason why the potentials produced by photoreceptors are referred to as graded potentials.

In a typical human eye, there are three fundamental cone photopigments, cyanolabe, chlorolabe, and erythrolabe. The cyanolabe-containing cones are referred to as short wavelength-sensitive cones (SWS or S-cones), the chlorolabe-containing cones as

middle wavelength-sensitive cones (MWS or M-cones), and the cones containing erythrolabe as long wavelength-sensitive cones (LWS or L-cones) (Yoonessi & Yoonessi, 2011).

Rods are most densely packed at about 20 degrees from the fovea, where they reach a peak density of about 150,000 rods/mm². There are no rods in the fovea (Curcio et al., 2000). The postreceptoral organization of the rod system is different from that of the cone system. The result is a duplex retina: a rod-dominated system operates under dim (scotopic) lighting conditions (less than $-3 \log \text{cd/m}^2$) and a cone-dominated system functions under daylight (photopic) conditions (more than $+1 \log \text{cd/m}^2$). Cones are most concentrated in the fovea where their density is 150 000 / mm², the same as the peak density of rods (figure 3.2). Although the density of cones is substantially reduced outside of the fovea, they are present throughout the retina (Boynton, 1979).

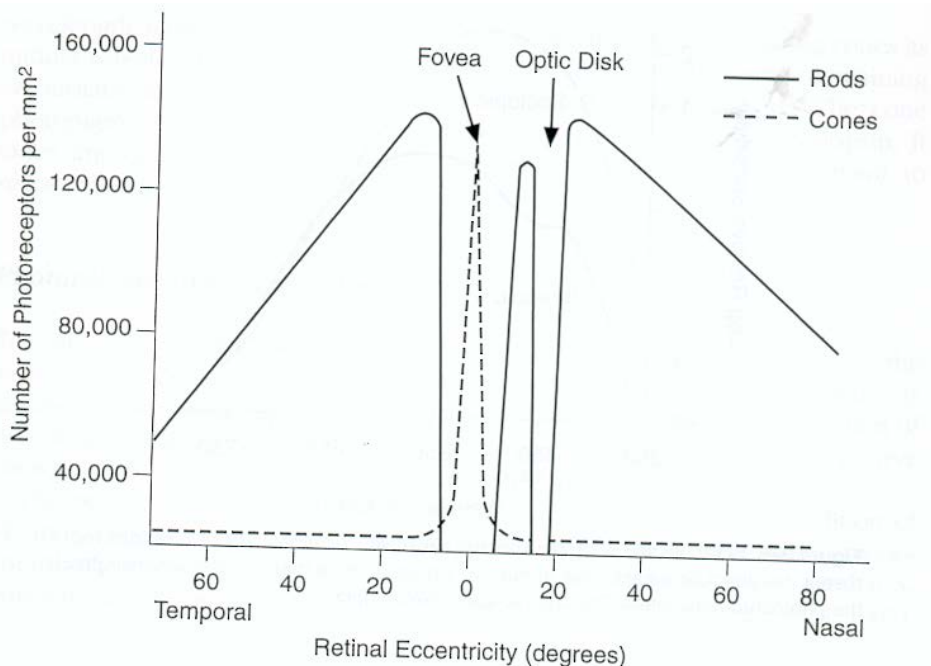


Figure 3.2 Retinal Distribution of rods and M- and L- cones (Osterberg, 1935, taken from Schwartz, 2004 figure 3-7, p34)

3.1.4 Spatial resolution and spatial summation - Photopic Vs Scotopic Conditions.

There is a trade-off between visual resolution and visual sensitivity, which is largely due to the manner in which the rods and cones are connected to the postreceptoral elements of the retina. A major distinction between the scotopic and photopic

systems, is that many more rods communicate with a ganglion cell than is the case for cones. The scotopic system manifests greater spatial summation than the photopic system. Spatial summation contributes to high scotopic sensitivity. The scotopic system has excellent sensitivity (a stimulus is seen), yet poor spatial resolution. In contrast, the photopic system shows less spatial summation, resulting in poor sensitivity, but excellent spatial resolution.

The photopic system is better able to distinguish two flashes of light separated by a brief interval in time. It has superior temporal resolution. This involves the notion of the critical duration, or critical period, in which there is total temporal summation. Scotopic vision, with its greater degree of temporal summation, shows a critical duration of about 100 milliseconds, whereas photopic vision manifests a critical duration in the order of 10 to 50 milliseconds (Sperling & Jolliffe, 1965; Krauskopf & Mollon, 1971; Swanson et al., 1987).

The photoreceptors have simple requirements for activation: diffuse light falling on their receptive fields elicits a response. At more proximal locations to the brain within the retina, the requirements for neural activation are more stringent. Ganglion cells, for example, are responsive only to stimuli that manifest spatial contrast. The retina is designed largely to extract contrast information.

The photoreceptor to bipolar cell to ganglion cell arrangement in the retina reflects the feed-forward, or centripetal, nature of retinal organization. Lateral interconnections also exist, which provide for the horizontal transmission of retinal information. Horizontal and amacrine cells are involved in this lateral integration. This allows feedback and inhibition mechanisms to occur.

In addition to the feed-forward and lateral interconnections, there is a centrifugal pathway, which allows feedback transmission of information. In this pathway, information is transmitted from the ganglion cell region back towards the photoreceptors by interplexiform cells (Linberg & Fisher, 1986).

3.1.5 Horizontal Cells

A large number of photoreceptors, which are distributed over a relatively large area of the retina, synapse with the widely dispersed dendritic tree of a single horizontal cell. Because light falling on any of these photoreceptors may affect the neural activity of the horizontal cell, it manifests substantial spatial summation.

There are two classes of horizontal cells – H1 and H2 cells (Dacheux & Raviola, 1990; Dacey et al., 1996; Martin, 1998). The H1 cells receive input primarily from the M- and L- cones, and little input from the S-cones. In comparison, H2 cells show strong connectivity with S-cones and also receive input from M- and L-cones.

Like photoreceptors, horizontal cells show graded responses and do not generate action potentials. Since photoreceptors and horizontal cells both hyperpolarize in response to light, the synapses connecting them are referred to as sign-conserving synapses.

3.1.6 Bipolar Cells

Bipolar cells are the first (i.e., most distal) retinal cells to display spatial antagonism. Like the photoreceptors and horizontal cells that precede them, bipolar cells do not generate action potentials.

The receptive field of an on-centre bipolar cell is similar to the on-centre ganglion cell receptive field (see later): light falling on the centre of the cell's receptive field causes excitation (depolarisation), whereas light falling on the surround causes inhibition (hyperpolarization). On-centre bipolar cells are characterized by an invaginating synapse that they make with photoreceptors in the outer plexiform layer (Famiglietti & Kolb, 1976; Stell et al., 1977).

Another class of bipolar cells show an inhibitory off-centre bordered by an excitatory on-surround. Unlike on-centre cells, off-centre bipolar cells form a conventional flat synapse with photoreceptors. Both on- and off-centre bipolar cells synapse with ganglion cells in the inner plexiform layer (IPL) at different sub layers with off-centre cells forming synapses in the outer sub-layer and on-centre cells synapsing in the inner sub-layer (Nelson et al., 1978; Peichi & Wassle, 1981).

The explanation for what occurs within the outer plexiform layer that causes some bipolar cells to have an on-centre arrangement and others to have an off-centre configuration, may involve the neurotransmitter glutamate (Slaughter & Miller, 1985, Yoonessi & Yoonessi, 2011)). It is thought that for on-centre bipolar cells, glutamate is inhibitory. Therefore, a reduction in its release causes a relative excitation (depolarisation) of the bipolar cell. For off-centre bipolar cells, the same neurotransmitter has the opposite effect. It is excitatory, and a reduction in its release, secondary to the hyperpolarization of a photoreceptor, causes a relative inhibition (hyperpolarization) of the bipolar cell.

In addition to being categorized as on- or off-centre, bipolar cells are also characterized as midget or diffuse (Boycott & Wässle, 1999). Compared to diffuse bipolar cells, midget bipolar cells have smaller soma and less extensive dendritic trees. An on-centre bipolar cell may be a midget or diffuse cell. The same is true for an off-centre bipolar cell. The receptive field centres of the primate midget bipolar cells that are located in the central and midperipheral retina manifest input from a single M or L cone (Wässle et al., 1994). Such an arrangement accounts for the high level of visual acuity seen in primates. In the periphery, the receptive field centres of midget bipolar cells receive input from more than one photoreceptor, consistent with the reduced visual acuity associated with the peripheral retina.

A diffuse bipolar cell's receptive field centre is formed by 5 to 10 cones (Boycott & Wässle, 1999). Since more than one cone type may form the centre, its spectral sensitivity is very similar to the surround, which also reflects a mixture of different cone types. The surround is formed by H1 cells that receive input from both M- and L-cones.

Figure 3.3 summarizes many of the connections regarding bipolar cells, showing the synaptic connections involved in the formation of diffuse on-centre, diffuse off-centre, midget on-centre, midget off-centre, and S-cone bipolar cells. There are also at least four other classes of bipolar cells.

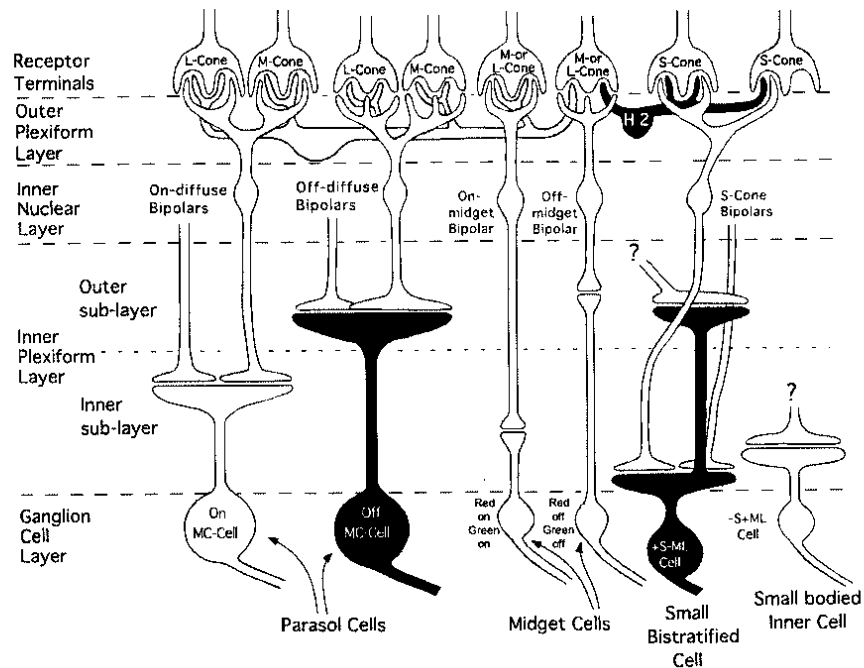


Figure 3.3. Schematic showing the organization of the primate retina. (taken from Schwartz, 2004, figure 12-11, p274)

The view that midget bipolar cells transmit both chromatic and acuity information is controversial. Some investigators believe that one class of retinal cells transmits a pure colour signal, while another class of cells process acuity information (e.g. Calkins & Sterling (1999).

3.1.7 Amacrine Cells

There are about 20 different types of amacrine cells. The complex cellular and synaptic arrangement of the retina points to a high degree of information processing within this structure. Many amacrine cells, like bipolar cells, show a centre-surround organization. An important feature that distinguishes them from bipolar and other more distal retinal cells is the time-related characteristics of their neural response. Amacrine cells tend to respond briefly to the stimulus onset and offset. Because of this characteristic, they are thought to play a critical role in coding movement. Amacrine cells are the first retinal neurons to display action potentials, in contrast to the graded potentials of photoreceptors, horizontal cells, and bipolar cells (Barnes & Werblin, 1986).

3.1.8 Ganglion Cells and Receptive Fields

The innermost cell body layer is the ganglion cell layer. There are two major classes of ganglion cells. The smaller midget, or parvo (P), cells comprise about 80 percent

of these cells and the larger parasol, or magno (M), cells about 10 percent (Lennie et al., 1990). In addition to these neurons, there are small bistratified ganglion cells.

The receptive field properties of ganglion cells reflect the collective properties of the neurons that precede them. They often have a centre-surround organization. Light falling on the receptive field's centre has the opposite effect to light falling on the surrounding area of the receptive field. This is often referred to as spatial antagonism or lateral inhibition (Kuffler, 1953). For a ganglion cell, light falling on the receptive field centre causes the frequency of action potentials to increase - the cell is excited. In contrast, light falling on the receptive field surround inhibits the cell and there is a reduction in the frequency of action potentials. Such a ganglion cell is said to have an on-centre and off-surround. Other ganglion cells have the reverse arrangement, with an off-centre and on-surround.

A strong stimulus for a ganglion cell can be made to occur using a sine wave grating as a stimulus. The bright bar can be made to fall on the receptive field's excitatory centre, resulting in an increased frequency of action potentials. The dark bars can be made to fall simultaneously on the receptive field's inhibitory surround, also increasing the frequency of action potentials and leading to an excitatory response. The result is that the spatial grating vigorously excites the cell. This helps to explain why ganglion cells are selective for spatial contrast, not diffuse illumination. Very early in the visual system, within the retina itself, contrast information is extracted.

Similarly a spot and annulus can elicit responses of opposite signs from the bipolar cell. This is because the spot falls on the bipolar cell receptive field centre, whereas the annulus falls on its antagonistic surround (see figure 3.4). The same effect is also found for the ganglion cell (Werblin & Dowling, 1969).

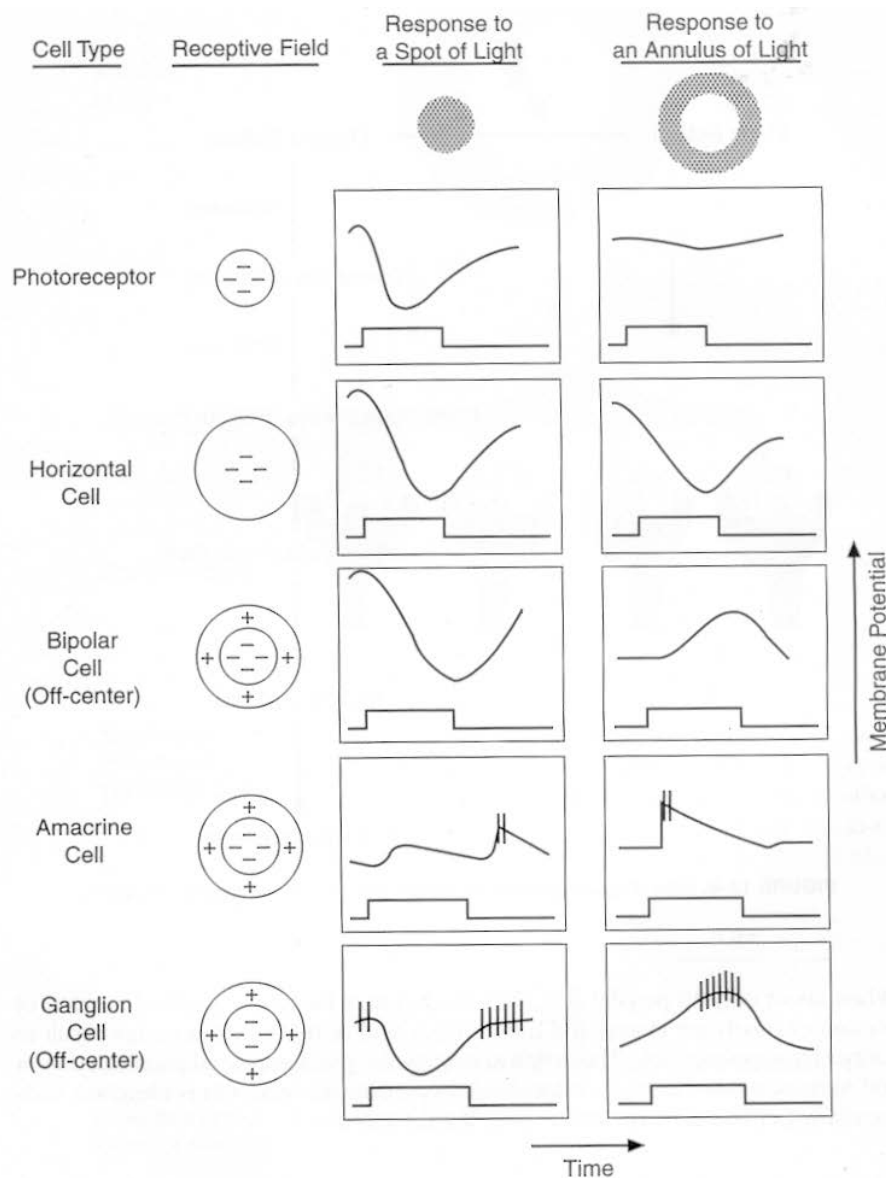


Figure 3.4. Intracellular recordings from the various neural elements in the mudpuppy retina (taken from Schwartz, 2004, figure 12-7, p269)

The centre-surround organization found in ganglion cells has its origins in the bipolar cells. On-centre midget bipolar cells synapse with on-centre midget ganglion cells, and off-centre midget bipolar cells synapse with off-centre midget ganglion cells. Midget ganglion cells are sometimes referred to as retinal parvo cells. On-centre diffuse bipolar cells synapse with on-centre parasol ganglion cells, and off-centre diffuse bipolar cells synapse with off-centre parasol ganglion cells. Parasol ganglion cells are sometimes called retinal magno cells. S-cone bipolar cells synapse onto a distinct class of ganglion cells, the small bistratified cells. The receptive fields of these neurons have an on-centre that is formed exclusively by S-cones (Dacey & Lee, 1994).

A key feature of central and midperipheral midget bipolar cells is the contribution of only one cone to the formation of the receptive field centre. This also holds true for midget ganglion cells located in the fovea. These cells receive input from only one midget bipolar cell, and hence from only one cone (Kolb & Dekorver, 1991). This limited spatial summation accounts for the extremely high visual acuity of central vision. In the peripheral retina, more than one bipolar cell feeds into a midget ganglion cell, increasing spatial summation and accounting for the periphery's reduced visual acuity. The increased spatial summation of peripheral midget ganglion cells is reflected in their larger receptive fields, compared to foveal cells (Rodieck, 1991). Parasol cells have large dendritic trees and presumably synapse with more than one diffuse bipolar cell. This contributes to the extensive receptive field that typifies these cells.

Similar to amacrine cells, ganglion cells generate action potentials. Action potentials, unlike graded potentials, do not decay over distance. This is critical because ganglion cell axons must traverse a substantial distance before they reach their primary destination, the dorsal lateral geniculate nucleus (dLGN).

Retinal cells distal to the amacrine cells communicate with each other through so-called slow potentials. Slow potentials actually spread very rapidly, allowing for fast communication between cells. A problem with slow potentials is that they decay as they move away from their origin, eventually dissipating. In comparison, action potentials do not decay, but they are very slow. The axons of ganglion cells become myelinated as they leave the eye at the disk to form the optic nerve. When a myelin sheath is present along an axon that generates action potentials, there is rapid electronic transmission, with the action potential being regenerated at the nodes of Ranvier at the gaps within the myelin sheath. This saltatory transmission allows rapid transmission of information over long distances to occur without signal decay.

Parasol ganglion cells respond transiently to a flash of light, and midget ganglion cells manifest a sustained response (DeMonasterio & Gouras, 1975). This difference may be due to the nature of the amacrine cell input, with parasol ganglion cells receiving substantial input from transient amacrine cells and midget ganglion cells receiving a large input from sustained amacrine cells (Werblin & Dowling, 1969).

The axons of midget and parasol ganglion cells synapse in the dLGN, forming the first leg of the parvo and magno retinocortical pathways. A third pathway, the konio pathway, is formed by the axons of the bistratified ganglion cells, which also synapse in the dLGN (Yoonessi & Yoonessi, 2011). After the dLGN, the parvo and magno pathways maintain various degrees of independence through the striate cortex, visual area 2, and specialized higher cortical centres (Livingstone & Hubel, 1988).

3.1.9 The dLGN

The pathway from the retina to the dLGN to the striate visual cortex is referred to as the retinocortical pathway. While the great majority of retinal ganglion cells contribute to this pathway, a smaller percentage contributes to the retinotectal pathway. The retinotectal pathway consists of the nerve fibres which connect the retina to the tectum of the midbrain. These axons synapse in the midbrain's superior colliculus (or tectum), bypassing the dLGN. The tectum apparently does not project to the cortex. This pathway appears to be important for encoding eye movements.

The dorsal lateral geniculate nucleus (dLGN) of monkeys and other primates have been found to be a laminated structure. The axons of most retinal ganglion cells synapse on the neurons in this laminated structure. A notable feature of the dLGN is its division into three distinct sections, each constituted of a different type of neuron. The two most ventral layers consist of large neurons referred to as magno cells, and the dorsal four layers consist of smaller neurons referred to as parvo cells (as mentioned on p77). In between these principal layers, in the interlaminar regions (intercalated layers), are collections of yet smaller cells called konio cells (Hendry & Yoshioka, 1994). These cells are hardly visible. Konio cells are diverse small cells with wide fields of input consisting of different cells types. Structurally, they are smaller than parvo cells. The physiological response of konio cells is not as well studied as the other two cell types, while they may play a role in seasonal mood changes and color constancy mechanism (Younessi & Younessi, 2011).

3.1.10 Parvo and Magno cells

Parvo cells are selective to colour contrast, but not to fast movement. In comparison, magno cells are largely monochromatic and very sensitive to movement (Schiller &

Malpeli, 1978). Although the division of the visual system into parallel pathways may be most apparent at the level of the dLGN, this division is also found in the retina (i.e., midget and parasol ganglion cells) and, to a lesser extent, in the striate cortex and higher cortical areas (DeMonasterio & Gouras, 1975; Livingstone & Hubel, 1987, 1988).

Retinal midget (parvo) and parasol (magno) ganglion cells manifest properties similar to their counterparts in the dLGN. A parvo neuron manifests a sustained response when presented with a long duration stimulus. Magno neurons respond to the same stimulus in a transient manner, with only a brief burst of activity at stimulus onset and offset. The transient nature of magno neurons may be due to a substantial input from transient amacrine cells (Werblin & Dowling, 1969). Behavioural studies in monkeys have shown that the parvo pathway is concerned with colour discrimination and visual acuity. Parvo cells manifest smaller receptive fields than magno cells, making them more sensitive to higher spatial frequencies. The receptive field centres of centrally located midget (parvo) ganglion cells are constituted of a single cone, contributing to the highly developed visual acuity manifested by primates. The magno system, in comparison, encodes movement and low spatial frequencies (Merigan & Maunsell, 1990; Schiller et al., 1990a,b).

Transient responses to rapid changes in illumination give magno neurons the capability to resolve high temporal frequency stimuli. Since sustained neurons respond to a stimulus for a longer period of time, they are better suited to code low temporal frequencies. Consistent with this, temporal modulation transfer functions (TMTFS) show that magno cells respond best to high temporal frequencies and parvo neurons respond best to low temporal frequencies (Lee et al., 1990).

Visual information appears to flow along distinct, but not independent, processing streams (Mishkin et al., 1983; Maunsell & Newsome, 1987; Merigan & Maunsell, 1993). One of these streams (variously referred to as the temporal, ventral, or "what" stream) is apparently critical for identifying and recognizing objects, whereas the other major stream (the parietal, dorsal, or "where" stream) plays a central role in motion perception and localization in visual space. Although the ventral and dorsal processing streams are adapted to analyse different aspects of visual information,

there is communication between the two pathways. The ventral and dorsal processing streams are commonly considered to be extensions of the parvo and magno pathways, respectively. The ventral processing stream is thought to receive its predominant input from the parvo retinogeniculate pathway, and the dorsal processing stream is thought to receive its predominant input from the magno pathway (Livingstone & Hubel, 1987, 1988). The larger diameter axons of magno neurons transmit action potentials faster than the smaller diameter axons of parvo neurons. Since the magno system is fast, this information rapidly reaches the cortex. The details of the alerting visual event are then analysed by the "what" system, which processes information that the "where" system does not encode, such as colour and spatial detail.

3.1.11 The Cortex

The cortex is constituted of four lobes: frontal, parietal, temporal, and occipital. These are separated from one another by particularly deep sulci. Neurophysiological, and brain imaging studies and anatomical tracings reveal that each of the lobes is organized into many different functional areas, or modules. Some of these areas (approximately 20) are predominantly devoted to analysing visual information (DeYoe & Van Essen, 1988; Van Essen et al., 1992). The anatomical organization of the cortex is, in some respects, the opposite of that of the retina. Whereas the retina manifests convergence from the photoreceptors to the ganglion cells, there is a divergence within the cortex, with information broadly distributed to a very large number of neurons throughout this structure.

3.1.12 The Striate Cortex

The striate cortex is so named because of the dense plexus of geniculate axons that forms a distinctive stria, referred to as the line of Gennari in layer 4B. It is also referred to as the primary visual cortex, visual area 1, VI, and Brodmann area 17. As is the case for all of cortex, the striate cortex is a layered tissue. The striate cortex is located within the occipital lobe.

The majority of striate cortical neurons are binocular (Pietrasanta et al., 2012), but most are dominated by one eye. Ocular dominance is laid out in a regular pattern of alternating right and left ocular dominance slabs, sometimes called ocular dominance columns (Hubel & Wiesel, 1965b, 1968). The striate cortex is organized into

orientation slabs as well as ocular dominance columns. A complete set of ocular dominance columns (both eyes) and orientation columns (all orientations) form a hypercolumn (Hubel & Wiesel, 1977; Hubel et al., 1978).

Although the striate cortex contains a representation of the entire visual field, it is dominated by the fovea. This cortical magnification of foveal vision occurs primarily due to the large area of cortex devoted to the fovea, rather than the high density of ganglion cells found in the fovea (Popovic et al., 2001).

The striate cortex projects not only to the extrastriate cortex, but it also sends a major reciprocal projection to the dLGN, as well as a projection to the pulvinar, a thalamic nucleus thought to be associated with visual attention, motion processing, and visually guided movement (Merabet et al., 1998). As a general rule, projections to lower visual centres (e.g., dLGN, pulvinar) originate from the deeper layers of the striate cortex (in particular, layer 6), whereas those to extrastriate cortex originate from more superficial layers (particularly, layers 2/3) (Lund et al., 1979; Miller, 2003). Information also flows back towards the striate cortex from the extrastriate cortex via reciprocal pathways (i.e., feedback loops). These feedback loops, which in some ways are analogous to the retinal centrifugal pathway and the reciprocal projection from the striate cortex to the dLGN, may be involved in the gating of information.

3.1.13 Simple and Complex Cells

Neurons in the cat striate cortex have been found to be sensitive to elongated stimuli, such as bars and edges (Hubel & Wiesel, 1959, 1962). Hubel & Wiesel divided these cells into two general categories: simple and complex cells. They later found comparable cells in the monkey cortex (Hubel & Wiesel, 1968).

Simple cells are most sensitive to an edge or bar of a specific orientation. The stimulus, if a bar, must be of a specific width. Moreover, the bar or edge must be properly positioned within the cell's receptive field. The receptive fields of simple cells are divided into antagonistic excitatory and inhibitory regions. It has been suggested that the receptive fields of simple cells result from the input of dLGN neurons whose receptive fields lie along a straight line. Like simple cells, complex cells respond best to an elongated stimulus of a specific orientation. However,

whereas stimulus position within the receptive field of a simple cell is critical, the stimulus can be positioned anywhere within a complex cell's receptive field. Many complex cells are characterized by direction selectivity - for the cell to be stimulated, the stimulus must move in a specific direction. A stimulus moving in the opposite direction, even if of the proper orientation, does not elicit a response. Unlike simple cells, the receptive fields of complex cells cannot be divided into separate excitatory and inhibitory regions.

The formation of increasingly complicated receptive field arrangements (e.g., simple cells) from less complicated arrangements (e.g., concentric dLGN cells) is referred to as serial, or hierarchical processing (Hubel & Wiesel, 1962, 1965a). It has been suggested that the receptive fields of complex cells are the result of this hierarchical processing (Hubel & Wiesel, 1962, 1965a). Similarly, the signals of dLGN cells are combined to produce a simple cell's receptive field, and the signals of simple cells are thought to be combined to produce a complex cell's receptive field. The manner in which these signals are combined is not fully understood. There is not simple linear addition of simple cells, as complex cells do not manifest separate excitatory and inhibitory areas. Other possibilities are that the summation may be non-linear. Non-linear dLGN cells (magno cells) may play a larger role in the formation of the receptive fields of complex cells than they do for simple cells (Hoffman & Stone, 1971; Stone et al., 1979).

Hubel & Wiesel (1965a) found that certain cortical neurons are sensitive to the length of the stimulus. These end-stopped neurons were originally classified as hypercomplex cells. Subsequent examination of the visual cortex revealed that sensitivity to stimulus length is a feature common to many cortical cells (Schiller et al., 1976; Gilbert, 1977). Consequently, hypercomplex cells are generally not considered to be a separate category of cortical neurons.

Cortical neurons respond well to sine wave gratings, and are selective for a particular spatial frequency (DeValois et al., 1982). One cell may be finely tuned to stimuli of 3 cycles/degree, whereas another cell is tuned to 6 cycles/degree. This is consistent with the hypothesis that the visual system operates as a Fourier analyser.

Parallel processing occurs in concert with hierarchical processing. The segregation of the visual system into parallel pathways continues, to some extent, into the striate cortex and beyond (Livingstone & Hubel, 1987, 1988). Staining striate cortex for cytochrome oxidase reveals an irregular pattern of blobs within its superficial layers and a regular pattern of stripes in adjoining visual area 2 (Wong-Riley, 1979). Striate blobs are rich with concentrically organized, double-colour opponent neurons that presumably result from parvo input (Ts'o & Gilbert, 1988). The superficial region of striate cortex between blobs, the interblob region, also appears to receive substantial parvo input. The magno pathway apparently bypasses blobs and the interblob regions. Cytochrome oxidase staining also reveals that visual area 2 contains so-called thin, pale, and thick stripes. These stripes may be specialized to code colour, orientation, and retinal disparity, respectively (Ts'o et al., 2001).

3.1.14 The Extrastriate Cortex

The striate cortex projects to the extrastriate cortex, which is the region of the visual cortex that is not distinguished by the line of Gennari. Other extrastriate areas are visual area 2 (V2 or Brodmann area 18), visual area 4 (V4), inferotemporal cortex (IT), and visual area 5 (V5), also referred to as the middle temporal cortex or (MT). Some of these labels are usually applied to the human cortex, while others are usually applied to the monkey cortex.

Although basic analysis of visual information occurs in the striate cortex, considerably more processing is required to produce the final image perceived. This analysis occurs in visual areas outside of the striate cortex, in the extrastriate cortex. Beyond the striate cortex there is a substantial divergence of information through projections to neighbouring cortical visual areas, which in turn send projections to numerous other higher visual areas, and so forth (Van Essen et al., 1992). In addition to this feed-forward distribution of information, there is feedback (through reciprocal connections) from the higher cortical areas to lower areas. The cortex contains at least 20 distinct visual areas, each containing a map of the visual field called a retinotopic map. It appears that these various areas, which can be conceptualised as specialized modules, play different roles in processing visual information.

3.1.15 Cortical Modularity

Certain higher visual areas are specialized modules that analyse specific attributes of the visual world. Cells in the inferotemporal cortex (IT) respond to complex forms, including faces, indicating a role in form perception (Gross, 1973; Tovée & Coben-Tovée, 1993; Rolls & Tovée, 1995). Both V4 and inferotemporal cortex are considered part of the ventral processing stream. Cells in V5 (also called the middle temporal cortex, or MT), a component of the dorsal processing stream, are well suited for the encoding of motion (Rodman & Albright, 1989).

Imaging studies such as functional magnetic resonance imaging (fMRI), reveal that the region of the brain that is most active depends on the task (Corbetta et al, 1990). Functional magnetic resonance imaging reveals cortical activity by detecting levels of oxygenation. If a human subject views an array of variously coloured, moving objects (for example, red and green objects) and is asked to attend to the green object, areas in the ventral stream show the most activity. In comparison, when the subject views the same array, but is asked to pay attention to the movement of the red objects, the dorsal stream manifests the most activity. If shape (or form) of the object becomes the focus, activity is greatest in the ventral processing stream.

3.1.16 Visual Area 4 and Inferotemporal Cortex

Visual area 4 (V4) and the inferotemporal cortex (IT) belong to the ventral processing stream, and contain cells that are responsive to colour and sophisticated forms, respectively. V4 is sometimes said to analyse colour information (Zeki, 1983), while IT is thought to analyse form information (Fuster & Jervey, 1981; Tanaka et al., 1991).

The receptive fields of cells in IT are large, thereby providing the basis to integrate information over an extensive area and analyse complex patterns (Gross, 1973; Rolls & Tovée, 1995).

The area of monkey cortex that is called IT is probably equivalent to the lateral occipital complex (LOC) in humans. Based on fMRI studies in human subjects, it appears that the LOC responds well to objects, but not to scrambled objects or object fragments (Grill-Spector et al., 2001). It seems to respond to all objects, not showing selectivity for a particular type.

More specialized properties are present in two nearby areas, the fusiform face area (FFA) (Yue et al., 2011) and the parahippocampal place area (PPA) (Tong et al., 1998). The FFA responds well to faces, but not other objects, and may be involved in face detection and/or recognition (Kansiwisher & Yovel, 2006). In comparison, the PPA is strongly activated by objects (e.g., a house) and places - but not by faces - indicating a possible role in perceiving scenes.

Information from the various cortical areas must be combined to result in an integrated percept (Schiller, 1993). For instance, motion and position information that is processed along the dorsal stream must be integrated with colour and form information that is processed along the ventral stream. Information from these two streams must be combined with memory. This integration is apparently coordinated in the prefrontal cortex, an area that has long been thought to play a role in cognition (Rao et al., 1997).

3.1.17 Visual Area 5

Cells in V5 have properties that enable them to perform a comparatively sophisticated analysis of motion information (Gilaie-Dotan et al., 2011), perhaps due to substantial input from the magno pathway (Albright, 1984; Maunsell et al., 1990).

Extracellular recordings in rhesus monkeys observing plaids, reveal that direction selective neurons in the striate cortex tend to respond strongly to the movement of the individual grating components of the plaid, but weakly to the movement of the plaid, itself (Movshon et al., 1985). In comparison, certain cells in V5 respond best to the movement of the plaid as a whole. These neurons encode what is perceived (i.e., the integrated movement of the plaid rather than the individual grating components) and apparently play an important role in global motion perception.

Additional support for V5 involvement in motion perception comes from human PET and fMRI studies (Watson et al., 1993). Transcranial magnetic stimulation (TMS) provides evidence that fast back projections from V5 to striate cortex are necessary for visual awareness of movement (Pascual-Leone & Walsh, 2001). Induced neural activity in V5 has been found to result in the perception of moving phosphenes.

The application of TMS to the striate cortex prior to stimulation of V5 does not affect the perception of moving phosphenes. However, when TMS is applied to V5 about 5 to 45 msec prior to its application in the striate cortex, the perception of movement is disrupted, suggesting that the stimulation of the striate cortex interferes with a signal presumably transmitted along a fast back projection from V5.

3.1.18 Bottom Up and Top Down Attention

Cells in lower visual areas may respond to the physical characteristics of the stimulus, and activity in the higher centres may reflect the perceptions the observer experiences. Bottom-up attention is said to occur for an observer's response to a sudden flash of light or movement in the periphery of the visual field. The attention that is induced by these stimuli is not voluntary or conscious, and can be considered to result from bottom-up processes (Millner, 2012, Steinman & Steinman, 1998). This form of attention can be contrasted with top- down visual attention.

Cortical cells have also been found to reflect a conscious choice of attention, a process sometimes referred to as top-down attention. This has been studied by performing extracellular recordings on cortical visual neurons while a monkey chooses to attend to a specific aspect of a stimulus. It has been observed that a red-sensitive neuron in V4 responds more when a red stimulus is in its receptive field. However, when the animal is required to attend to the green stimulus, the response is diminished (Moran & Desimone, 1985; Motter, 1994).

3.2 The Decline in Acuity with Eccentricity

3.2.1 Introduction

In the next sections are explanations from the literature for the decline in acuity from central fixation to the periphery, concentrating on the foveal area up to an eccentricity five degrees either side of fixation and the use of the Landolt ring stimulus. The research literature puts forward a variety of reasons for why acuity may fall with eccentricity. The literature has also found or suggested that there are different trends in the fall of acuity with eccentricity, such as suggesting that there is a straight line relationship between acuity and eccentricity, or increased or decreased foveal magnification leading to deviations from a straight line relationship.

3.2.2 Straight – Line Relationship between Visual Acuity and Eccentricity

Weymouth (1958) used Landolt rings to find a virtually linear rate of increase in visual acuity from the foveal value. A shutter was used to expose the Landolt ring, for a short, unspecified exposure time. Weymouth (1958) suggested that this gradient could be related to other spatial thresholds and perceptual tasks via a neural substrate such as ganglion cell separation. Weymouth (1958) suggested that for many pattern recognition tasks, the function which fitted threshold size, plotted against angular eccentricity in the central fields, could therefore be approximated by a straight line (Figure 3.5).

To aid their studies into the fall in acuity with eccentricity, Daniel & Whitteridge (1961) defined cortical magnification (M) as the linear distance in millimetres of the cortical projection on the striate area, corresponding to 1° in visual space (units mm (of striate) / degree (of visual space)). Many researchers have subsequently examined cortical magnification. Drasdo (1977) examined data on ganglion cell receptive field density, D_r , (in receptive fields per solid degree) to see if it could be used to relate to M at every point in the receptive field. Like Weymouth (1958), Drasdo (1977) also suggested that there may be a straight-line relationship, between eccentricity and visual acuity.

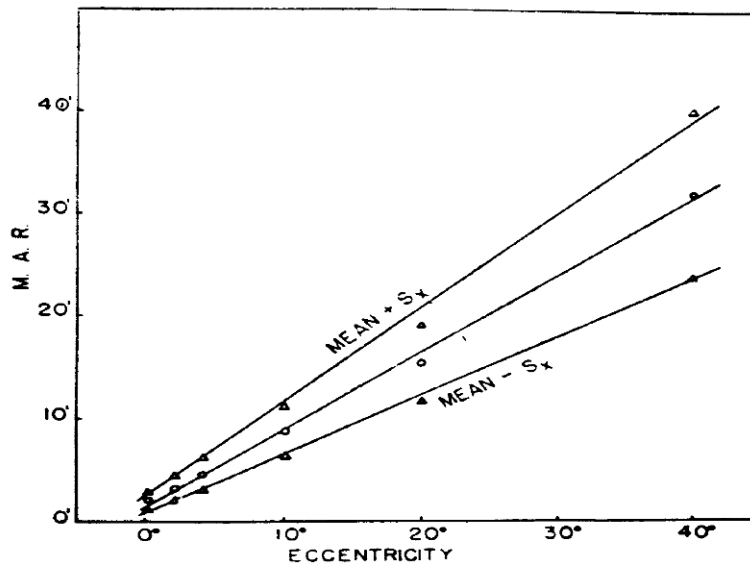


Fig. 2 (Weymouth). Mean minimal angle of resolution and points, one standard deviation above and one standard deviation below, as functions of retinal eccentricity. Data from 20 observers, one eye only.

Figure 3.5 Mean minimal angle of resolution, one standard deviation above and one standard deviation below, as functions of retinal eccentricity. Data from 20 observers, one eye only, Weymouth (1958).

3.2.3 Cortical Magnification Factor

A possible explanation for the trend of decreasing acuity with eccentricity suggests that there is cortical magnification, which increases from the periphery to the central fovea (Palomares et al., 2011).

Numerous studies have been made concerning cortical magnification. For instance, Daniel & Whitteridge (1961) examined retinal topography and related it to visual acuity to find a monotonic decrease with eccentricity, which was ambiguous as to whether a straight - line trend should occur. They used the data of Weymouth (1958) to compute the variation in MAR with eccentricity. Daniel & Whitteridge (1961) found that the decrease in cortical magnification factor from the foveal to the peripheral projection area in the rhesus monkey was very similar to the fall in visual

acuity in man from the fovea to the periphery. Recording electrodes were used on dissected monkeys and baboons to detect the effect of a stimulus in different parts of the visual field. Their findings suggested that the visual field was mapped out on the cortex. They concluded that cortical magnification was responsible for the increased foveal representation at the calcarine cortex.

3.2.4 Experiments with Landolt Rings

Weymouth's study (1958) with Landolt rings suggested a linear decrease in acuity with eccentricity existed. However, subsequent research with Landolt rings has produced variable results. The variation in results may have occurred due to normal experimental variation or due to other factors being involved in influencing the decline of acuity with eccentricity.

Millodot (1966) performed experiments on the variation of acuity with eccentricity using Landolt rings and compared his results to the cone density data of the human retina compiled by Le Grand (1956). This led to the suggestion that the curve of visual acuity was very similar to the cone density variation up to around 4° or 5°. However beyond this, visual acuity was found to drop more rapidly than cone separation.

Jacobs (1979) suggested that contours around the Landolt ring appeared to increase the Minimum Angle of Resolution. Jacobs (1979) suggested the cause of contour interaction was neural rather than retinal. At the very centre, Jacobs (1979) said contour interaction had less effect. His results did not produce a straight line relationship.

Virsu et al., (1987) performed tests using Landolt rings with a presentation time of 500 ms. It was suggested that there could be many reasons for cortical magnification scaling failures. They considered neural network differences, differences between M_r and M_c , (retinal magnification factor and cortical magnification factor), receptive field size rather than sampling density as a determinant of performance and the effects of undersampling. Their stimulus presentation times were 500 ms, which suggests that P cells rather than M cells were stimulated. Figure 3.6 illustrates their results.

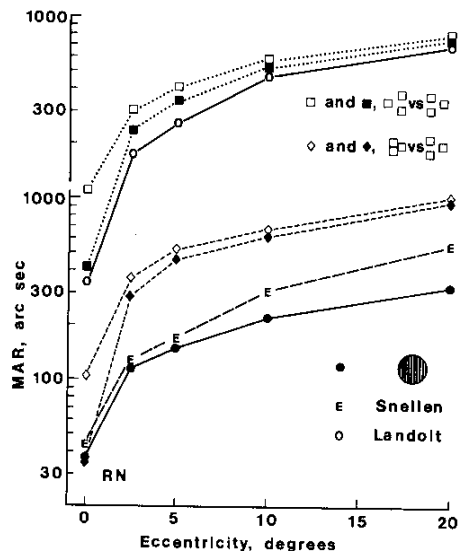


Figure 3.6 MAR as a function of eccentricity on the horizontal meridian in five visual acuity tasks: grating acuity (filled circles) Snellen (E 's) Landolt (O 's), dot direction (squares), dot separation (dots) Open symbols refer to measurement from the middle of dots in the dot tests. Filled symbols refer to measurements from the nearest edges of the dots, (Virsu et al., 1987).

Researchers have suggested that some optical factors may influence the variation in acuity with eccentricity which may involve features that are specific to the Landolt rings. Virsu et al., (1987) suggested that the gap in the Landolt ring became a line, which would increase acuity for Landolt rings, into vernier acuity type levels. Millodot (1966), on the other hand, suggested that oscillations were needed to allow the Landolt ring to be detected via stimulating different parts of the retina due to the oscillations' movements, and that the light flux from the ring may be unable to provide direct stimulation.

3.2.5 Cone and Ganglion Cell Density

Research on cone size has often supported the existence of decreasing acuity with eccentricity, but has not always suggested whether there should be a straight-line relationship or not. For instance, Song et al., (2011) used high resolution adaptive optics scanning laser ophthalmoscope (AOSLO) systems to image the retina. Cone photoreceptor packing density was found to be higher close to the fovea and decreased with increasing retinal eccentricity from 0.18 to 3.5 mm (around 0.6–12°).

Earlier, Young (1971) also found that cone size and cone spacing increased with eccentricity. Young (1971) examined the renewal of retinal rod and cone outer

segments using radio-autography in rhesus monkeys. Electron microscope pictures were taken which were examined by light microscopy. The concentration of cones dropped sharply in the parafovea, then declined gradually in the far periphery.

Young (1971) referred to previous researchers to point out that in man and the rhesus monkey, cone outer segments are long and thin in the fovea and increasingly shorter and thicker towards the periphery. He also pointed out that slight tapering of the outer segments of foveal cones has also been observed in the human retina.

The distribution of ganglion cells has also often been used to account for the decrease in acuity with eccentricity, to suggest this decrease may be linear or otherwise. However, this has been related more to areas outside the central 5 degrees surrounding fixation.

For instance, Weymouth (1958) suggested that the cone density near the centre, where there was an excavation of ganglion cells, and the ganglion cell density outside the area of excavation were the determinants of a straight – line relationship between acuity and eccentricity. Weymouth (1958) derived a graph using the data from Fick (1898) and Polyak (1941) to support the view that the cones near the fovea produced a straight-line relationship.

Similarly, Jennings & Charman (1981) used figure 3.7 below to suggest that ganglion cell interval has a better correlation with acuity, rather than cone or optical data. They mentioned that this relationship broke down at small eccentricities because of the ganglion - free nature of the fovea.

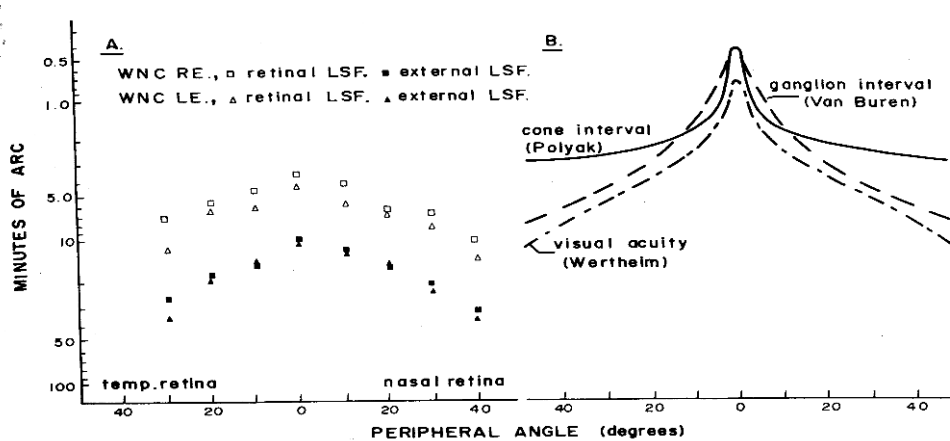


Fig. 10. A. The variation in the square root of the product of the vertical and horizontal halfwidths as a function of peripheral angle. The halfwidths are those occurring at the peripheral angle indicated, with the central best spherical refraction. Both retinal and external line-spread function halfwidths are shown. Subject WNC, right and left eyes, cycloplegia, 7.5 mm diameter pupil. B. The variation of cone separation and visual acuity with peripheral angle (after Harrison, 1953). The cone interval data are from Polyak (1941) and the visual acuity data from Wertheim (1894). Also shown is the variation in retinal ganglion cell interval with peripheral angle from Van Buren (1963).

Figure 3.7 A Retinal and External Line Spread Functions for Subject WNC B The variation of Cone Separation and Visual Acuity (in minutes of arc) with Peripheral Angle, and the variation in Retinal Ganglion cell interval with Peripheral Angle, (Jennings & Charman, 1981).

In figure 3.7B above the cone interval data comes from Polyak (1941), the visual acuity data from Wertheim (1894) and the ganglion cell interval data from Van Buren (1963). At small eccentricities, the visual acuity curve appears to follow the cone separation curve. However unlike Weymouth (1958), Jennings & Charman (1981) did not explicitly suggest that there should be a straight line relationship.

Rolls & Cowey (1970) also acknowledged that the ganglion cell density – cortical magnification relationship would break down near the fovea due to the foveal excavation of ganglion cells, as noted by Jennings & Charman (1981). Unlike Weymouth (1958), Rolls & Cowey (1970), and Jennings & Charman (1981) did not suggest there should be a straight – line relationship between acuity, ganglion cell density and eccentricity.

3.2.6 Ganglion cell Receptive Field Density

Drasdo (1977) examined data on ganglion cell receptive field density, D_r , (in receptive fields per solid degree) to see if it could be used to relate to M at every point in the receptive field.

Drasdo (1977) believed M^2 to be proportional to D_r so that the receptive field curve could be used to estimate M at any peripheral angle θ . He further evaluated this relationship by correlating the $1 / \sqrt{D_r}$ values with $1/M$ derived from studies of cortical phosphenes, visual acuity and migraine scotomata. This led Drasdo (1977) to conclude that $1 / M$ is almost exactly proportional to $1 / \sqrt{D_r}$. Drasdo (1977) suggested that the linear relationship, $V = k (1 + 0.59\theta)$, gave a useful approximation when θ is less than 30° , where V is the spatial threshold, ganglion cell sampling interval, or M^{-1} at any eccentricity or peripheral angle θ° ; k is the foveal value of V .

Receptive field density was also studied by Rovamo & Virsu (1979), who measured the contrast sensitivity function at 25 locations in the visual field by determining the contrast required for determining the direction of movement or orientation of sinusoidal gratings, or for detecting them in central and peripheral vision. Rovamo & Virsu (1979) compared published data on the density D of the receptive fields of retinal ganglion cells and the cortical magnification factor M , which lead them to suggest that M^2 is directly proportional to D in primates. Unlike Drasdo (1977), Rovamo & Virsu (1979) did not suggest that a straight line relationship may be a useful approximation at small eccentricities.

Drasdo (1991) & Weymouth (1958) both suggested that different tasks could lead to different intercepts and slopes in the straight line relationship. Similarly, Deeley & Drasdo (1987) also suggested that different acuity tasks may be affected differently by optical degradation to give different slopes or intercepts.

3.2.7 Ganglion Cell Receptive Field Size

Researchers have found an inverse relationship between receptive field size and eccentricity similar to the inverse relationships found by others, concerning receptive field density and eccentricity (e.g. Drasdo, 1977).

For instance, Smith et al., (2001) used functional resonance IMAGUBG (fMRI) to estimate the average receptive field size of neurons in each of several striate and extrastriate areas of the visual areas of the human cerebral cortex. Their fMRI results were qualitatively in accord with the findings from primate neurophysiology studies.

Smith et al., (2001), pointed out that linearity may break down in and near the fovea ($<5^\circ$), where receptive fields have been found to be bigger than that expected from a linear relationship, despite being at their smallest.

Virsu et al., (1987) excluded the possibility of the size of the receptive fields of the visual cells determining the decline of acuity with eccentricity in their results with Landolt rings. Their results suggested that if the size of the receptive fields of the visual cells had determined acuity, then less foveal magnification would have occurred. They discounted this from applying to their Landolt ring acuity versus eccentricity results, because their results produced greater foveal magnification.

Virsu et al., (1987), however, also commented that although an explanation based on field sizes rather than receptive field density had been excluded, as an explanation for their M scaling failures, it was possible that the two aspects of sampling were so closely matched, so that no distinction between them as causative factors could be easily made.

3.2.8 Stimulus Presentation Time

Stimulus presentation time has been suggested to be a factor in determining acuity as a shorter stimulus presentation time may stimulate M cells rather than P cells, and through reducing the effect of the oscillations of the eye. Different studies have used different stimulus presentation times. This could provide an explanation for deviations from a straight line relationship, due to reasons such as different cells being stimulated. A longer stimulation time has been shown to increase acuity for Landolt rings under photopic conditions (Mandelbaum & Sloan, 1947). Mandelbaum & Sloan (1947) found that at the highest brightness Landolt ring central acuity increased from 0.75 to 1.13 when the exposure time was increased from 1/5 second to several seconds. In the paracentral areas the difference was less marked.

Drasdo, Thompson & Deeley (1990) performed psychophysical experiments with gratings to suggest that there are two gradients of neural sampling in peripheral vision. Their physiological model suggested that the threshold for a low contrast briefly presented grating would depend on M neurons. P neurons would be dominant

for a prolonged presentation at high contrast. Drasdo, Thompson & Deeley (1990) pointed out that previous psychophysical studies had suggested that the sustained channel has a low pass response and the transient channel responds maximally at 5 to 9 Hz (Kulikowski & Tolhurst, 1973) or 7 to 13 Hz (Anderson & Burr, 1985).

Drasdo, Thompson & Deeley (1990) generated static and 8 Hz counterphasing grating patterns with sinusoidal temporal and spatial luminance profiles on a video monitor, to separate out the M and P cell responses (figure 3.8).

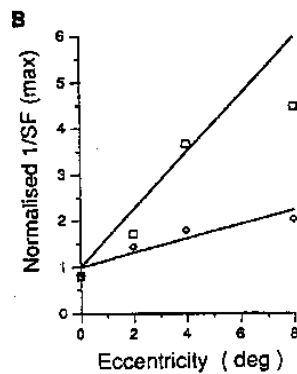


Figure 3.8 Plots of the spatial frequency $^{-1}$ for the CSF peak value, against eccentric visual angle for counterphasing and static stimuli Drasdo, Thompson & Deeley (1990).

In figure 3.8, the spatial frequency $^{-1}$ for the CSF peak value, against eccentric visual angle for counterphasing and static stimuli were normalized with respect to the foveal value. The results demonstrated that the transient system had a flatter gradient (diamonds), compared to the sustained system (squares). The points of figure 3.8 were suggested by Drasdo, Thompson & Deeley (1990) to represent a straight-line relationship. However, the points do not appear to fit the line that well, and there are not many data points, which suggests their assumption of a straight line relationship may not be entirely accurate. The straight lines appear to have been drawn using linear regression analysis.

It was found that the spatial dimensions for the P/sustained stimuli varied more markedly with eccentricity from the fovea than did those for the M/transient stimuli. The foveal resolution for the P stimulus was found to be 2.4 times greater than for the M stimulus. This was despite the effects of optical degradation. This was assumed to

reflect the local difference in sampling density for different sets of M and P neurons. This appeared to be most marked in the central field up to 5 degrees angular radius. This coincides with the area of excavation, where the different types of ganglion cell are displaced laterally, making it difficult to evaluate their various densities

Baseler & Sutter (1997) also examined the P and M cells, by using VEPs (visual evoked potentials) to favour contributions from either P or M pathways. Their findings suggested that the ratio of P to M contributions decreased with eccentricity out to 7.8 degrees. Like Drasdo, Thompson & Deeley (1990), they concluded that the P pathway was more active or numerous in the fovea, and decreased steeply with eccentricity relative to the M pathway.

3.2.9 Neural Factors

Neural factors have been put forward by researchers to explain the decline of acuity with eccentricity. Such research did not always suggest whether there should be a straight – line trend. Virsu et al., (1987) found increased foveal magnification and one of the reasons for this was put forward as being due to differences in neural networks. Jacobs (1979) suggested contour interaction reduced Landolt ring acuity, and proposed that neural factors may also be involved.

Cortical tissue and its links to ganglion cells has also been studied, resulting in more reasons being suggested for why acuity may fall with eccentricity. Azzopardi & Cowey (1993) examined the additional neural circuitry allocated to ganglion cells. It was found that more cortical volume was allocated to the central ganglion cells, suggesting that a declining trend would occur for acuity with eccentricity. They used a retrograde transneural tracer from the cortex to the retina to relate cortical tissue directly to the number of ganglion cells projecting to marked areas of the striate cortex. They reported that the ganglion cells near the fovea were allocated 3.3 to 5.9 times more cortical tissue than more peripheral ones. They concluded that the cortical representation of the central retina was much greater than expected from the density of the ganglion cells. They suggested that the expansion of foveal representation might accommodate the additional neural circuitry required for the additional visual processing needed in the central visual field.

An example of possible neural changes may be provided by Virsu et al., (1987), who pointed out that the most often suggested reason for the failure of M scaling was that the neural networks are qualitatively different in foveal and peripheral projections. A scaling failure is then bound to occur due to the nature of the connections between cells. In their tests, grating acuity and Snellen acuity behaved quite similarly, whereas the Landolt and dot tests gave lower acuity values in the periphery. They suggested that the features in question required some kind of relational and cortical processing, as the failures occurred in tasks requiring binocular interactions and the analysis of spatial relationships.

Grüsser (1995) drew the fortification scintillations of his migraine phosphenes, within the visual field. Controlled perimetric drawings were performed every 1-2 minutes during the aura state. Grüsser (1995) suggested that the number of striate cells available to process a region of unit size decreases with eccentricity. This caused the size of the migraine aura to increase with eccentricity, when the migraine spread along the visual cortex. This suggestion seems to be similar to the view put forward by Azzopardi & Cowey (1993). However, Grüsser (1995) used regression analysis to find a straight-line relationship between acuity and eccentricity, unlike Azzopardi & Cowey (1993) whose research was more aimed at finding the relationship between cortical tissue and ganglion cells. Like Weymouth (1958) and Drasdo (1977), Grüsser (1995) also suggested that there was a straight – line relationship between acuity and eccentricity.

Hirsch & Curcio (1989) suggested that cone density could not explain the reduced acuity at the fovea. This is in contrast to the research by Jennings & Charman (1981), mentioned earlier, whose graphs suggested that at small separations, cone separation may determine visual acuity.

Hirsch & Curcio (1989) examined the retina of a 35-year-old male corneal transplant donor. Photomicrographs were taken of the retina. Human cone centre to centre spacings were measured to determine whether foveal and near-foveal acuity were predicted by retinal sampling grain. It was found that cone cross-sectional area increased and cone density decreased with eccentricity. The resolution of the retinal sampling grain was compared with actual human acuity data and plotted on a graph

from tasks using Snellen Letters (Ludvigh, 1941), Landolt C (Sloan, 1968) and gratings (Weiskrantz & Cowey, 1963; Westheimer, 1982).

Hirsch & Curcio (1989) suggested that the visual acuity tasks performed achieved results at or near the Nyquist limit at 1 and 2 degrees retinal eccentricity. The Nyquist frequency was derived from the sampling theorem from Helmholtz. Helmholtz, (1911) reasoned that the resolution of gratings, consisting of light and dark bars, required that at least one row of un-stimulated cones associated with the dark bars lies between at least two rows of stimulated cones associated with the light bars. At 0 and 0.2 degrees, Hirsch & Curcio (1989) found that all the visual tasks performed below the anatomical Nyquist frequencies. This led them to conclude that at the foveal centre, the sampling theorem applied to cone spacing tended to overestimate the measured resolving power. They suggested that either foveal, optical or neural processing beyond the sampling stage, may be the other factors that had led to a loss in spatial resolution.

3.2.9 Optical Factors

Studies concerning the variation of aberrations with eccentricity have concentrated on eccentricities outside the central five degrees either side of fixation. Aberrations have been found to increase away from the centre of the visual field and to be dominated by defocus and astigmatism (Mathur et al., 2009, Atchison & Scott, 2002). Atchison & Scott (2002) used a Hartmann–Shack wavefront sensor with five subjects to measure wave aberrations in 5° steps out to ±40° in the horizontal visual field. They noted higher

amounts of third-order root-mean-square (RMS) aberrations in the nasal visual field than in the temporal field but little change of fourth-, fifth-, and sixth-order RMS aberrations. Atchison (2006) found linear rates of change in horizontal coma and quadratic changes in spherical aberration and secondary astigmatism along the horizontal visual field. Mathur et al., (2008) measured aberrations across the central 42° x 32° of the visual field in 5 emmetropes. Oblique and with/against the rule astigmatism was found to have increased quadratically from the centre to the periphery of the visual field along the 45°– 225° meridian and 0°–180° meridian, respectively, and decreased along the meridians perpendicular to these. Vertical coma

was found to have increased at a linear rate from the superior to the inferior visual field and horizontal coma increased at a linear rate from the nasal to the temporal visual field. Spherical aberration, higher-order RMS, and total RMS (excluding defocus) aberrations did not show any trend across the visual field.

Many of the recent studies have been initiated by research into the causes of myopia. For instance Jaeken & Artal (2012), observed a significant tendency to have relative hyperopia in the periphery of the myopic eyes. In a study of 202 eyes on 101 subjects, the relative peripheral refraction (RPR) was found to be significantly different between the emmetropic and myopic eyes from 15°–40° in the temporal retina and from 20°–40° in the nasal retina.

In earlier research, Virsu & Rovamo (1979) suggested that the attenuation of contrast could lead to a decrease in foveal acuity. They measured the minimum contrast required for discriminating the direction of movement or orientation of sinusoidal gratings or for detecting them in central and peripheral vision. Virsu & Rovamo (1979) suggested that at the highest spatial frequencies, contrast sensitivity functions could not be scaled adequately due to the attenuation of contrast in the retinal images. In the fovea and near fovea, high cortical spatial frequencies corresponded to high retinal spatial frequencies and these retinal images were considerably attenuated in contrast already. Therefore Virsu & Rovamo (1979) suggested that cortical resolution and high – frequency sensitivity must remain much lower in foveal rather than peripheral representations in spite of the deterioration of optical quality as a function of eccentricity, when the eye's optics transmits the retinal images. The optical degradation affected high frequencies the most.

Jennings & Charman (1981) however thought there was constant image quality, in the central 20-30°, which led them to suggest that aberrations could not explain the decrease in visual acuity with eccentricity. Jennings & Charman (1981) examined monochromatic aberrations in the central area. They used a "double-pass" photo-electric method to measure the vertical and horizontal external line-spread functions of the human eye. The central 80° of the horizontal meridian of both eyes of one subject was measured. Comparison of the shapes of the acuity curve using data from

Wertheim (1894) showed that acuity deteriorated very quickly with eccentricity whereas the optical quality remained relatively constant over the central 20-30°. This made them conclude that the variation in visual acuity with peripheral angle was attributable to neural rather than optical factors. Jennings & Charman (1981) suggested that visual acuity was instead, limited by the *neurological organisation of the visual pathway* from the retina to the cortex.

Millodot et al., (1975) similarly looked at oblique astigmatism and concluded that this type of aberration alone could not explain the decline of acuity with eccentricity either. Landolt rings were used by Millodot et al., (1975) at eccentricities of 20, 40 and 60 degrees, under photopic (245 cd/m²) and low luminance (2.45 cd/m²) conditions, with and without correction of peripheral refractive error. The peripheral correction used was principally due to oblique astigmatism. Their data also suggested that the poor quality of the peripheral dioptics could not account for the degradation of acuity in the peripheral visual field.

It should be noted however that the studies of Jennings & Charman (1981) and Millodot, et al., (1975) covered eccentricities that were rather wider than the foveal / near foveal eccentricities considered by Virsu & Rovamo (1979).

3.2.11 Multiple Factors

Many researchers have suggested that there is more than one spatial factor influencing acuity tasks and eccentricity, such as a combination of cone or ganglion cell density, cortical magnification, neural and optical factors.

For instance, Poirier & Gurnsey (2005) suggested that gradients of eccentricity dependent losses may differ and that there are many different sources of eccentricity dependent resolution loss. As one moves from the fovea to the periphery, there are fewer cortical V1 cells per retinal ganglion cell (Azzopardi & Cowey, 1993). There is also less overlap of cortical receptive fields (Dow al.,1981); Hubel & Wiesel (1974), and there is a decrease of parvocellular to magnocellular contributions to visually evoked potentials (Baseler & Sutter, 1997). Poirier & Gurnsey (2005) suggested these factors may work in combination to give different gradients of eccentricity losses.

Banks et al., (1991) also suggested that multiple factors were involved in producing a monotonic trend of decreasing acuity with eccentricity. Banks et al., (1991) measured acuities at eccentricities of 0, 2.5, 5 and 10 degrees. Grating acuity was measured with square-wave gratings covering a square area of side length equal to 6 cycles. Vernier acuity fell off about twice as much as grating acuity over the eccentricities tested.

Banks et al., (1991) pointed out that optical, receptor and other retinal properties vary in many ways across the retina. They pointed out that the OTF of the eye slowly becomes poorer with increasing eccentricity; cone density declines more rapidly and nearly linearly; outer segment length decreases precipitously in the central 2 degrees and slowly thereafter; and the convergence of cones onto retinal ganglion cells increases slowly and steadily across the whole retina. They suggested that these factors were bound to influence performance in spatial visual tasks probably in different ways in different tasks.

3.2.12 Equations describing the variation of acuity with eccentricity.

Researchers have often produced equations to relate acuity and eccentricity. For instance, Strasburger et al., (2011) used the equation:

$$S = S_0 \cdot (1 + E / E_2) \quad (3)$$

where S is the stimulus size at eccentricity E , S_0 is the threshold size at $E = 0$, i.e., in the centre of the fovea, and E_2 is a constant related to the slope b of the function, which is given by

$$b = S_0 / E_2: \quad (4)$$

The parameter E_2 can be used as a single summary descriptor providing a quick way of comparing the eccentricity dependencies across visual tasks. It corresponds to the eccentricity at which S is twice the foveal value.

It has been suggested that to equalize performance across the visual field, scaling along non-spatial stimulus dimensions, in particular pattern contrast, is required along with size scaling (Melmoth & Rovamo, 2003; Strasburger et al., 1994). Results of recent fMRI studies support this spatial-scale model for which Strasburger et al.,

(2011) have summarized empirical values and derived a logarithmic retinocortical mapping function which matches the inverse linear law.

3.2.13 Mesopic Levels

Research into the variation of acuity under mesopic conditions has mainly consisted of measurements of acuity versus eccentricity under lower light levels, to cover a range of levels from photopic to mesopic to scotopic light levels. Different results have been obtained under mesopic or scotopic conditions, compared to photopic conditions. The decrease in acuity with eccentricity is generally thought to follow the rod distribution more closely, as scotopic light levels are reached, since the cones become less active under lower light conditions. The scotopic region, within which only rods operate, starts at absolute rod threshold and ends at cone threshold. The photopic region, within which only cones operate, begins at rod saturation and extends to the highest illumination levels. Finally, between cone threshold and rod saturation lies the mesopic region, within which both rods and cones operate (Stockman & Sharpe, 2006). Mesopic light levels range from luminances of approximately 0.001 to 3 cd/m².

Virsu & Rovamo (1979) examined contrast sensitivity via gratings and concluded that cortical magnification factor was mainly applicable only to photopic conditions. Virsu & Rovamo (1979) used control experiments to decrease the average retinal illuminance to scotopic levels. Completely different results were obtained. Foveal thresholds decreased dramatically. This change in results led them to suggest that their results were valid for photopic levels of average retinal illuminance, but not to mesopic or scotopic vision.

The decreased rod distribution near the centre can be seen in the following graph:

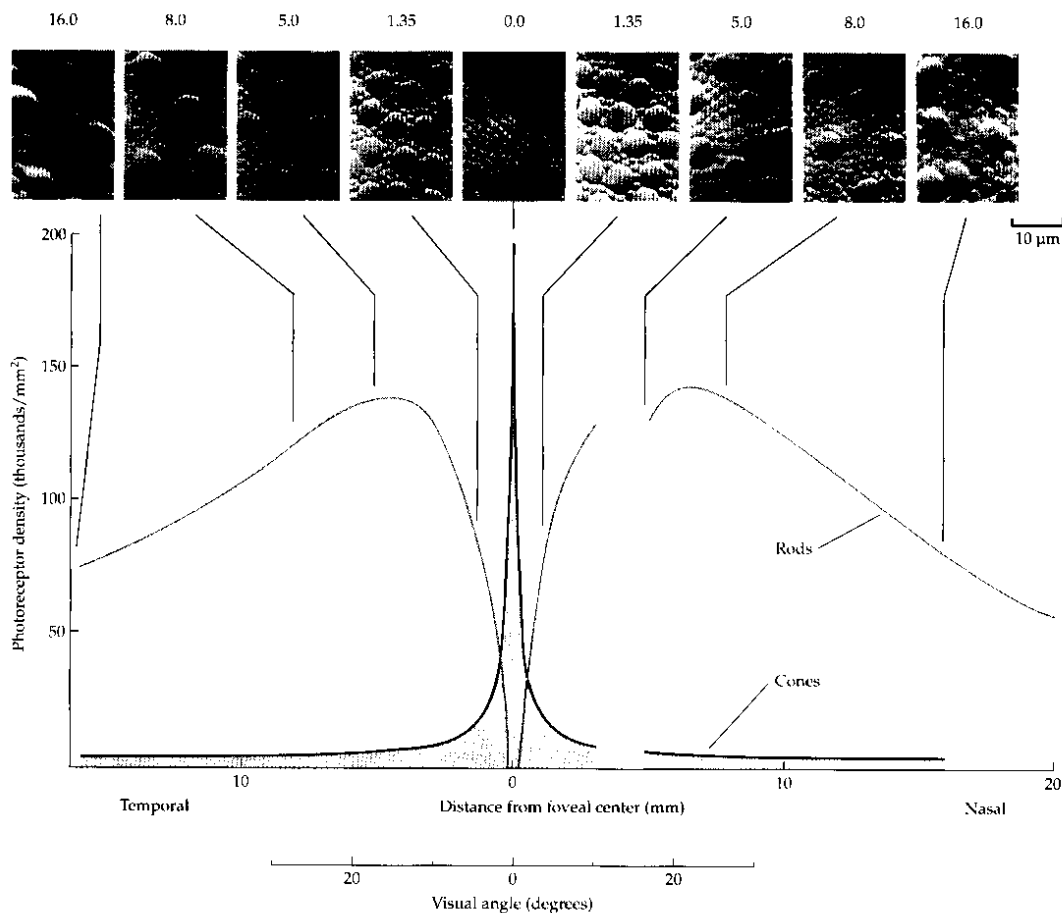


Figure 3.9 Photoreceptor Densities as Functions of Eccentricity along the Horizontal Meridian (Oyster, 1999).

In figure 3.9 above, the photomicrographs are optical sections through the photoreceptor inner segments. They show photoreceptors at different distances from the centre of the fovea (0.0). The distances are given in millimetres above each photograph, and their locations are correlated with the rod density curve below. Except for the central panel (0.0), which contains only cones, the larger cells are cones and the smaller ones are rods. The break on the nasal side of the graph marks the location of the optic nerve head. Consequently, the decrease in acuity with eccentricity is generally found to have greatly elevated central thresholds under lower mesopic and scotopic light conditions, as the cones progressively lose their sensitivity, whilst the rods become more sensitive. Under mesopic conditions there would be a mixture of rod and cone stimulation.

It should also be noted however that recent research has suggested that the sensitivity of the retina at a given mesopic adaptation level is not only the result of the size and

density of rods and cones in the area concerned, but also depends on the interaction between them (Matesanz et al., 2011). This consists of a change in cone sensitivity caused by dark-adapted rods (Zeile et al., 2008).

Similarly, Weymouth (1958) drew the following graph from the data of Fick (1898), relating Minimum Angle of Resolution to eccentricity for photopic and scotopic vision:

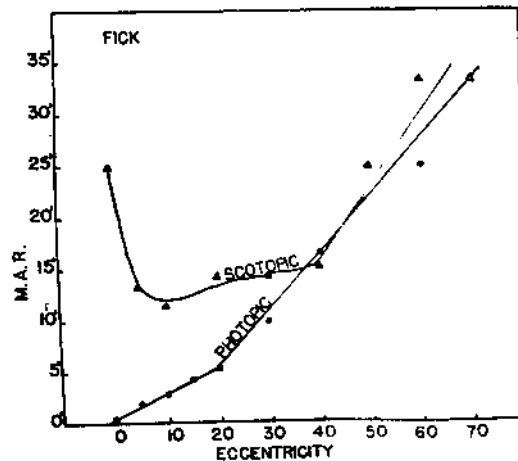


Figure 3.10 Minimal angle of resolution of the light and dark adapted eye as functions of retinal eccentricity. Data from Fick (1898), (Weymouth, 1958).

It can be clearly seen in figure 3.10 that the scotopic acuity levels are elevated. The mesopic levels would probably lie somewhere in between the photopic and scotopic levels.

Mandelbaum & Sloan (1947) measured central and peripheral Landolt ring visual acuity under a range of illumination from the photopic level at 9 log microlamberts to the scotopic level at 4.3 log microlamberts. The minimum visual angle at which 75 per cent of the presentations were properly identified determined visual acuity. Measurements at 17 brightness levels were taken on one subject from the fovea to 30 degrees. The Landolt rings were flashed on a screen for exposures of 1/5 a second, for the parafoveal measurement, to ensure the subject did not move his fixation while making an observation. Exposure time was not limited for the central measurement, because the researchers thought this was the best way to get an accurate central measurement.

Central acuity decreased more rapidly than peripheral acuity with diminution in light intensity. At intensity levels, below 6.3 log microlamberts, paracentral acuity exceeded foveal acuity (figure 3.11).

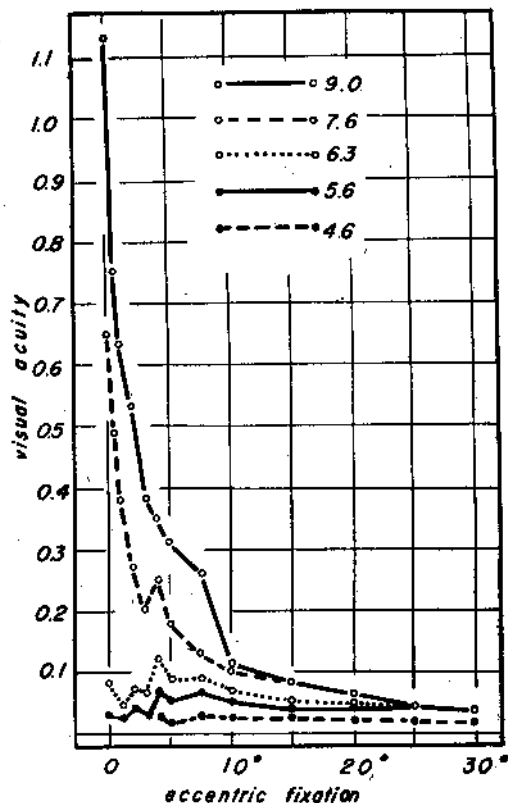


Figure 3.11 Visual acuity using Landolt rings along the horizontal meridian of the temporal retina at five different intensity levels ranging from 4.9 to 9.0 log microlamberts, Mandelbaum & Sloan (1947).

Similarly, Sloan (1968) experimented with Landolt rings with a 2 second presentation time at different background levels. Sloan (1968) used single Landolt ring targets with openings in the up, down, right and left positions. Each target was mounted at the centre of a white plastic square. A similar white square concealed the test objects between exposures. The cover was moved aside by hand to expose the target for intervals of about two seconds. The acuity at each level of illumination was determined at which the minimum visual angle at which 6 of 8 presentations of the Landolt ring were correctly identified as to the location of the opening. Acuties were measured over a range of background luminances from about +3 to -2 log mL. Sloan

(1968) found that at high luminances foveal acuity was much higher than the nearby paracentral retinal region. With decreasing luminance the superiority of the fovea decreased, and at $-2 \log \text{mL}$, the paracentral acuity exceeded that of the fovea (Figure 3.12). A weakness of Sloan's (1968) study was that only two subjects were used.

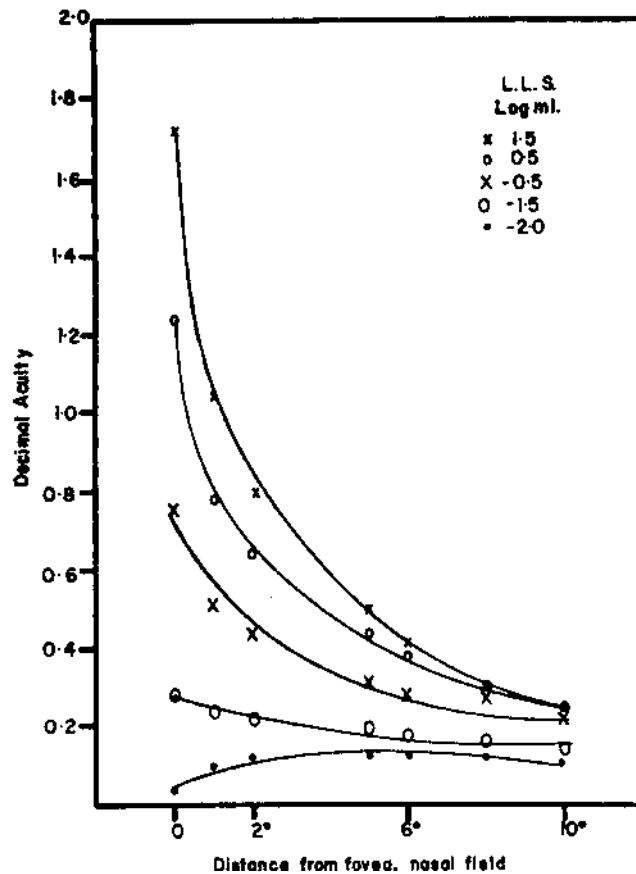


Figure 3.12 Change of acuity with retinal location for different background luminances, Subject L.S. (Sloan,1968).

Chapter Four

4. Initial Investigations of Parameters affecting the CAA Test

4.1 The CAA Test

The Contrast Acuity Assessment (CAA) test has been developed to assess functional visual performance under both daytime and low levels of ambient illumination (Chisholm et al. 2003). It was designed to assess orientation discrimination based on contrast acuity over a field of $\pm 5^\circ$, corresponding to the functional visual field.

The CAA test employed a Landolt ring stimulus.

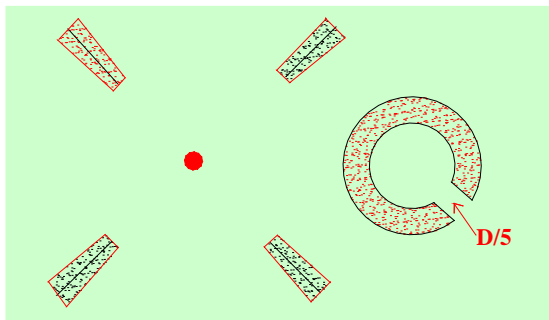


Figure 4.1 CAA Test Fixation spot and Fixation flankers, and Landolt Ring (with gap of diameter/5 (D/5)).

The single Landolt ring stimulus had an orientation of 45° to the vertical and a gap size that comprised of 20° of the ring. Contrast was defined as $\delta L/L_b$ where δL was the difference in luminance between the target and background and L_b denoted background luminance (grey in colour). This is equivalent to the Michelson contrast corresponding to periodic stimuli but is suitable for specifying higher target contrasts when dealing with positive increments and periodic stimuli, as were used in this study.

Michelson contrast is commonly used for patterns where both bright and dark features are equivalent and take up similar fractions of the area. Michelson contrast is defined as:

$$(L(\text{target})-L(\text{background})) / (L(\text{target})+L(\text{background})) \quad (4.1)$$

The denominator represents twice the average of the luminance, with $L(\text{target})$ and $L(\text{background})$ representing the target and background luminance.

4.2 CAA Test Apparatus - Equipment and Set-up

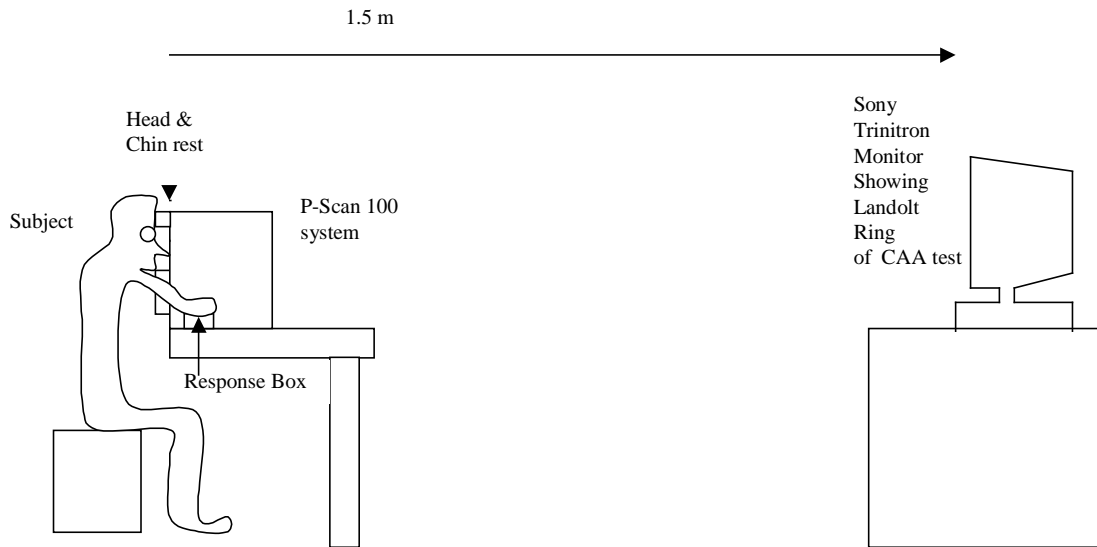


Figure 4.2 CAA Test Apparatus Setup

Figure 4.2 shows the CAA test apparatus setup. The subject was required to view a computer screen 1.5 m away which displayed a briefly presented Landolt ring stimulus in one of four positions. The subject was required to press a button on a response box to indicate in which position the gap of the Landolt ring was seen.

The stimulus was presented randomly at the following eccentricities in the visual field: -5° , -2.5° , -1.25° , 0° , $+1.25^\circ$, $+2.5^\circ$, $+5^\circ$ along the horizontal meridian. Four oblique guides surrounded the fixation target to aid central fixation. The stimulus duration was 120 ms to ensure that the stimulus would not trigger a saccadic eye movement that could precede the onset of the stimulus (Barbur et al., 1988). The screen was viewed from a distance of 150 cm in order to ensure that the resolution of the screen did not affect the definition of the smallest target generated. In each of the experiments, the target was presented at the seven different stimulus locations in a random order. A four-alternative, forced-choice procedure was used to determine the

threshold for the variable in question, (i.e. upper left, upper right, lower left, lower right). The subject was required to press one of four response buttons to indicate the position of the gap in the ring.

The contrast acuity thresholds were measured using a staircase procedure driven by the subject's responses. An adaptive staircase method was used in which the size of the stimulus was increased following a 'no' or incorrect response, but a decrease in size required the target to be seen or identified correctly on two consecutive occasions (1-up, 2-down). The up and down steps were of equal size. Such a strategy gives a performance at threshold of 70.7% correct (Lee et al., 1997). If the gap could not be resolved, a guess was made and a button pressed, with a single incorrect guess resulting in an increase in target size.

Under photopic conditions, the monochromatic Landolt ring had a 24% contrast, with a 12 cd/m^2 background luminance. Under mesopic conditions the monochromatic Landolt ring had a 48% contrast, with a 0.05 cd/m^2 background luminance.

The CAA Test apparatus was previously developed to test the visual performance of pilots (Chisholm, 2003). The City University CAA, Scatter (Chapter 7), and Contrast Sensitivity tests were run on the P-SCAN 100 system (Barbur et al., 1987; Alexandridis et al., 1991). This allows presentation of either positive or negative contrast stimuli on a 21" high resolution Sony Trinitron monitor (model 500PS, 1280 x 1024 pixels, 60Hz, maximum luminance of 100 cd/m^2), driven by an ELSA Gloria XL 10 bit graphics card. The LUMCAL program developed by Barbur and colleagues was used in conjunction with a LMT 1000 luminance meter to calibrate the luminance characteristics of the monitor every month throughout the study. This involved determining the luminance versus applied voltage relationship for each gun. The spectral output of each phosphor was measured using a Gamma Scientific Telespectoradiometer (model 2030-31) and this provided the chromaticity coordinates of each phosphor. The monitor was allowed to warm up for a minimum of 20 minutes before use on each occasion to allow the luminance output to stabilise.

All tests were completed in a darkened room where the only light came from a current-regulated halogen spotlight (11.5 Volts) directed towards a white diffuser on the ceiling above the visual display. This arrangement contributed negligible light to the actual display but prevented dark adaptation. The surrounding walls were painted matt black and all other surfaces visible to the subject were coated with a non-reflecting black felt material. This included the inside of the housing for the patient, consisting of a head and chin rest of adjustable height positioned behind the infrared transmitting mirror of the P-SCAN 100 system. This dichroic mirror was set at 45° to the line of sight and transmitted 95% of visible light while reflecting infrared light. The calibration was always undertaken through the mirror to simulate the normal viewing condition. The two infrared cameras were located below the line of sight as were the pulsed infrared sources. A matt black cloth was used to cover all but the lens of each camera during testing to eliminate their reflection in the mirror.

The subjects wore their own glasses or contact lenses where possible but if their current prescription was unsuitable, full aperture trial lenses were placed in a frame before the eye under test. All subjects underwent a subjective refraction to determine the appropriate refractive correction for the testing distance of 150 cm for the CAA test. Although small degrees of defocus have no significant effect on the measurement of the scatter function of the eye (Barbur, 1997), the appropriate correction was used throughout since defocus is known to significantly alter contrast thresholds, particularly for low contrast targets (Ho & Bilton, 1986; Lohmann et al., 1991). In all cases, the correcting lens was cleaned before use to ensure that it scattered as little light as possible. For subjects who had both eyes suitable for testing, only the dominant eye was examined. The dominant eye was determined by asking the subject to extend their arms. Then with both eyes open the subject aligned the index finger with a distant object. The subject observer then alternately closed the eyes to determine which eye was viewing the object with the least amount of shift in position. The eye which observed the least shift of position was the dominant eye. The other eye was occluded throughout the experimental procedure. If the subject was found to be equidominant, with neither eye producing a least shift in position when occluded, the eye with the least refractive error, or the same eye as the patient's favoured hand would have been used. However all subjects were found to produce

one eye as being dominant, when the alignment test was used. All subjects underwent a brief trial run for each experiment before the actual measurements were taken.

4.3 General Test Parameters

A background light level of 12 cd/m^2 was selected for photopic test measurements. This figure falls within the photopic range, but because it is much lower than the average daylight luminance, less pupil constriction occurs making the test more sensitive to aberrations and forward light scatter.

4.4 Mesopic Testing:

In preparation for mesopic testing, the subject was required to wear a light-proof patch over the selected eye while sitting in a darkened room for a minimum of 15 minutes to induce a state of adaptation appropriate for the mesopic background luminance employed. Mesopic light levels were achieved by viewing the display through a spectrally calibrated neutral density filter (nominal optical density of 2). The display was viewed through the P-Scan 100 chin rest set-up to ensure that only light that had passed through the filter could reach the subject's eye. The spectral absorption of the filter was taken into account to ensure that the luminance chromaticity specified remained unaffected by the non-uniform spectral transmittance of the filter.

The contrast acuity test required accurate and steady fixation throughout. The P-SCAN 100 system allowed fixation to be monitored, with verbal instruction if the subject's eye wandered.

Investigations were made to test for stimulus onset time and crowding effects, by altering the contrast of the guides and stimulus onset time (the time between the fixation target offset and the onset of the test target). In addition, contrast sensitivity effects with artificial pupils were examined as a test to parallel the artificial pupil tests performed with the artificial pupil CAA tests and scatter tests (see later), to determine whether the artificial pupil results could be linked to the contrast sensitivity results.

4.5 Previous CAA Test Results

The results from a previous study made at City University for a group of 62 normal subjects, who had completed gap discrimination tasks with size as the variable, under both photopic (24% contrast, 12 cd/m² background) and mesopic (48% contrast, 0.05 cd/m² background) conditions (Chisholm, 2003; Chisholm et al., 2003), were used as a starting point for our investigations. The same method and apparatus were also used to test new subjects.

The previous study's results revealed that acuity thresholds increased linearly with eccentricity at photopic light adaptation levels, except in the foveal region where the thresholds were higher than predicted on the basis of the linear relationship predicted by Drasdo (1977). Under mesopic light adaptation levels, visual inspection of the contrast acuities in the foveal region suggests that the trend of higher thresholds in the foveal region is even more pronounced, even for targets of 48% contrast (figure 4.2). An ANOVA test showed the photopic and mesopic mean Landolt ring gap acuities to be significantly different statistically ($P = 0$, at all eccentricities).

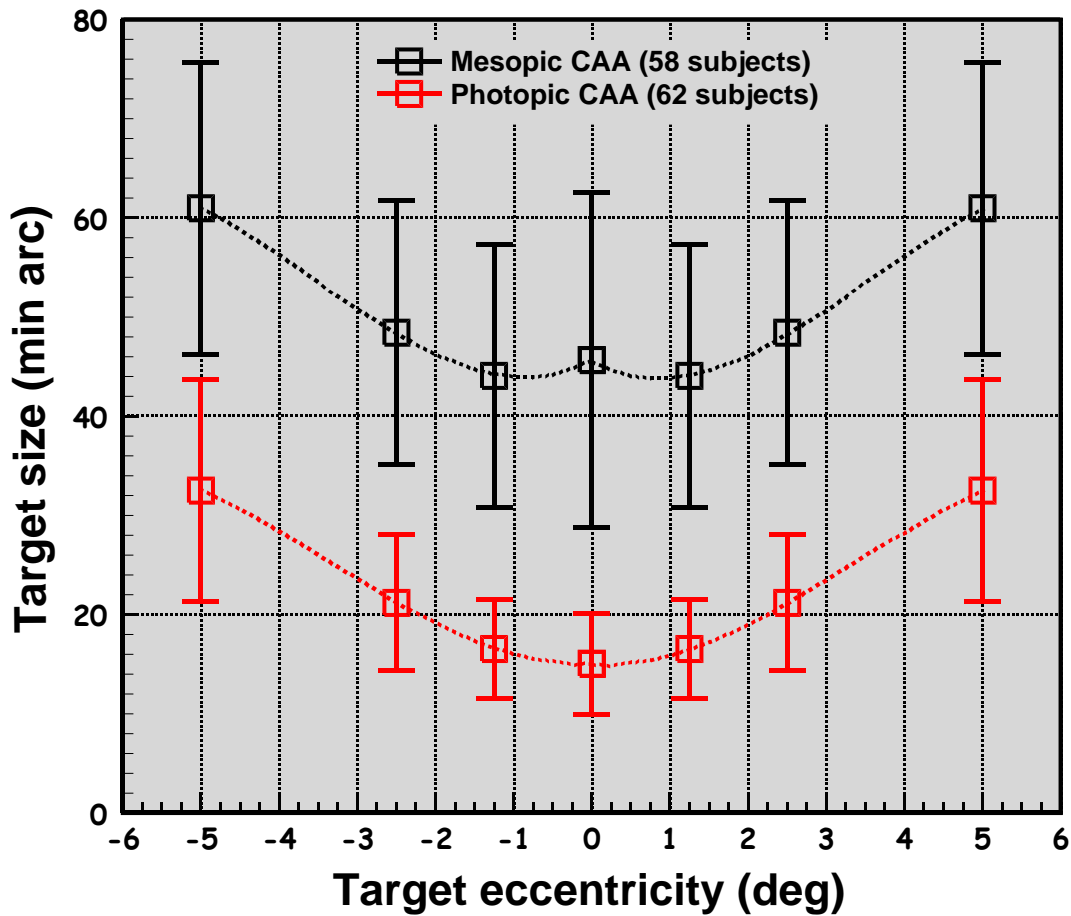


Figure 4.3 Averaged Photopic and Mesopic CAA test results. Target Size versus Eccentricity. The error bars represent 2 standard errors (Chisholm et al., 2003).

These elevated photopic and mesopic gap acuities were regarded as foveal dips. We defined the foveal dip as the difference between an extrapolated linear result compared to the actual increased threshold leading to a gap acuity that was not as great as the threshold that would result from a linear graph, at the centre of fixation.

In figure 4.3, the foveal dips are shown by the distances ab, under mesopic conditions and cd under photopic conditions.

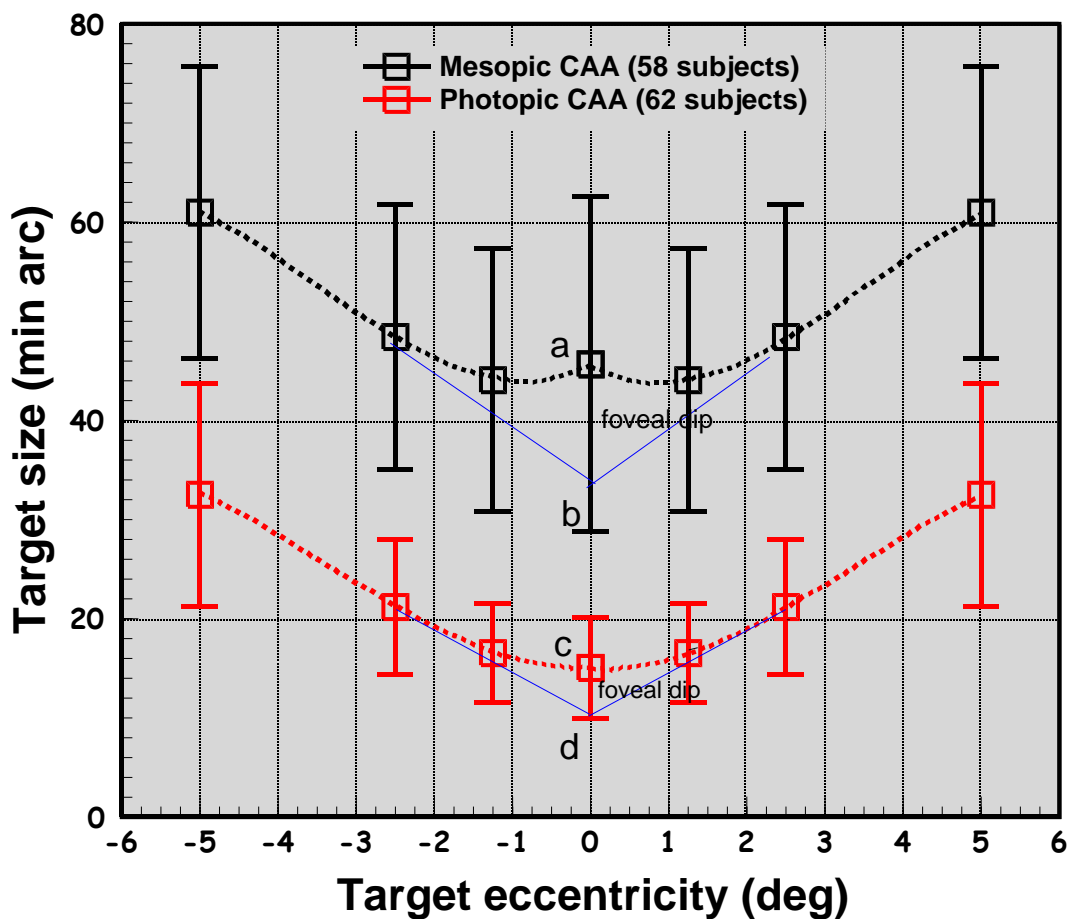


Figure 4.4 Illustration of Foveal Dips under photopic and mesopic conditions. Error bars are two standard errors.

The extrapolated straight line results were derived by extrapolating straight lines from the $\pm 2.5^\circ$ and $\pm 5^\circ$ eccentricities, to where they intercepted the zero fixation points. These gave slightly different values depending on which side (the negative side or the positive side) the extrapolation took place. These were averaged to determine the extrapolated values at the zero eccentricity central fixation points (points b and d in figure 4.3), from which the foveal dips were derived. The size of the foveal dip was found by subtracting the extrapolated straight line values from the central gap acuity values (distances a-b and c-d in figure 4.4).

Researchers such as Drasdo (1977), Weymouth (1958) and Grusser (1993) have suggested that the variation of acuity with eccentricity could be approximated by a straight line relationship. For this reason a straight line was extrapolated from the $\pm 5^\circ$ eccentricities to the $\pm 2.5^\circ$ eccentricities. These eccentricities rather than the $\pm 1.25^\circ$ eccentricities were chosen in order to reveal larger discrepancies between the theoretical straight line results and our actual CAA test results. These discrepancies

were denoted by us by the term ‘foveal dips’, and were made the subject of further investigations.

Under photopic conditions, the higher foveal threshold was initially thought to have been accounted for by the following explanations:

- 1) Ganglion cell sampling interval was not as high in the foveal region as predicted from the linear relationship.
- 2) The retinal image was degraded by increased scatter and aberrations in some subjects and this may have caused the observed increase in foveal acuity threshold.
- 3) Crowding and stimulus onset time effects induced by the preceding fixation spot for foveal measurements caused a reduction in sensitivity and hence the increased thresholds.

At mesopic light adaptation levels the CAA test results also showed the foveal region to give a significantly higher threshold, even for targets of 48% contrast.

To try to account for the much higher foveal thresholds under mesopic conditions, various hypotheses were considered:

- 1) The effective ganglion cell population changes in the mesopic range and this could have resulted in an even greater reduction in sampling density in the foveal region.
- 2) The involvement of rod receptors was significant at this light level and rod receptors are absent in the central foveal region. ((1) & (2) are closely related). The raised thresholds may be partly related to the greater absence of rods near fixation, and the rods may have played a greater role in the mesopic levels.
- 3) The larger pupil size in the mesopic range resulted in increased aberrations and scattered light.

4) Stimulus onset time and crowding effects played an even greater role in the mesopic range.

4.6 Patient selection and characteristics

All the subjects were unpaid volunteers, recruited from City University and Imperial College staff and students, or through social contacts.

The research followed the tenets of the Declaration of Helsinki and informed consent was obtained from all subjects prior to testing. This followed a detailed explanation of the nature of the study along with any possible consequences. Both the University and Departmental Research and Ethics Committees approved the study in advance.

A detailed history was taken for each potential subject to allow identification and exclusion of pregnant women and subjects with systemic disease such as diabetes, or medication that might influence visual function. A subjective refraction was undertaken to ensure that all subjects were fully corrected prior to testing and achieved a minimum visual acuity of 6/9. Ocular health was examined to exclude eyes with any pathology, including lens opacities classified using the LOCS III system (Chylack et al., 1993). Any lens opacities patients were excluded, meaning that the cut – off grade was 0.2 or higher under the LOCS III system. No potential subjects were rejected using this lens opacity criterion, possibly because the subjects were relatively young. The primary investigator, YCT, a researcher at City University, examined all subjects.

4.7. Initial Investigation 1 Contrast Sensitivity Effects and Artificial Pupils

4.7.1 Introduction

Kay & Morrison (1985) observed that under monochromatic light, in a perfectly diffraction-limited system, image contrast declined approximately linearly with spatial frequency until the cut-off frequency determined by dh (d is pupil diameter and h is wavelength) is reached (Westheimer, 1964). Kay & Morrison (1985) pointed out that

additional marked attenuation of contrast occurs, particularly in the range of intermediate spatial frequencies, due to the effects of geometrical aberrations. These aberration effects are reduced as pupil diameter decreases until an approximately diffraction-limited system is attained at pupil diameters of 2.0-3.0 mm (van Meeteren, 1974; Howland & Howland, 1977). Kay & Morrison (1985) conducted experiments to try to eliminate the effects of retinal illuminance by increasing screen luminance for a 3 mm artificial pupil size.

4.7.2 Hypothesis

We used artificial pupils to investigate the effects of aberrations on contrast sensitivity. Our intention was to investigate the effect of 6 mm and 3 mm artificial pupils on the CAA test. We decided to also examine the effects of 6 mm and 3 mm artificial pupils on contrast sensitivity, so that we could determine whether CAA changes could be due to contrast sensitivity changes or visual resolution changes.

4.7.3 Methods

Contrast Sensitivity was measured on eight dilated (phenylephrine 2.5% & tropicamide 1 %) subjects using 6 and 3 mm artificial pupils. The drops chosen for dilation were a powerful combination to ensure a strong dilation was achieved, which ensured the pupils achieved a pupil size in excess of the 6 mm artificial pupils. The City University Contrast Sensitivity Test (described below) was used. A test distance of 250 cm was used for the Contrast Sensitivity test.

4.7.4 The City University contrast sensitivity test apparatus:

The contrast sensitivity apparatus has been described before (Hennelly, 2000). A high resolution CRT display (1280 x 1024 pixels) was used to generate vertical sine wave grating stimuli. The test field subtended a visual angle of five degrees, at a viewing distance of 3 metres and had a surround luminance of 34 cd/m². The background illuminance was set at 12 cd/m² for the 6 mm artificial pupil. To compensate for decreased retinal illuminance for the 3 mm artificial pupil, the background illuminance was increased to 48 cd/m² (= 12 cd/m² x (6²/3²)). Pupil centration was

performed by visual inspection of the subject's eyes and the artificial pupil. The subjects were adapted for at least three minutes to the grey background. The subjects were then asked to fixate the central target test area (a yellow cross on the visual display unit), and instructed to press the YES button when any vertical lines were observed. As the measurement of contrast sensitivity may be influenced by the number of tests, each subject completed a training session, to reduce potential practice effects.

A random 'yes/no' staircase, with variable step size and stimulus presentation time of 250 ms, was used to obtain contrast threshold. Contrast threshold was measured at three spatial frequencies - 1.2, 6.1, and 19.1 cpd. . All measurements were taken monocularly. It was initially thought that the apparatus was designed to take six measurements of contrast sensitivity at each spatial frequency. However it later transpired that only one measurement was taken at each spatial frequency. Time constraints did not allow more readings to be taken.

The parameters used to conduct the CS test can be seen in table 4.1.

Staircases:	Coarse	Fine
No of reversals analysed:	6	6
Reversals ignored:	4	4
Start increment:	0.15	0.05
End increment:	0.04	0.01.

Table 4.1 - The parameters used to conduct the City University CS test. The first 4 reversals were ignored.

4.7.5 Subjects

Eight subjects were tested, aged 20 to 28. They consisted of volunteers from the City University optometry department and the Imperial College optics department. Their details are listed in Table 4.2. They had all had previous experience of

psychophysical testing through being City University staff or students. None of the subjects were contact lens wearers except for subject MY.

Subject	Age	Refractive Error	Pupil Size mm	Dominant Eye
AP	21	-0.50/-0.25 116	7.82	Right
SL	28	-0.75/-0.75 x 90	8.77	Right
AnP	20	-0.25/-0.25 x 10	7.83	Left
MS	21	plano / -0.25 x 172	7.83	Right
CO	21	plano	7.17	Right
JK	23	-0.50/-0.25 x 90	7.01	Right
MY	22	-2.50/-0.50 x 2 ½	8.07	Right
LDS	29	+2.75/-1.00 x 170	7.51	Right

Table 4.2 Subjects used for the artificial 6 mm, 3 mm Pupil Contrast Sensitivity Study.

4.7.6 Results

Most of the results showed a trend of decreasing contrast sensitivity with increased pupil size. Five of the eight subjects had improved contrast sensitivity at all three points tested. Three had contrast sensitivity improvements at two out of three points. One subject went against the trend and had decreased contrast sensitivity with a 3 mm pupil at two points and improved contrast sensitivity at one point.

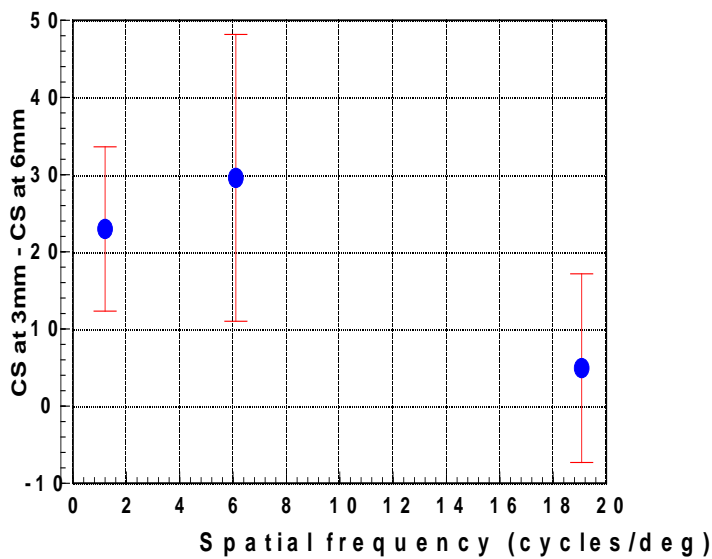


Figure 4.5 Contrast Sensitivity (CS) Differences for 8 subjects for 3 mm and 6 mm pupils. Error bars are 2 standard errors.

The overall results for the eight subjects are shown above in Figure 4.5. A trend of increased contrast sensitivity for the 3 mm pupils is shown.

							Differences		
	3mm pupil			6mm pupil			3mm - 6mm results		
	Spatial frequency			Spatial frequency			Spatial frequency		
Subject	1.2	6.1	19.1	1.2	6.1	19.1	1.2	6.1	19.1
AP	109.98	57.77	7.16	92.16	47.14	8.01	17.82	10.63	-0.85
SL	113.26	90.83	6.63	59.05	38.88	4.18	54.21	51.94	2.45
AnP	76.17	112.22	50.42	66.62	48.99	11.18	9.55	63.24	39.25
MS	66.76	46.72	50.88	48.60	28.58	36.05	18.16	18.14	14.83
CO	93.45	76.10	18.27	65.00	62.18	36.12	28.45	13.92	-17.85
JK	90.03	76.65	7.95	84.87	90.40	18.93	5.16	-13.75	-10.98
MY	110.42	93.11	40.12	88.86	50.84	34.24	21.57	42.26	5.88
LDS	76.13	68.85	11.20	47.36	18.57	4.59	28.77	50.28	6.62
Mean	92.02	77.78	24.08	69.06	48.20	19.16	22.96	29.58	4.92
S.D.	17.97	20.84	19.71	17.68	21.83	14.27	15.06	26.28	17.28

Table 4.3 Contrast Sensitivity for Each Subject.

Paired sample t tests for 3 mm minus 6 mm artificial pupil contrast sensitivities, for eight subjects with seven degrees of freedom were carried out. The paired sample t test for the mean 3 mm contrast sensitivity minus the mean 6 mm contrast sensitivity at each spatial frequency, showed statistically significant differences for the middle ($P = 0.015$) and lower spatial frequencies ($P = 0.004$) (1.2 and 6.1 cpd), but not for the

highest 19.1 cpd spatial frequency ($P = 0.447$),. The differences are shown in table 4.3.

The mean percentage change for the low 2.1 cpd result was +24.9%. The mean percentage change for the middle 6.1 cpd was +38.0 %. The mean percentage change for the high 19.1 cpd was +20.4%.

There was a large variation in results, due to only one reading of contrast sensitivity being taken at each spatial frequency and pupil size due to time constraints. Ideally six readings at each artificial pupil size and spatial frequency would have been taken. The mean spatial frequencies and standard deviations are shown in Table 4.3 and show the large S.D.s (standard deviations).

4.7.7 Discussion

Hernandez et al., (1996) examined the effect of different factors on the CSF, such as pupil size. The study was done with a natural pupil and with a 3 mm artificial pupil. The average luminance of the monitor was kept steady at 15 cd/m^2 at all times. Unlike our results, in the low frequency zone, the results with an artificial 3 mm pupil were lower, than those corresponding to the larger natural pupil, indicating decreased contrast sensitivity. Hernandez et al., (1996) attributed this to reduced retinal illumination. Similarly, to our results, in the high frequency zones, the results tended to be different compared to the low frequency results. Their two CSFs overlapped.

This may be contrasted to our results in which the larger 6 mm pupils produced lower contrast sensitivity results, probably due to spherical aberration. There was no statistically significant difference between the mean contrast sensitivities of the high cpd results. This is in line with the results of Cox & Holden (1990) who suggested that spherical aberration reduces image contrast rather than image resolution.

A notable difference between Hernandez et al., (1996) and our experiments was that we compensated for retinal illumination. This may explain the differences between

our results. Hernandez et al., (1996) also used square wave gratings, whilst we used sine wave gratings.

As in our contrast sensitivity experiments, Kay & Morrison (1987) measured contrast sensitivity to sinusoidally modulated grating patterns generated on a cathode ray tube (CRT). They examined four subjects. Artificial pupil diameters from 2 - 8 mm with and without homatropine eye drops were used. Kay & Morrison (1987) suggested that contrast sensitivities at low spatial frequencies had been found by others to be attenuated with a larger pupil diameter (Green & Campbell, 1965), and that spherical aberration provided a further complication.

In contrast to our experiments, Kay & Morrison (1987) studied pupil diameter effects in the absence of compensation for changes in retinal illumination, to reproduce natural viewing conditions. We instead chose to compensate for the effects of retinal illumination to try to determine the effects of increased aberrations on contrast sensitivity.

In the homatropinized eye, Kay & Morrison (1987) found that viewing with the 3 mm artificial pupil tended to improve contrast sensitivity, which is in line with our results. However, Kay & Morrison (1987) concluded that their results were not significant and suggested that changes in pupil diameter, without correction for the change in retinal illumination, had no significant effect on contrast sensitivity for their 3 mm and 6 mm pupil results.

Kay & Morrison (1987) suggested that cycloplegic drugs could in theory adversely affect contrast sensitivity measurements and that should the cycloplegic drug diffuse into the retina, neuronal activity may also be affected. Therefore, they took the precaution of repeating their experiments in a number of subjects without homatropine to check against such possible effects, and their results revealed no significant effects. This may suggest that our results may have been similarly unaffected by the use of phenylephrine and tropicamide, but we can not be absolutely sure of this.

4.7.8 Conclusion

A statistically significant difference between the mean contrast sensitivities for the 3 mm Contrast Sensitivity minus the 6 mm Contrast Sensitivity occurred for the low 2.1 cpd and middle 6.1 cpd spatial frequencies, but not for the high 19.1 cpd results. This may have been due to spherical aberration affecting contrast sensitivity at the low and middle spatial frequencies. Spherical aberration may therefore have less effect on visual acuity, due to its lesser effect at high spatial frequencies. This suggests spherical aberration may not have led to the foveal dip.

4.8 Investigations with the CAA Test Parameters:

4.8.1. Initial Investigation 2: High Contrast versus Low contrast CAA Tests:

4.8.2 Hypothesis:

We decided to examine whether there was an association between target contrast and foveal dip. The foveal dip of the CAA Test may also have occurred due to low contrast targets being used rather than high contrast targets. Therefore the effect of using high contrast rather than low contrast CAA test targets was investigated.

4.8.3 Methods:

CAA gap acuity was examined with 6 mm and 3 mm artificial pupils, for eccentricities of 0 and 2.5 degrees, to determine by how much the use of lower contrast targets (24% contrast) or higher contrast targets (125% contrast) may have affected the CAA test results. Compensation was made with the background illumination to make retinal illumination constant, as for the contrast sensitivity artificial pupil tests. Pupils were dilated with 1.0% tropicamide and 2.5 % phenylephrine, to keep the dilating drops the same as those used to measure aberrations using the Hartmann-Shack aberrometer at Imperial College.

4.8.4 Subjects

5 subjects, recruited from City University optometry students (aged 20 to 28) were examined.

Subject	Age	Refractive Error	Dominant Eye
AP	21	-0.50/-0.25 116	Right
SL	28	-0.75/-0.75 x 90	Right
AnP	20	-0.25/-0.25 x 10	Left
MS	21	Plano / -0.25 x 172	Right
CO	21	Plano	Right

Table 4.4 Subjects examined for the artificial 6 mm, 3 mm Pupil High & Low Contrast CAA Test Study.

The subjects' details are listed in Table 4.4. They had all had previous experience of psychophysical testing through being City University students. None of the subjects were contact lens wearers.

4.8.5 Results

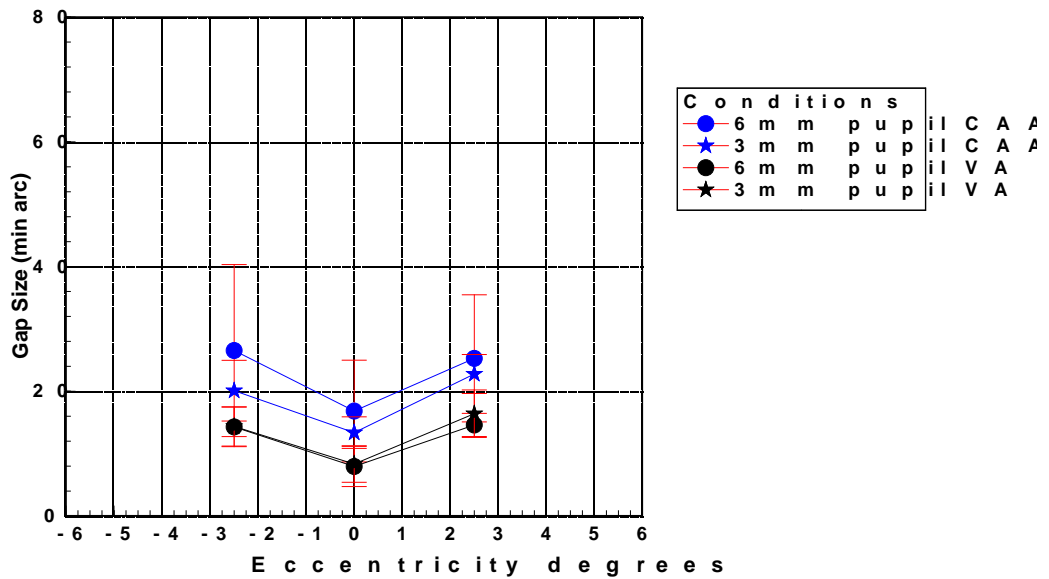


Figure 4.6: Photopic Gap Acuity results at high and low contrast for 5 subjects. Error bars are 2 standard errors. VA was used in the legend as the high 125% contrast test becomes similar to the high contrast VA tests used in clinical practice.

Figure 4.6 shows photopic gap acuity results at high and low contrast for 5 subjects. Higher acuity is shown for the higher contrast targets, together with smaller changes due to pupil size differences. This suggests aberrations and scatter due to increased pupil size may affect the CAA test due to its low 24% contrast levels. The pupil size performance changes at high contrast are very small, causing the points to coincide. Better performance with high contrast targets are also revealed by the individual graphs in Appendix One.

The better performance with the high contrast targets could suggest that the low contrast of the CAA test might be a factor in producing the foveal dip. Similarly the slightly greater differences with the low contrast targets may suggest that there could be a minor role for aberrations and scatter to influence the CAA test and produce a foveal dip.

Mesopic gap acuities using high contrast (192%) CAA test targets were also measured for three subjects. This resulted in photopic levels of gap acuity being achieved. This could suggest that the elevated mesopic thresholds may have occurred due to low contrast targets being used.

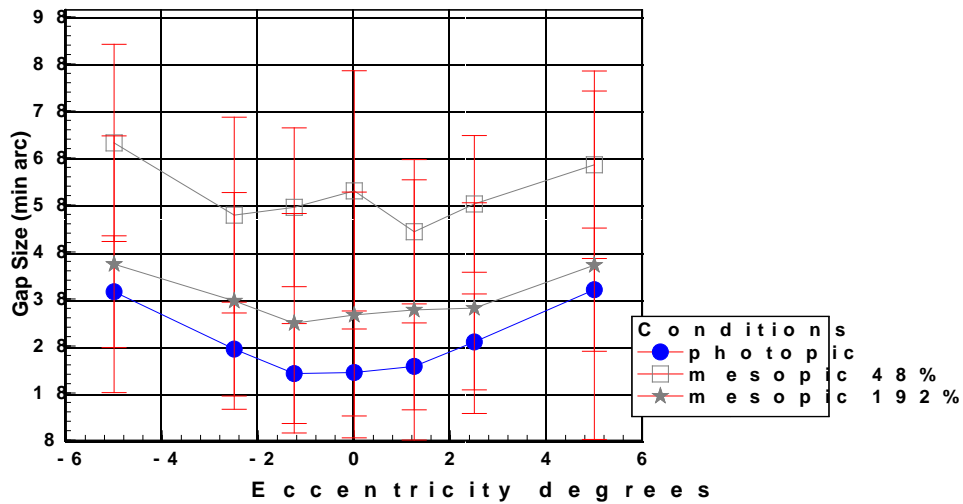


Figure 4.7: Mesopic Gap Acuity results at high and low contrast for 3 subjects. Error bars are 2 standard errors.

Mesopic Gap Acuity results at high and low contrast for 3 subjects are shown in figure 4.6. It can be seen that the mesopic 192% contrast gap size acuities are no longer as elevated when they were at 48% contrast. The 192% mesopic levels appear to be improved compared to the 48% mesopic acuities. The overlapping error bars suggest that the results are not statistically significant. An ANOVA test to examine the effect of high contrast on the mesopic results did not yield statistically significant results at any eccentricities ($P = 0.22$ at the central zero eccentricity).

The results for these three subjects individually are shown in appendix one. Two of the three subjects followed the trend, of high contrast mesopic results achieving similar levels of acuity compared to the photopic results. The other subject did not follow the same trend.

4.8.6 Discussion

High contrast targets under mesopic conditions appear to have raised mesopic contrast acuity levels near to photopic levels. This suggests that part of the explanation for the mesopic foveal dip may be due to the use of low contrast CAA test targets. The high contrast photopic and mesopic acuity results may also be in line with the observation that standard visual acuity tests in clinical practice may not pick up decreases in visual performance due to aberrations or cataract (Elliott & Hurst, 1990; Keir et al., 2011).

The improved acuities with high contrast targets are also in line with Strasburger et al., 's findings. Strasburger et al., (2011) produced equations to show relationships between stimulus size, contrast and eccentricity, using ten Roman digits in a serif font as stimuli on more than 20 young observers. These equations confirmed that there was a size contrast trade off at each eccentricity. The resulting graphs appeared to be fairly linear in the central 10°. These results confirmed the need for scaling non-spatial variables and the crucial role played by contrast. Melmoth and Rovamo (2003) similarly confirmed that scaling of letter size and contrast equalizes perception across eccentricities.

Our results concerning the use of 6 mm and 3 mm artificial pupils with the CAA test were not statistically significant, which is in line with the view expressed by Cox & Holden (1990) who suggested that spherical aberration affects contrast sensitivity rather than spatial discrimination. Figure 4.5 shows a slight trend towards greater differences being generated by the different pupils at lower contrast. This suggests aberrations or scatter may have decreased CAA test performance more at low 24% contrast levels, rather than at high 125% levels.

Jenkins (1963) also assessed the changes in VA using Landolt rings, under photopic conditions, with artificial pupils, dilated pupils and with and without keeping retinal illumination constant. Jenkins (1963) found slight improvements in VA with and without keeping retinal illumination constant for 3 mm pupils compared to 6 mm pupils for 14 subjects. Differences between our experimental conditions, involved the use of non computer generated 6 / 6 sized Landolt ring targets. Jenkins (1963) moved

the targets to different distances to vary their size. Artificial pupils over a wider range of pupil diameters (1.5 - 8 mm) were also used by Jenkins (1963), who attributed the improvement in VA to the decrease in spherical aberrations for the smaller pupil sizes. His significant results may have occurred due to the larger number of subjects used.

4.8.7 Conclusion

For the artificial pupil results, in the case of the contrast sensitivity test, only the lower and middle spatial frequencies were changed by the use of different pupil sizes. This may have occurred due to increased aberrations or scatter. High contrast targets under mesopic conditions appears to have raised mesopic contrast acuity levels to near photopic levels. Similarly greater differences were generated at low contrast by the 6 mm compared to the 3 mm artificial pupils under photopic conditions. This may mean that the contrast of the target may be an important factor in producing the foveal dips under mesopic and photopic conditions.

4.9 Investigation 3: Crowding Effects

4.9.1 Introduction

Strasburger et al., (2011) acknowledged that there are many theories concerning crowding, and that many issues remain unresolved. They suggested that crowding is the loss of form vision as a consequence of target patterns appearing in the spatial context of distracter patterns. It occurs when the surrounding patterns are closer than a critical distance specified by Bouma's law (1970). Bouma formulated a rule of thumb stating that the critical flanker distance d , below which crowding sets in, when expressed as free space between the letters, is about 50% of the target's eccentricity. Strasburger et al., (2011) also suggested that a way to understand crowding was to consider it as a two-stage theory of feature detection and feature combination.

4.9.2 Hypothesis

A possible reason for the CAA Test foveal dip was due to the effect of crowding. The effect of crowding on the CAA Test was therefore examined by reducing the contrast of the guides.

4.9.3 Methods

Under photopic conditions, guide contrast was reduced, by changing the parameter, l (luminance of the guides), from 35 to 17 cd/m^2 . Under mesopic conditions, guide contrast was reduced, by changing the parameter, l , from 0.35 to 0.1 cd/m^2 . This changed the guide contrast under photopic conditions from 192% to 42% and under mesopic conditions from 600% to 100%.

4.9.4 Subjects

Three subjects were tested, aged, 23, 26 and 29 years old. They were City University student volunteers.

Subject	Age	Refractive Error	Dominant Eye
LDS	29	+2.75/-1.00 x 170	Right
DT	26	-5.00/-0.50 x 180	Left
JK	23	-0.50/-0.25 x 90	Right

Table 4.5 Subjects examined for the decreased guide contrast and increased stimulus onset time experiments.

The subjects' details are listed in Table 4.5. They had all had previous experience of psychophysical testing through being City University optometry students or staff. Subject DT sometimes wore contact lenses, whilst the other subjects were non contact lens wearers.

4.9.5 Guide Contrast Effects Results

One subject showed better performance under these conditions, supporting the notion that the CAA foveal dip may have occurred due to the crowding effect of the guides. However the other two subjects did not follow the same trend. Therefore the results were inconclusive.

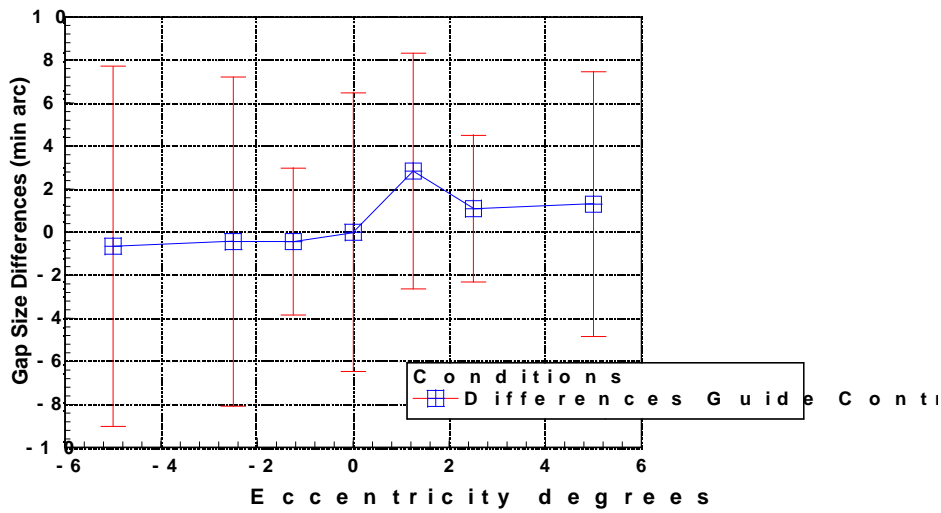


Figure 4.8 Guide Contrast reduced, Photopic CAA Test Differences for three Subjects. Error bars are two standard errors.

Photopic Gap acuity at normal Guide contrast - Photopic Gap acuity at the reduced guide contrast is shown in figure 4.8. None of the differences are statistically significantly different from zero, as suggested by the error bars crossing the zero y axis.. An ANOVA test to examine the effect of reduced guide contrast on the means of the photopic results did not yield statistically significant results at any eccentricities (P = 1.0 at the central zero eccentricity).

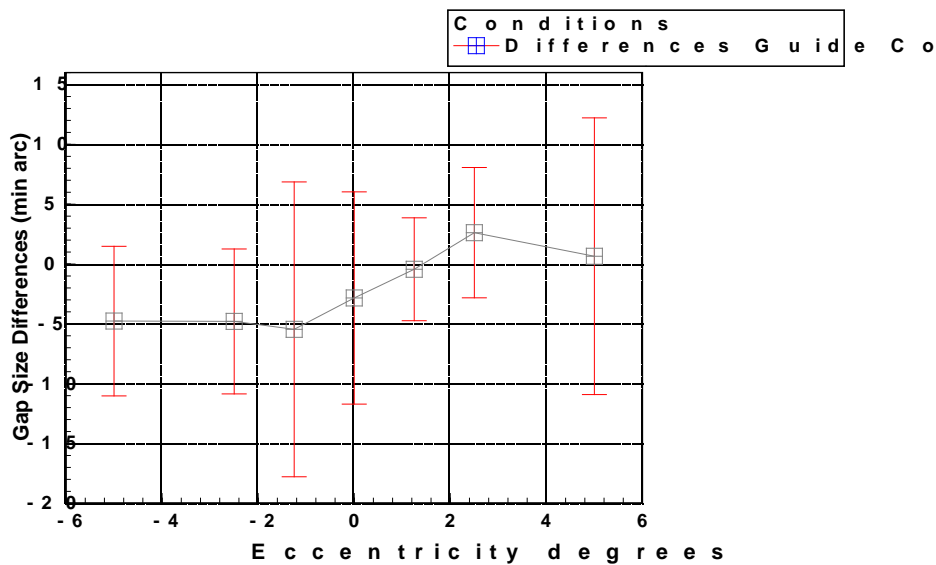


Figure 4.9 Guide Contrast reduced, Mesopic CAA Test Differences for three Subjects. Error bars are two standard errors.

Mesopic Gap acuity at normal Guide contrast - Mesopic Gap acuity at the reduced guide contrast is shown in figure 4.9. None of the differences are significantly different from zero, as suggested by the error bars crossing the zero y axis line. An ANOVA test to examine the effect of reduced guide contrast on the means of the mesopic results did not yield statistically significant differences at any eccentricities ($P = 0.7$ at the central zero eccentricity).

The individual results for the three subjects are shown in Appendix One.

4.9.6 Discussion

No definite trends were found, although it would have been difficult to find statistically significant results, if they had existed, with only three subjects. Our results can be compared to other studies involving lateral masking and crowding. Lateral masking appears to be a complex process, which may explain the variability in our results. For instance, Danilova & Bondarko (2007) presented letters of high-contrast black figures (5 cd/m^2) on a bright background (either 70 cd/m^2 , 80 cd/m^2 or 210 cd/m^2). This difference in the background luminance resulted in a contrast change from 94 to 98%. Experiments were run in a room dimly lit with tungsten

bulbs. Variable sizes of the test Landolt C were used for all 5 observers participating in their study. All the masking functions were found to be U-shaped.

Danilova & Bondarko (2007) suggested that foveal contour interaction and crowding effects were not simple phenomena that can be explained by a single process of either lateral masking, or the physics of the stimulus, or physiological inhibition, or optical factors. They suggested that the combination of several mechanisms can contribute to the crowding effects even in its more simple form at the resolution limit of the visual system.

Zenger-Landolt & Koch (2001) studied lateral interactions in the periphery by measuring how contrast discrimination of a peripheral Gabor patch is affected by flankers. Their results found that in the presence of collinear flanks, contrast discrimination thresholds first decreased with increasing pedestal contrast, then increased (as in the classical dipper function), then decreased again, and finally often increased again, resulting in a W-shaped curve. To account for these data, they proposed a model, which assumed that flankers provided divisive inhibition to the target unit for low target contrasts, but provided subtractive inhibition for higher target contrasts. The transition between divisive and subtractive inhibition occurred at a target contrast similar to the flanker contrast. This may also be reflected in our results, which showed variations in response to changes in flanker contrast. A lot of noise or variations were also found in their results. However, the stimuli used by Zenger-Landolt & Koch (2001) were quite different to our CAA test landolt ring targets.

Another theory suggests that crowding is also subject to modulations induced by transient and sustained attention (Fang & He, 2008). The details of the interaction between these attentional factors with feature detection and position coding are still unresolved (Strasburger et al., 2011). Such unresolved theories of crowding make it difficult to provide full explanations for our results.

4.9.7 Conclusion:

The CAA test produced a mixture of results when guide contrast was reduced under photopic and mesopic conditions. Therefore the results were inconclusive. It is uncertain whether the foveal dips may have been caused by the contrast of the guides.

4.10 Initial Investigation 4: Timing Effects

4.10.1 Introduction

As mentioned in chapter 3, along the visual pathway, there are cells that are more sensitive to detail, i.e. parasol bipolar cells, P cells in the ganglion cell layer, and there are cells that are more suited to movement detection, e.g. retinal amacrine cells, parvo bipolar cells and M cells in the ganglion cell layer.

4.10.2 Hypothesis.

We investigated the effect of stimulus onset time to determine whether this may affect the variation of acuity with eccentricity. This could affect the variation of acuity with eccentricity by simulating a different mixture of M cells or P cells. P and M cells are distributed differently in the retina. We aimed to examine whether stimulus onset time effects in the CAA test, may be altered by adjusting stimulus onset time.

4.10.3 Method

The effect of stimulus onset time on the CAA Test, under photopic and mesopic conditions, was examined, by increasing the stimulus onset time. These subjects were tested with an increased delay between the offset of the fixation guide and the onset of the stimulus. This was achieved by changing the delay time parameter from 453 ms to 1000 ms.

4.10.4 Subjects

Three subjects were tested, aged, 23, 26 and 29 years old. They were City University optometry student and staff volunteers. Their details are listed in Table 4.4.

4.10.5 Results

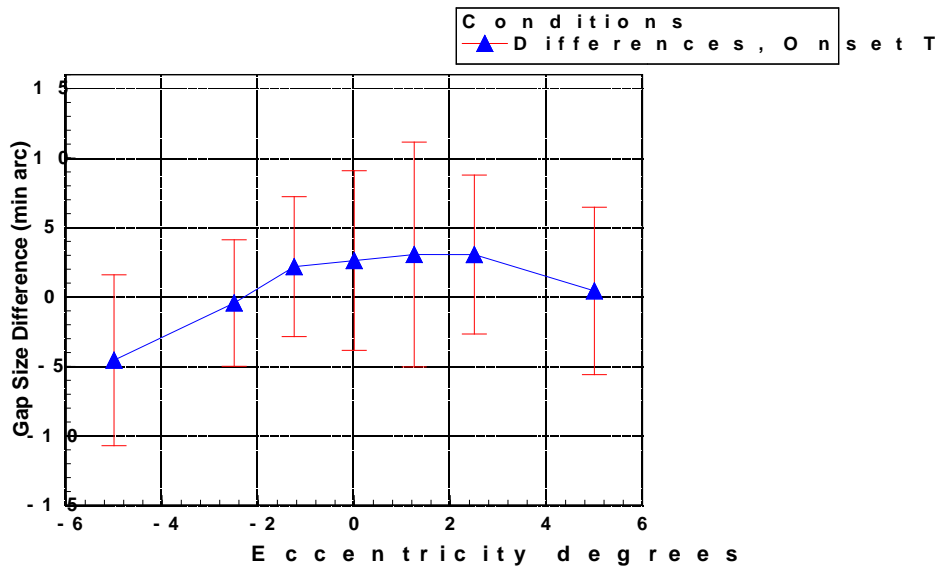


Figure 4.10 Stimulus Onset Time increased, Photopic CAA Test Differences for three Subjects. Error bars are two standard errors

Photopic Gap acuity at normal Stimulus Onset Time - Photopic Gap acuity at the increased stimulus onset time is shown in figure 4.10. None of the differences are significantly different from zero.. An ANOVA test to examine the effect of increased stimulus onset time on the means of the photopic results did not yield statistically significant differences at any eccentricities ($P = 0.55$ at the central zero eccentricity).

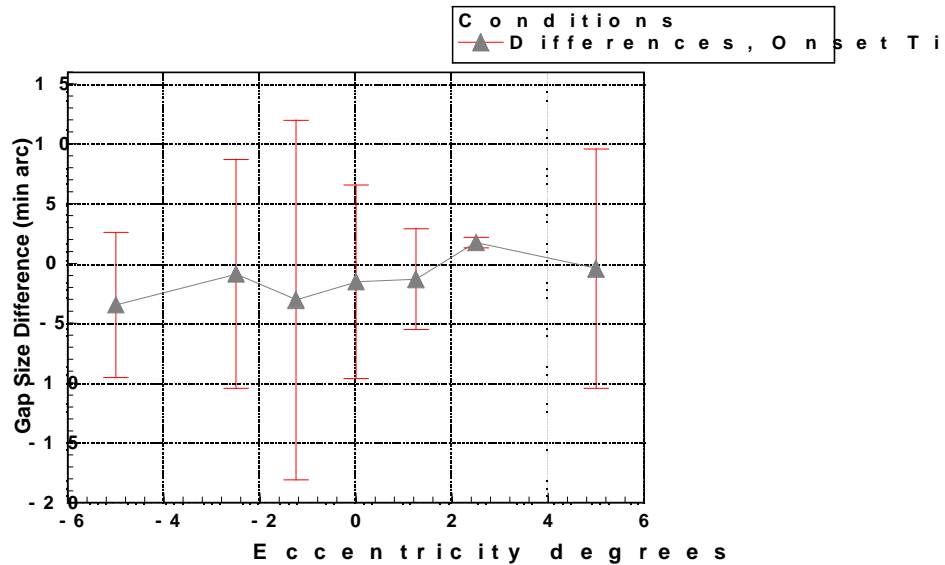


Figure 4.11 Stimulus Onset Time increased, Mesopic CAA Test Differences for three Subjects. Error bars are two standard errors.

Mesopic Gap acuity at normal Stimulus Onset Time - Mesopic Gap acuity at the increased stimulus onset time is shown in figure 4.10. An ANOVA test for the effect of increased stimulus onset time on the means of the mesopic results did not yield statistically significant differences in the means at any eccentricities ($P = 0.84$ at the central zero eccentricity).

4.10.6 Discussion

Inconclusive results were found, which may be due to the small number of subjects used, or the change in stimulus onset time may not have been enough to produce significant changes in results. Or it could be that stimulus onset time might have no effect on gap acuity. Ideally around eight subjects would have been tested instead of just three to increase the chances of finding a statistically significant difference if one existed. Even if a statistically significant result had been found, there would still be a chance that the result may not be clinically significant, as clinical significance can be a more relevant factor. It would also have been better to have been able to test more delay time parameters, if there had been more time available to perform the

experiments. The three subjects involved had undergone other tests in the study as well. Caution had to be used in allowing the subjects to take rests whenever tired. Each test lasted around ten minutes. Research examining the effect of stimulus time has changed the presentation time in different ways (e.g. Drasdo, Thompson & Deeley (1990). Therefore their results are not directly comparable with ours.

4.11 Conclusions

The guide contrasts results did not yield significant results or trends. Neither did the onset of stimulus time increase, although only three subjects were tested, due to time constraints. This suggests that there is no evidence that either guide contrast or stimulus onset time had a role in producing the foveal dip.

The artificial pupil contrast sensitivity results yielded statistically significant results for differences in the means at the lower 1.2 and middle 6.1 cpd spatial frequencies. The contrast sensitivity results did not yield statistically significant results for the difference in the means at high spatial frequencies. This is in line with only slight trends occurring with the use of artificial pupils in the photopic CAA test. A slight trend of increased differences due to the use of 6 mm and 3 mm artificial pupils on the CAA test at low contrast may suggest that aberrations and scatter could play a minor role in producing a foveal dip.

The better acuities yielded with higher contrast targets under mesopic and photopic conditions, also suggest that low contrast may be an important factor in producing the foveal dip.

Chapter Five

The Effect of Natural Aberrations on the CAA Test

5.1 Overall Aim

The aim of the study described in this chapter is to investigate the association between higher order aberrations and gap acuity measured by the CAA test under photopic and mesopic conditions. To do this, we investigated the effect of aberrations on performance in the CAA test for normal subjects.

5.2 Apparatus and Procedures: Hartmann Shack:

The Shack-Hartmann wavefront sensor was built at Imperial College, London (Diaz-Santana, 2000; Diaz-Santana & Dainty, 2000). The light source used was a super luminescent diode (SLD) at 543 nm (Davies et al., 2003). In the Shack-Hartmann wavefront sensing technique, a narrow collimated laser beam forms a spot on the retina, and the light reflected and emerging from the eye is sampled by a rectangular lenslet array placed on a plane that is conjugate to the eye's pupil. A CCD camera, placed on the focal plane of the lenslet array and conjugate with the retina, was used to record the spot pattern of the wavefront. Deviations from the ideal Shack-Hartmann spot pattern were proportional to the local slopes of the wave aberration. The estimated slopes were fitted to a sixth-order Zernike polynomial (27 terms) expansion using a least-mean square procedure.

The size of each lenslet was 0.8×0.8 mm over the pupil plane, and the focal length was 35 mm. A maximum of 48 sampling lenslets covered a pupil of diameter 6.5 mm. The measured power reaching the cornea was <500 nW in every case, and the retinal image of the source was used as a fixation marker. A dental bite bar was used to maintain steady fixation, and a cathode ray tube (CRT) monitor with a concentric circular grating was used to monitor fixation. The spacing between lines in the circular grating over the CRT corresponded with 1 mm spacing over the pupil plane. Consequently, the repositioning error was approximately ± 500 μm . If done very carefully, accuracy could probably be improved, but on the other hand, accuracy could be affected by the operator's visual acuity, parallax due to his/her positioning

with respect to the CRT, illumination conditions, and contrast on the screen. The aligning arm of the system did not include an eye-tracking device; consequently, recording of the positioning was not performed. The dental bar permitted a steadier fixation than that provided by a chin rest and a forehead support bar. The subject grasped the bite bar and was asked to fixate on the fixation marker. The position of the bite bar was adjusted by horizontal (x and z) and vertical (y) translations. A CCD monitor was used to aid pupil alignment.

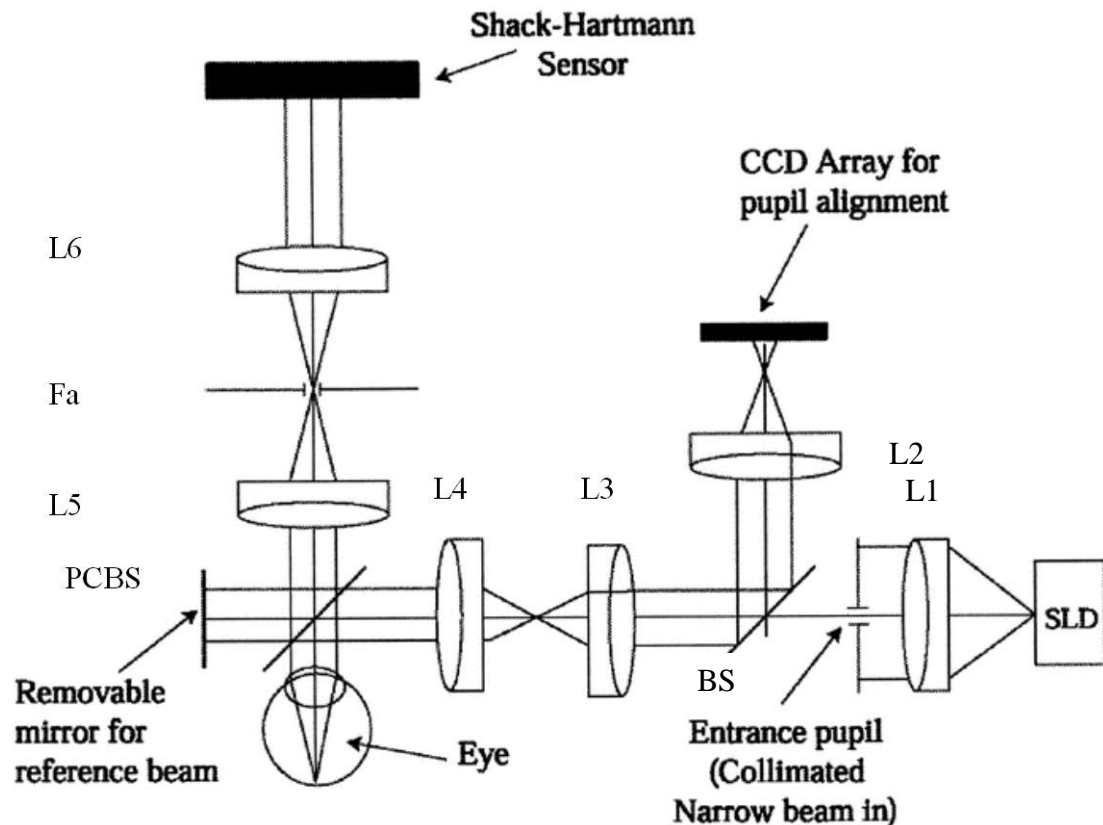


Figure 5.1. Optical layout of wavefront sensor.

In the Shack-Hartmann wavefront sensor in figure 5.1, light coming from a super luminescent diode (SLD) formed a point on the retina. L1 and L2 were collimating lenses. L3, L4 and L5, L6 were relay systems in the illumination and imaging channels, respectively. The diameter of the entrance pupil aperture was 1.5 mm, and Fa was a field aperture. Light reflected off the retina was imaged by a Shack-Hartmann sensor on to a cooled CCD camera. Images of the pupil were projected onto

a CCD camera and this monitored pupil centration. BS was a pellicle beam splitter, and PCBS was a polarizing cube beam splitter.

5.3 Examining the Foveal Dip

The following hypotheses were put forward in Chapter 4 to explain the presence of the foveal dip:

Under photopic conditions, the higher foveal threshold could have been accounted for by the following:

- 1) Ganglion cell sampling interval was not as high in the foveal region as predicted from the linear relationship.
- 2) The retinal image was degraded by increased scatter and aberrations in some subjects, which may have caused the observed increase in foveal acuity threshold.
- 3) Crowding and stimulus onset time effects induced by the preceding fixation spot for foveal measurements caused a reduction in sensitivity and hence the increased thresholds.

To try to account for the much higher foveal thresholds under mesopic conditions, the following hypotheses were considered:

- 1) The effective ganglion cell population changes in the mesopic range and this could have resulted in an even greater reduction in sampling density in the foveal region.
- 2) The involvement of rod receptors was significant at this light level and rod receptors are absent in the central foveal region. ((1) & (2) are closely related). The raised thresholds may be partly related to the greater absence of rods near fixation, and the rods may have played a greater role in the mesopic levels.
- 3) The larger pupil size in the mesopic range resulted in increased aberrations and scattered light.
- 4) Stimulus onset time and crowding effects played an even greater role in the mesopic range.

5.3.1 Hypothesis

We aimed to investigate the effect of aberrations on normal subjects with natural pupils on the photopic and mesopic CAA test, to determine whether they may have influenced the foveal dip.

5.3.2 Method:

Wavefront aberration measurements over a 6 mm diameter pupil were taken. Linear regressions were performed on higher order aberrations and the CAA test results, to determine whether aberrations may have contributed to the foveal dip, under photopic and mesopic conditions.

If aberrations had contributed to the foveal dip, then there should have been a trend of increased aberrations being associated with increased CAA foveal dip results. This was investigated by recruiting subjects, performing the CAA test on them and measuring their aberrations.

5.3.3 Subjects

14 normal subjects, aged 23-54, were examined with natural pupils, under photopic conditions and 10 normal subjects, aged 23-54, were tested under mesopic conditions with the CAA test. The subjects were volunteers, recruited from City University and Imperial College Staff, students and social contacts.

A detailed history was taken for each potential subject to allow identification and exclusion of pregnant women and subjects with systemic disease such as diabetes, or medication that might influence visual function. A subjective refraction was undertaken to ensure that all subjects were fully corrected prior to testing and achieved a minimum visual acuity of 6/9. Ocular health was examined to exclude eyes with any pathology, including lens opacities classified using the LOCS III system (Chylack et al., 1993).

The subjects' details are listed in Table 5.2. Subjects CL, SM, LDS, LW MW, PM RY, & JAB had all had previous experience of psychophysical testing through being

City University staff or students. Subjects KH, JOB, SC, STG, SIG & AD had had no previous experience of psychophysical testing. Subjects LW, RY, SC & STG were part time contact lens wearers. The other subjects were non contact lens wearers.

Subject	Age	Refractive Error	Dominant Eye
CL	38	-2.00 /-0.50 x 175	Right
KH	23	-1.00/-0.50 x 94	Right
SM	25	0.25 DS	Right
LDS	29	+2.75/-1.00 x 170	Right
LW	30	-4.25/-1.00 x 7	Right
JOB	23	+0.25 DS	Right
MW	54	-2.25 DS Add +1.50	Right
SC	24	-.4.50/-1.00 x 27	Right
PM	37	-0.50/-0.25 x 63	Left
RY	35	-3.75 DS	Right
STG	23	-1.50/-4.00 x 15	Left
JAB	50	-0.50 DS	Right
SIG	45	+0.50/ -1.00 x 32.5	Left
AD	26	+2.00/-2.00 x 163	Left

Table 5.1 Subjects used for the natural aberrations versus CAA Test Study.

5.3.4 Results

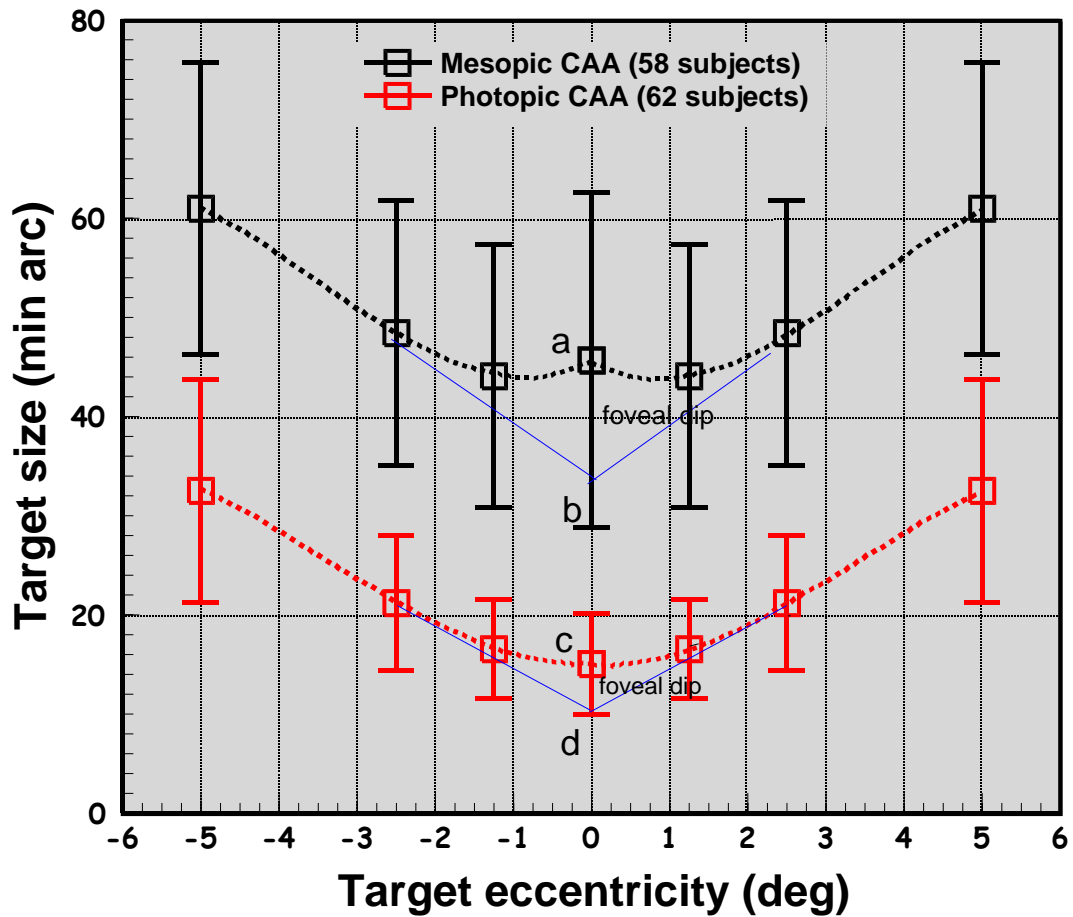


Figure 5.2 Calculation of Foveal Dip

Photopic foveal dips were calculated for each subject by subtracting the extrapolated straight line result ‘d’ under photopic conditions from the subjects’ photopic central gap acuity value.

Similarly, mesopic foveal dips were calculated for each subject by subtracting the extrapolated straight line result ‘b’ under mesopic conditions from the subjects’ mesopic central gap acuity value.

The mean extrapolated straight line results were calculated to be 9.9 mins arc (photopic, point d in figure 5.2) and 38.6 mins arc (mesopic, point b in figure 5.2). This enabled the foveal dips to be calculated (Table 5.1).

Subject	Photopic Central Gap Acuity mins arc	Mesopic Central Gap Acuity mins arc	Photopic Foveal Dip mins arc	Mesopic Foveal Dip mins arc	Higher Order Aberrations RMS microns - Pupil Size 6 mm
CL	10.49	35.4	0.62	-0.47	0.280
KH	11.14	56.37	1.28	20.5	0.526
SM	11.43	35.63	1.57	-0.24	0.450
LDS	11.80	50.47	1.94	14.6	0.257
LW	12.45	55.71	2.59	19.85	0.268
JOB	12.45	34.74	2.59	-1.13	0.176
MW	14.12	58.49	4.25	22.62	0.264
SC	14.42	51.78	4.56	15.92	0.210
PM	15.08	58.99	5.21	23.12	0.300
RY	15.46	62.52	5.60	26.65	0.177
STG	15.73	64.23	5.87	28.37	0.277
JAB	16.39	63.02	6.52	27.16	0.505
SIG	16.39	73.41	6.52	37.54	0.168
AD	16.39	45.23	6.52	9.36	0.130
mean	13.84	53.28	3.98	17.42	0.285
se	0.57	3.17	1.15	6.34	0.034

Table 5.2 Photopic & Mesopic Gap Acuities, Foveal Dips & Higher Order Aberrations.

Regressions of foveal dip against higher order aberrations RMS did not yield statistically significant trends at photopic ($P = 0.268$) and mesopic ($P = 0.999$) light levels (figures 5.3 & 5.4).

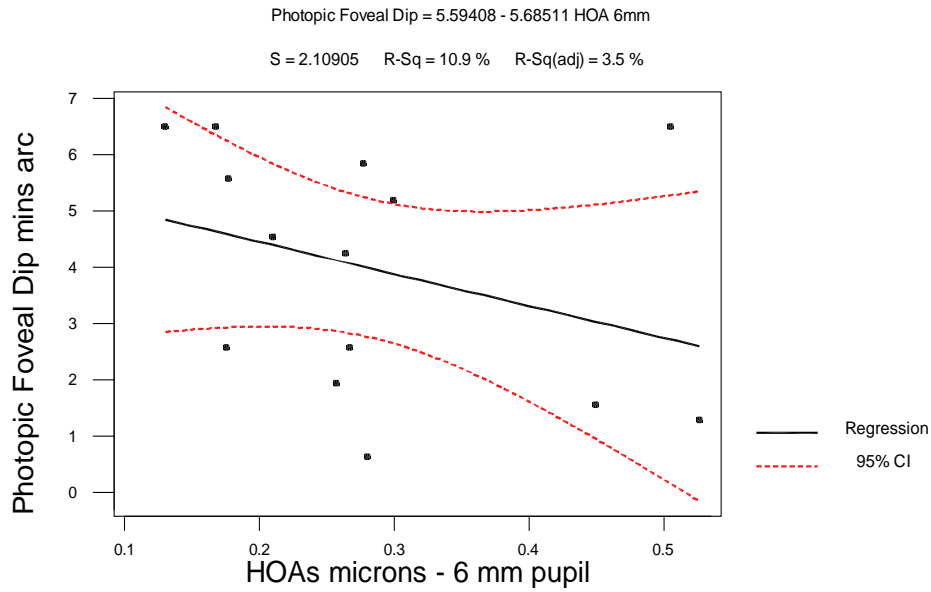


Figure 5.3 Photopic Foveal Dip vs Higher Order Aberrations: Pupil size 6 mm

Higher Order aberrations (HOAs) were represented by the wavefront RMS error over a 6 mm pupil size for third orders and above. The above regression plot shows that no statistically significant trend for photopic CAA foveal dip versus higher order aberrations ($P = 0.248$, adjusted $R^2 = 3.5\%$) was found.

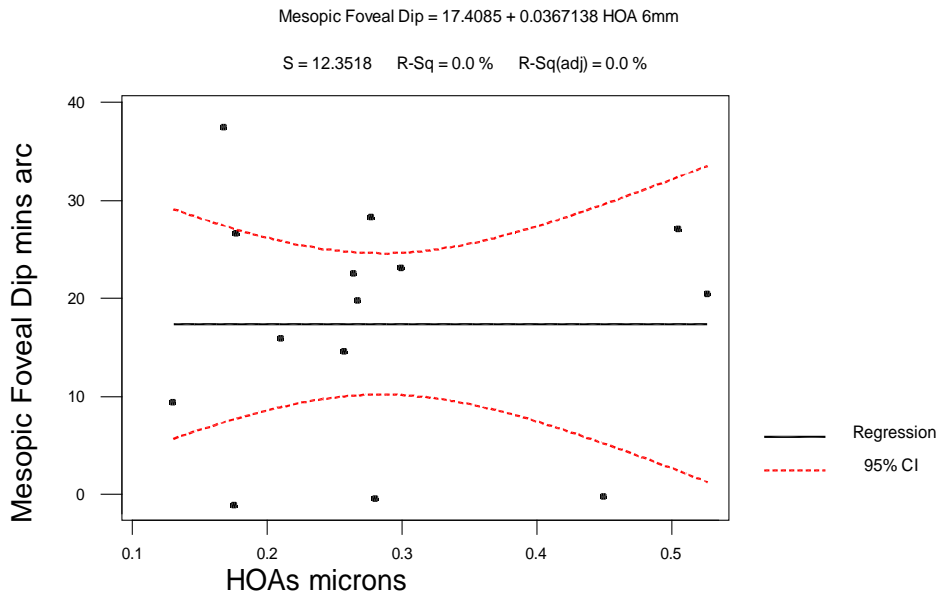


Figure 5.4: Mesopic Foveal Dip vs Higher Order Aberrations: Pupil size 6 mm

The above regression plot shows that no statistically significant trend for mesopic CAA foveal dip versus higher order aberrations ($P = 0.999$, adjusted $R^2 = 0\%$) was found.

5.3.5 Discussion

The trend of mesopic foveal dip against HOAs was flat which may be unexpected, as under mesopic conditions some researchers have found a more significant trend between HOAs and visual performance (e.g. Applegate et al., 2006).

There was no facility for measuring pupil sizes under the CAA test mesopic or photopic conditions. Such a facility would have allowed us to scale the aberration measurements to the actual size of the pupil under test conditions, which could have lead to different results. Therefore we were limited to measuring aberrations over a 6 mm pupil diameter and we compared this to CAA test performance under mesopic and photopic conditions.

Reseachers have found the VSOTF (visual Strehl ratio based on optical transfer function) showed greater predictability than higher order aberrations RMS, to predict

visual performance (Buhren et al., 2009, Marshack et al., 2004). Unfortunately the data were not available for this variable to be calculated.

The results show no statistical relationship between RMS aberrations and foveal dip or central CAA threshold. This agrees with results found by Joslin and associates (2003) who examined eighteen eyes of nine myopic subjects fitted with corneal refractive therapy (CRT) contact lenses. CRT contact lenses for myopia were found to have significantly increased higher order aberrations, whereas there was no significant effect on visual acuity. Similarly, modification in the overall aberration pattern of the eye induced by accommodation was not associated with any significant effect on image quality (Artal et al., 2002).

More recently, Su & Hu (2009) examined 40 eyes of 20 patients who underwent cataract surgery and were randomly assigned to receive a spherical IOL in one eye and an aspheric IOL in the contralateral eye. Although, compared to the conventional spherical IOL, the aspheric IOL significantly reduced total ocular and spherical aberration, it did not result in better contrast acuity under mesopic or photopic conditions. The researchers suggested that the small pupil size observed under the test conditions may have been a factor, which limited the beneficial effect of aspheric IOLs on visual performance.

It may be noted however that Young et al., (2011) suggested that the nature of the visual task is important when determining which aberrations have the greatest impact on visual performance. Young et al., (2011) assessed reading performance using text with a simulated monochromatic aberration (defocus, coma, or secondary astigmatism). They found that the rate of decline in reading performance with increasing aberration amplitude was smaller for coma than for secondary astigmatism or defocus. Defocus and secondary astigmatism were found to have a more significant impact on word identification, unlike coma. The CAA test was quite a specific test, so it may be the case that if the same subjects had been made to perform other tasks, relationships may have been found between their aberrations and visual performance. The CAA test results for normal subjects are also in line with some studies on super normal vision, which have found little relation between aberrations and visual

performance. For instance, Levy et al., (2005) investigated the higher order aberrations from the third to the eighth orders in a selected sample of 70 eyes with supernormal vision. The amount of ocular aberrations in these eyes were found to be considerable and the magnitudes were comparable to those of myopic eyes, including those before refractive surgery without supernormal vision.

Similarly, Amesbury & Schallhorn (2003) found that a group of naval aviators with supernormal vision did not have lower higher order aberrations (HOAs) than those without this level of high uncorrected vision. Some higher-order terms were actually higher in the aviator group, such as coma. They suggested, therefore, that the RMS wavefront error of normal eyes has a low correlation with visual performance and that attempts to correct HOAs may provide little or no functional benefit to most normal eyes without highly irregular corneas.

Applegate et al., (2003) put forward reasons for why at lower levels of aberrations; the RMS wavefront error is not a good predictor of visual acuity. This low correlation was attributed to the variation in the neural transfer function between the subjects, the low sensitivity of common clinical measures to low levels of aberration, and the fact that a combination of aberrations may interact to improve or reduce visual performance, depending on their radial orders, sign, and angular frequency.

There have been a instances where researchers have found relationships between aberrations and visual performance in quite specific areas.

Researchers have found relationships between aberrations and visual performance in subjects with supernormal vision, in contrast to Levy et al., (2005). For instance, Applegate et al., (2006) found that the ability of the metrics of retinal image quality to predict logMAR acuity improved as luminance and/or contrast were lowered for normal subjects. Pesudovs et al., (2004) examined cataract surgery subjects and found that wave aberration metrics correlated better with mesopic low contrast visual acuity.

Over a large range of RMS errors (an equivalent dioptric range of around 3 dioptres), it has been found that visual acuity decreases with increasing RMS error of the corneal first surface (Applegate et al., 2000), on subjects with pathology and refractive surgery subjects. Hence, it was suggested that minimizing higher order aberrations by wavefront-guided refractive surgery would improve visual performance. However, this inverse correlation between ocular aberrations and visual performance has been found only in data sets with a high magnitude of aberrations and acuities. In our CAA test results using normal subjects, such large ranges of aberrations were not examined. This led us to induce large aberrations on subjects by using contact lenses with large Q values (chapter 6).

It has been demonstrated that the manner in which the Zernike modes are combined significantly impacted measured acuity in a way that RMS wave-front error and equivalent dioptric error could not predict. A reason suggested for this was that RMS wavefront error specified only the standard deviation of the wavefront error over the pupil. It does not contain information as to how this wavefront error is distributed within the pupil (Applegate, Marsack et al., 2003). This may help to explain why we found no relationships in our normal subjects between RMS wavefront error and the foveal dip or central CAA test performance.

5.4 Conclusions

No relationship or trend was found between the higher order aberration 6 mm pupil RMS aberration values and the CAA test results for the foveal dips under mesopic or photopic conditions. These results occurred even though the use of artificial pupils produced lower contrast sensitivity at the middle and lower spatial frequencies in Chapter 4. These aberration results, which were not statistically significant, may also be contrasted with the slightly greater differences generated by the 6 mm and 3 mm artificial pupils at low contrast for the 0 and 2.5 degree eccentricities in chapter 4. This suggests that retinal factors or scatter, rather than aberrations may have contributed more to the elevated photopic and mesopic thresholds. Aberrations may only have played a very small or no role in producing the foveal dips.

Chapter Six

6. The Effect of increased Spherical Aberration on the CAA Test

6.1 Introduction

Spherical aberration, in the past, has often increased following refractive surgery. We investigated its effects by using custom made soft contact lenses with specified asphericities as determined by their Q values.

We aimed to investigate whether our tests could pick up changes in visual performance due to increased levels of spherical aberration using Q value contact lenses. These results could then be related to the foveal dip observed in Chapter 4 (figure 4.2). Q values were selected to simulate the Q values found in normal and post refractive surgery subjects, to induce significant (non-physiological) amounts of positive and negative spherical aberration. The spherical aberration generated also depended on the pupil size and the way in which the contact lens settled on the eye.

The value of Q is 0 for a sphere, -1 for a parabola, $-1 < Q < 0$ for a prolate ellipsoid and $Q > 0$ for an oblate ellipsoid. Most human corneas are prolate, flattening from the centre to the periphery (giving negative asphericity; $Q < 0$) (Mastropasqua et al., 2006). The physiological Q value in an untreated cornea ranges between 0.50 and -0.88, with an average value of -0.26, which is correlated with low spherical aberration (Mandell & St Helen, 1971; Kiely et al., 1982). Conventional myopic laser surgery reverses the normal corneal shape to an oblate profile, steepening the shape from the centre to the periphery to often give a positive asphericity of $Q > 0$. Hersh et al., (2003) examined the corneal topography of 20 eyes which had undergone laser in situ keratomileusis, laser-assisted subepithelial keratectomy, and photorefractive keratectomy for myopia. The mean Q asphericity was found to be $+ 0.92 \pm 0.70$ postoperatively, corresponding to an oblate profile, and hence increased positive spherical aberration.

Pop & Bains (2005) examined Q value asphericity after customized aspheric treatment zone (CATz) topography ablation in one eye and optical path difference

guided customized aspheric treatment (OPDCAT wavefront guided) in the other eye. The resulting Q values after surgery were -0.3009 ± 0.3174 (CATz) and -0.4119 ± 0.5269 (OPDCAT). Similarly post op Q values of $+0.47 \pm 0.46$ for wavefront guided LASIK and $+0.50 \pm 0.49$ for Custom Q LASIK (LASIK aiming for an optimal Q value) were found by Koller et al., (2006).

Corneal asphericity changes due to LASIK ablation for hyperopic subjects have been studied by Chen et al., (2002) for prolate hyperopic corneas. They found that the prolate corneas became more prolate and that Q changed by up to -2 , giving a range of post op Q values between 0 and -2.5 approximately.

More recently, Bottos et al., (2011), in a study involving 177 myopic eyes and 32 hyperopic eyes, found the mean Q value to be $+0.35$ sd 0.44 and -0.64 sd 0.31, respectively, postoperatively after wavefront-guided laser in situ keratomileusis.

Ang et al., (2009) examined 170 eyes with preoperative myopia and myopic astigmatism, to compare an aspheric LASIK ablation algorithm to a tissue saving (control group) LASIK ablation algorithm, using the Technolas 217z100 excimer system. Eyes in the aspheric group had significantly lower Q values. For a corneal diameter of 7 mm the aspheric group had a mean Q value of $+0.466$ sd 0.341 range -0.140 to 1.5410 compared to the tissue saving control group. which had a mean Q value of -0.737 s.d. 0.373 range 0.080 to 1.960 . More recent studies have found spherical aberration to be less of a problem due to improved wavefront technology.

In addition, spherical aberration has been shown to increase with age due to the decreasing compensation of positive corneal spherical aberration by negative lenticular spherical aberration (Artal, Berrio et al., 2002). Spherical aberration has also been shown to increase depth of field, e.g. in studies examining the use of intra-ocular lenses in cataract surgery (Nochez et al., 2011).

6.2. Initial Study

6.2.1 Hypothesis

We decided to investigate whether increased levels of higher order aberrations, similar to those following laser refractive surgery could affect visual performance as measured by the CAA test.

6.2.2 Subjects

3 subjects were recruited, aged 23 (subject SS), 24 (subject JC) and 27 (subject DT). They were City University optometry students. Inclusion criteria were no ocular pathology and 0.50 DC or less of astigmatism.

6.2.3 Apparatus

6.2.3.1 Q Value Contact Lenses

9 sets of front surface aspheric contact lenses were made with different Q values for the main study and 3 sets of contact lenses were used for the initial study. Cambridge Precision Contact Lenses manufactured the custom designed contact lenses.

The soft contact lenses were made of PHEMA 40% with a BOZR of 8.7 - 8.5 mm and TD of 14.3 mm. The Q value lenses in the initial study consisted of Q = -2, Q = 0 and Q = +1.5 lenses. BVPs were made to correct the subjects' spherical error. The front surface conics (aspheric) were made with the following Q values for the main study:

Lens	1	2	3	4	5
Q	-2.0	-1.0	0.0	1.0	1.5

Table 6.1 Q values of the aberration controlled Contact Lenses

The asphericity (or "conic constant") Q was used to describe a conic section with the following equation: -

$$Z = \frac{y^2}{r + \sqrt{r^2 - (Q+1)y^2}} \quad \text{equation 6.1}$$

where Z is the surface sagitta, y is the radial distance from the surface apex and r is the apical radius of curvature. It may be useful to note that $p = Q + 1$ where p is the "asphericity" or simply "p-value", is used by a number of authors to describe conic sections.

The contact lenses were rinsed and rubbed with Renu multipurpose solution, manufactured by Bausch & Lomb. They were also stored in Renu multipurpose solution. This method of cleaning and storing the contact lenses was not expected to produce significant contact lens parameter changes. Researchers have found that other methods of cleaning and storing lenses could produce greater parameter changes, such as in the case of hydrogen peroxide systems and heat based systems, by altering the water content, (e.g. Harris et al., 1989). Peroxide based systems have also been shown to influence the base curve of contact lenses (Janoff, 1985). The contact lenses were soaked in fresh multipurpose solution for several hours if they had not been used for several days or more.

Digital rubbing of contact lenses has also been shown to induce parameter changes, within the tolerance range of the ISO (the International Organization for Standardization,) by Mutalib & Lee (2010). Therefore care was taken not to rub the lenses too vigorously.

6.2.3.2 WASCA Aberrations and Pupil Size Measurement

The Asclepion WASCA (Wavefront Aberration Supported Cornea Ablation, Carl Zeiss Meditec, Jena, Germany) workstation is a wavefront analyser whose main purpose is for measuring aberrations. It can also measure pupil diameter objectively (Schmitz et al., 2003). It utilizes a Hartmann-Shack sensor to investigate the eye's aberrations. The eye is illuminated by a plane infrared wave emitted by a superluminescent diode (850 nm, 45 μ W). The light is focussed on the retina by the refractive power of the cornea and the lens. It generates a wavefront into the fovea. This wavefront is reflected backwards. The pupil is the smallest part of the optical system, which is passed by the measuring laser and the wavefront. Therefore the diameter of the passing wavefront is equivalent to the diameter of the pupil. The

aberrometer determined the pupil diameter indirectly by measuring the diameter of the distribution pattern of the reflected wavefront using the Hartmann-Shack principle.

6.2.3.3 WASCA Procedure

The following procedure was used to measure the aberrations using the WASCA machine. The subject was first of all aligned to the instrument. The Start Button was then clicked, which made the video display an image, which was focused, to make the eye clear and centred. The iris image was centred in the rectangle of the window. The instrument was aligned to centre the pupil in the X and Y directions. The joystick was rotated clockwise to raise the measurement instrument, and anti-clockwise to lower it. The joystick was adjusted left to right to move the stage more precisely on the table. The instrument was focused on the iris image. The stage was locked when the iris was focused.

Six dots were shown around the image of the pupil, which were a corneal reflection of six illumination LEDs in the instrument. Their appearance and symmetric position on the display showed that the eye was almost perfectly centred. Optimal alignment of the eye in front of the examination window would produce a sharp and clear picture in the centre of the frame lines. The six light dots were made to appear symmetric with respect to the pupil and crossbar. The subject's aberrations were then measured by pressing the "refract" button. Several readings were taken for each subject, from which the mean was taken for each subject.

6.2.4 Methods

Aberration controlled contact lenses with Q values of 0, +1.50 and -2 were used to determine the effect of raised spherical aberration levels on CAA test performance under photopic and mesopic conditions. These contact lenses had originally been used on another study concerning accommodation.

6.2.5 Results

The CAA test differences generated by the Q value contact lenses show that larger differences were generated under mesopic conditions compared to photopic conditions (Tables 6.2 and 6.3).

		Photopic						
		Eccentricity						
	Subject	-5	-2.5	-1.25	0	1.25	2.5	5
Q = -2	DT	20.8	10.5	16.4	12.4	16.4	24.9	33.8
	JC	18.2	13.7	9.8	1.3	9.8	12.4	19.5
	SS	50.1	44.5	42.6	53.8	63.6	60.8	40.3
Q = 1.5	DT	26.0	15.0	13.8	11.8	13.8	32.1	41.0
	JC	32.5	32.7	28.8	21.0	22.9	34.7	57.9
	SS	83.9	68.0	63.6	59.0	75.3	65.4	55.3

Table 6.2 Pilot Study Differences in photopic gap acuities generated by Q =-2 and Q = +1.5 contact lenses.

		Mesopic						
		Eccentricity						
Q value	Subject	-5	-2.5	-1.25	0	1.25	2.5	5
Q = -2	DT	60.5	49.7	60.3	66.8	59.0	68.7	66.3
	JC	15.61	18.97	15.07	18.35	22.3	17.7	10.4
Q = +1.5	DT	61.1	45.1	59.6	53.1	59.0	50.4	48.1
	JC	59.2	42.5	47.2	57.0	63.0	51.0	54.6

Table 6.3 Pilot Study Differences in mesopic gap acuities generated by Q =-2 and Q = +1.5 contact lenses.

This is shown graphically (Figures 6.1).

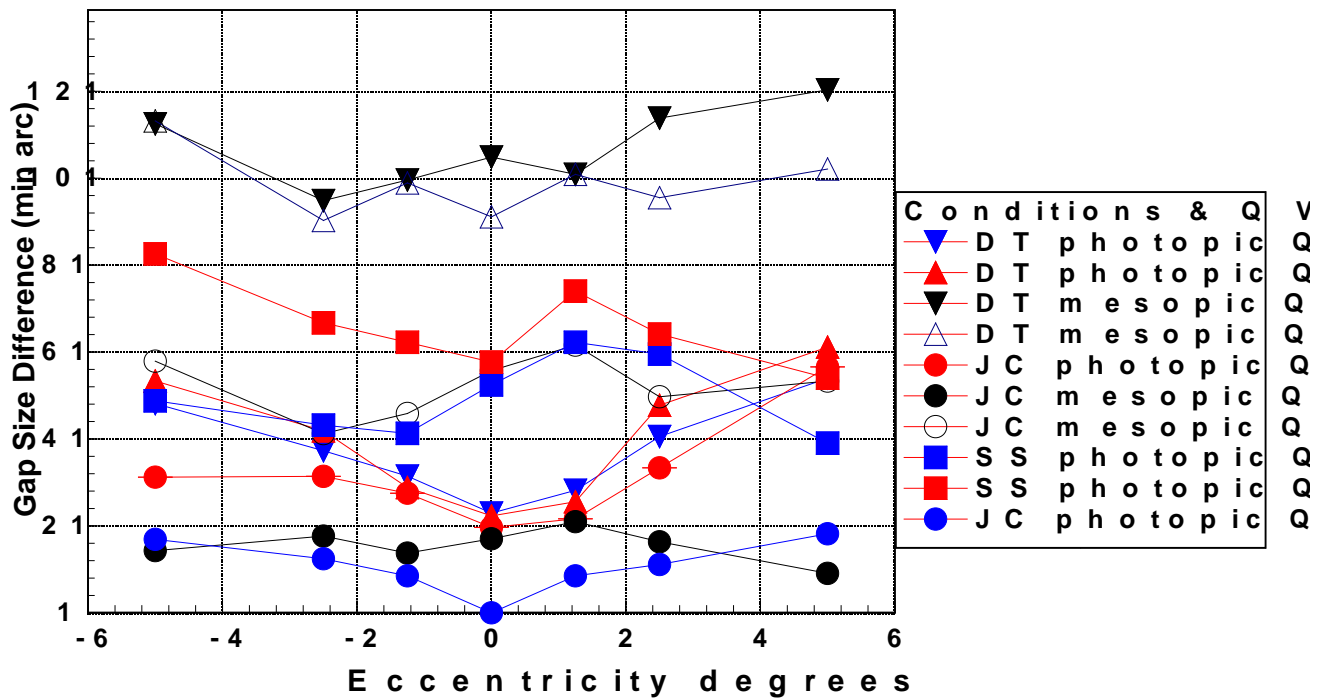


Figure 6.1 Initial Study Photopic & Mesopic Gap Size Differences generated by Q = -2 and Q = +1.5 contact lenses for three subjects compared to the Q = 0 values.

Figure 6.1 shows the gap size differences generated by the Q = -2 and Q = +1.5 contact lenses under photopic and mesopic conditions for subjects DT and JC, and under photopic conditions for subject SS. The gap size difference for subject DT for the Q = -2 lenses, was calculated by subtracting the Q = 0 gap acuities from the Q = -2 gap acuities, and are denoted as DT photopic Q_{m2} - Q₀ in the legend of the graph. Similarly the gap size difference for the Q = + 1.5 lens is denoted by DT photopic Q_{p15} - Q₀.

The largest differences occurred for subject DT with the +1.50 and -2 Q value lenses under mesopic conditions. The smallest differences occurred with subject JC under photopic conditions. There was a large variation in the results, but the Q = +1.5 and Q = -2 lenses in the various conditions produced worse gap acuity results, than the plano Q = 0 lenses. Subject SS was unable to complete the mesopic test, which explains why there are only two mesopic results.

6.2.6 Discussion.

The results showed that the Q value contact lenses produced definite changes in visual performance. Greater changes were observed under mesopic conditions, possibly due to the larger pupil sizes leading to a greater effect from the increased spherical aberration. Therefore we proceeded to recruit more subjects to carry out more extensive tests using contact lenses with an increased number of Q values. The results were used to select contact lenses with Q values of 0, +1.50, +1.00, -2 and -1 (table 6.1).

6.3 Main Study

6.3.1 Hypothesis.

We decided to further investigate the effect of using contact lenses with different Q values to determine their effect on visual performance as well as on other parameters such as spherical aberration or other aberrations. This could then be used to determine whether the effect of aberrations induced by Q value lenses could then be assessed in respect of visual performance with the CAA test under mesopic and photopic conditions. The results could also be related to the CAA test foveal dip.

6.3.2 Main Study Subjects:

Subject Initials , dominant eye, RX	Age	BVP
RS RE -3.00/-0.25 x 30	32	-3.00 DS
CG RE -1.25 DS	26	-1.25 DS
KT LE -2.75 DS	26	-2.75 DS
PP LE +0.25 DS	30	+0.25 DS
CT LE +0.25/-0.25 x 45	25	+0.25 DS
KF RE -2.50/-0.50 x 85	31	-2.50 DS
JBO LE -2.75 DS	32	-2.75 DS
KAP RE -2.50/-0.50 x 167	28	-2.50 DS
KRP RE -0.25/-0.25 x 135	20	-0.25 DS

Table 6.4 Patients used for the main Aberration controlled contact lens study.

A further nine subjects were recruited, but two subjects dropped out. They consisted of students from City University, Imperial College, and social contacts. Their details are listed in Table 6.4. Subjects were excluded from the study if their astigmatism was more than 0.5 DC, or if they had significant ocular pathology. Subjects RS, KF, JBO & KAP were contact lens wearers. The other subjects were non contact lens wearers. Their corneas were checked using the slit lamp with fluorescein to check for the absence of corneal staining. The contact lenses were allowed to settle for ten minutes before testing began. The pupil diameters tended to vary with which contact lens was worn. The +1.50 Q value lenses tended to produce the smallest pupil diameters. The Q = 0 contact lenses tended to produce the largest pupil diameters. The pupil diameters were assessed by the WASCA aberration measurements. The pupil diameters ranged from just under 4 mm to just under 7 mm.

The subjects were allowed sufficient time to rest between each test, to avoid tiredness and aid concentration. The whole series of tests would last three to four hours

altogether, and this was broken down into not testing more than two lenses at a time, under photopic and mesopic conditions as it was not practicable to test for longer than about an hour or two. The order in which the lenses were tested was randomised. Clinical notes were made on the fit of the contact lenses to ensure good centration, and non excessive lens movement occurred.

6.3.3 Main Study methods

The CAA test was used to assess visual performance. The remaining seven subjects had their aberrations measured using the Wasca wavefront analyser at City University. Minitab 13.32 and Stanford Graphics v3 was used to analyse the data.

6.3.4 Results

For six subjects, regressions were performed to show that the Q value definitely changed the spherical aberration. For most subjects the relationship was found to fit a linear model very well. In other cases the fit was less good, with merely an inverse relation being found. Noise in the measurement of aberrations may have produced the wide range of spherical aberration values for some subjects. This may have been caused by accommodation or lens movement.

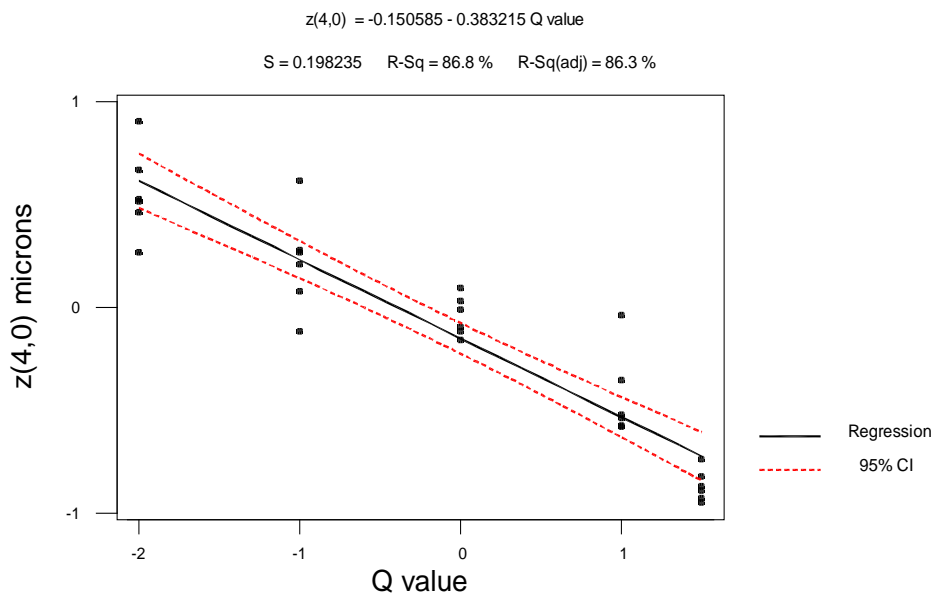


Figure 6.2 Q Value vs Z (4,0) Spherical Aberration over a 4.5 mm Pupil, for 6 subjects.

Q Value vs Zernike Spherical Aberration for 6 subjects over a 4.5 mm Pupil is shown in figure 6.2. This shows an inverse relation between Q and spherical aberration. With an adjusted R^2 of 86.3% and $P = 0$, the relationship between Q and spherical aberration is shown to be a statistically significant linear fit for these 6 subjects (subjects CG, CRT, KT, KAP, PP and RS. The inverse relationship found is actually not in line with other studies concerning Q value and spherical aberration (see discussion later).

Subjects JBO & KF dropped out of the study). It was not possible to measure aberrations over a 4.5 mm pupil for subject KRP in respect of the $Q = +1.5$ contact lenses, because the pupil size of the subject became too small when wearing the $Q = +1.5$ lenses. 4.5 mm was chosen as the aberration measurement diameter, to aim for a pupil size which would allow a relationship between spherical aberration and visual performance to be found if one existed. Ideally a larger pupil size would have been used, but this was not possible as the $Q = + 1.50$ lenses tended to reduce the pupil diameters to below 5 mm.

The Q value lenses were also found to produce changes in Z (2,0) defocus. This was due to the fact that defocus, like spherical aberration is determined by the Q value (Gatinel et al., 2004). This is similar to the effect of the circle of least confusion being shifted, as explained by Dietze & Cox, 2005.

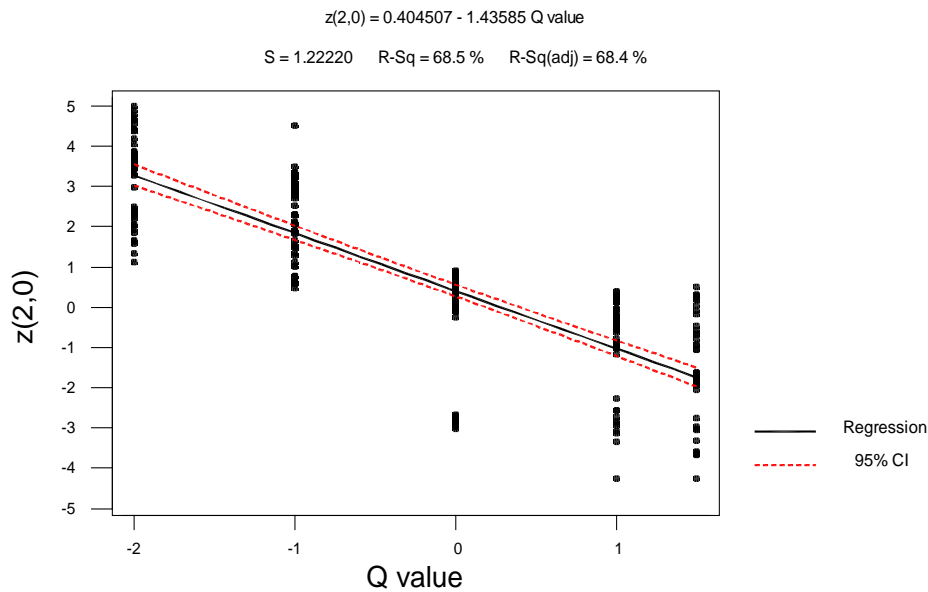


Figure 6.3 Q Value vs Z (2,0) Defocus over a 4.5 mm Pupil, for 6 subjects.

Q Value vs Zernike Defocus for 6 subjects over a 4.5 mm pupil is shown in figure 6.3. This shows an inverse relation between Q and Defocus. With an adjusted R^2 of 68.4% and $P = 0$, the relationship between Q and spherical aberration is shown to be a statistically significant linear fit for these 6 subjects (subjects CG, CRT, KT, KAP, PP and RS). As for the case with Z (4,0) spherical aberration, the inverse relationship found is actually not in line with other studies concerning Q value and spherical aberration, or defocus.

6.3.4.4 Analysis of results using Quadratic Regressions

Quadratic regressions were performed on the data. This was to examine whether positive and negative values both decreased visual performance on the CAA test. The use of a quadratic regression would also allow us to compare our results to a study performed by Parker et al., (2009), and determine a possible value for the optimal amount of spherical aberration to achieve the best or least reduced visual performance.

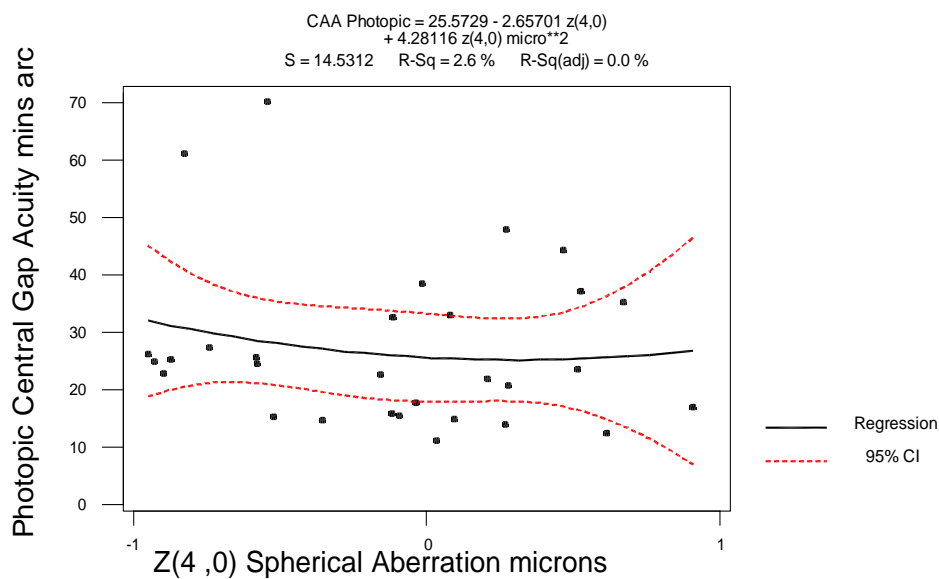


Figure 6.4: Z (4,0) Spherical Aberration (for a 4.5 mm pupil) vs Photopic Gap Acuity Quadratic Regression.

No quadratic trend is shown in figure 6.4 for photopic gap acuity versus Z (4,0) spherical aberration ($P = 0.697$, adjusted $R^2 = 0$) for 6 subjects. (The minitab regression equation was calculated to give a minimum at $Z (4,0) = +0.310 \mu\text{m}$. However the graph clearly suggests there was no significant quadratic regression.)

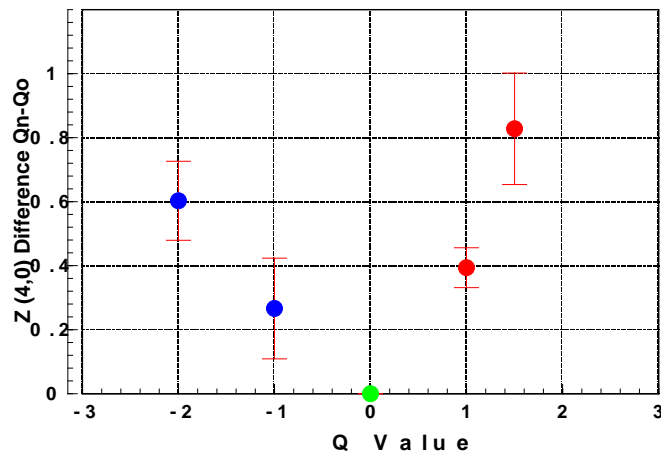


Figure 6.6 Z (4,0) Spherical Aberration Differences generated by the Q = -2 and Q = -1 Contact Lenses compared to the Q = +1.5 and Q = +1 differences. Error bars are two standard errors. (Differences are shown in absolute values.).

Figure 6.6 shows that a greater magnitude of difference for z (4,0) spherical aberration was generated by the Q = +1.5 contact lenses (($Q_{p15} - Q_o$) mean = $-0.828 \mu\text{m}$ s.e. = 0.087) compared to the Q = -2 contact lenses (($Q_{m2} - Q_o$) mean = $0.603 \mu\text{m}$ s.e. = 0.062). A greater difference of magnitude for z (4,0) spherical aberration was also generated by the Q = +1 contact lenses (($Q_{p1} - Q_o$) mean = $-0.394 \mu\text{m}$ s.e. = 0.062) compared to the Q = -1 contact lenses (($Q_{m1} - Q_o$) mean = $0.266 \mu\text{m}$ s.e. = 0.079).

It may be expected that the Q = -2 asphericity would generate more spherical aberration than a Q = +1.5 asphericity. This may suggest that the Q value lenses were mislabelled. The Q = -2 and Q = -1 lenses may have been mislabelled as the Q = +1.5 and Q = + 1 lenses and vice versa, due to an error by the manufacturer. This would then explain the negative regressions, which we would have expected to be positive, in line with the research literature (see discussion).

6.3.4.5 Regressions Against other Variables

A few other variables were also found to give significant regressions. An example of this is Seidel coma.

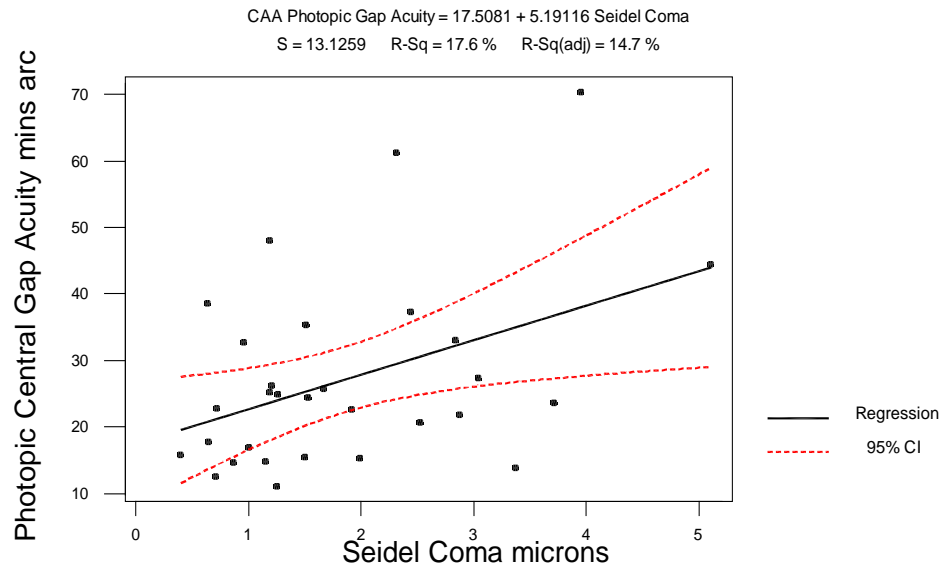


Fig 6.7 Seidel Coma for a 4.5 mm pupil vs Central Photopic Gap Acuity for six Subjects

Figure 6.7 shows Seidel coma over a 4.5 mm pupil vs central photopic gap acuity for six subjects. A significant ($P = 0.021$) positive trend is shown between increasing Seidel coma and photopic central gap acuity. The adjusted R^2 value is quite low (14.7%). This may reflect the variations between subjects in the effect of the Q value contact lenses in unintentionally generating coma. This may have contributed to the photopic spherical aberration quadratic regression curve not being a statistically significant fit to the data. This low adjusted R^2 value may be of interest as it is in line with the suggestion by Parker et al., (2009) that other aberrations could influence visual performance when using contact lenses with defined levels of spherical aberration.

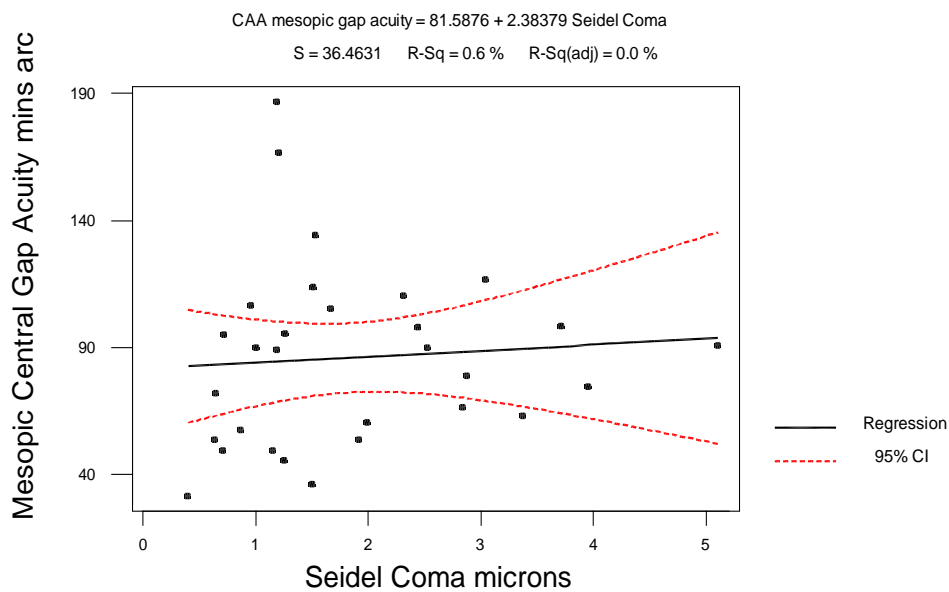


Fig 6.8 Seidel Coma vs Central Mesopic Gap Acuity for 6 Subjects

Figure 6.8 shows Seidel coma over a 4.5 mm pupil vs central mesopic gap acuity for six subjects. No statistically significant trend was found ($P = 0.689$, adjusted $R^2 = 0\%$) between increasing Seidel coma and mesopic central gap acuity.

This result goes against the trend of the spherical aberration quadratic regressions becoming more significant under mesopic conditions than under photopic conditions.

Seidel astigmatism produced a similar statistically significant positive linear regression under photopic conditions. This is shown in appendix 2.

6.3.4.6 Q Value lenses vs CAA Test Performance

The main findings were that the larger the Q values or spherical aberration, the less good was the performance on the CAA test.

Overall the individual results provided a mixture of outcomes. The plano Q value lens usually gave the best results. Which lenses then followed varied. The mesopic graphs appeared to be flatter or more raised centrally. Sometimes there was a lot of overlapping of the graphs. Occasionally, contact lenses of higher Q values gave better results than contact lenses of lower Q value. Sometimes the positive Q value lenses provided better results than the minus Q value lenses, or the reverse occurred.

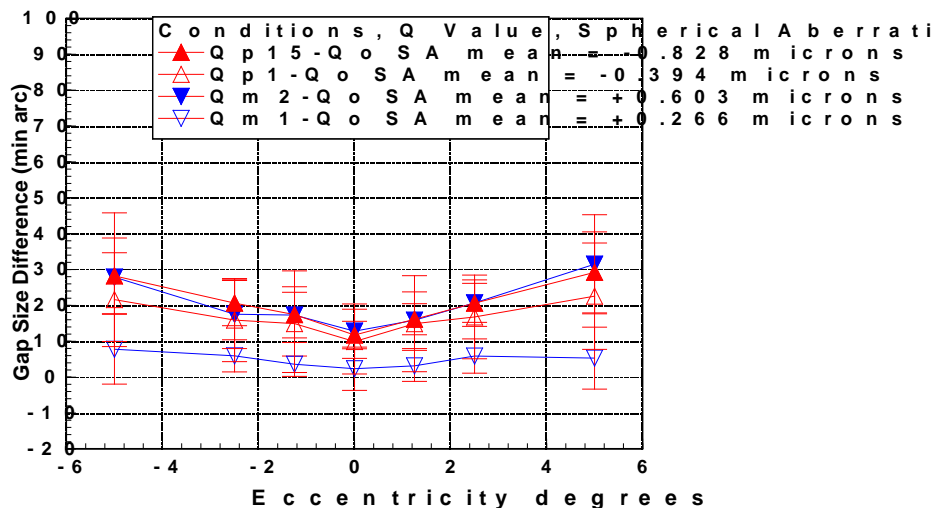


Figure 6.9 Main Study Photopic Gap Size Differences Error bars are 2 standard errors.

The photopic results for seven subjects are shown in figure 6.9. Gap size difference means of the seven subjects (subjects CG, CRT, KAP, KRP, KT, PP and RS) are shown and the error bars show two standard errors. The average Z (4,0) spherical aberration difference is also shown over a 4.5 mm pupil in the legend for six subjects (subjects CG, CRT, KAP, KT, PP and RS).

The Q = -1 lenses produced by far the least differences. The Q = + 1 lenses produced the next least differences. There appears to be a slight trend of the gap differences

being greater at the peripheral points instead of at the central points. The $Q = -2$ lenses and $Q = +1.5$ lenses produced fairly similar gap size differences.

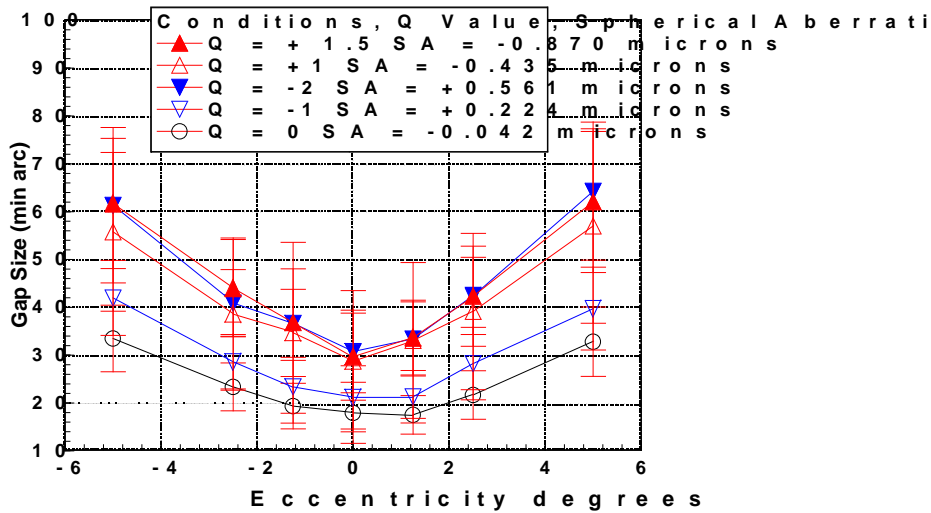


Figure 6.10 . Photopic Gap acuities for the $Q = -2, -1, 0, +1, +1.5$ lenses for Seven Subjects. Error bars are 2 standard errors.

Photopic Gap acuities for the $Q = -2, -1, 0, +1, +1.5$ lenses for seven subjects are shown in figure 6.10. Mean gap acuities of the seven subjects (subjects CG, CRT, KAP, KRP, KT, PP and RS) are shown and the error bars show two standard errors. The average Z (4,0) spherical aberration is also shown over a 4.5 mm pupil in the legend for six subjects (subjects CG, CRT, KAP, KT, PP and RS).

Overall the +1.5 and -2 Q value lenses gave the most elevated gap acuities. However the +1 Q value gap acuities were almost as elevated. The $Q = 0$ gap acuities were the smallest, and the $Q = -1$ gap acuities were also markedly better than the $Q = -2, +1.5$ and +1 Q value acuities.

Generally, under mesopic conditions, the greater the Q value, the more elevated were the gap acuity thresholds, but exceptions to this general trend often occurred.

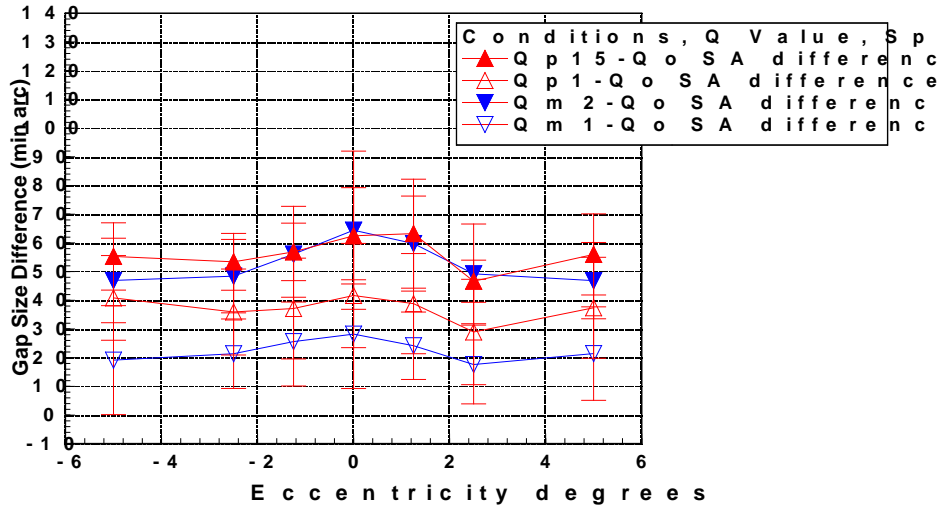


Figure 6.11 Main Study Mesopic Gap Size Differences Error bars are 2 standard errors.

Figure 6.11 shows the mesopic gap size difference results for 7 subjects. The Q = -1 lenses again produced the least differences followed by the Q = +1 lenses. The Q = +1.50 and Q = -2 lenses produced the greatest gap size differences. In contrast to the photopic results, the central points yielded greater gap acuity differences than the peripheral points.

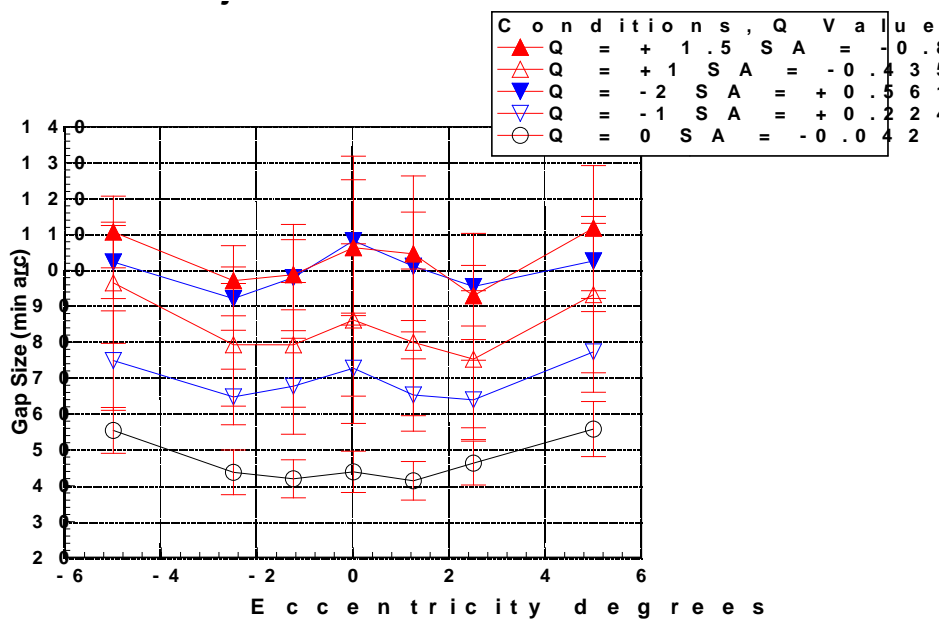


Figure 6.12 Mesopic Gap acuities for the $Q = -2, -1, 0, +1, +1.5$ lenses for Seven Subjects. Error bars are 2 standard errors.

Mesopic Gap acuities for the $Q = -2, -1, 0, +1, +1.5$ lenses for the same seven subjects are shown in figure 6.12. Mean gap acuities of the seven subjects (subjects CG, CRT, KAP, KRP, KT, PP and RS) are shown and the error bars show two standard errors. The average Z (4,0) spherical aberration is also shown, over a 4.5 mm pupil in the legend for six subjects (subjects CG, CRT, KAP, KT, PP and RS).

Overall the +1.5 and -2 Q value lenses gave the most elevated gap acuities. Unlike the photopic results, the +1 Q value gap acuities appear to be distinctly better than the $Q = +1.5$ and $Q = -2$ value results. The $Q = 0$ gap acuities were the smallest, and the $Q = -1$ gap acuities were also markedly better than the $Q = -2, +1.5$ and $+1$ Q value acuities. The central points appear to be more elevated than the 1.25 and 2.5 peripheral points, especially for the larger Q values. This may suggest that the central area became more sensitive to the effects of aberrations under mesopic conditions. This may help to explain why the foveal dip was larger under mesopic conditions.

Overall the results shown in figures 6.11 & 6.12 suggest that the plus Q (+1.00 and +1.50) value contact lenses generated negative spherical aberration which affected the subjects' CAA test results by a greater amount, compared to the positive spherical aberration generated by the negative Q (-1 and -2) value lenses.

This may be partly explained by examining the differences in magnitude of the spherical aberration generated by the $Q = -2$ and $Q = -1$ lenses, compared to the $Q = +1.5$ and $Q = +1$ lenses (figure 6.5).

6.4 Discussion

6.4.1 Q Value vs Spherical Aberration and Defocus.

Our results gave a negative relationship between Q value and spherical aberration. However other researchers have found a positive relationship between Q value and spherical aberration, in agreement with what would be expected theoretically. For instance, Mastropasqua et al., (2006) analyzed ocular wavefront error and corneal asphericity (Q) in patients treated with aspheric PRK and conventional PRK to correct myopia and myopic astigmatism. A positive correlation was found between increasing Q value and spherical aberration. The WASCA aberrometer was used to measure the spherical aberration. Tuan & Chernyak (2006) found similar results when studying LASIK patients, using a VISX aberrometer.

Similarly Calossi (2007) produced a conversion chart for corneal asphericity notations with the corresponding spherical aberration, which showed Q value to be positively correlated with spherical aberration.

This suggests that the negative relationship between our Q values and spherical aberration may have been due to the contact lens manufacturer specifying their Q values with a sign change. This sign change may have occurred due to the software being used by the contact lens manufacturer. Alternatively, it may be that the manufacturer mislabelled the contact lenses, or that our particular WASCA software induced a sign change in the measurement of spherical aberration.

Similarly the Q value contact lenses changed the Z (2, 0) defocus term in a similar way to the Z (4,0) term, since Z (4,0) and Z (2,0) are linked,mathematically. We did not compensate for this change in contrast as did other researchers such as Li et al., (2009), because our aim was to keep the Q value as the only parameter that was changed from one experiment to the next.

6.4.2 CAA Test Results: Q value vs Visual Performance

Our results showed definite trends of increasing Q values leading to increased contrast acuity levels under photopic and mesopic conditions. Furthermore, only under mesopic conditions, with the presence of non physiological amounts of spherical

aberration, slightly greater differences in CAA test visual performance at the central zero fixation point were produced compared to the peripheral points (figures 6.8-6.11). This suggests that natural aberrations would probably be unable to reduce CAA test results centrally rather than peripherally to produce a foveal dip.

Our results may be compared to refractive surgery studies in which corneal asphericity has been studied in conjunction with visual performance. These studies on Q value versus visual performance were however based on direct measures of corneal asphericity, whilst our Q values were based on the contact lens Q values. Therefore these studies may not be directly comparable to ours.

Various researchers have found a mixture of results, concerning Q value and visual performance. For instance, Ang et al., (2009) compared two groups of eyes, which underwent LASIK, an aspheric group with significantly lower Q values and a control group. The control group had higher positive Q values after refractive surgery (0.682 s.d. 0.417 compared to 0.163 s.d. 0.277 over a 5 mm pupil). The aspheric group comprised 86 eyes and the control group, 84 eyes. Although high- and low-contrast corrected distance visual acuity (CDVA) was similar between the groups, the aspheric group gained more lines of low-contrast CDVA.

Mastropasqua et al., (2006) analyzed corneal asphericity (Q) and visual performance in patients treated with an aspheric photorefractive keratectomy profile and compared their results to patients having conventional PRK to correct myopia and myopic astigmatism. They found that their measures of mean high-contrast best corrected VA and low contrast VA revealed less good visual performance with the conventionally corrected PRK group which had higher positive Q values. Their Logmar results are in line with our CAA test results of higher Q values leading to decreases in performance. The aspheric profile PRK group showed more prolate corneal asphericities (mean Q of 0.15 ± 0.26) than the conventional group (mean Q of 0.45 ± 0.26), with increasing oblateness for higher attempted corrections. It may be noted that the range of Q values found in Mastropasqua et al., (2006)'s study (mean Q of 0.45 ± 0.26) and Ang et al., (2009)'s study was below that of the +1 and +1.5 Q values used in our CAA tests. The number of subjects used were larger in these studies, which may explain

why statistically significant results for acuity were found for lower Q values. In the Ang et al., (2009) study, the aspheric group comprised 86 eyes and the control group, 84 eyes. In the Mastropasqua et al., (2006) study, 50 eyes were treated with aspheric profile PRK, and 24 eyes were treated with standard PRK. The tests using Logmar acuity charts were also different to our Landolt ring based CAA tests.

Anera et al., (2003) analyzed the effect of postsurgery asphericity on contrast-sensitivity function (CSF) under photopic conditions. CSF measurements were found to have deteriorated after LASIK. This deterioration was attributed to the effect of increasing corneal asphericity. The p factors post op ranged from +0.91 to +2.04 which are equivalent to Q values from -0.09 to +1.04. Anera (2003)'s study was based on measuring the CSF whilst our study was based on the CAA test, so his study is not directly comparable to ours. Different luminance conditions were also used in his study.

The results with our negative Q value aberration controlled contact lenses may be compared with Chen et al., (2002)'s results for 23 hyperopic subjects who were originally prolate. Their post op asphericities became more prolate by up to -2 to give a range of Q values of 0 to -2.5. No relationship was found between Q values and visual performance. A factor which may have caused the results to differ, was the use of Snellen charts by Chen et al., (2002).

Similarly low post op Q values and good visual outcomes have been reported by Koller et al., (2006). Post op Q values of $+0.47 \pm 0.46$ for wavefront guided LASIK and $+0.50 \pm 0.49$ for Custom Q LASIK (LASIK aiming for an optimal Q value) resulted in insignificant postoperative changes in glare acuity and low-contrast acuity. However this study was aimed more at assessing differences between surgical techniques rather than relating Q values to visual performance. This study found similar post op Q values to the Holladay et al., (1999) study, and yet no significant changes in visual performance were found.

Holladay et al., (1999) performed corneal topography on post op myopic LASIK patients and found that all corneas became oblate after LASIK to a mean Q-value of -0.47 ± 0.40 . Low contrast VA (13%) at low illumination levels produced the largest decreases in visual performance. The decrease in visual performance was attributed to the oblate corneas rather than corneal micro irregularities, because visual acuity was most affected under dark conditions, which induced large pupil sizes, which would allow the oblateness to have more effect.

In line with Holladay et al., (1999), Budak et al., (1999) examined computerized videokeratographs of emmetropic, myopic, and hyperopic eyes and found that corneal Q-values lower than -0.3 were associated with reduced optical performance of the cornea.

Various researchers have put forward reasons for why negative asphericity should decrease visual performance. For instance, Santos et al., (1987) attributed the loss of one or two lines of best corrected visual acuity in the Prospective Evaluation of Radial Keratotomy (PERK) study to the large blur circle created by negative asphericity. Applegate & Gansel (1990) concluded that negative aspheric radial keratotomy corneas create significant image aberration.

It should be noted that since the signs of our Q value lenses may have been reversed, e.g. due to the contact lens manufacturer software, our conclusions concerning Q value and visual performance may be similar, but with the Q values reversed in sign.

6.4.3 Spherical Aberration and Visual Performance.

The negative Q value lenses tended to produce positive spherical aberration which affected the CAA test results less than the positive Q value lenses. This may be partly due to less positive spherical aberration being generated by the $Q = -2$ and $Q = -1$ lenses. This may also have occurred because positive spherical aberration is present in most subjects naturally. Therefore the subjects may be less affected by positive spherical aberration, than by negative spherical aberration.

The smaller pupil size under photopic conditions may have also contributed to the finding of no statistically significant relationship being found between the CAA test photopic results and spherical aberration. This would be in line with the results of Su & Hu (2009), who found that although, compared to conventional spherical IOLs, aspheric IOLs significantly reduced total ocular and spherical aberration, this did not result in better contrast acuity under mesopic or photopic conditions. The researchers suggested that the small pupil size observed under the test conditions may have been a factor, which limited the beneficial effect of aspheric IOLs on visual performance.

In line with this, Tuan & Chernyak (2006) made the observation that Q value is more closely correlated with mesopic spherical aberration rather than photopic spherical aberration. (Mesopic spherical aberration was taken to be spherical aberrations corrected for mesopic pupil size, and photopic spherical aberration was taken to be spherical aberration corrected for photopic pupil size).

The research literature has found that higher levels of spherical aberration may reduce visual performance. However, researchers have also suggested that small amounts of spherical aberration can improve visual performance.

Fleming (1993) has put forward theoretical reasons for why spherical aberration may improve or decrease visual performance in his radial keratotomy patients. Fleming (1993) suggested that negative asphericities of radial keratotomy patients could cause vision to deteriorate by creating a defocusing effect by increasing the blur circle due to aberrations. However this could sometimes be overcome by the depth of field being increased due to undercorrected spherical aberration, or by the retina intercepting a caustic shape induced by high levels of negative asphericity at a favourable position. These various theoretical effects of spherical aberration may help to explain why the aberration controlled contact lenses had various effects on the CAA test results.

Optical aberrations also reduce image contrast and induce spatial phase shifts in the retinal image. Ravikumar et al., (2010) studied the effects of spatial phase shifts on object recognition, by simulating image blur computationally for defocus,

astigmatism, coma, and spherical aberration. It was found that in the presence of positive spherical aberration, acuity loss due to phase errors was more for hyperopic defocus than for myopic defocus, because the contrast of phase-reversed components was much higher for hyperopic defocus. 180° phase shifts were found to reduce visual acuity, whereas those with a phase shift of less than 180° (coma, for example) had less effect. These different interactions may also help to explain the variability in our results.

Our significant mesopic spherical aberration results are broadly in line with the findings of Applegate, Ballentine et al., (2003) who found linear relationships to exist between various Zernike modes and visual performance measured on high and low contrast aberrated LogMAR charts. Z(4,0) at low contrast gave the best linear fit. However these tests were performed under photopic conditions, on three subjects, with dilated pupils and 3 mm artificial pupils, with Chart illumination maintained at 100 cd/m². This may be contrasted to our conditions of natural pupils being used under mesopic (0.05 cd/m² background light level) and photopic conditions (background light level of 12 cd/m²), and our spherical aberration values ranged more widely from -0.870 (s.e. 0.063) μm to +0.561 (s.e. 0.175) μm, for a 4.5 mm pupil.

Tanabe et al., (2004) have also found a significant correlation between visual performance and spherical-like aberrations. However they used the root-mean-square of fourth-order Zernike components (Z_4^{-4} to Z_4^4) over a 4 mm pupil to represent spherical-like aberrations and the logarithm of the minimal angle of resolution low contrast VA was used to measure visual performance.

Our significant z (4,0) spherical aberration mesopic visual performance results are also broadly in line with Applegate et al., (1998) who quantified in radial keratotomy patients, the area under the log contrast sensitivity function (AULCSF) and corneal first surface wavefront variance for two artificial pupil sizes (3 and 7 mm). Radial keratotomy was found to have induced an increase in the optical aberrations of the eye and the increase for large pupils (7 mm) was found to be correlated to a decrease in contrast sensitivity. Radial keratotomy was found to shift the distribution of aberrations from third order dominance (coma-like aberrations) to fourth order

dominance (spherical-like aberrations). Therefore the changes found could resemble the increased spherical aberration generated by our Q value contact lenses.

More recently, Li et al., (2009) used adaptive optics to find that when all aberrations were corrected, a decrease in visual acuity occurred when enough positive or negative spherical aberration was induced. Their results are in line with our significant mesopic spherical aberration CAA test quadratic regression result. Similarly to our experiments, black Landolt C optotypes under a staircase method were used to test visual acuity. However, their study differs in that they used adaptive optics to induce more exact amounts of spherical aberration, whilst in our study the amount of spherical aberration induced varied between the subjects. Also, their acuity tests were performed under green light, with 6 mm artificial pupils, with dilation and cycloplegia. All their procedures were performed after defocus and astigmatism were corrected using trial lenses. Decentration could have led to astigmatism and coma being induced by the Q value contact lenses. This would have been less likely to be produced by the adaptive optics system when generating spherical aberration, due to its greater accuracy in alignment.

Some researchers have sometimes found no statistically significant differences when examining refractive surgery subjects in respect of the link between spherical aberration and visual performance. For instance, Alio et al., (2008) examined the aberrations for patients who had undergone Excimer laser surgery for hypermetropia. The primary spherical aberration coefficient $Z(4,0)$ was found to have changed from positive to negative values. Objective visual quality, as measured by the point spread function and strehl ratio was found to have not been significantly affected. The spherical aberration in their study was measured over a 6 mm pupil so their results are difficult to compare with our 4.5 mm spherical aberration results for the Q value contact lenses. No statistically significant results were found between spherical aberration and visual performance.

Small amounts of spherical aberration have been shown to improve visual performance, in support of Fleming (1993)'s theories. Parker et al., (2009) examined the effect of defined levels of spherical aberration induced with wavefront guided soft contact lenses and their effect on logMAR high contrast visual performance on twelve

subjects. Their results showed that the subjects' best logMAR high contrast VA occurred with the presence of positive residual spherical aberration. This may be in line with our $Q = -1$ contact lens results which produced small amounts of positive spherical aberration, together with relatively good CAA test visual performance results (see figures 6.3-6.6). Parker et al., (2009) found high contrast visual performance worsened with greater amounts of positive or negative spherical aberration and a quadratic fit to the data peaked at +0.209 mm.

Our results for the photopic data gave a peak photopic acuity for $z(4,0)$ of $0.310 \mu\text{m}$ over a 4.5 mm pupil. However the minitab graph clearly suggested there was no significant quadratic regression. In contrast to this, under mesopic conditions the minimum CAA gap acuity occurred at $Z(4,0) = -0.013 \mu\text{m}$.

Parker et al., (2009) suggested that lens movement and decentration may have influenced the results, and that spherical aberration was not the only aberration influencing visual performance, or the higher order aberrations induced. Decentration can lead to coma and astigmatism being induced. This is in line with our finding of Seidel coma and Seidel astigmatism producing significant regressions under photopic conditions. Parker et al., (2009) used mydriatic drops combined with artificial 6 mm pupils under photopic conditions, with high contrast logmar charts. This differs from our use of natural pupils with the CAA test and our use of low contrast landolt rings, under mesopic and photopic conditions. Their results were quite variable in line with our results for different individual subjects.

Similarly, Nochez et al., (2011) evaluated 54 eyes which underwent cataract surgery with aspheric IOL implantation. A final target ocular spherical aberration between $0.07 \mu\text{m}$ and $0.10 \mu\text{m}$ was considered to be the best compromise between subjective depth of focus and objective contrast sensitivity. Their findings reinforced the theory that some residual total ocular spherical aberration was a better choice for enhancing the quality of vision.

Wang & Koch (2007) also found that most eyes achieved the best image quality with a small amount of residual ocular 4th-order spherical aberration, when trying to

optimise intraocular lens asphericity. However the optimal spherical aberration varied widely between subjects and their calculations were theoretical.

Other researchers on the other hand, in contrast to Parker et al., (2009) have found that small amounts of negative spherical aberration can improve visual performance. For instance, Rae et al., (2009) performed experiments with customised spherical aberration controlled soft contact lenses. High and low contrast acuities were found to be significantly better in the group wearing the contact lenses with negative spherical aberration. Similarly, Legras et al., (2004) measured the amount of aberration required to produce a just-noticeable blur and found that optimal clarity was achieved by adding a small negative amount of spherical aberration.

Our results differ from other studies, which corrected for defocus and cylinder after spherical aberration had been induced. This may be expected to affect the results. Rae et al., (2009) pointed out that if the focus was non-optimal, reduced visual acuity may be expected and changing the sign of the spherical aberration would be expected to optimise focus and hence retinal image quality and visual acuity. Similarly Rae et al., (2009) suggested that controlled amounts of negative spherical aberration may be beneficial in spherical soft contact lens wearers with larger cylinders and/or larger pupils.

6.4.4 Coma and CAA Test results.

In our studies, a statistically significant result was found showing that Seidel coma affected the CAA test results under photopic conditions. Other studies have also found relationships between coma and visual performance, but usually they have measured coma using the Zernike polynomials. For instance, Fernandez-Sanchez et al., (2008), investigated the effect of 3rd order aberrations on subjects wearing contact lenses with a 5.0 mm artificial pupil. Coma and trefoil were induced with purpose designed soft contact lenses. A significant reduction in high contrast VA and low contrast VA was found only for their highest coma and trefoil values of around 1 μm . These results are not directly comparable to our Seidel coma results as Seidel coma is computed differently to the Zernike coma values. The test of VA involved letter charts in contrast to our Landolt rings. Artificial 5 mm pupils were used in contrast to the use of natural pupils in our study with the CAA test.

De Gracia et al., (2011) examined 20 patients with different amounts of coma added to 0.5 D of astigmatism. Adding coma (0.23 μm for a 6 mm pupil) to astigmatism resulted in a clear increase of VA in 6 subjects, consistent with theoretical optical predictions, while VA decreased when coma was added to astigmatism in 7 subjects. The effects were related to the presence of natural astigmatism and whether this was habitually corrected or uncorrected. The expected performance occurred mainly in eyes with no natural astigmatism. This led the researchers to suggest that relevant neural adaptation effects in eyes normally exposed to astigmatic blur had influenced the results.

Rouger et al., (2010) used adaptive optics to simulate seven levels of Zernike coma aberrations in four subjects. High and low contrast Landolt ring acuity and contrast sensitivity were found to be reduced by the different Zernike coma modes. This is broadly in line with our Seidel coma results.

Our coma results are also broadly in line with the results of Oshika et al., (2006) who found that coma-like aberration measured over a 4 mm pupil, showed a significant correlation with low-contrast VA. The root-mean-square of the third-order Zernike coefficients was used to represent comalike aberrations (whilst we used Seidel coma to represent such aberrations). 10% Logmar charts were used to measure low contrast VA.

Coma in refractive surgery is normally associated with decentration of the ablation in keratorefractive procedures, even at subclinical levels. Alio et al., (2008) also suggested that the peripheral ablation of hyperopic procedures is more sensitive to subtle levels of decentration and could be a factor in the aberrations seen in this type of surgery. This is in line with our Q value contact lenses which appeared to generate coma, even though the intention was just to generate spherical aberration.

The results of Applegate et al., (2000) may also illustrate that coma can influence visual performance. Corneas with increased wavefront variance showed a decrease in visual performance. Their sample of patients included many patients with large

asymmetric aberrations (coma-like aberrations), in contrast to studies, which had concentrated on refractive surgery patients who had increased spherical-like symmetric aberrations.

Applegate et al., (2000) speculated that rotationally symmetrical aberration may be more forgiving in terms of the adverse influence on visual images, whereas rotationally asymmetrical aberration (i.e., third-order comalike aberration) causes greater degradation of visual images. This may be contrasted to De Gracia et al., (2011)'s research which suggested that 180° phase shifts caused by spherical aberration degraded the image more than coma, where the phase shift was less than 180°.

Data from research on wave-guided versus non wave-guided refractive surgery can also be used to illustrate the influence of coma on visual performance which supports our significant Seidel coma results. For instance, Zhang et al., (2008) compared the visual acuity, higher-order aberration, and contrast sensitivity of wavefront-guided LASIK with iris-registration in 94 eyes and conventional LASIK in 117 eyes. They found that the increase of coma aberration in the wavefront-guided LASIK group was significantly lower than that in the conventional group. They suggested that this may explain why there was an improvement of visual performance and contrast sensitivity in the wavefront-guided LASIK iris registration group compared to the conventional group. In this study coma was represented by the RMS of 3rd order coma – the square root of the sum of the squared coefficients of Z_3^{-1} and Z_3^{+1} .

Their results are also not directly comparable to our results due to the different pupil sizes used to measure the aberrations. The aberrations for our Q value subjects were measured over a 4.5 mm pupil, whilst the aberrations for the Zhang et al., (2008) study were measured over a 6 mm pupil.

6.4.6 Contact Lens advantages for aberration generation:

Rae et al., (2009) pointed out that contact lenses have advantages for the correction of higher order aberrations over spectacle lenses because of the maintained alignment with the optical axis on eye movement away from primary gaze.

One of the aims of our study was to simulate the changes in corneal shape or spherical aberration produced by refractive surgery, by using aberration controlled soft contact lenses with various Q values. The advantages of using a conic section are that, in the normal population, it is a good approximation. It is also mathematically simple with just a single value representing the departure of the surface from a spherical shape.

6.5 Limitations of the study with Aberration Controlled contact lenses

6.5.1 Movement and Centration

Limitations in the potential benefits of aberration correction with contact lenses exist due to lens movement and centration (Guirao et al., 2001). This may lead to increased coma or astigmatism.

6.5.2 Adaptation

Other studies (e.g. Artal et al., 2004) indicate that the nervous system compensates for previous aberrations and that the human brain adapts to the eye's natural aberrations. Therefore this is a limitation of our aberration controlled contact lens study, as our study did not allow for adaptation.

6.5.3 Binocularity

An aspect that was not covered by our research was the influence of aberrations on binocular visual performance. For instance, Jiménez et al., (2008) analyzed the influence of higher order aberrations on binocular visual performance under mesopic conditions, on 35 emmetropic observers with a Wasca aberrometer. It was found that binocular summation and maximum disparity significantly decreased with increasing interocular differences in higher order aberrations (total, coma, and spherical aberration).

6.5.4 Corneal Modelling

A disadvantage of using a conic section for contact lenses to model the cornea is that these contact lenses would not completely reflect all changes as the profile of the cornea may be more complicated than the profile induced by the soft contact lenses. Gonzalez-Méijome et al., (2007) assessed anterior corneal Q values with different

corneal diameters and compared them with values assessed by a commercial videokeratoscope. Statistically significant differences in Q values were found with different reference points from the central cornea, demonstrating that a single conic shape assuming a constant Q value does not always account for the actual corneal shape. They suggested that the corneal flattening ratio changes as one goes from the central cornea in an almost linear fashion, with the cornea becoming more prolate as the corneal diameter increases.

Many studies have almost invariably assumed that the corneal profile can be approximated by a conic section, with a single Q value (e.g. Kiely, 1982; Guillon, 1986). Although this is sufficient over most of the cornea it cannot model the rapid change in curvature that occurs towards the limbus without the addition of higher-order aspheric terms (Hull 1999). In addition, this method must be restricted to individual meridians so that astigmatic corneas are modelled correctly (a conventional conicoid is rotationally symmetric).

Corneal astigmatism was also not simulated by our aberration controlled contact lenses. Gonzales-Méijome et al., (2007) have found that this also changed Q values at different corneal diameters. Budak (1999) made similar observations to explain why their Q values were slightly different to others findings due to their Q values being measured for a 4.5 mm diameter.

6.6 Conclusion

Under photopic conditions the Q value contact lenses gave no statistically significant differences compared to the mesopic conditions for regressions of spherical aberration versus central CAA gap acuity. Spherical aberration versus CAA gap acuity produced a statistically significant quadratic regression under mesopic conditions. Other aberrations such as Seidel coma also produced significant regressions under photopic conditions. The smaller pupil size under photopic conditions may have lead to spherical aberration not influencing the photopic CAA test significantly, allowing other aberrations such as Seidel coma to influence results instead. Under mesopic conditions, the enlarged pupil size may have allowed the CAA test to be influenced by

spherical aberration. This confirms the CAA test is capable of picking up changes under mesopic conditions, due to increased non-physiological spherical aberration. This suggests that aberrations were unlikely to have played a major role in producing the CAA test foveal dip, because only non-physiological amounts of aberrations, under mesopic conditions, reduced CAA test performance in the central compared to the peripheral areas.

Chapter Seven

7. Scatter and Visual Performance

7.1.1 Introduction.

Apart from diffraction, the two main optical effects that can decrease visual performance are aberrations and scatter. The effect of aberrations has been covered in Chapter 5 and 6. Within the normal eye, there are four major sources that contribute to the total amount of straylight: the cornea, the iris and sclera, the lens, and the fundus (Weale, 1986, Vos & Bouman, 1964). Contact lenses can provide an additional source of scatter. In this chapter the effects of scatter were investigated to determine whether it could lead to an increased foveal dip or whether it could be correlated to an increase in spherical aberration. There are various methods of measuring scatter as outlined in Chapter 2. The City University Scatter Test was used to see if trends could be found between scatter and the CAA test, spherical aberrations and the effect of pupil size.

7.2 Subjects

Eleven of the subjects in the group who performed the CAA test in Chapter 5 were also measured for scatter with the City University Scatter test. Graphs were plotted to see if there was a relationship between k' and the foveal dip. The subjects details are listed in Table 7.1..

Subject	Age	Refractive Error	Dominant Eye
CL	38	-2.00 DS	Right
KH	23	-1.00 /-0.50 x 94	Right
LDS	29	+2.75 /-1.00 x 170	Right
LW	30	-4.25 /-1.00 x 7	Right
JOB	23	+0.25 DS	Right
SC	24	-4.50 /-1.00 x 27	Right
PM	37	-0.50 /-0.25 x 63	Left
RY	35	-3.75 DS	Right
STG	23	-1.50 /-4.00 x 15	Left
SIG	45	+0.50 /-1.00 x 32.5	Left
AD	26	+2.00 /-2.00 x 163	Left

Table 7.1 Subjects used for the Scatter versus CAA Test Study.

Subjects CL, LDS, LW, PM & RY had all had previous experience of psychophysical testing through being City University staff or students. Subjects KH, JOB, SC, STG, SIG & AD had no previous experience of psychophysical testing. Subjects LW, RY, SC & STG were part-time contact lens wearers. The other subjects were non contact lens wearers

Scatter was measured on 4 subjects, dilated with 2.5% phenylephrine using 6 mm and 3 mm artificial pupils. The aim was to determine whether changes in pupil size could lead to increased scatter, which could in turn cause an increased foveal dip.

The subjects details are listed in Table 7.2.

Subject	Age	Refractive Error	Dominant Eye
MS	21	plano / -0.25 x 172	Right
SL	28	-0.75/-0.75 x 90	Right
JLB	49	-0.50 DS	Right
LDS	29	+2.75/-1.00 x 170	Right

Table 7.2 Subjects used for the Scatter versus Pupil Size Study.

All the subjects had had previous experience of psychophysical testing through being City University staff or students. None of the subjects were contact lens wearers.

Scatter was measured on 3 subjects using 5 different Q values of contact lenses, to see if the aberration controlled contact lenses affected scatter. The subjects' details are listed in Table 7.3.

Subject	Age	Refractive Error	Dominant Eye
CG	26	-1.25 DS	Right
CT	25	+0.25/-0.25 x 45	Left
KRP	20	-0.25/-0.25 x 135	Right

Table 7.3 Subjects used for the Scatter versus Q Value Study.

All the subjects had had previous experience of psychophysical testing through being City University staff or students. None of the subjects were contact lens wearers.

A further two subjects complaining of glare / dry eyes / photophobia (one of whom had an intraocular lens implant) were assessed for scatter. These were previously untested subjects. Their results were compared to the pupil size, normal subject and aberration controlled contact lens results. The subjects' details are listed in Table 7.4.

Subject	Age	Refractive Error	Dominant Eye
LH	45	R +1.50 / -0.50 X 170 L + 0.50 / -2.00 x 168 Add + 1.00	Right (both eyes tested)
PG	41	+0.25 DS	Right

Table 7.4 Subjects used for the Scatter Study concerning abnormal conditions.

Neither subject had previous experience of psychophysical testing and they were not contact lens wearers.

7.32 Methods

The measurement of scattered light was made using the flicker compensation technique. The luminance of a large scattering annulus was modulated sinusoidally and this produced scattered light over the image of the test target on the retina. This was located in the centre of the annulus, (see figure 7.1). The luminance of the test target on the screen was then modulated in counterphase so as to cause the same modulation in the retinal illuminance of the image of the target. This is illustrated in figure 7.2, which shows how the sinusoidal modulation of the screen luminance cancels out the temporal modulation caused by the scattered light. When the retinal illuminance of the test target caused by scattered light equalled that caused by the temporal modulation of the screen luminance, little or no flicker was perceived. The screen luminance of the test target at minimum flicker was therefore a measure of the retinal illuminance caused by scattered light for that annulus and eccentricity. The process was then repeated for a range of annulus sizes.

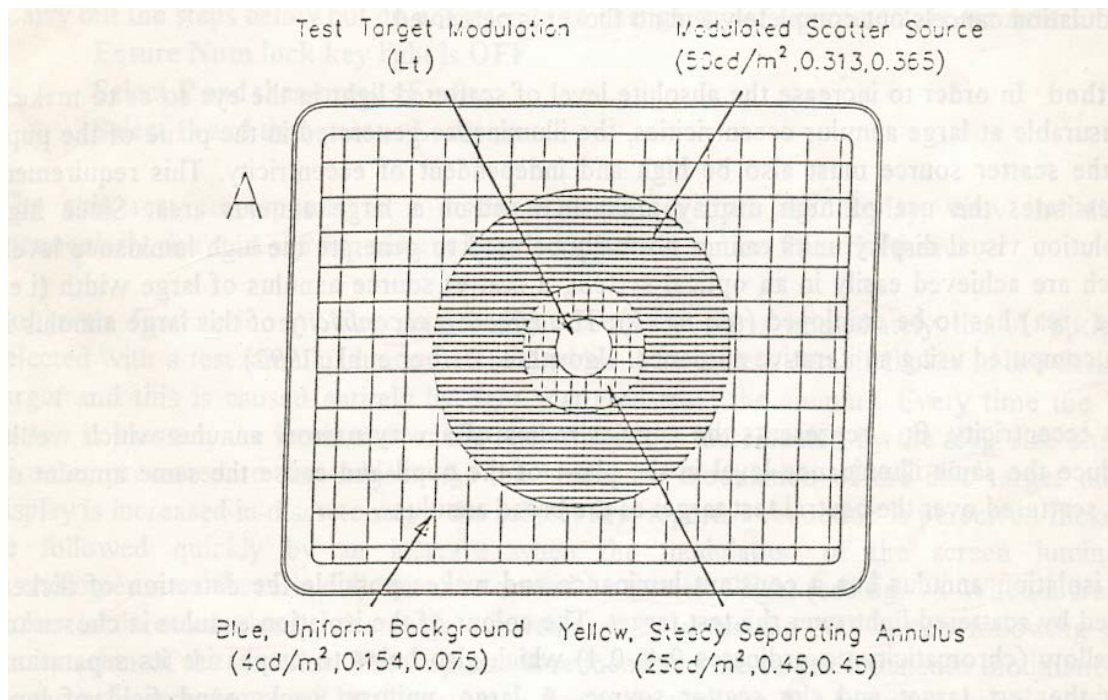


Figure 7.1. Schematic diagram showing the stimulus arrangement for the light scatter test.

The light scatter test made use of a high-resolution display monitor, driven by a 60 Hz, non-interlaced graphics adapter with a resolution of 1280 x 1024 pixels and has been described before (Hennelly 2000, Kvensakul 2005, Chisholm 2003). A chin/forehead rest was provided for the positioning of the subject's head. The viewing distance used was 50 cm and the remaining parameters appropriate for use with this display were stored as default settings in the scatter program. In order to maintain good control of phosphor luminances, the maximum luminance of the display for white light (i.e., chromaticity co-ordinates, $x = 0.305$, $y = 0.323$) was limited to 100cd/m^2 . The technique employed worked by measuring the luminance of an external stimulus, which generated the same retinal illuminance as that caused by the scattering source. The scatter program measurement was taken when the subject observed little or no flicker in the central annulus and pressed the 'GO' response button on a response box.

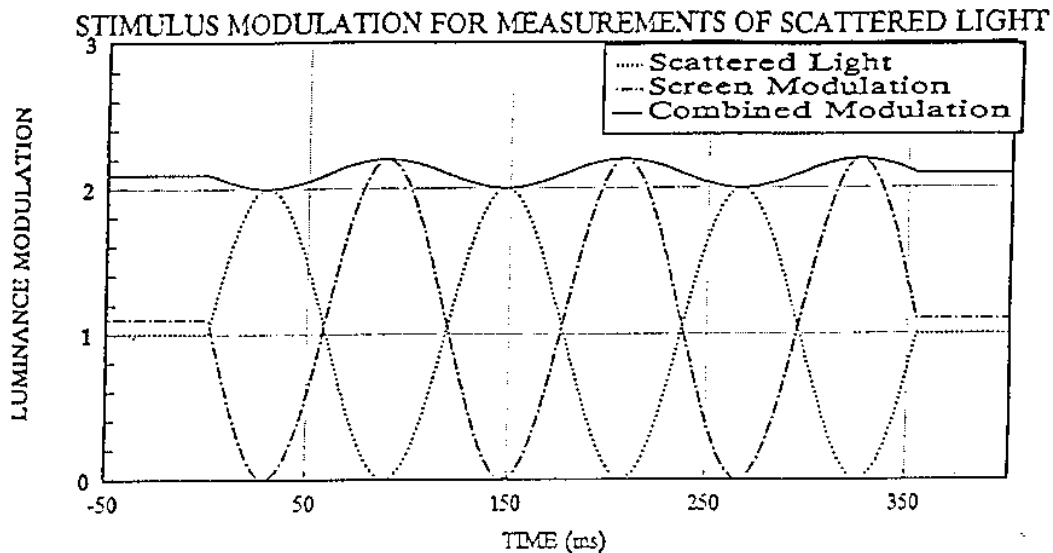


Figure 7.2. Illustration of the sinusoidal modulation of retinal illuminance over the central test target caused by light scattered from the modulated annulus and its compensation, achieved by counterphase modulation of the screen luminance (Barbur & Goodbody, 1995).

In order to increase the absolute level of scattered light in the eye so as to make it measurable at large annulus eccentricities, the illuminance generated in the plane of the pupil by the scatter source also had to be high and independent of eccentricity. This requirement necessitated the use of a high display luminance and/or a large annulus area. Since high resolution visual display units cannot normally be used to generate the high luminance levels which were achieved easily in an optical system, a scatter source annulus of large width (i.e., large area) had to be employed (see figure 7.1).

The effective eccentricity of this large annulus was then computed using an iterative numeric algorithm (Barbur et al., 1992). This eccentricity represented the angular radius of a very narrow annulus, which would produce the same illuminance level in the plane of the pupil and cause the same amount of light scattered over the central test target as the broad annulus.

The isolation annulus had a constant luminance and made possible the detection of flicker caused by scattered light over the test target. The colour of the isolation annulus was chosen to be yellow (chromaticity co-ordinates 0.4, 0.4) which also helped to emphasise its separation from the test target and the scatter source. A large, uniform background field of low luminance helped to maintain a steady state of light adaptation and fill the display area outside the scatter source annulus (see figure 7.1).

The area of the scattering annulus changed appropriately with the annulus eccentricity so as to keep the illuminance in the plane of the pupil constant and independent of annulus eccentricity. The light scattered over the test target was measured for five annulus sizes corresponding to five eccentricities of the scattering source. The luminance of the scatter source annulus was modulated at a frequency of 8.6 Hz for a duration of 0.35 s, as shown in figure 7.2. 100% modulation was employed. This caused a burst of flicker in the scatter source and the consequent detection of flicker in the centre test target was caused by scattered light.

A procedure was used to measure the mean luminance of the test stimulus, which minimised or eliminated the detection of flicker caused by scattered light. A response button box was used with the functions allocated to the buttons as follows:-

Function	Button Label
Increase target luminance modulation	YES
Decrease target luminance modulation	NO
Record threshold setting	GO
Repeat stimulus without change	Other buttons

The display was warmed up for at least 10 minutes before measurements were carried out. The display was viewed monocularly.

7.4 Subject's instructions.

The measurement sequence started with a test stimulus luminance of 0 cd/m^2 . The subject detected flicker in the dark test target and this was caused entirely by light scattered from the annulus. Every time the YES button was pressed, the luminance of the test stimulus was incremented by the step size and the stimulus presented to the subject. As the luminance modulation of the disc target on the display was increased in discrete steps, the subject would first notice a reduction in perceived flicker. This would be followed quickly by an increase, when the modulation of the screen luminance compensated the retinal illuminance caused by scattered light (see figure 7.2). When increased, and flicker was detected clearly, the subject was required to press the NO button following each presentation of the stimulus. This caused the step size to be reduced and the screen luminance modulation of the target was decreased by the new step size every time the NO button was pressed until the position of no flicker was reached. If in doubt about seeing flicker, the press of any other button would cause the stimulus to be presented again without any change. When the position of minimum or no flicker was reached the GO button was pressed, causing the measurement to be recorded and another annulus size was then used.

Six estimates of scattered light level were obtained for each annulus eccentricity and the corresponding standard errors were calculated.

When the experiment was finished, computation of the effective eccentricities occurred. Regression analysis was used to compute the light scatter model parameters which best fitted the measured experimental data.

7.5 Results

7.5.1 Scatter and the CAA Test:

The data was analysed to see whether there was a difference in scatter which could account for the differences in visual performance on the CAA test in the 10 normal subjects tested in chapter 5. A large variation in the scatter results occurred and there were no statistically significant differences. Regressions were plotted to see if there

was a relationship between k' and the foveal dip. k' was selected as the regression variable instead of n or k because n and k can influence each other.

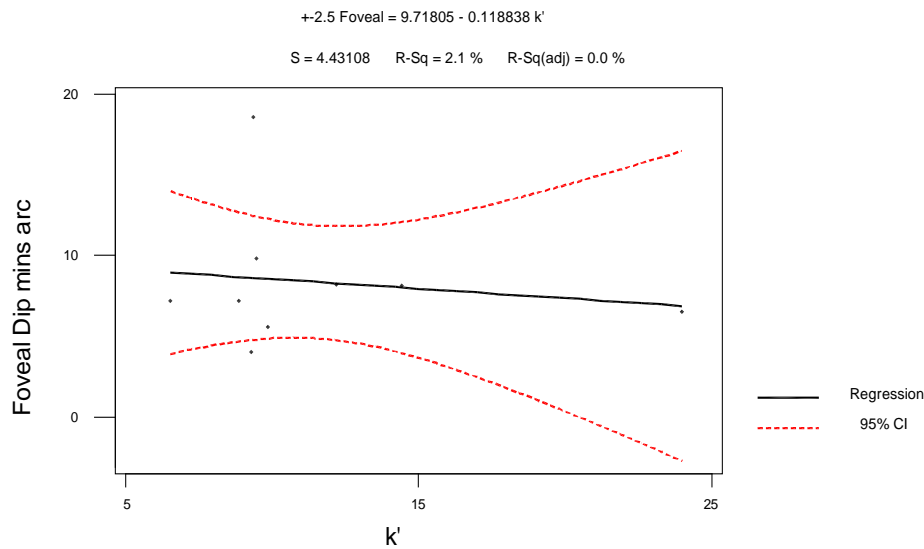


Figure 7.3: Mesopic Foveal Dip vs Scatter k'

A regression plot of Mesopic Foveal Dip vs Scatter k' is shown in figure 7.3. The trend was not statistically significant. ($P = 0.71$, adjusted $R^2 = 0\%$) No statistically significant trends were found for n and k against foveal dip. The photopic equivalents similarly gave no statistically significant trends.

7.5.2 Scatter and Pupil Sizes

Scatter was measured in 4 subjects, dilated with 2.5% phenylephrine using 6 mm and 3 mm artificial pupils, to determine whether scatter would increase with the larger pupil size. However a large variation in results occurred. The aim was to determine whether the foveal dip of the CAA test could be accounted for, by increased scatter, due to enlarged pupils.

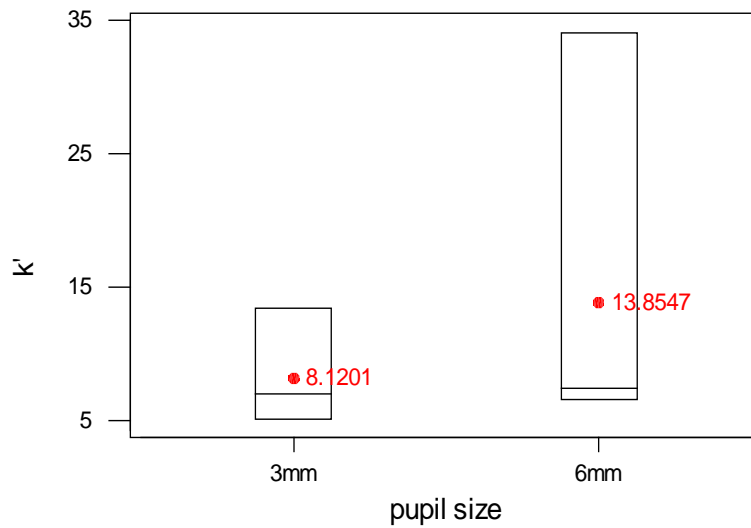


Figure 7.4 Scatter k' versus Pupil Size. Means are in red. Medians are shown by the horizontal lines. 95% confidence intervals are denoted by the box plots boundaries.

Figure 7.4 shows Box Plots of Scatter k' versus Pupil Size. A paired sample t test to determine whether there was a difference in the mean value of k' at the different pupil sizes, did not produce statistically significant results ($P = 0.331$), although only four subjects were tested (subjects LD, JLB, MS and SL). It would have been preferable to measure more subjects, given the volatility of the readings, however this was not possible due to time constraints. Individual scatter plots also gave slight increases of scatter with the 6 mm pupil sizes (see Appendix three).

Overall the results revealed a weak, trend of increased scatter with increasing pupil diameter, which was not statistically significant.

7.5.3 Scatter and Q value

Scatter was measured for 3 subjects using 5 different aberration controlled contact lenses, to see if the aberration controlled contact lenses affected the scatter. The

results showed no definite trends. Sometimes the scatter from the lenses with high Q values gave more scatter. Sometimes they gave less scatter.

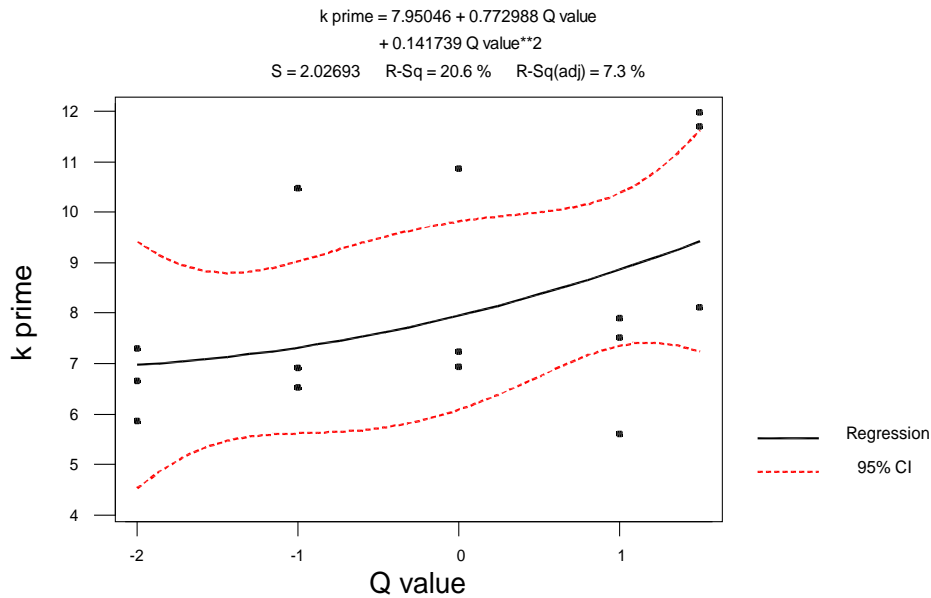
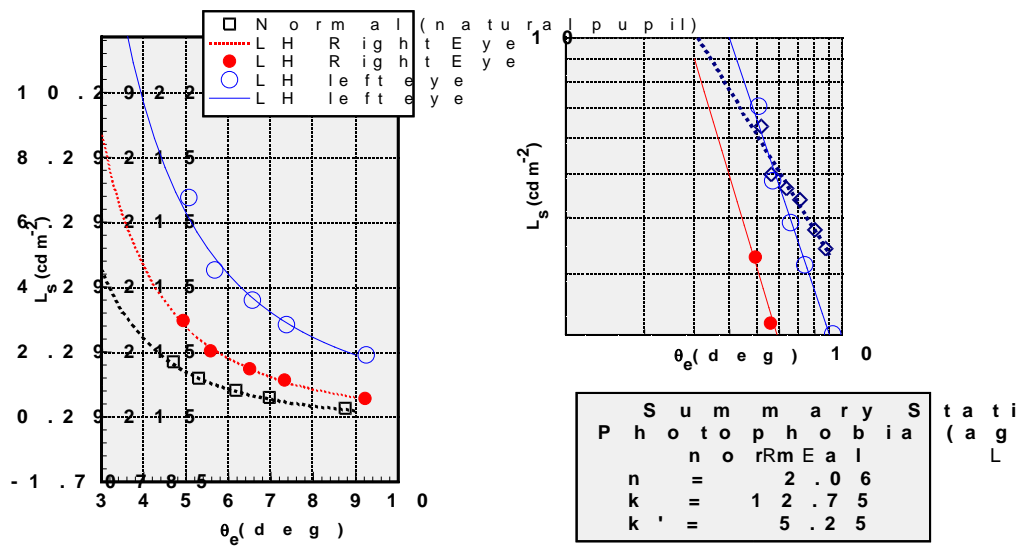


Figure 7.5 Scatter k' vs Q value Quadratic regression

Figure 7.5 shows a quadratic regression of Scatter k' against Q value, which was not found to be statistically significant. The P value was 0.74 and the adjusted R² was 7.3%. A quadratic regression was chosen to examine whether increasing Q values could be associated with increasing values of k'.

7.5.4 Scatter and two case study subjects:

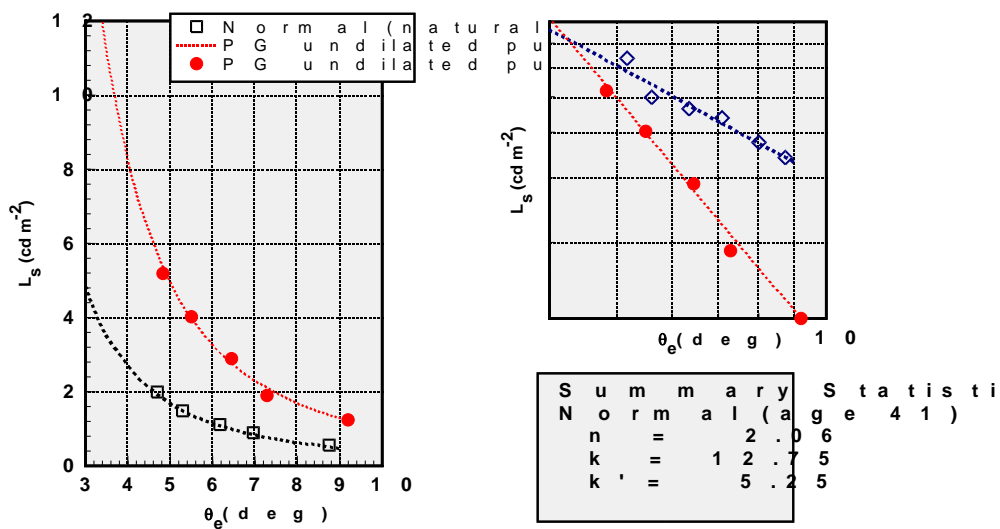
Two subjects complaining of glare / dry eyes / photophobia (one of whom had an intraocular lens implant) were assessed for scatter and were found to have increased scatter.



Scatter function of the eye. Subject LH. The inset shows the same data on a logarithmic scale. The empirical scatter function, L_s .

Figure 7.6. Scatter Function for subject LH suffering from photophobia.

The results for a subject suffering from photophobia are displayed in figure 7.6. LH RE and LH LE denotes LH's right and left eyes. The results appear to show elevated scatter functions for the right and left eyes. The k' values are high which reflect the elevated scatter functions. The left eye k' value was especially high, as was the elevation of the left eye scatter function.



Scatter function of the eye. Subject ~ 4 mm. The inset shows the same predictions based on empirical data.

Figure 7.7 Scatter Function for subject suffering from dry eye and photophobia – Subject PG.

The results for subject PG, suffering from dry eye and photophobia, after a cataract operation, are displayed in figure 7.7. An elevated scatter functions is shown. The k and k' values are very high – far higher than the k' values for the artificial 6 mm pupils for normal subjects. These two case studies illustrate that the 6 mm pupil or the different Q value contact lenses did not lead to much increased scatter in the normal subjects compared to the increases in scatter for subjects with pathological conditions.

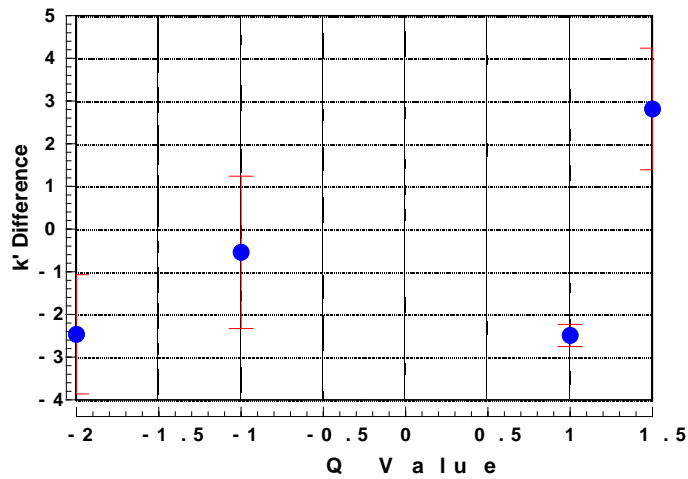


Figure 7.8 Scatter k' Differences generated by changes in Q values. Error bars are two standard errors.

Scatter k' differences generated by changes in Q values are shown in Figure 7.9. For the changes in Q values, the Q = 0 k' values were subtracted from the Q = -2, -1 +1 & +1.5 values. The differences in k' are less than three, which is less than the differences generated by subjects PG and LH who had pathological conditions (Figure 7.10).

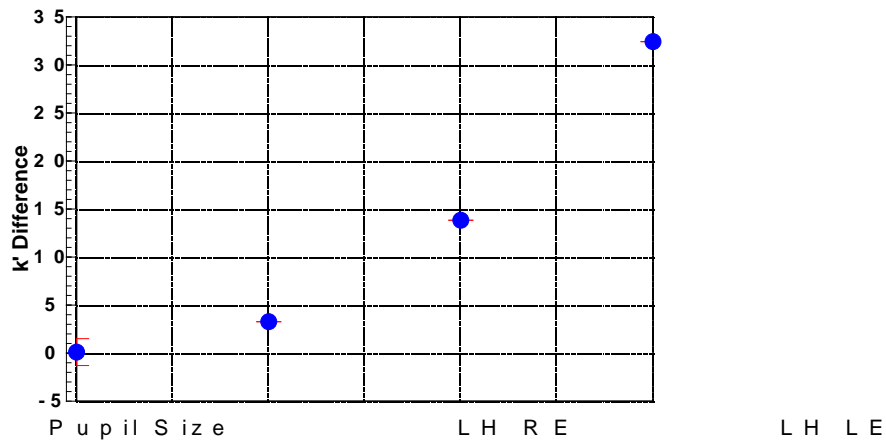


Figure 7.9 Scatter k' Differences generated by Pupil Size, & pathology. Error bars are two standard errors.

Scatter k' differences generated by pupil size and pathology, and are shown in figure 7.10. The difference in k' due to pathology, was calculated as k' for the abnormal eye minus k' for a normal eye. LH RE denotes subject LH Right Eye. Similarly PG LE denotes subject PG LE. The data for the subjects with pathology are the same as the data in figures 7.6 & 7.7.

Figure 7.10 shows that the k' values of left eyes of subjects LH and PG are significantly greater than the differences in k' generated by the changes in pupil sizes or changes in Q values.

7.6 Discussion

No statistically significant differences were found between measures of scatter (n , k and k') and the CAA test for mesopic central gap acuity with normal subjects. This agrees with the results of Van den Berg (2008), who pointed out that scatter concerns the area outside the middle of the PSF, whilst VA relates to the central area of the PSF.

When relationships have been found between glare and visual performance, the amounts of glare have been large, such as when glare occurs due to cataract, or car headlights. Most of our subjects on the other hand were normal subjects, so there was less likelihood of finding a relationship between scatter and visual acuity. Such

subjects would only have had small amounts of scatter. Two case study subjects did however show increased scatter due to corneal abnormalities.

Our results are in line with Rubin et al., (1993) who examined cataract subjects before and after surgery. The Brightness Acuity Tester was used to measure glare. Prior to surgery there was significant disability glare that was not correlated with acuity. Following surgery, improvements in disability glare were independent of improvements in acuity.

However our results are not in line with Carlsson et al., (1984) who examined the effect of glare caused by floodlights. Their results indicated that the vision of details was impaired by glare. Similarly, Puell et al., (2004) found that drivers who experienced difficulty driving at night and had poor visual acuity presented with worse mesopic contrast sensitivity and greater glare sensitivity. These studies examined the effects of large quantities of glare, which can be contrasted with our inconclusive results relating smaller quantities of scatter and CAA gap acuity.

A large variation in our results in relating the effect of pupil sizes and scatter occurred. This is in line with Franssen et al., (2007) who suggested that for natural pupils (between 2 and 7 mm diameter), straylight only weakly depended on pupil diameter (within 0.2 log units). For large scatter angles and small pupil diameters, it was suggested that eye wall translucency contributed significantly to straylight in a wavelength and pigmentation dependent manner. However Franssen et al., (2007) suggested that the pupil size would have to be around 2 mm or less for eye wall translucency to affect scatter in the eye, whilst the smallest pupil size used in our experiments was 3 mm.

Franssen et al., (2007) argued that the suggestion that in darkness pupil dilation allows more glaring light to have an effect on the retina, was misleading, because larger pupils also allow more light from the dark scenery to reach the retina, thus counteracting the effect of the glaring light. It was suggested that in fact, one might expect both effects to balance each other out precisely, because quantitatively the

increase in glare light would equal the increase in direct light. Thus for uniform light-scattering over the pupil plane little effect of pupil size would be expected by Franssen et al., (2007).

Apart from the effect of eye wall translucency, another confounding factor suggested by Franssen et al., (2007) would occur at very large pupil sizes of around 8 mm or more. At these large pupil sizes straylight in the zonular area of the eye lens could provide an extra source of straylight at the extreme periphery of the eye lens. In this region, the zonular area may scatter light much more strongly than more central parts of the lens. However the largest pupil size that we used was 6 mm, so our results would be unaffected by this confounding factor.

Masket (1992) examined a group of 40 postoperative cataract patients with a Miller-Nadler glare test performed before and after midpupillary pharmacologic dilation. Their results indicated that pupillary enlargement was associated with increased glare disability, in contrast to Fransen et al., (2007). The difference in results may have been due to the use of abnormal subjects in Masket (1992)'s study, compared to the normal subjects used in Fransen (2007)'s study.

Similarly, Veraart et al., (1992) found stray light values to be increased by a factor of 1.4 for 4 mm sized pupils and 2.0 for 8 mm sized pupils in nineteen patients who had undergone radial keratotomy.

Our results suggest that the marginal differences in scatter produced with the 6 mm and 3 mm artificial pupils can probably not be used to explain why the elevated CAA test acuities or foveal dips under photopic and mesopic conditions occurred. No statistically significant scatter results were produced by the different Q value lenses, which also suggests that the changes in the CAA test results associated with the different Q values (see Chapter 6) were not the result of increased scatter.

Our regression of k' versus CAA test was not found to be statistically significant which also suggest that the foveal dips were not caused by increased scatter. The scatter in the two subjects with known problems was more than the scatter induced by the increased pupil sizes or the contact lenses with increased Q value and spherical aberration. This also suggests that neither increased Q value, spherical aberration, nor increased pupil sizes increased scatter by significant amounts. This in turn may suggest that the foveal dips were probably not caused by increased scatter, as neither increased spherical aberration (caused by the Q value contact lenses) nor pupil size increased the scatter by a statistically significant amount. It should be noted however that very small numbers of subjects were examined due to time constraints, so finding statistically significant results, if they had existed, would have been difficult to achieve.

Chapter Eight

7. Summary & Conclusions

8.1 Summary of Results

The following factors were found to produce definite trends in the CAA test: Spherical aberrations, as induced by aberration controlled contact lenses, produced definite changes in visual performance. This suggests that if refractive surgery produces large amounts of spherical aberration, visual performance may be reduced outside the normal range of the CAA Test. Increases in contrast in the photopic and mesopic CAA tests produced improved gap acuity. The consistently better results with the use of high contrast targets in the CAA test may be related to the high contrast VA tests used in optometric practice, which demonstrates that VA performance may be high, but the effects of scatter or aberrations may not be detected. There were variable results using 6 mm and 3 mm pupil sizes on the CAA test, contrast sensitivity test and scatter test, reducing the contrast of the guides in the CAA test, and increasing stimulus onset time. This may suggest that changing parameters of the various visual tests by small amounts has a more variable effect on the results, whilst large changes in the stimulus will lead to larger effects and more easily observable trends. For small changes, other individual factors such as concentration or tiredness may influence the results, and cause some of the variability, whilst for large changes, factors such as varying concentration levels may play a less significant role.

Multiple factors, which may be retinal, cortical, or optical, may have influenced the results of the tests, which may have interplayed with each other to produce the variable results. Previous research literature has attributed the variation of visual acuity with eccentricity to be related to cone, ganglion cell or receptive field density, receptive field size or cortical factors. However it may be that although these factors are influential, the stimulus used and stimulus conditions are factors that can easily change the variation of acuity with eccentricity. This may in turn change the influence of various factors such as the distribution of cells stimulated in the retina, which may then affect the size or density of the receptive fields, causing the

information to be processed differently in the visual cortex. Different areas of the visual cortex may be affected by different stimuli under different conditions, leading to different variations of acuity with eccentricity.

8.2 Conclusions

The following conclusions have been made concerning aberrations, scatter, pupils and visual performance.

8.2.1 Chapter 4 – Experimental investigations on Visual performance Changes with Eccentricity.

The guide contrasts results did not yield statistically significant results or trends. Neither did the onset of stimulus time increase, although only three subjects were tested, due to time constraints.

The artificial pupil contrast sensitivity results yielded statistically significant results for the lower 1.2 and middle 6.1 cpd spatial frequencies. The use of artificial pupils with low and high contrast targets showed variable results, which are in line with the contrast sensitivity results not revealing significant results at high spatial frequencies. A slight trend towards greater differences being generated by 6 mm artificial pupils under photopic conditions occurred, which was not statistically significant. The better acuities yielded with higher contrast targets by two of the three subjects, at mesopic levels, may reflect that the higher contrast targets were more easily detected by the less active cones and more active rods at the mesopic levels. This suggests that low target contrast may be an important factor in producing the foveal dip.

More investigations under a wider variety of conditions could be made, with increased numbers of subjects to obtain more reliable results. A greater range of spatial frequencies could be assessed for the contrast sensitivity experiments, with an increased number of different pupil sizes. The effect of different target contrasts, background illumination levels and target durations, onset times and target types are worthy of further investigation.

8.2.2 Chapter 5 – Effect of Natural Aberrations on the CAA Test

No relationship or trend was found between the aberrations and the CAA test results for the foveal dips or central thresholds under mesopic or photopic conditions for normal subjects.

More subjects may be required to generate more reliable results. To link aberrations with visual performance, metrics other than RMS values are probably required, and more research is needed in this area.

8.2.3 Chapter 6 – The effect of Q value and Spherical Aberration on the CAA Test.

Spherical aberration was shown to be significantly negatively correlated with the Q values, which goes against the positive correlations found in the research literature. This may be due e.g. to the software used by the contact lens manufacturer. The Q value contact lenses gave significant quadratic regressions for spherical aberration against mesopic CAA central gap acuity. Seidel coma and Seidel astigmatism were also correlated with elevated gap acuities under photopic conditions.

It was only under mesopic conditions with large non-physiological amounts of spherical aberration that a foveal dip type result was produced, with the central areas becoming raised compared to the peripheral areas. This suggests that non – physiological amounts of aberration probably did not contribute significantly to the foveal dip.

Further work could involve the same investigations being performed with different contact lens types and materials, and with different Q values. Different tests and instruments for aberration measurement could also be used to verify the results. The effect of spherical aberration on natural pupil size seems to be worthy of further investigation, since higher Q values appeared to give rise to smaller pupil sizes. Pupil size seemed to be most affected by the +1.50 Q value lenses. Pupil sizes could be measured simultaneously, while the visual performance tests are being performed to gain a greater insight into the relationships between aberrations, scatter, pupil sizes, crowding, eccentricity and visual performance.

8.2.4 Chapter 7 – Scatter and Visual Performance

The foveal dips were probably not caused by increased scatter, as in the normal subjects increased scatter was not associated with decreased CAA test performance. Changes in Q values, or increases in spherical aberration also did not increase the scatter. This suggested the changes in the CAA test caused by the aberration controlled contact lenses were not the result of increased scatter. The marginal increases in scatter produced with the 6 mm artificial pupils suggests that the foveal dips were also not significantly influenced by differences in scatter.

The scatter in the two subjects with known problems was more than the scatter induced by the increased pupil sizes or the Q value contact lenses with increased spherical aberration. This suggests that neither the spherical aberration, nor increased pupil sizes increased scatter by significant amounts.

The measures of scatter were subjective, and the experiments could be re – examined by using objective methods of measuring scatter. The experiments could be repeated under different conditions, with different contact lens materials, more subjects and different background illuminations. The experiments were performed under largely monochromatic conditions. Chromatic conditions and other experimental conditions could bring different results.

8.5 Achievements of the Project:

The ineffectiveness of physiological amounts of aberrations as measured by RMS wavefront error for predicting CAA test visual performance among normal subjects has been confirmed. Evidence for the probable importance of retinal factors rather than aberrations or scatter, in producing raised thresholds and the foveal dip in the CAA test under photopic and mesopic conditions has been produced.

A firm relation between spherical aberration and CAA test performance under mesopic conditions has been shown for our Q value contact lenses.

8.6 Concluding Remarks:

Insights have been provided into the effects of aberrations, Q value, scatter, crowding, stimulus onset time and pupil size on visual performance, as measured by the CAA Tests and contrast sensitivity. The research is original mainly due to the use of aberration controlled contact lenses with different Q values to assess the effect of aberrations on visual performance, together with the manipulation of different parameters in the CAA test.

Appendix 1

A1.1 CAA Test Artificial Pupil Results

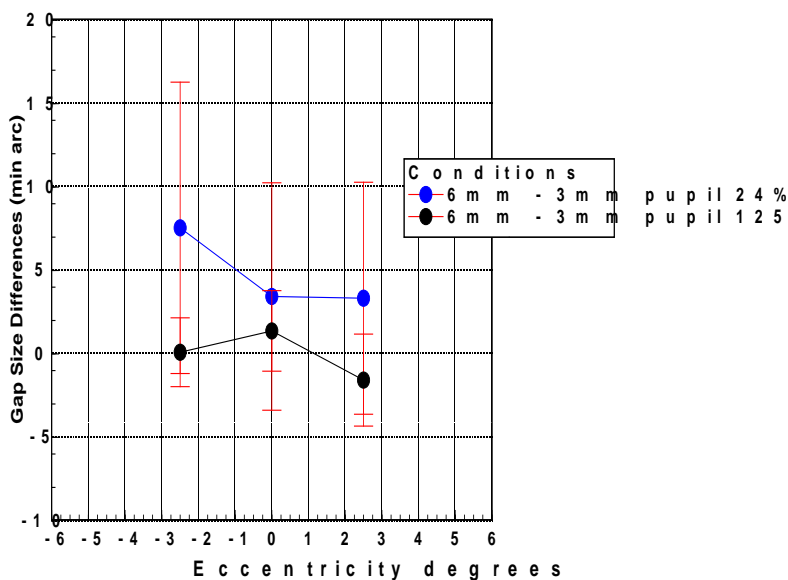


Figure A1.1. Differences in Photopic Gap Acuties due to 6 mm and 3 mm pupil sizes at 24% and 125% contrast. Error bars are 2 standard errors.

The results of five subjects combined (subjects MS, AnP, AP, CO, SL) are shown in figure A1.1. Differences in gap acuity are shown (= CAA 6 mm gap acuity – CAA 3 mm gap acuity). The lower contrast 24% differences appear to be larger than the 125% differences, although the differences are not statistically significant. This suggests aberrations and scatter due to increased pupil size may affect the CAA test due to its low 24% contrast levels.

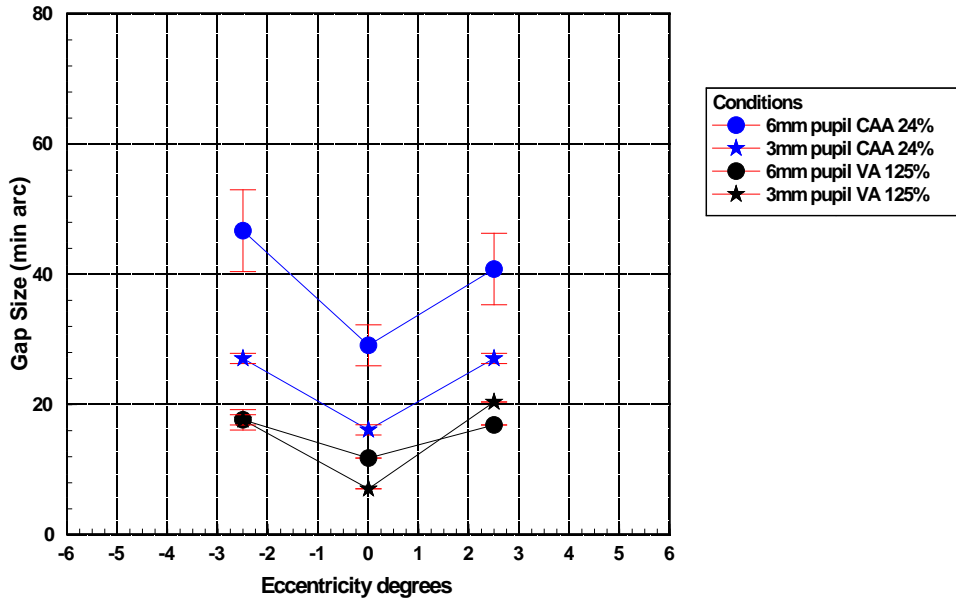


Figure A1.2: Photopic Gap Acuity results at high and low contrast for subject MS. Error bars are 2 standard errors

Subject MS shows improved acuities for the higher contrasts, with the lower contrasts giving a large difference between the 6 mm and 3 mm artificial pupil results, possibly due to the aberrations having a larger effect at the lower contrast level. The CAA test 125% test targets were similar to a VA test room target in terms of contrast, so they are denoted as VA 125% in the legend.

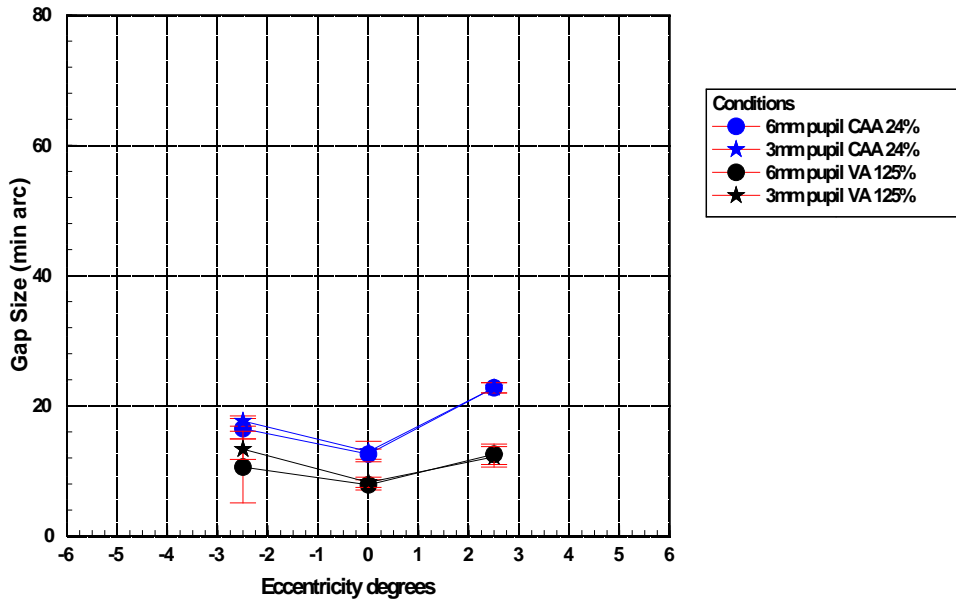


Figure A.1.3: Photopic Gap Acuity results at high and low contrast for subject AnP. Error bars are 2 standard errors.

Subject AnP shows little variation due to artificial pupil changes, but a larger change due to the contrast changes, as shown in figure A1.3

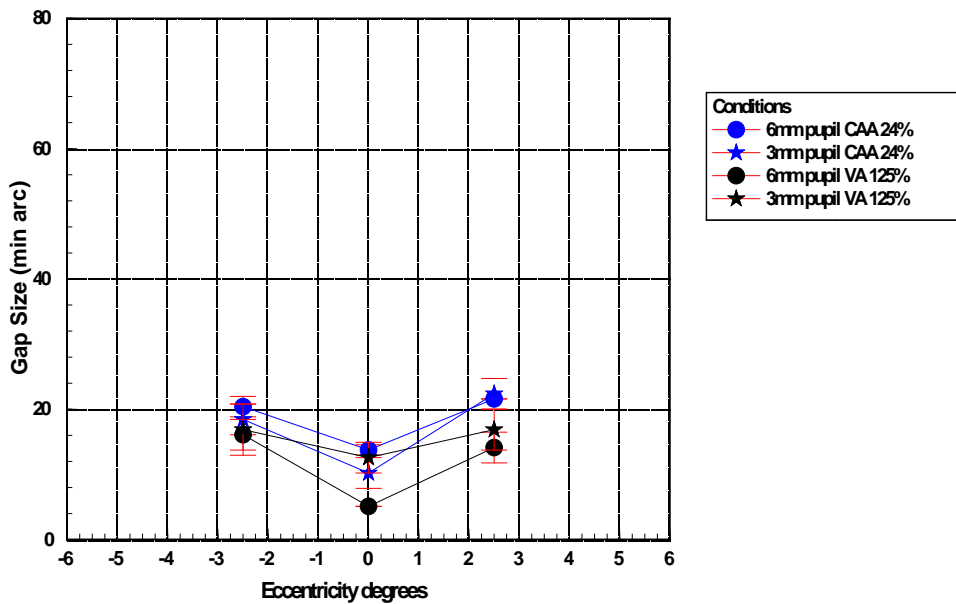


Figure A1.4: Photopic Gap Acuity results at high and low contrast for subject AP. Error bars are 2 standard errors.

Subject AP appears to show less variation for the 6 mm vs 3 mm pupils results at low contrast, as shown in figure A1.4. Surprisingly, more variation is shown for the high

contrast central results, and it is surprising that the 6 mm high contrast acuity is higher than the 3 mm high contrast acuity.

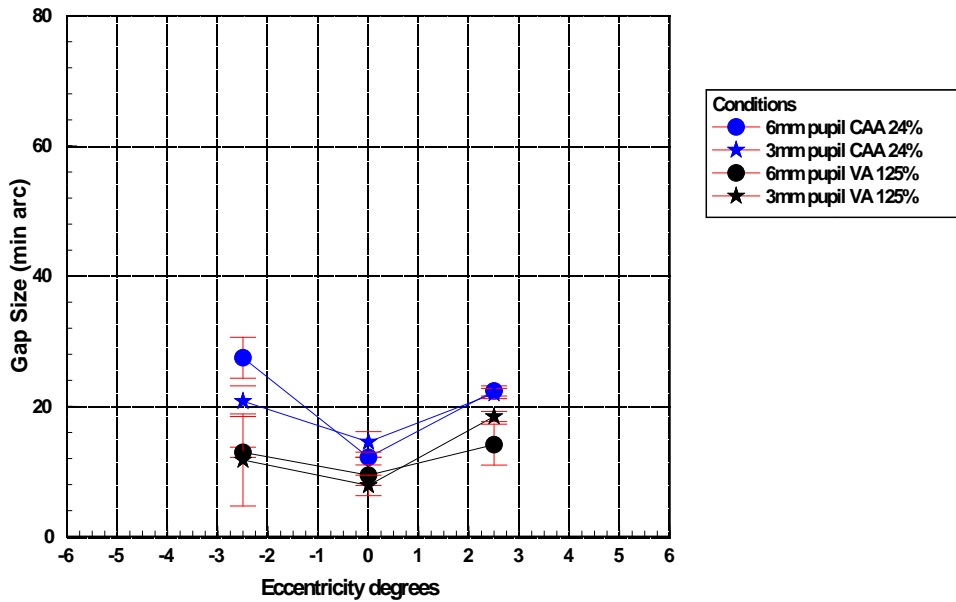


Figure A1.5: Photopic Gap Acuity results at high and low contrast for subject CO. Error bars are 2 standard errors.

Subject CO produced most changes due to the changes in contrast of the Landolt rings, as seen in figure A1.5. The changes in pupil size have had little effect at the -2.5 eccentricity at high 125% contrast. At the low 24% contrast, better acuity resulted with the 3 mm pupil diameter. The opposite occurred at the zero eccentricity position. At the +2.5 position, at low contrast the results are the same, whilst at high contrast, the 3 mm pupil displays inferior gap acuity compared to the 6 mm pupil result.

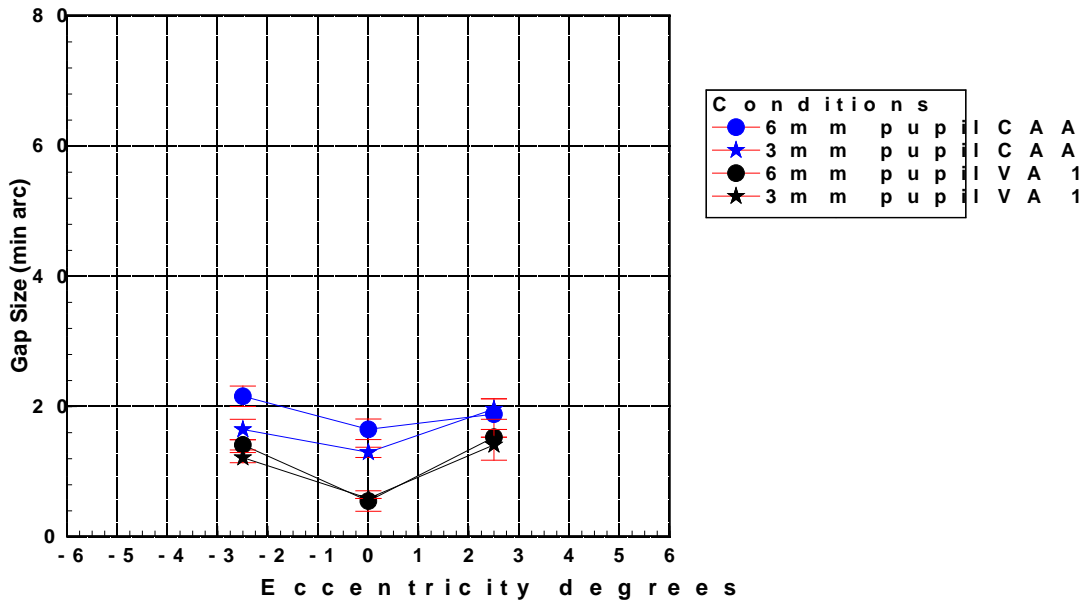


Figure A1.6: Photopic Gap Acuity results at high and low contrast for subject SL. Error bars are 2 standard errors.

Subject SL also gave most changes due to the changes in contrast of the Landolt rings, as seen in figure A1.6. The 125% contrast targets clearly give improved acuity results. For pupil size effects, the greatest effects occur with the low contrast targets at the 0 and -2.5 positions, here the 3 mm pupil size gives better low contrast acuity. The changes in pupil size have had little effect for the high contrast targets.

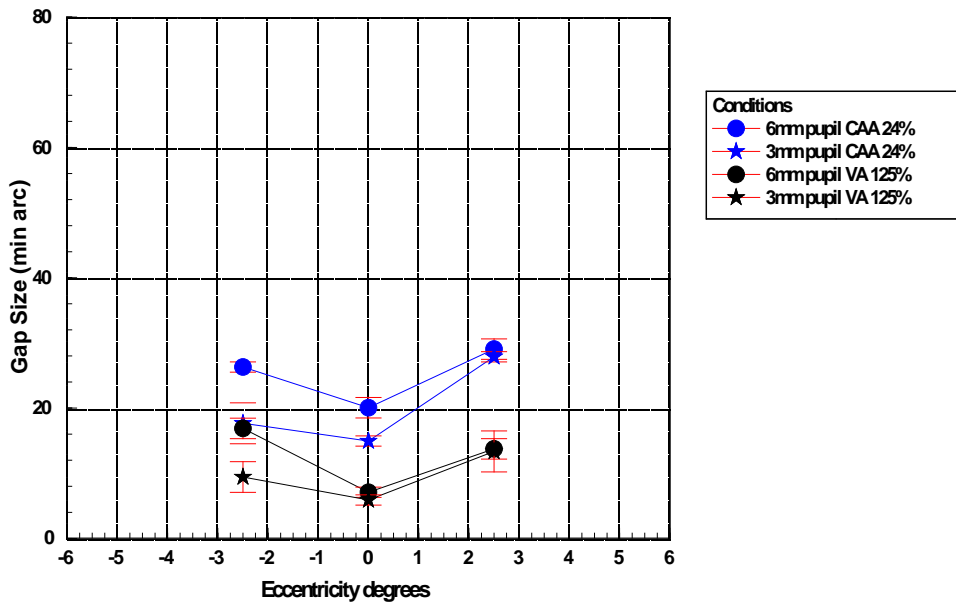


Figure A1.7 Photopic Gap Acuity results at high and low contrast for subject MS – a repeat run. Error bars are 2 standard errors.

A repeat run is shown for subject MS in figure A1.7. The differences are less marked for subject MS on the second attempt.

A1.2 Further Guide Contrast Results

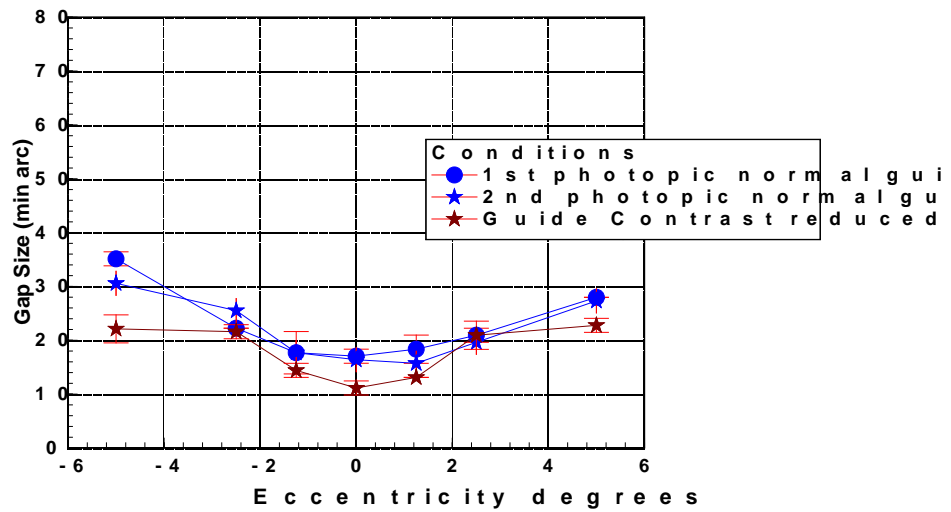


Figure A1.8. CAA Guide contrast changed - Photopic Tests - subject DT. Error bars are 2 standard errors.

The results for subject DT (age 27) with the guide contrast reduced are shown in figure A1.8. Improved gap acuity is shown for all the points except the 2.5 eccentricity points. Photopic runs were repeated and the CAA test here shows good repeatability.

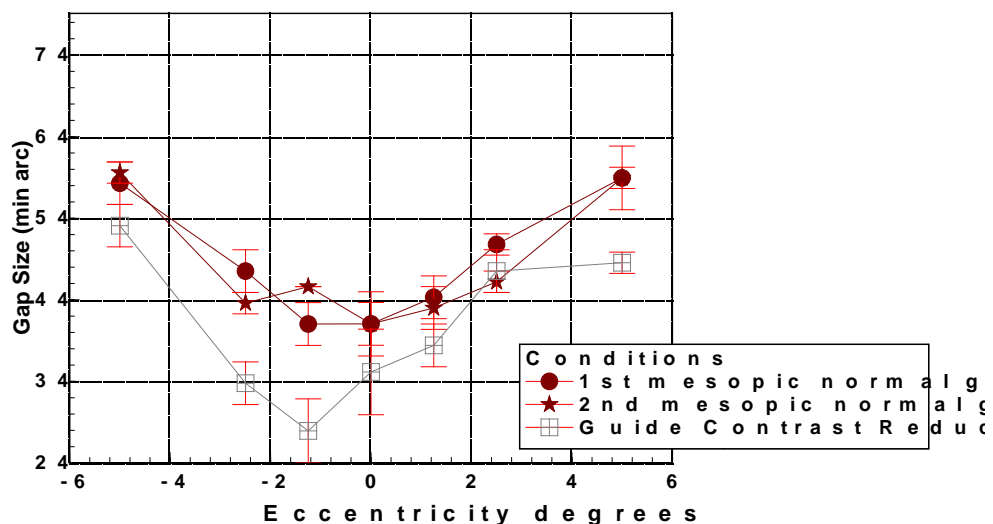


Figure A1.9 Guide Contrast reduced Mesopic Gap Acuity Tests - subject DT. Error bars are 2 standard errors.

The results for subject DT with the guide contrast reduced under mesopic conditions are shown in figure A1.9. Improved gap acuity is shown for all the points except for one 2.5 eccentricity point and one 5 degree eccentricity point. Mesopic runs without guide contrast reduction were repeated and the CAA test here shows good repeatability too. The highest gap acuity is shown to appear at the -1.25 eccentricity. This may have been due to the patient not being properly aligned.

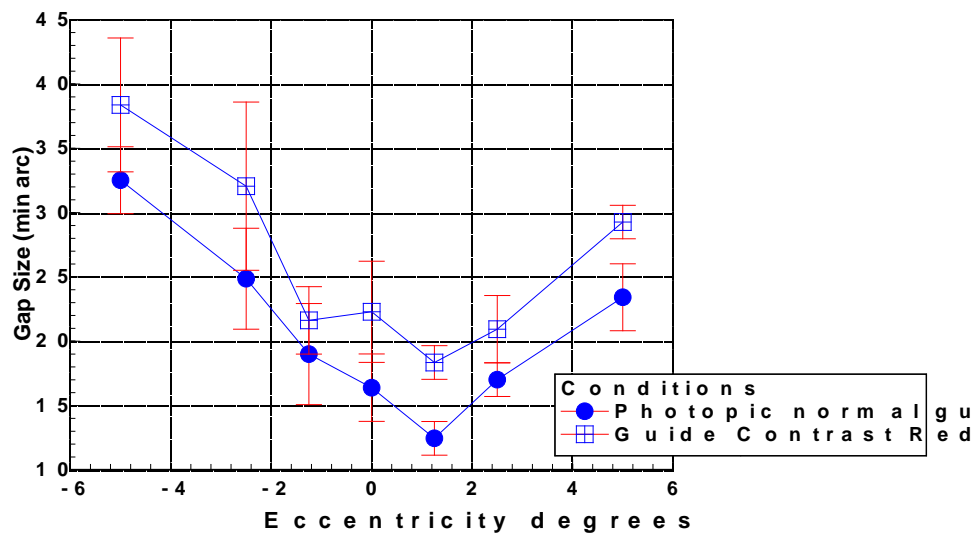


Figure A1.10 Guide Contrast reduced Photopic CAA Tests - subject JK. Error bars are 2 standard errors.

The results for subject JK with the guide contrast reduced under photopic conditions are shown in figure A1.10. Decreased gap acuity is shown for all the points, when guide contrast is reduced, which is the opposite result compared to subject DT (figure A4.7). The highest gap acuity here is shown to appear at the $+1.25$ eccentricity. This may have been due to the patient not being properly aligned.

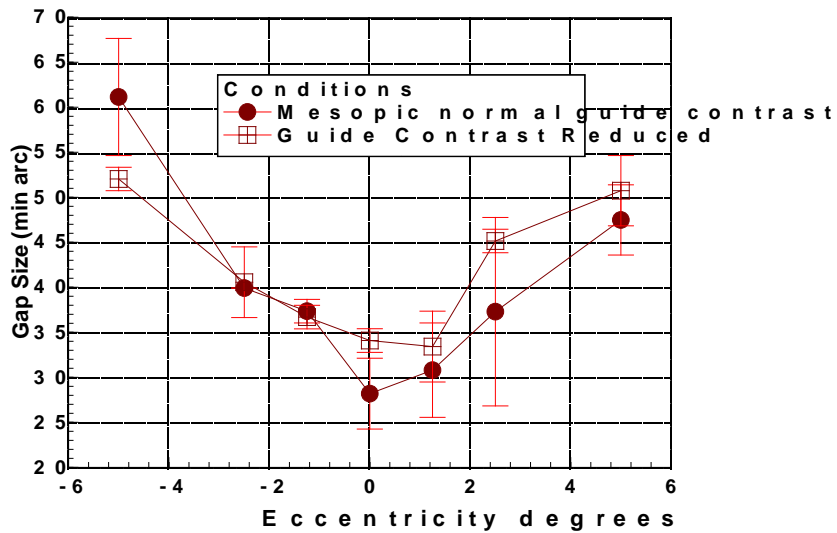


Figure A1.11 Guide Contrast reduced Mesopic CAA Tests - subject JK Error bars are 2 standard errors.

The results for subject JK with the guide contrast reduced under mesopic conditions are shown in figure A1.11. Decreased gap acuity is shown for four of the seven points, when guide contrast is reduced. Two points show no change when guide contrast is reduced. Only one point reveals better gap acuity with reduced guide contrast (at the -5 eccentricity). Therefore a mixture of results has occurred.

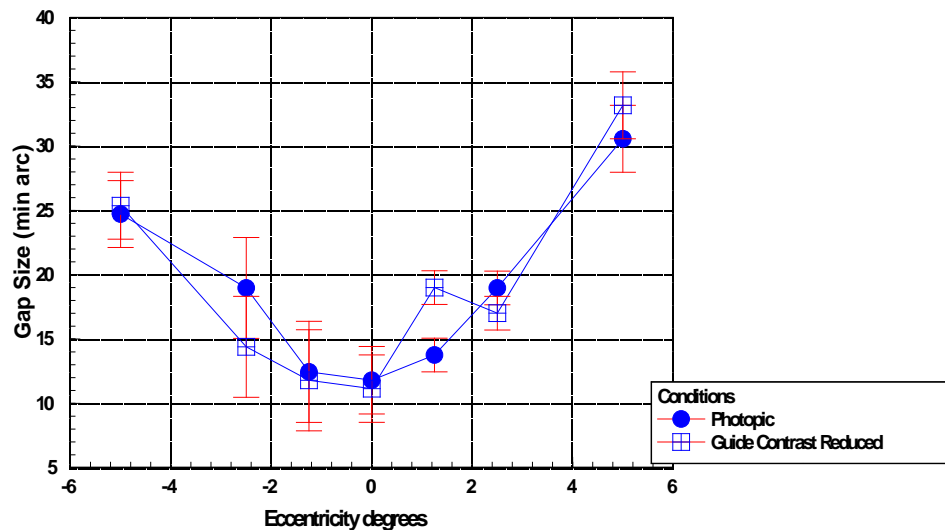


Figure A1.12 Guide Contrast reduced, Photopic CAA Tests - subject LD. Error bars are 2 standard errors.

The results for subject LD with the guide contrast reduced under photopic conditions are shown in figure A1.12. Increased gap acuity is shown for four of the seven points, when guide contrast is reduced. Three points show reduced gap acuity when guide contrast is reduced. Therefore a mixture of results has occurred.

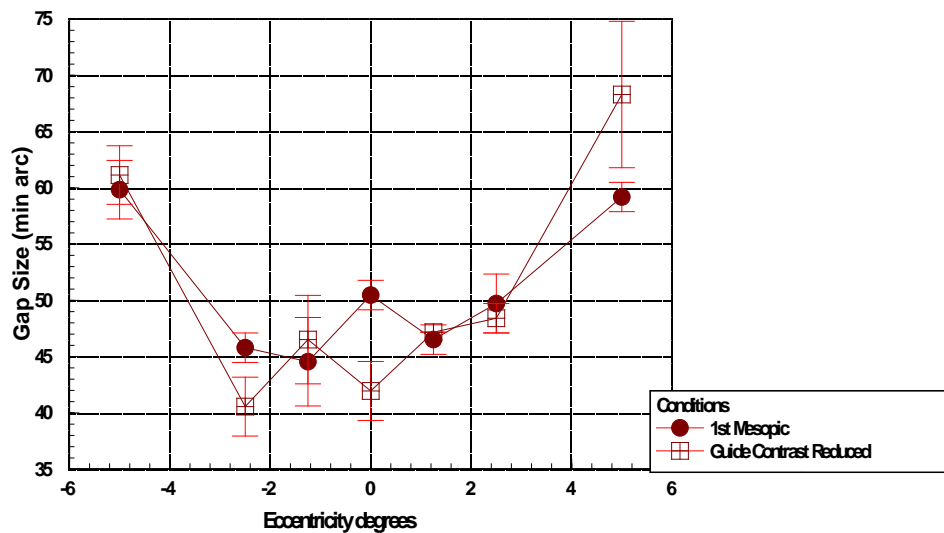


Figure A1.13 Guide Contrast reduced, Mesopic CAA Tests - subject LD. Error bars are 2 standard errors.

The results for subject LD with the guide contrast reduced under mesopic conditions are shown in figure A1.13. Increased gap acuity is shown for three of the seven points, when guide contrast is reduced. Three points show reduced gap acuity when guide contrast is reduced. One point shows no change. Therefore a mixture of results has occurred.

A1.3 Further Stimulus Onset Time Results

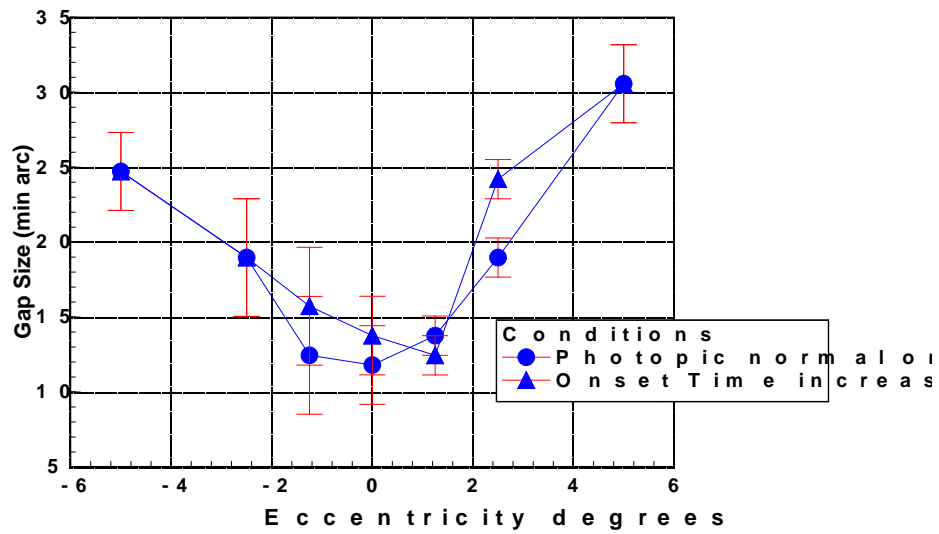


Figure A1.14: Stimulus Onset Time increased, Photopic Gap Acuity Tests for subject LD. Error bars are 2 standard errors.

The results for subject LD with the onset of the stimulus time increased under photopic conditions are shown in figure A1.14. Decreased gap acuity is shown for three of the seven points, when the stimulus onset time is increased. Increased gap acuity is shown for one of the points, at the +1.25 eccentricity. The other points for normal stimulus onset time and increased stimulus onset time approximately coincide. A mixture of results has occurred, with no definite trend being shown.

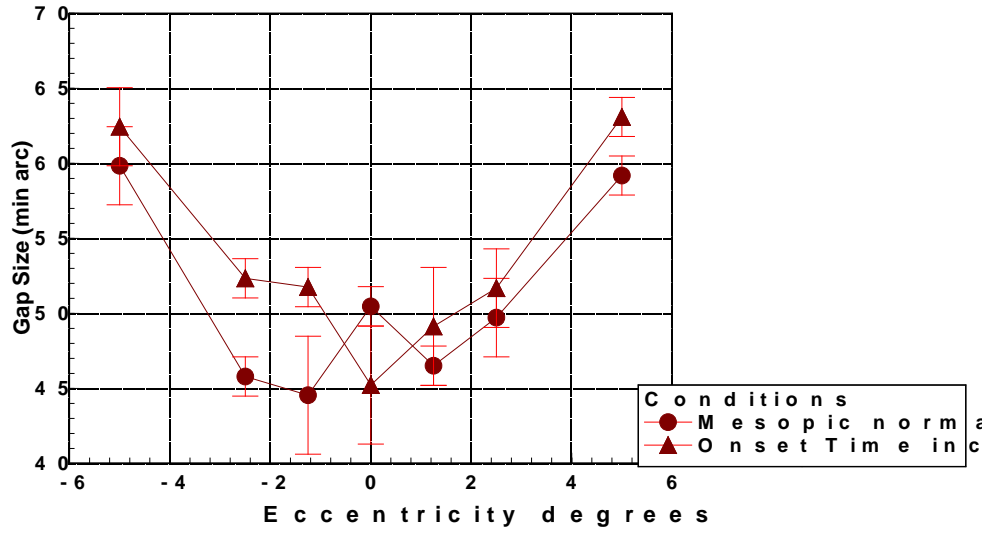


Figure A1.15: Stimulus Onset Time increased, mesopic Gap Acuity Tests - subject LD. Error bars are 2 standard errors.

The results for subject LD with the onset of the stimulus time increased under mesopic conditions are shown in figure A1.15. Decreased gap acuity is shown for six of the seven points, when the stimulus onset time is increased. Increased gap acuity is shown for one of the points, at the zero degree eccentricity. Therefore there seems to be a slight trend towards improved gap acuity in this instance.

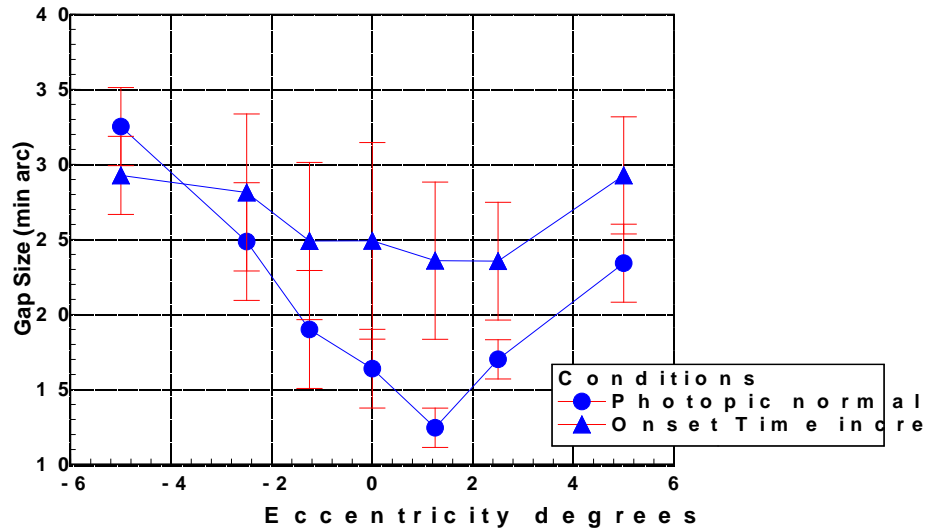


Figure A1.16 Stimulus Onset Time increased, photopic Gap Acuity Tests - subject JK Error bars are 2 standard errors.

The results for subject JK with the onset of the stimulus time increased under photopic conditions are shown in figure A1.16. Decreased gap acuity is shown for six of the seven points, when the stimulus onset time is increased. This shows the opposite trend to the results of DT . The changes appear to be statistically significant for only two of the seven points. The subject may have been misaligned, leading to the best contrast acuity occurring at the +1.25 eccentricity. The standard errors are large for this subject.

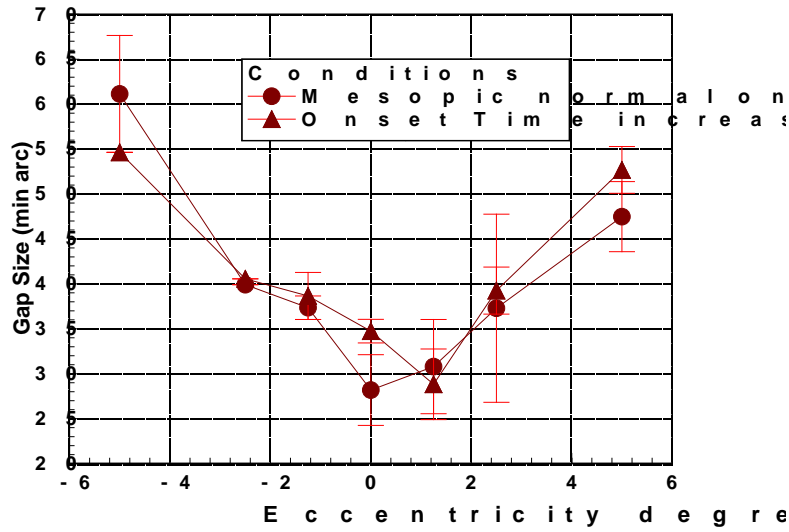


Figure A1.17: Stimulus Onset Time increased, mesopic Gap Acuity Tests - subject JK. Error bars are 2 standard errors.

The results for subject JK with the onset of the stimulus time increased under mesopic conditions are shown in figure A1.17. Decreased gap acuity is shown for two of the seven points, when the stimulus onset time is increased. Increased gap acuity is shown for one of the points. The other points for normal stimulus onset time and increased stimulus onset time approximately coincide. A mixture of results has therefore occurred in this instance, with no definite trend being shown.

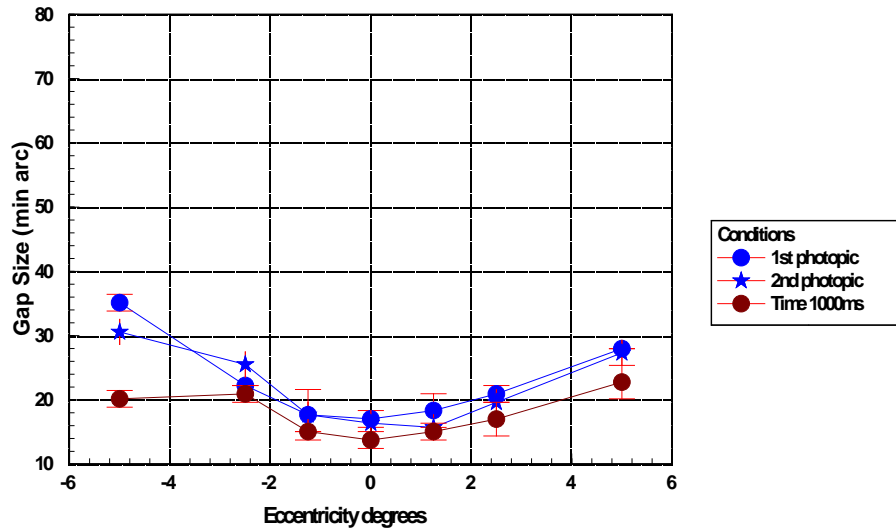


Figure A1.18 Stimulus Onset Time increased, photopic Gap Acuity Tests - subject DT. Error bars are 2 standard errors.

The results for subject DT with the onset of the stimulus time increased under photopic conditions are shown in figure A1.18. Increased gap acuity is shown for all of the seven points, when the stimulus onset time is increased. The changes are not statistically significant except at the 5 degree eccentricity points.

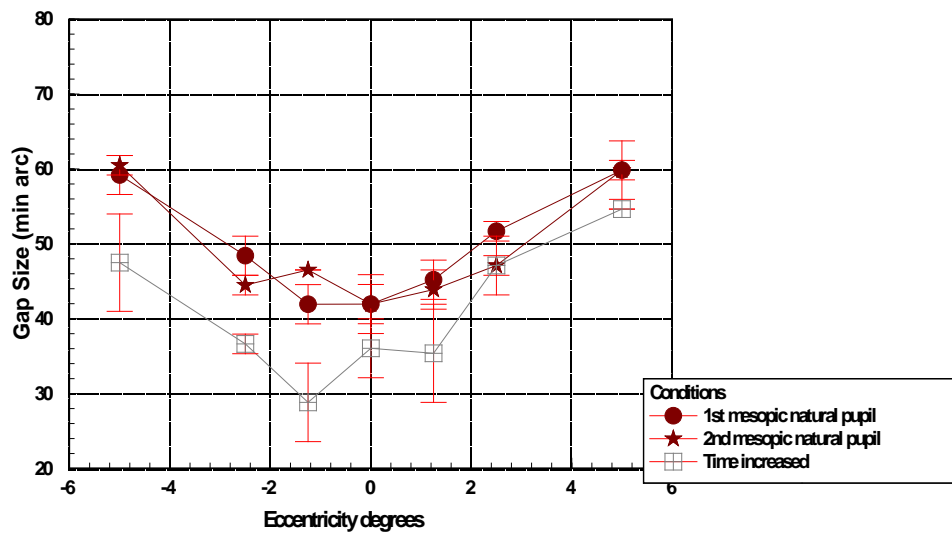


Figure A1.19: Stimulus Onset Time increased, mesopic Gap Acuity Tests - subject DT. Error bars are 2 standard errors.

The results for subject DT with the onset of the stimulus time increased under mesopic conditions are shown in figure A1.19. Increased gap acuity is shown for six of the seven points, when the stimulus onset time is increased.

Overall, a mixture of results occurred. Subject DT showed improvements in gap acuity with increased stimulus onset time. JK showed less good performance with increased stimulus onset time, though her results were quite variable. LD also showed variable results, with a slight trend towards improvements in gap acuity under mesopic conditions with increased stimulus onset time.

A1.4 Effect of High Contrast on Mesopic Results

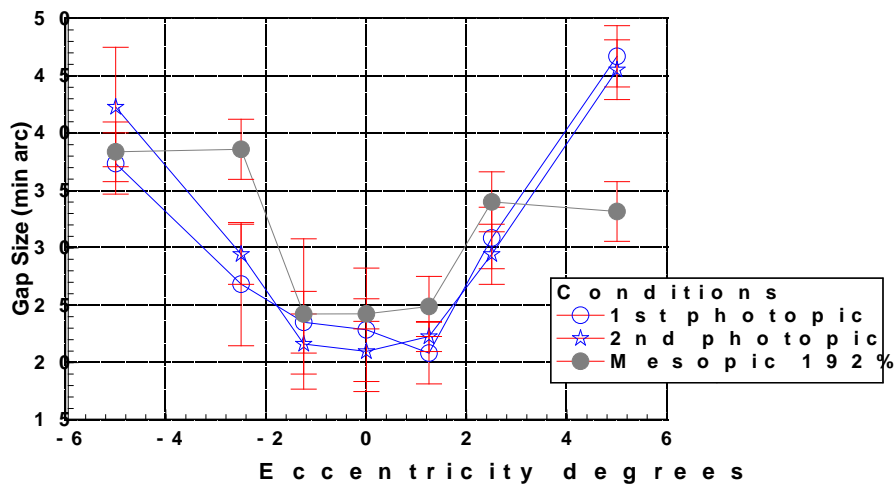


Figure A1.20: Mesopic Gap Acuity results at high and low contrast for subject GB. Error bars are 2 standard errors

Mesopic Gap Acuity results at high and low contrast for subject GB are shown in figure A1.20. It can be seen that the mesopic 192% contrast gap size acuities are no longer as elevated when they were at 48% contrast (e.g. see figure 4.2). At the peripheral +5 position, the mesopic 192% contrast acuity is better than the photopic acuity. This result is almost repeated at the +5 position too. This may reflect the lower numbers of cones being present at this periphery position, compared to a larger number of rods.

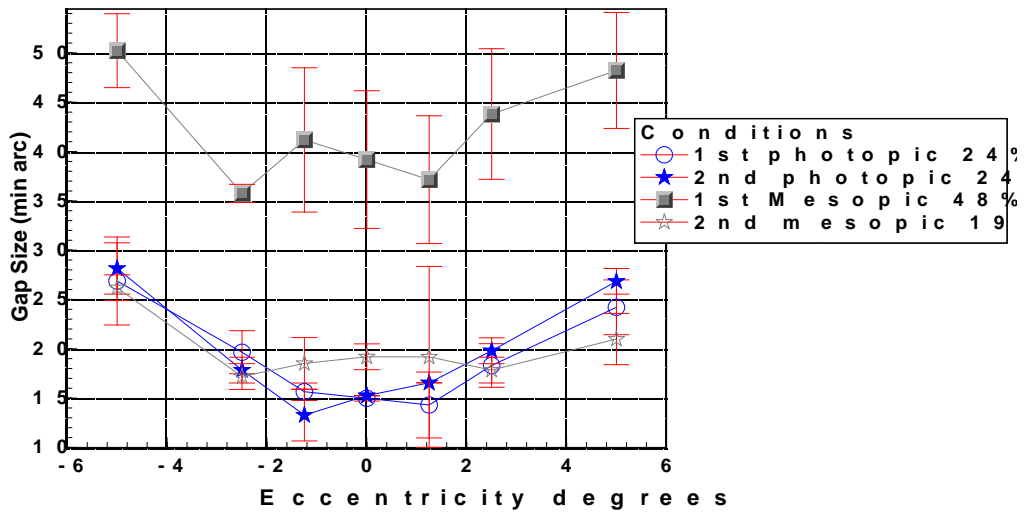


Figure A1.21: Photopic and Mesopic Gap Acuity results at high and low contrast for subject PM. Error bars are 2 standard errors.

Photopic and Mesopic Gap Acuity results at high and low contrast for subject PM (age 29) are shown in figure A1.21. Subject PM appears to have given the expected results of higher contrast giving better acuity results. Like GB's results, the mesopic high 192% contrast results of PM become closer to the photopic results. Low 48% mesopic contrast acuity results are also shown, showing elevated thresholds.

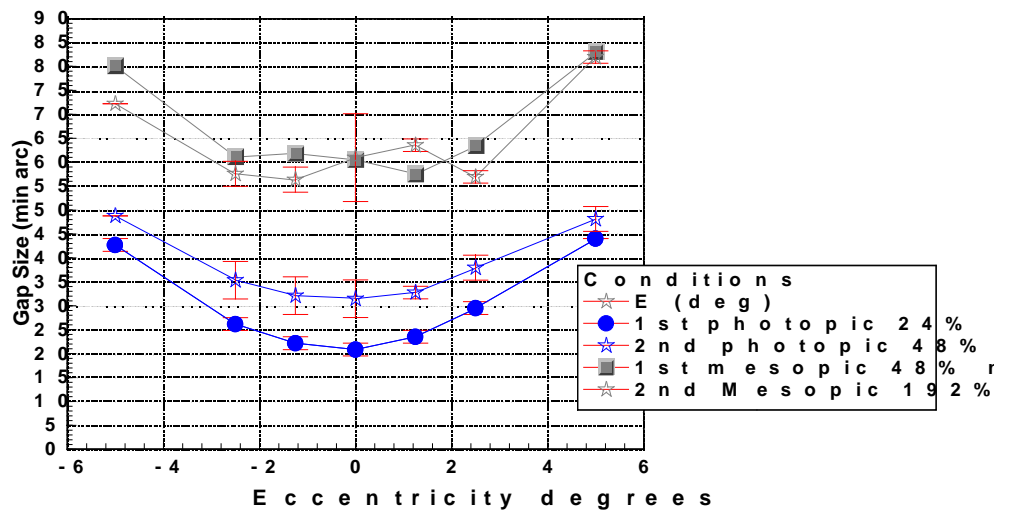


Figure A1.22: Photopic and Mesopic Gap Acuity results at high and low contrast for subject HF. Error bars are 2 standard errors.

Photopic and Mesopic Gap Acuity results at high and low contrast for subject HF (age 28) are shown in figure A1.22. Subject HF does not appear to have given the expected results of higher contrast giving better acuity results. Unlike PM's & GB's results, the mesopic high 192% contrast results of HF have not become closer to the photopic results. Low 48% mesopic contrast acuity results are also shown, showing similar thresholds to the 192% mesopic thresholds.

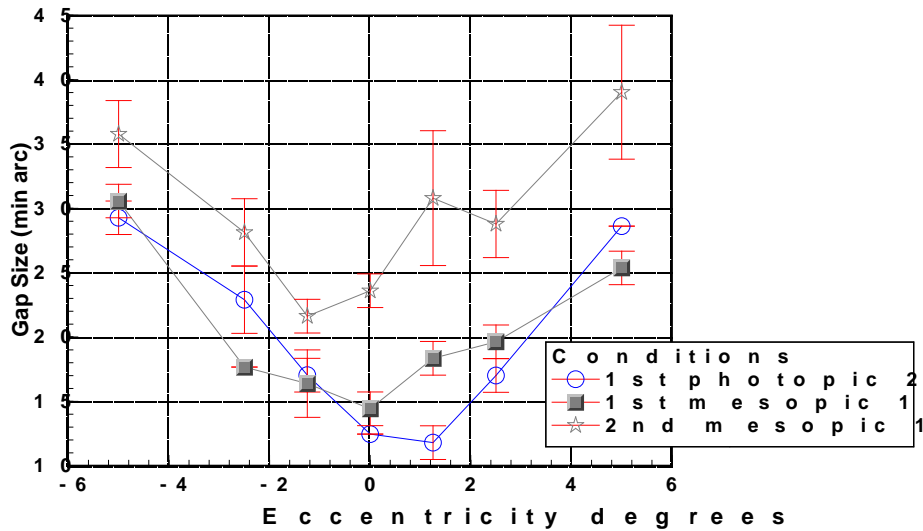


Figure A1.23: Effect of artificial 3 mm pupil on high contrast Mesopic Gap Acuity for subject LW. Error bars are 2 standard errors

The effect of an artificial 3 mm pupil on high contrast mesopic gap acuity, and of high contrast on the mesopic results, for subject LW is shown in figure A1.23. Subject LW shows high contrast mesopic thresholds reaching photopic levels, whilst the use of a 3 mm artificial pupil raises the contrast acuity thresholds as the artificial pupil reduces the size of the pupil to below the ideal pupil size (Campbell & Gregaory, 1960). The use of the artificial pupil reducing contrast acuity even at high contrast levels may reveal the importance of large pupils being required to achieve high acuity to increase retinal illuminance in spite of the increase in aberrations.

Appendix 2

A2. Other Significant Regressions

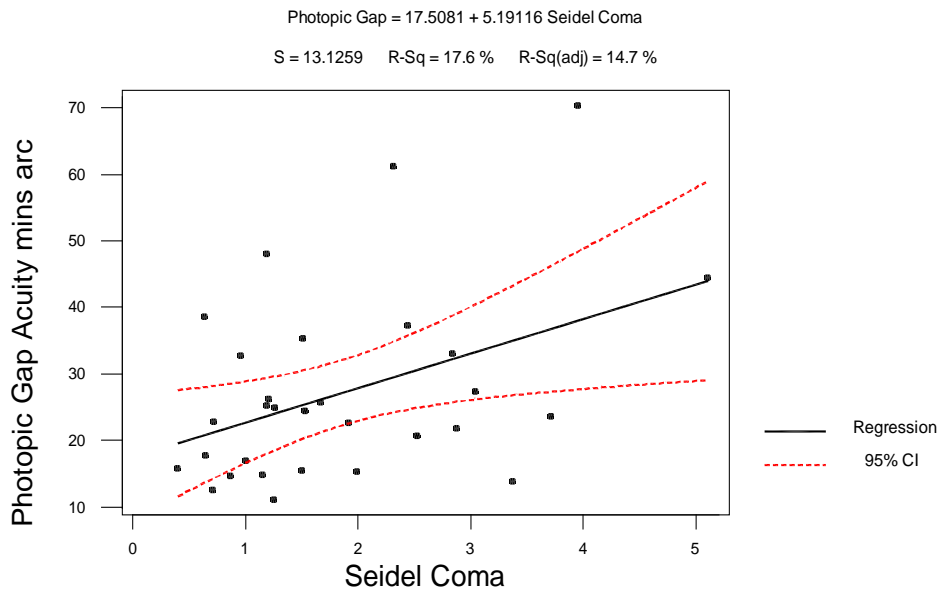


Figure A2.1 Linear regression between photopic central gap acuity and Seidel Coma

Figure A2.1 shows a statistically significant positive linear regression between photopic gap acuity ($P = 0.021$ adjusted $R^2 = 14.7\%$) and Seidel coma. Under mesopic conditions a linear regression between CAA gap acuity and Seidel Coma was not statistically significant ($P = 0.689$).

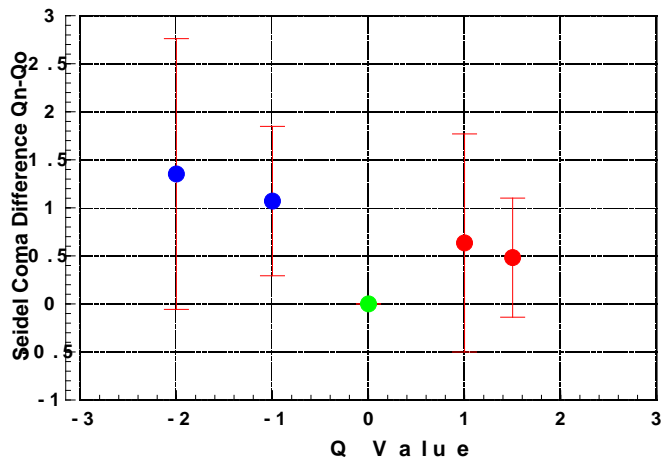


Figure A2.2: Seidel Coma Differences generated by the Q value lenses. Error bars are 2 standard errors.

Figure A2.2 shows that the Q value lenses generated changes in Seidel coma which may have led to the photopic results being influenced by Seidel coma. Mean differences generated by the Q value lenses appear to be greater for the negative value lenses rather than the positive value lenses. However the large overlapping standard error bars suggest that the differences are not statistically significant.

This may help to explain why smaller differences of spherical aberration were generated by the minus Q = -2 and Q = -1 contact lenses, compared to the positive Q = +1.5 and Q = +1 lenses (Chapter 6, Figure 6.5).

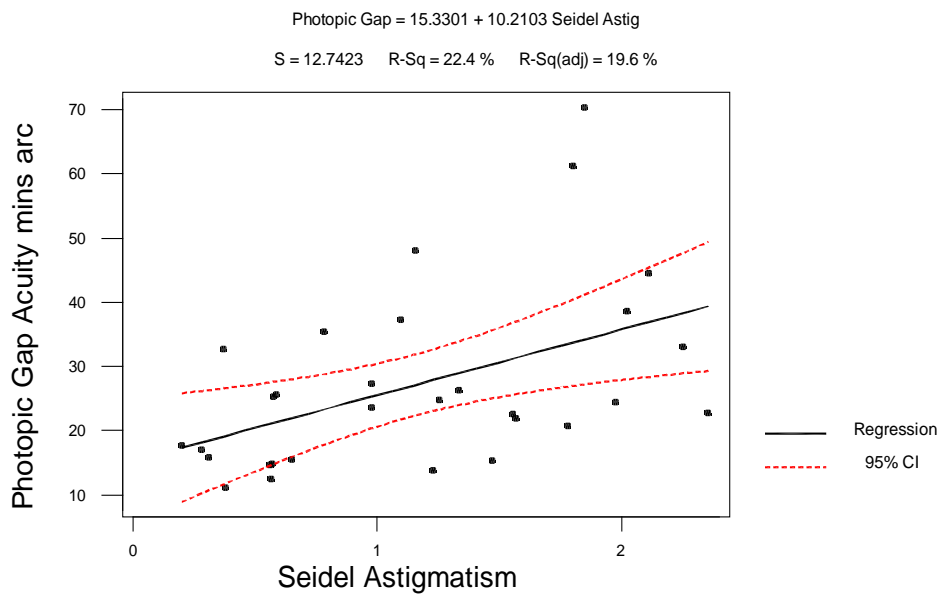


Figure A2.3 Linear regression between photopic central gap acuity and Seidel Astigmatism.

Figure A2.3 shows a positive linear regression between photopic gap acuity ($P = 0.008$ adjusted $R^2 = 19.6\%$) and Seidel astigmatism. Under mesopic conditions a linear regression between photopic CAA gap acuity and Seidel astigmatism gave no statistically significant trend..

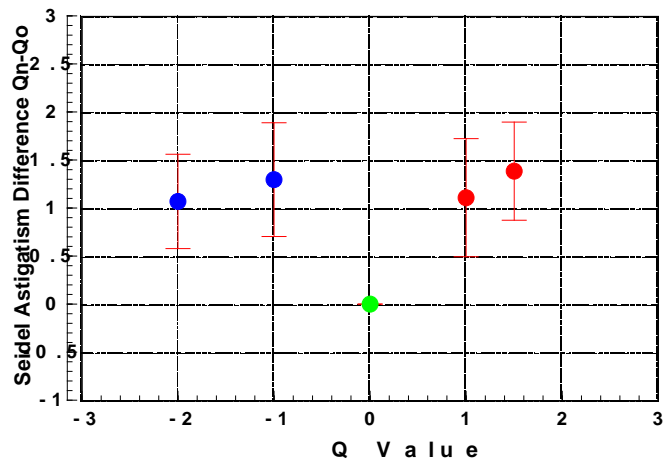
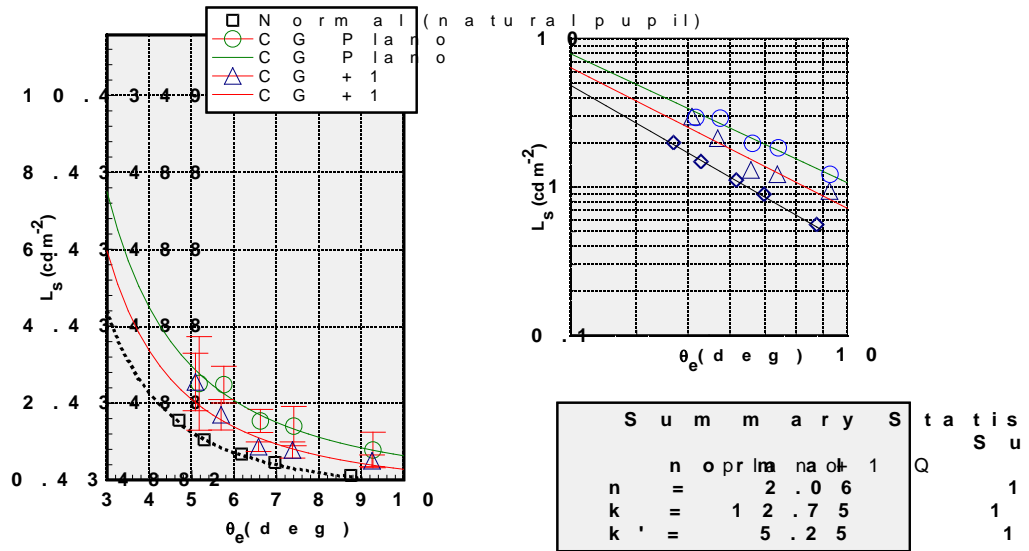


Figure A2.4: Seidel Astigmatism Differences generated by the Q value lenses. Error bars are 2 standard errors.

Figure A2.4 shows that the Q value lenses generated changes in Seidel astigmatism, which may have led to the photopic results being influenced by Seidel astigmatism. Mean differences generated by the Q value lenses appear to be similar for the negative value lenses and the positive value lenses.

Appendix 3

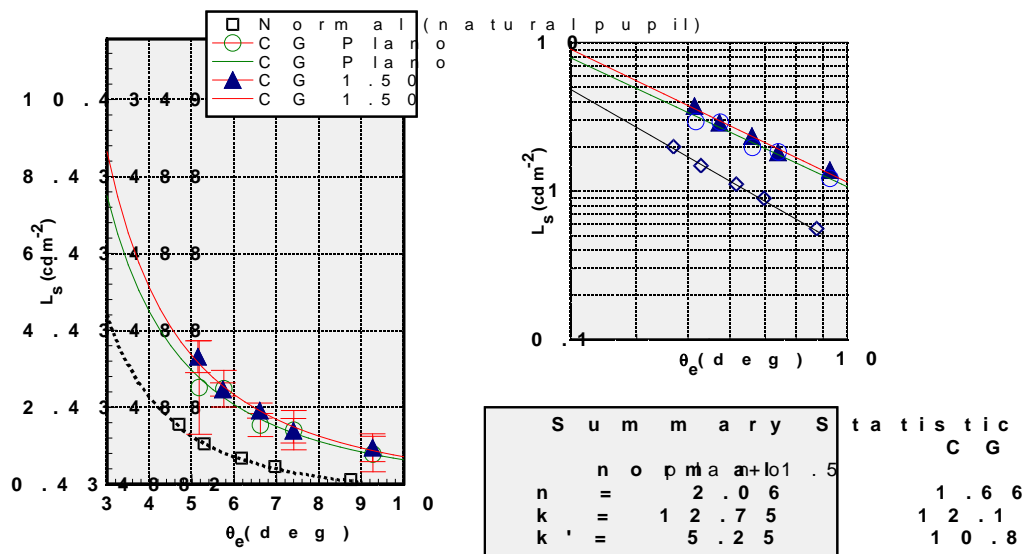
A3.1 Scatter and Spherical Aberration



The inset shows the same data on a log-log scale. The main plot shows the scatter function L_s (cd m⁻²) versus θ_e (deg) for four conditions: Normal (natural pupil), CG Plano, CG +1, and CG +1. The inset shows the same data on a log-log scale. A summary statistics table is provided below the plots.

Figure A3.1: Scatter function of the eye. Subject CG, Right eye tests. Q value plano and +1.00 Contact Lenses compared. Error bars represent two standard errors.

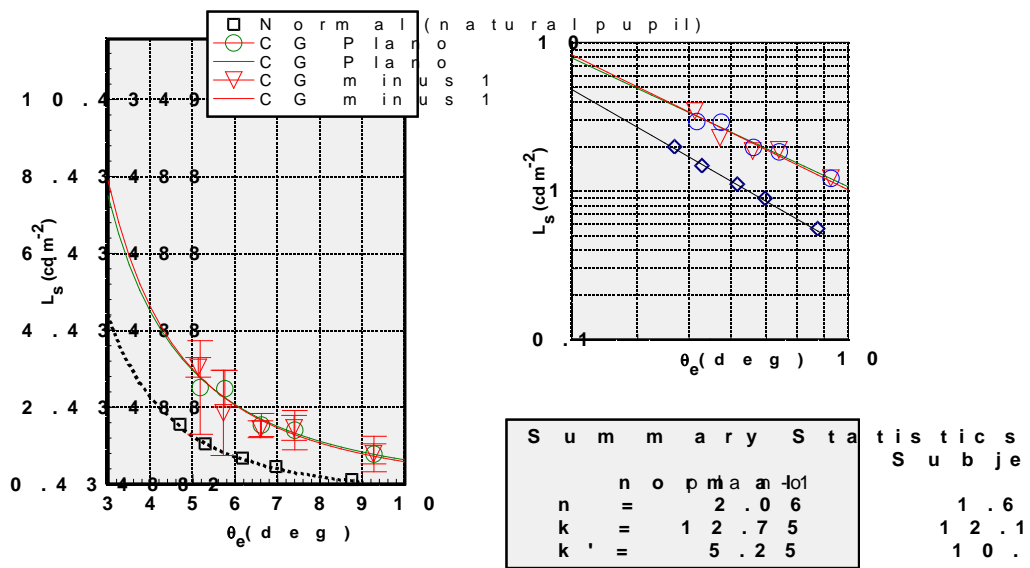
The scatter functions for subject CG for +1 and plano Q value contact lenses are shown in figure A3.1. The scatter index n values are decreased for the contact lenses, which suggests that there was increased angular distribution of scatter. The k values are also decreased, suggesting the straylight parameter was slightly decreased. However the integrated straylight parameter k' has increased, which suggests the scatter could have led to decreased visual performance. This elevated scatter function may have occurred due to the properties of the contact lenses, rather than the aberrations of the contact lenses. The plano contact lens appears to actually give a more elevated scatter function than the +1 Q value contact lenses, although the difference does not appear to be statistically significant, since their error bars overlap.



The inset shows the same data on a log-log scale of the empirical scatter function, L_s .

Figure A3.2: Scatter function of the eye. Subject CG Right eye tests, Q value plano and +1.50 Contact Lenses compared. Error bars represent two standard errors.

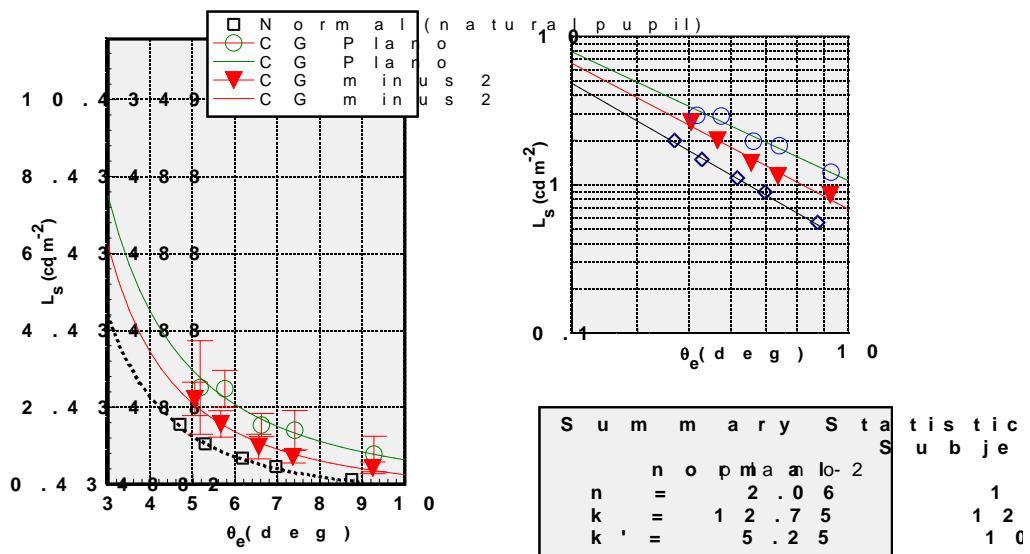
The Scatter function of the eye for subject CG comparing the results for Q value plano and +1.50 contact lenses are shown in figure A3.2. Like before, elevated scatter functions are shown for the +1.50 and plano contact lenses, compared to a normal eye. The scatter functions are graphically very similar for the contact lenses in the left hand diagram. The k and k' values are highest of all for the +1.5 contact lenses, indicating increased scatter, but the graphs on the left hand side suggest that the differences between the scatter generated by the +1 and 1.5 Q value lenses are not statistically significant, since the error bars overlap. The increases in scatter may have occurred due to the contact lenses themselves scattering light, rather than due to their different Q values.



The inset shows the same data on a log-log scale of the empirical scatter function, L_s .

Figure A3.3: Scatter function of the eye. Subject CG Right eye tests, Q value plano and -1.00 Contact Lenses compared. Error bars represent two standard errors.

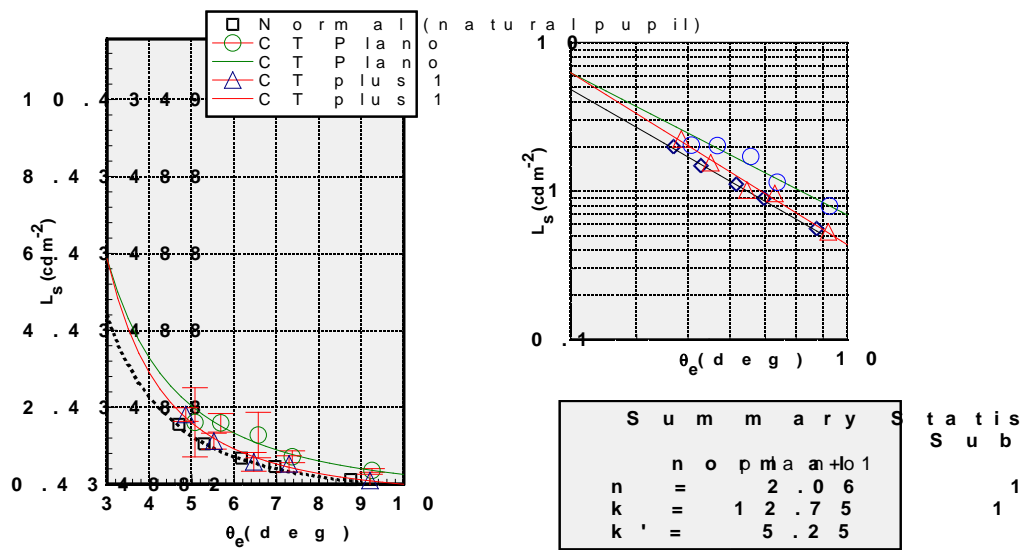
The Scatter function of the eye for subject CG comparing the results for Q value plano and -1.00 contact lenses are shown in figure A3.3. Elevated scatter functions are shown for the -1.00 and plano contact lenses, compared to a normal eye. The scatter functions are also graphically very similar for the contact lenses in both diagrams. The n, and k values are slightly higher for the -1.00 contact lenses, denoting increased scatter index n, or greater angular distribution of scatter, and increased straylight parameter k. However the integrated straylight parameter k', is slightly less for the -1.00 contact lens, indicating decreased scatter, despite the increase in Q value and aberrations.



The inset shows the same data on a log-log scale. The main plot shows the scatter function L_s (cd m⁻²) versus θ_e (deg) for three conditions: Normal (natural pupil), CG Plano, and CG minus 2. The inset shows the same data on a log-log scale, highlighting the power-law relationship between L_s and θ_e .

Figure A3.4: Scatter function of the eye. Subject CG, Right Eye, Q value plano and -2.00 Contact Lenses compared. Error bars represent two standard errors.

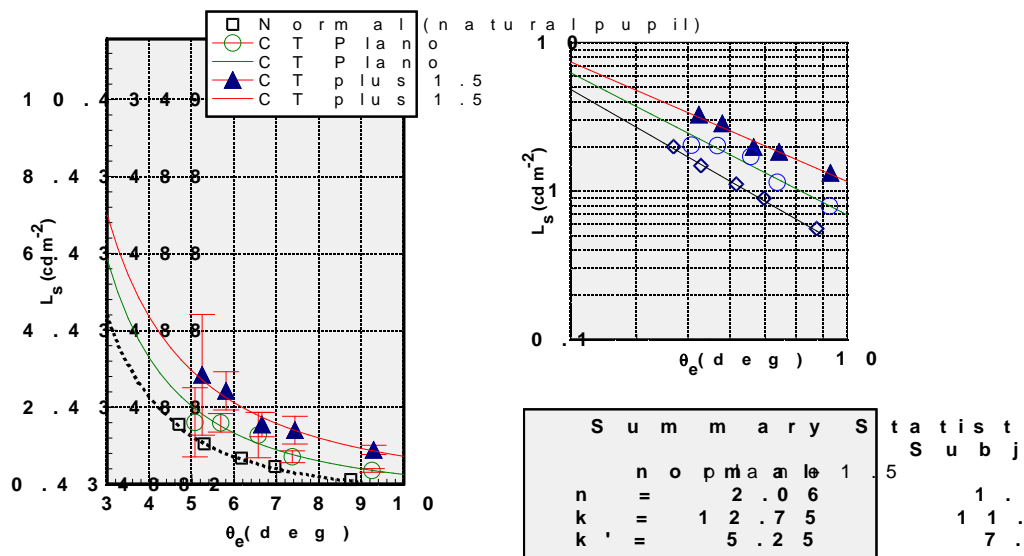
The Scatter function of the eye for subject CG comparing the results for Q value plano and -2.00 contact lenses are shown in figure A3.4. Elevated scatter functions are shown for the -2.00 and plano contact lenses, compared to a normal eye. The scatter functions are not as similar for the contact lenses as with the previous comparison. The n, and k values are slightly higher for the -2.00 contact lenses, denoting increased scatter index n or greater angular distribution of scatter, and increased straylight parameter k. However, the integrated straylight parameter k', is slightly less for the -2.00 contact lens, indicating decreased scatter, despite the increase in Q value and aberrations. This follows the trend for the -1.00 Q value contact lenses.



The inset shows the same data on a log-log scale. The main plot shows the scatter function L_s (cd m⁻²) versus the angle θ_e (deg). The inset shows the same data on a log-log scale, highlighting the power-law relationship between L_s and θ_e .

Figure A3.5: Scatter function of the eye. Subject CT, Left Eye, Q value plano and +1.00 Contact Lenses compared. Error bars represent two standard errors.

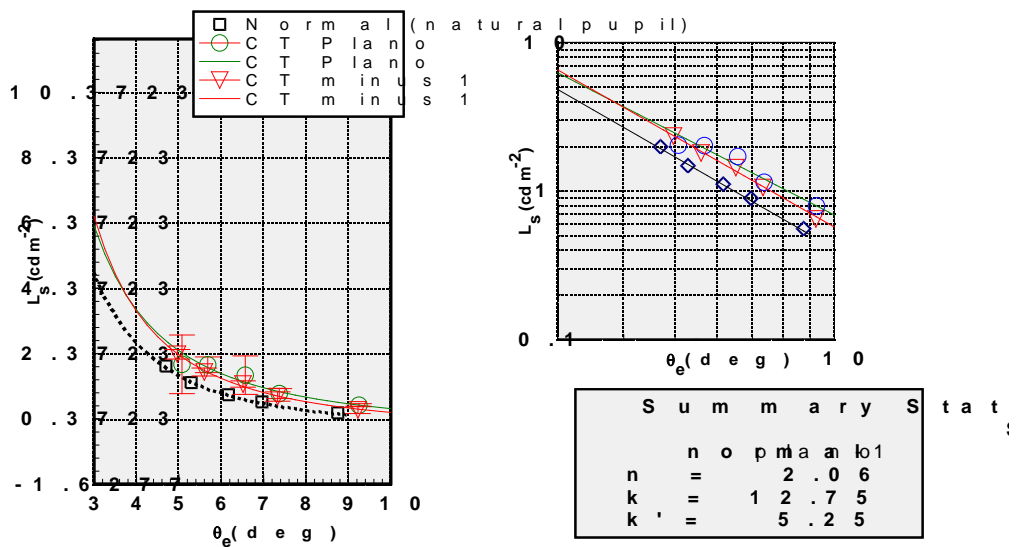
The Scatter function of the eye for subject CT comparing the results for Q value plano and +1.00 contact lenses are shown in figure A3.5. Only slightly elevated scatter functions are shown for the plano and +1.00 contact lenses, compared to a normal eye. All three scatter functions for a normal eye and the plano and +1.00 Q value contact lenses seem quite similar. For this subject, however, the plano contact lens gives the most elevated scatter function. The n and k values are slightly lower for the plano contact lenses, denoting decreased scatter index n or decreased angular distribution of scatter, and decreased straylight parameter k. However the integrated straylight parameter k', is slightly more for the +1.00 contact lens, indicating increased scatter. Conversely, for the +1.00 Q value contact lens, n and k was larger than the plano and normal eye values, but the k' value was very similar to the normal scatter function value. This made the +1.00 contact lens scatter function quite similar to the normal scatter function.



The inset shows the same data on a log-log scale. The main plot shows the scatter function L_s (cd m⁻²) versus θ_e (deg) for four conditions: Normal (natural pupil), CT Plano, CT plus 1.5, and CT plus 1.5. The inset shows the same data on a log-log scale. A summary statistics table is provided below the plots.

Figure A3.6: Scatter function of the eye. Subject CT, Left Eye, Q value plano and +1.50 Contact Lenses compared. Error bars represent two standard errors.

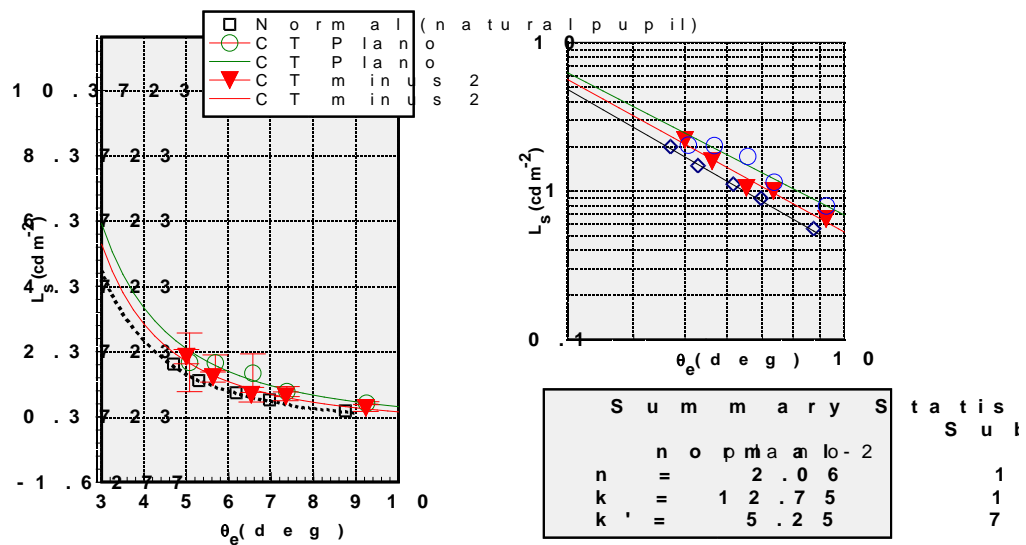
The Scatter function of the eye for subject CT comparing the results for Q value plano and +1.50 contact lenses are shown in figure A3.6. Elevated scatter functions are shown for the plano and +1.50 Q value contact lenses, compared to a normal eye. The scatter functions for the +1.50 Q value contact lens is more elevated, than the plano Q value contact lens scatter function, which in turn is more elevated than the scatter function of the normal eye. This could be used as an example of the increased aberrations appearing to affect the scatter function. However this example has not often been replicated and is actually a minority instance of such an occurrence. The n and k values are lower for the +1.50 Q value contact lenses, denoting decreased scatter index n or reduced angular distribution of scatter, and a decreased straylight parameter k. However, the integrated straylight parameter k', is more for the +1.50 contact lens, indicating increased scatter, compared to the plano Q value and normal scatter functions.



The inset shows the same data on a logarithmic scale for the empirical scatter function, L_s .

Figure A3.7: Scatter function of the eye. Subject CT, left eye, Q value plano and -1.00 Contact Lenses compared. Error bars represent two standard errors.

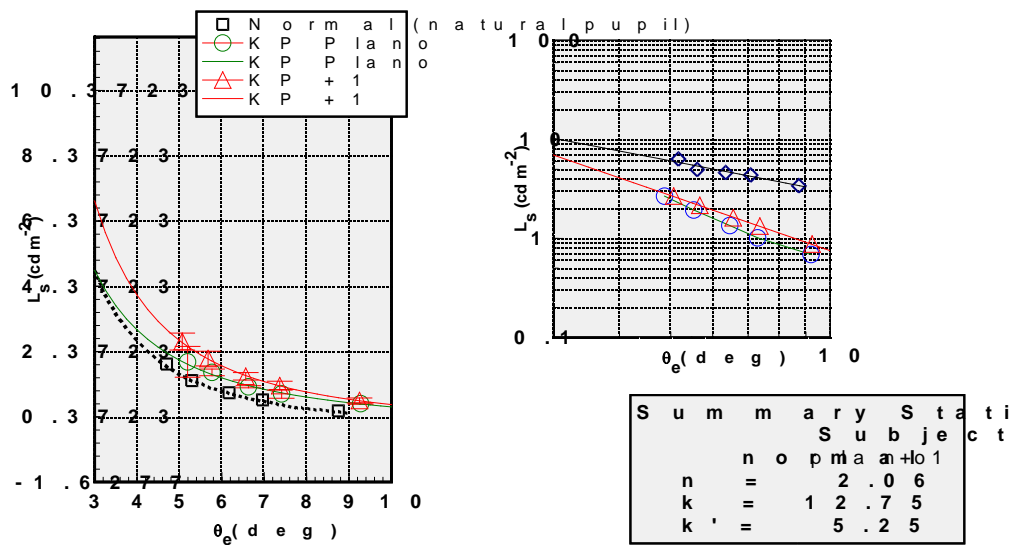
The Scatter function of the eye for subject CT comparing the results for Q value plano and -1.00 contact lenses are shown in figure A3.7. Only slightly elevated scatter functions are shown for the plano and -1.00 contact lenses, compared to a normal eye. The scatter functions for a normal eye and the plano and -1.00 Q value contact lenses seem to be quite similar. The n and k values are slightly lower for the plano contact lenses, denoting a decreased scatter index n or a decreased angular distribution of scatter, and a decreased straylight parameter k . However the integrated straylight parameter k' , is slightly more for the -1.00 contact lens, indicating increased scatter. For the -1.00 Q value contact lens, n and k are larger than the plano and normal eye values, but the k' value of the -1 Q value contact lens lies between the plano lens and normal scatter function value.



The inset shows the same data on a log-log scale. The main plot shows the scatter function L_s (cd m⁻²) versus θ_e (deg) for subject CT, left eye, comparing Q value plano and -2.00 Contact Lenses compared. Error bars represent two standard errors.

Figure A3.8: Scatter function of the eye. Subject CT, left eye, Q value plano and -2.00 Contact Lenses compared. Error bars represent two standard errors.

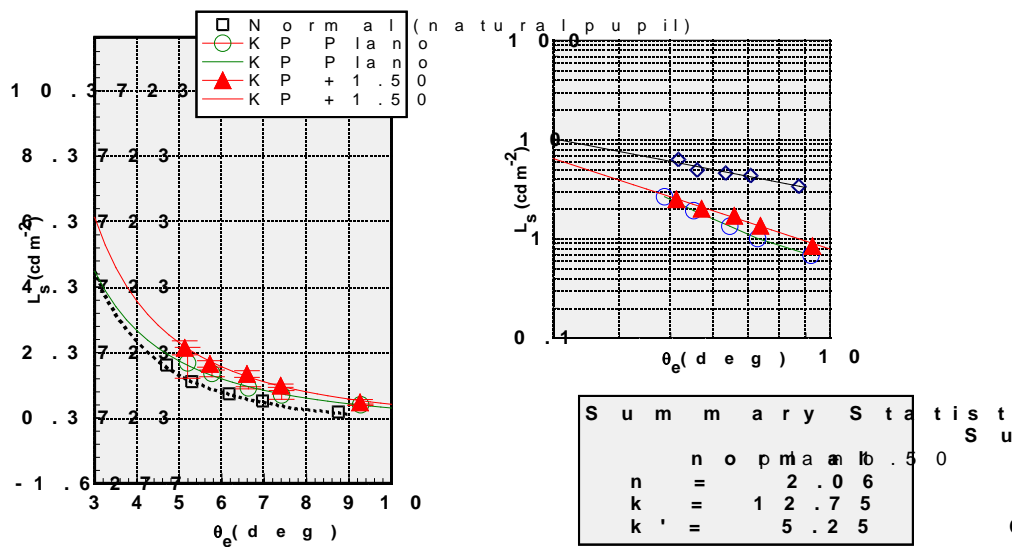
The Scatter function of the eye for subject CT comparing the results for Q value plano and -2.00 contact lenses are shown in figure A3.8. Only slightly elevated scatter functions are shown for the plano and -2.00 contact lenses, compared to a normal eye. The scatter functions for a normal eye and the plano and -2.00 Q value contact lenses seem to be quite similar. The n and k values are slightly lower for the plano and -2 Q value contact lenses, denoting decreased scatter index n or decreased angular distribution of scatter, and decreased straylight parameter k. However the integrated straylight parameter k', is slightly more for the -2.00 contact lens, indicating increased scatter. For the -2.00 Q value contact lens, the n, k and k' values lie between the plano and normal eye values. In this instance the -2 Q value contact lens scatter function also lies between the normal eye scatter function and plano contact lens, which suggests the -2 Q value aberrations created less scatter.



The inset shows the same data on the empirical $L_s \propto \theta_e^{-k}$ scatter function, L_s

Figure A3.9: Scatter function of the eye. Subject KP, right eye, Q value plano and +1.00 Contact Lenses compared. Error bars represent two standard errors.

The Scatter function of the eye for subject KP comparing the results for Q value plano and +1.00 contact lenses are shown in figure A3.9. Only slightly elevated scatter functions are shown for the plano and +1.00 contact lenses, compared to a normal eye. The scatter functions of the plano and +1.00 Q value contact lenses seem to be quite similar. The n and k values are slightly lower for the plano Q value contact lenses, denoting decreased scatter index n or decreased angular distribution of scatter, and a decreased straylight parameter k. However, the integrated straylight parameter k', is slightly more for the +1.00 and plano contact lens, than the normal eye k', indicating increased scatter. For the +1.00 Q value contact lens the k and k' values are greater than the plano and normal eye values, which gives an elevated scatter function.

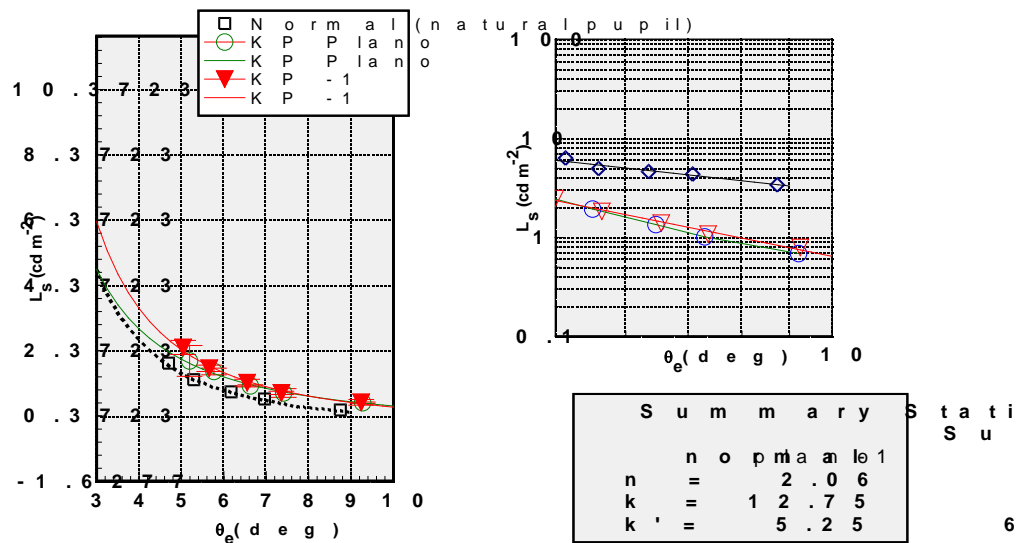


The inset shows the same data on the empirical scatter function, L_s

Figure A3.10: Scatter function of the eye. Subject KP, right eye, Q value plano and +1.50 Contact Lenses compared. Error bars represent two standard errors.

The Scatter function of the eye for subject KP comparing the results for Q value plano and +1.50 contact lenses are shown in figure A3.10. Like many of the results before, only slightly elevated scatter functions are shown for the plano and +1.50 contact lenses, compared to a normal eye. The scatter functions of the plano and +1.50 Q value contact lenses appear to be quite similar. The n and k values are lower for the plano Q value contact lenses, denoting decreased scatter index n or increased angular distribution of scatter, and a decreased straylight parameter k . However, the integrated straylight parameter k' , is greater for the +1.50 and plano contact lenses, than the normal eye k' , indicating increased scatter. For the +1.50 Q value contact lens the k' value is greater than the plano and normal eye values, which gives an

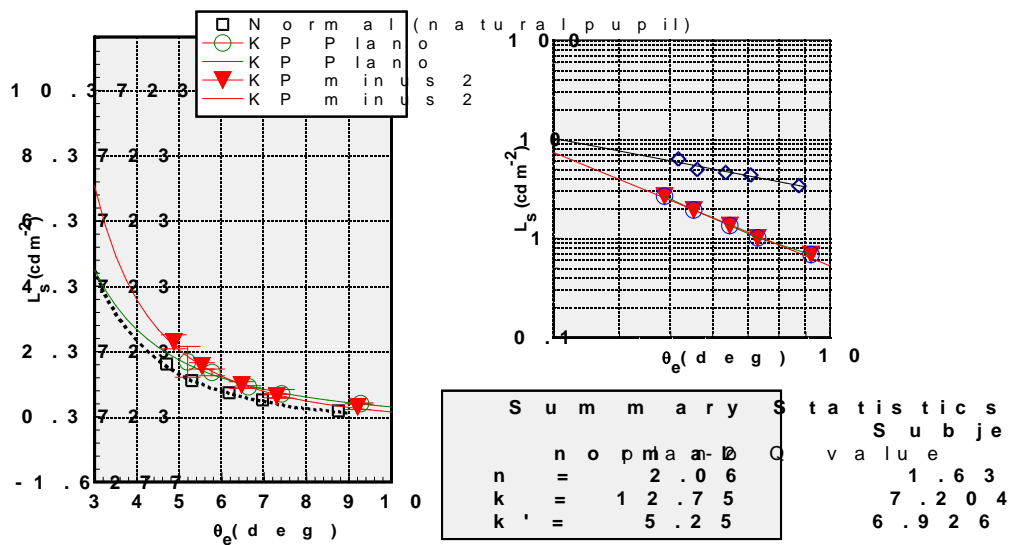
elevated scatter function.



The inset shows the same data on the empirical $L_s \propto \theta_e^{-k}$ scatter function, L_s

Figure A3.11: Scatter function of the eye. Subject KP, right eye, Q value plano and -1.00 Contact Lenses compared. Error bars represent two standard errors.

The Scatter function of the eye for subject KP comparing the results for Q value plano and -1.00 contact lenses are shown in figure A3.11. Only very slightly elevated scatter functions are shown for the plano and -1.00 contact lenses, compared to a normal eye. The scatter functions for the plano and -1.00 Q value contact lenses appear to be quite similar. The n and k values are lower for the plano and -1.00 Q value contact lenses, denoting decreased scatter index n or increased angular distribution of scatter, and a decreased straylight parameter k. However, the integrated straylight parameter k', is greater for the -1.00 and plano contact lenses, than the normal eye k', indicating increased scatter. For the -1.00 Q value contact lens, the k' value is only very slightly less than the plano contact lens values.



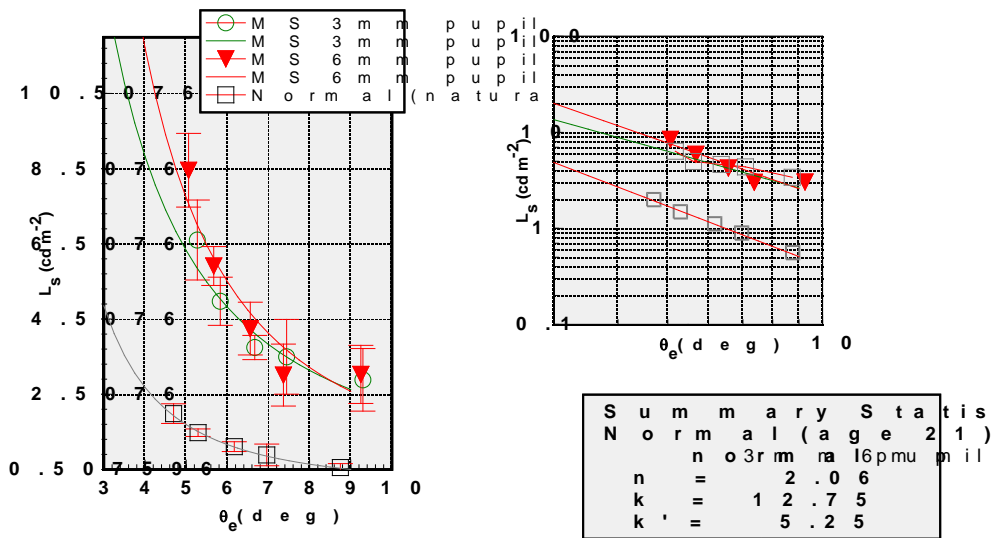
The inset shows the same data on a log-log scale. The main plot shows the empirical scatter function, L_s , versus the angle θ_e .

Figure A3.12: Scatter function of the eye. Subject KP, right eye, Q value plano and -2.00 Contact Lenses compared. Error bars represent two standard errors.

The Scatter function of the eye for subject KP comparing the results for Q value plano and -2.00 contact lenses are shown in figure A3.12. Like the previous results for this subject, only very slightly elevated scatter functions are shown for the plano and -2.00 contact lenses, compared to a normal eye. The scatter functions for the plano and -2.00 Q value contact lenses appear to be quite similar. The n and k values are lower for the -2.00 Q value contact lenses, denoting decreased scatter index n or increased angular distribution of scatter, and a decreased straylight parameter k . However, the integrated straylight parameter k' , is greater for the -2.00 and plano contact lenses, than the normal eye k' , indicating increased scatter. For the -2.00 Q value contact lens, the k' value is slightly less than the plano contact lens values. Subject KP appears to have shown very little variation between the different aberration controlled contact lenses, whilst subjects CT and CG showed more variation, but no definite trends.

A3.2 Scatter and Pupil Sizes

Scatter was measured in 4 subjects, dilated with 2.5% phenylephrine using 6 mm and 3 mm artificial pupils. A large variation in results occurred. The aim was to determine whether an increase in pupil size lead to more scatter in contrast to an increase in aberrations.



Scatter function of the eye. Subject MS. The inset shows the same data on a log-log scale. The empirical Akaike scatter function, L_s .

Figure A3.13 Scatter Function for 6 and 3 mm pupils for Subject MS

The results for subject MS are displayed in figure A3.13. The results appear to show increased elevated scatter functions for the 6 and 3 mm pupils, compared to a normal eye. The n values are lowest of all for the 6 mm pupil, and the k and k' are highest for the 6 mm pupil, which suggests the 6 mm pupil gave the most scatter, followed by the 3 mm pupil.

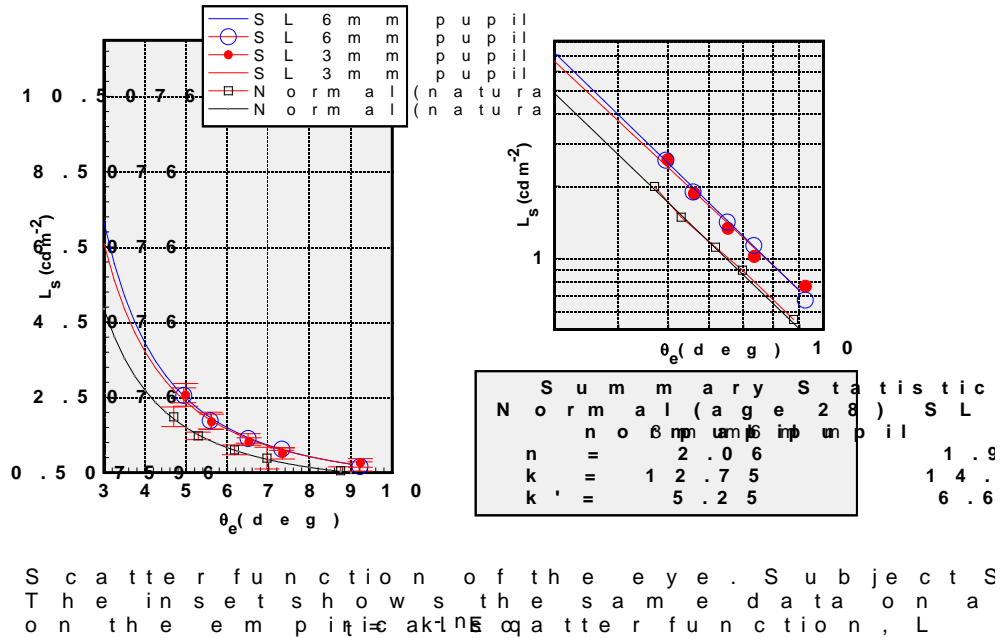


Figure A3.14. Scatter Function for 6 and 3 mm pupils for Subject SL

The results for subject SL are displayed in figure A3.14. The results appear to show very slightly elevated scatter functions for the 6 and 3 mm pupils, compared to a normal eye. The scatter functions for the 6 and 3 mm pupils appear to be graphically very similar. The n values are lowest of all for the 3 mm pupil, and the k and k' are highest for the 6 mm pupil, which suggests the 6 mm pupil gave the most scatter, followed by the 3 mm pupil. However the difference in k' values is very small and the graphs show very small differences, which suggests that for this subject, the 3 and 6 mm artificial pupils had little effect on scatter.

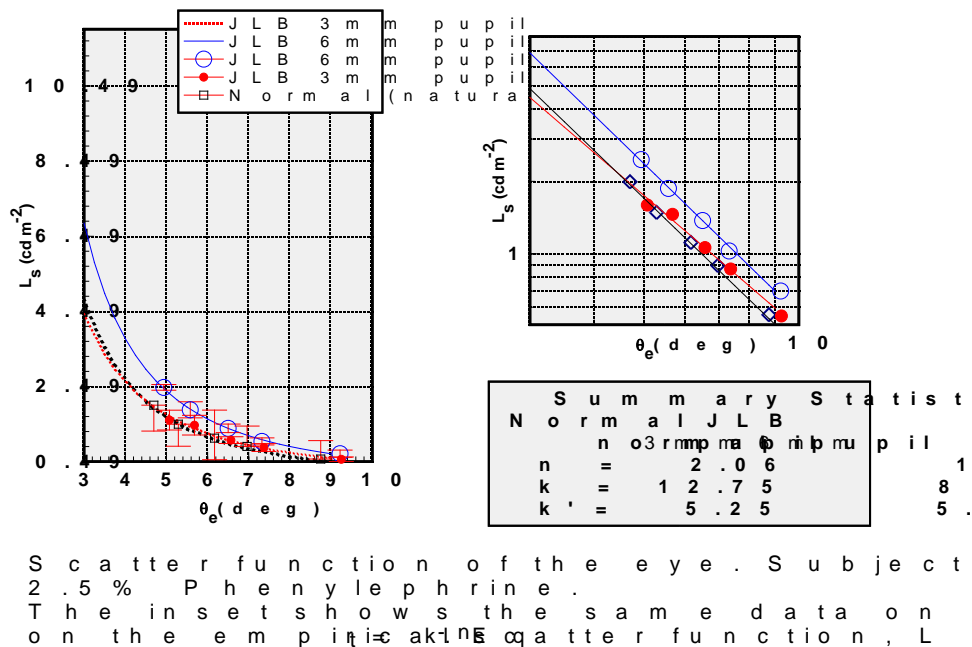


Figure A3.15. Scatter Function for 6 and 3 mm pupils for Subject JLB

The results for subject JLB are displayed in figure A3.15. The results appear to show very slightly elevated scatter functions for the 6 mm pupils, compared to a normal eye, but the artificial 3 mm pupil appears to give a scatter function very similar to the normal scatter function.. The n values are lowest of all for the 3 mm pupil, and the k and k' are highest for the 6 mm pupil, which suggests the 6 mm pupil gave the most scatter. The 3 mm pupil gives the smallest k and k' values, suggesting it resulted in the smallest amount of scatter compared to the normal and 6 mm pupil. The 6 mm pupil k and k' values gave the greatest values, suggesting that the 6 mm pupil gave the greatest scatter.

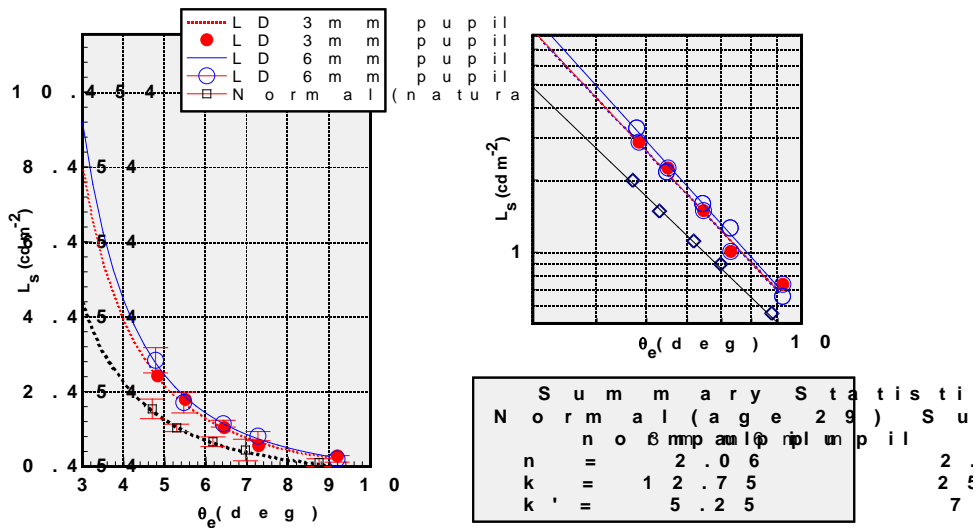


Figure A3.16. Scatter Function for 6 and 3 mm pupils for Subject LD

The results for subject LD are displayed in figure A3.16. The results appear to show elevated scatter functions for the 6 and 3 mm pupils, compared to a normal eye. The n , k and k' values are highest of all for the 6 mm pupil. The 3 mm pupil gives n , k and k' values between the normal scatter values and the k' values. The 6 mm pupil k and k' values gave the greatest values, suggesting that the 6 mm pupil gave the greatest scatter. These results for subject LD suggest that the 6 mm pupil gave the most amount of scatter followed by the 3 mm pupil. Overall the results revealed a general trend of increased scatter with increasing pupil diameter, but the trend was quite weak.

Reference List

1. Alarcon A, Anera RG, Villa C, Jimenez dB, Gutierrez R. Visual quality after monovision correction by laser in situ keratomileusis in presbyopic patients. *J Cataract Refract Surg.* 2011;37:1629-35.
2. Albright TD. Direction and orientation selectivity of neurons in visual area MT of the macaque. *J Neurophysiol.* 1984;52:1106-30.
3. Alexandridis E, Leendertz JL, Barbur JL. Methods for studying the behaviour of the pupil. *J Psychophysiol.* 1991;5:223-39.
4. Alio JL, Pinero DP, Espinosa MJ, Corral MJ. Corneal aberrations and objective visual quality after hyperopic laser in situ keratomileusis using the Esiris excimer laser. *J Cataract Refract Surg.* 2008;34:398-406.
5. Allen MJ, VOS JJ. Ocular scattered light and visual performance as a function of age. *Am J Optom Arch Am Acad Optom.* 1967;44:717-27.
6. Amesbury EC, Schallhorn SC. Contrast sensitivity and limits of vision. *Int Ophthalmol Clin.* 2003;43:31-42.
7. Anderson NJ, Beran RF, Schneider TL. Epi-LASEK for the correction of myopia and myopic astigmatism. *J Cataract Refract Surg.* 2002;28:1343-7.
8. Anderson SJ, Burr DC. Spatial and temporal selectivity of the human motion detection system. *Vision Res JID - 0417402.* 1985;25:1147-54.
9. Anera RG, Jimenez JR, Jimenez dB, Hita E. Changes in corneal asphericity after laser refractive surgery, including reflection losses and nonnormal incidence upon the anterior cornea. *Opt Lett.* 2003;28:417-9.
10. Ang RE, Chan WK, Wee TL, Lee HM, Bunnapradist P, Cox I. Efficacy of an aspheric treatment algorithm in decreasing induced spherical aberration after laser in situ keratomileusis. *J Cataract Refract Surg.* 2009;35:1348-57.
11. Ansari EA, Morgan JE, Snowden RJ. Psychophysical characterisation of early functional loss in glaucoma and ocular hypertension. *Br J Ophthalmol.* 2002;86:1131-5.
12. Applegate RA, Gansel KA. The importance of pupil size in optical quality measurements following radial keratotomy. *Refract Corneal Surg.* 1990;6:47-54.

13. Applegate RA, Howland HC, Sharp RP, Cottingham AJ, Yee RW. Corneal aberrations and visual performance after radial keratotomy. *J Refract Surg JID* - 9505927. 1998;14:397-407.
14. Applegate RA, Hilmantel G, Howland HC, Tu EY, Starck T, Zayac EJ. Corneal first surface optical aberrations and visual performance. *J Refract Surg*. 2000;16:507-14.
15. Applegate RA, Sarver EJ, Khemsara V. Are all aberrations equal? *J Refract Surg*. 2002;18:S556-S562
16. Applegate RA, Ballentine C, Gross H, Sarver EJ, Sarver CA. Visual acuity as a function of Zernike mode and level of root mean square error. *Optom Vis Sci*. 2003;80:97-105.
17. Applegate RA, Marsack JD, Ramos R, Sarver EJ. Interaction between aberrations to improve or reduce visual performance. *J Cataract Refract Surg*. 2003;29:1487-95.
18. Applegate RA, Marsack JD, Thibos LN. Metrics of retinal image quality predict visual performance in eyes with 20/17 or better visual acuity. *Optom Vis Sci*. 2006;83:635-40.
19. Arbelaez MC, Aslanides IM, Barraquer C, et al. LASIK for myopia and astigmatism using the SCHWIND AMARIS excimer laser: an international multicenter trial. *J Refract Surg*. 2010;26:88-98.
20. Artal P, Marcos S, Iglesias I, Green DG. Optical modulation transfer and contrast sensitivity with decentered small pupils in the human eye. *Vision Res*. 1996;36:3575-86.
21. Artal P, Fernandez EJ, Manzanera S. Are optical aberrations during accommodation a significant problem for refractive surgery? *J Refract Surg*. 2002;18:S563-S566
22. Artal P, Berrio E, Guirao A, Piers P. Contribution of the cornea and internal surfaces to the change of ocular aberrations with age. *J Opt Soc Am A Opt Image Sci Vis*. 2002;19:137-43.
23. Artal P, Chen L, Fernandez EJ, Singer B, Manzanera S, Williams DR. Neural compensation for the eye's optical aberrations. *J Vis*. 2004;4:281-7.

24. Atchison DA, Smith G. Monochromatic aberrations of schematic eyes. In: Anonymous *Optics of the human eye*. Οξφόρδ: Butterworth-Heinemann., 2000:
25. Atchison DA, Scott DH. Monochromatic aberrations of human eyes in the horizontal visual field. *J Opt Soc Am A Opt Image Sci Vis*. 2002;19:2180-4.
26. Atchison DA. Higher order aberrations across the horizontal visual field. *J Biomed Opt*. 2006;11:34026
27. Azzopardi P, Cowey A. Preferential representation of the fovea in the primary visual cortex. *Nature JID - 0410462*. 1993;361:719-21.
28. Bababeygy SR, Zoumalan CI, Manche EE. Visual outcomes of wavefront-guided laser in situ keratomileusis in eyes with moderate or high myopia and compound myopic astigmatism. *J Cataract Refract Surg*. 2008;34:21-7.
29. Babizhayev MA, Deyev AI, Yermakova VN, et al. Image analysis and glare sensitivity in human age-related cataracts. *Clin Exp Optom*. 2003;86:157-72.
30. Banks MS, Sekuler AB, Anderson SJ. Peripheral spatial vision: limits imposed by optics, photoreceptors, and receptor pooling. *J Opt Soc Am A JID - 8402086*. 1991;8:1775-87.
31. Barbur JL, Thomson WD, Forsyth PM. A new system for the simultaneous measurement of pupil size and two-dimensional eye movements. *Clin Vis Sci*. 1987;2:131-42.
32. Barbur JL, de Cunha D, Harlow AJ, oodward EG. Methods for the measurement and analysis of light scattered in the human eye. *J Opt Soc Am*. 1993;Non-invasive Assessment of the Visual System (Technical Digest Series):170-3.
33. Barbur, J. L and Goodbody, A. Expt. No 14 - The Measurement & Analysis of Light Scattered in the Human Eye. 1995. Ref Type: Unpublished Work
34. Barbur, J. L. The influence of defocus on the City University Light Scatter Program. 1997. Ref Type: Personal Communication
35. Barbur JL, Forsyth PM, Findlay JM. Human saccadic eye movements in the absence of the geniculocalcarine projection. *Brain*. 1988;111 (Pt 1):63-82.
36. Barbur JL, Harlow AJ, Sahraie A. Pupillary responses to stimulus structure, colour and movement. *Ophthalmic Physiol Opt*. 1992;12:137-41.

37. Barbur JL, Edgar DF, Woodward EG. Measurement of the scattering characteristics of the eye in relation to pupil size. *Optical Society of America*. 1995;1:250-3.
38. Barnes S, Werblin F. Gated currents generate single spike activity in amacrine cells of the tiger salamander retina. *Proc Natl Acad Sci U S A*. 1986;83:1509-12.
39. Baseler HA, Sutter EE. M and P components of the VEP and their visual field distribution. *Vision Res*. 1997;37:675-90.
40. Beckman C, Abrahamsson M, Sjostrand J, Hard S. Evaluation of a clinical glare test based on estimation of intraocular light scatter. *Optom Vis Sci*. 1991;68:881-7.
41. Benito A, Redondo M, Artal P. Temporal evolution of ocular aberrations following laser in situ keratomileusis. *Ophthalmic Physiol Opt*. 2011;31:421-8.
42. Bottos KM, Leite MT, Aventura-Isidro M, et al. Corneal asphericity and spherical aberration after refractive surgery. *J Cataract Refract Surg*. 2011;37:1109-15.
43. Bouma H. Interaction effects in parafoveal letter recognition. *Nature*. 1970;226:177-8.
44. Boycott B, Wassle H. Parallel processing in the mammalian retina: the Proctor Lecture. *Invest Ophthalmol Vis Sci*. 1999;40:1313-27.
45. Boynton RM. *Human Color Vision*. New York: Holt, Rinehart, and Winston, 1979:
46. Bricola G, Scotto R, Mete M, Cerruti S, Traverso CE. A 14-year follow-up of photorefractive keratectomy. *J Refract Surg*. 2009;25:545-52.
47. Budak K, Khater TT, Friedman NJ, Holladay JT, Koch DD. Evaluation of relationships among refractive and topographic parameters. *J Cataract Refract Surg*. 1999;25:814-20.
48. Bühren J, Pesudovs K, Martin T, Strenger A, Yoon G, Kohnen T. Comparison of optical quality metrics to predict subjective quality of vision after laser in situ keratomileusis. *J Cataract Refract Surg*. 2009;35:846-55.
49. Calkins DJ, Sterling P. Evidence that circuits for spatial and color vision segregate at the first retinal synapse. *Neuron*. 1999;24:313-21.

50. Calossi A. Corneal asphericity and spherical aberration. *J Refract Surg.* 2007;23:505-14.
51. Campbell CE. Matrix method to find a new set of Zernike coefficients from an original set when the aperture radius is changed. *J Opt Soc Am A Opt Image Sci Vis.* 2003;20:209-17.
52. Campbell FW, Gregory AH. Effect of size of pupil on visual acuity. *Nature.* 1960;187:1121-3.
53. Carlsson L, Knave B, Lennerstrand G, Wibom R. Glare from outdoor high mast lighting: effects on visual acuity and contrast sensitivity in comparative studies of different floodlighting systems. *Acta Ophthalmol Suppl.* 1984;161:84-93.
54. Cervino A, Bansal D, Hosking SL, Montes-Mico R. Objective measurement of intraocular forward light scatter using Hartmann-Shack spot patterns from clinical aberrometers. Model-eye and human-eye study. *J Cataract Refract Surg.* 2008;34:1089-95.
55. Cervino A, Gonzalez-Meijome JM, Linhares JM, Hosking SL, Montes-Mico R. Effect of sport-tinted contact lenses for contrast enhancement on retinal straylight measurements. *Ophthalmic Physiol Opt.* 2008;28:151-6.
56. Charman WN. Optical aberrations of the eye, Part I. *Optician.* 2003;225:18-22.
57. Charman WN. Wavefront aberration of the eye: a review. *Optom Vis Sci JID -* 8904931. 1991;68:574-83.
58. Charman WN. Understanding ocular wavefront aberration. Part 1. *Optician.* 2005;230:24-9.
59. Chen CC, Izadshenas A, Rana MA, Azar DT. Corneal asphericity after hyperopic laser in situ keratomileusis. *J Cataract Refract Surg.* 2002;28:1539-45.
60. Cheng, X., Bradley, A., Thibos, L. N., and Ravikumar, S. Impact of monochromatic aberrations on vision [Abstract]. *Invest Ophthalmol Vis Sci* 44 (Suppl). 2003. Ref Type: Abstract
61. Cheng X, Bradley A, Thibos LN. Predicting subjective judgment of best focus with objective image quality metrics. *J Vis.* 2004;4:310-21.

62. Chisholm, C. M. Assessment of visual performance: comparison of normal subjects and post-refractive surgery patients. 2003. Ref Type: Thesis/Dissertation
63. Chisholm CM, Evans AD, Harlow JA, Barbur JL. New test to assess pilot's vision following refractive surgery. *Aviat Space Environ Med.* 2003;74:551-9.
64. Chylack LTJ, Wolfe JK, Singer DM, et al. The Lens Opacities Classification System III. The Longitudinal Study of Cataract Study Group. *Arch Ophthalmol.* 1993;111:831-6.
65. Coe CD, Bower KS, Brooks DB, Stutzman RD, Hammer JB. Effect of blast trauma and corneal foreign bodies on visual performance. *Optom Vis Sci.* 2010;87:604-11.
66. Corbetta M, Miezin FM, Dobmeyer S, Shulman GL, Petersen SE. Attentional modulation of neural processing of shape, color, and velocity in humans. *Science.* 1990;248:1556-9.
67. Cox I, Holden BA. Soft contact lens-induced longitudinal spherical aberration and its effect on contrast sensitivity. *Optom Vis Sci.* 1990;67:679-83.
68. Curcio CA, Owsley C, Jackson GR. Spare the rods, save the cones in aging and age-related maculopathy. *Invest Ophthalmol Vis Sci.* 2000;41:2015-8.
69. Dacey DM, Lee BB. The 'blue-on' opponent pathway in primate retina originates from a distinct bistratified ganglion cell type. *Nature.* 1994;367:731-5.
70. Dacey DM, Lee BB, Stafford DK, Pokorny J, Smith VC. Horizontal cells of the primate retina: cone specificity without spectral opponency. *Science.* 1996;271:656-9.
71. Dacheux RF, Raviola E. Physiology of HI horizontal cells in the primate retina. *Proc R Soc Lond B Biol Sci.* 1990;239:213-30.
72. Daniel PM, Whitteridge ED. The representation of the visual field on the cerebral cortex in monkeys. *J Physiol (Paris) JID - 9309350.* 1961;159:203-21.
73. Danilova MV, Bondarko VM. Foveal contour interactions and crowding effects at the resolution limit of the visual system. *J Vis.* 1912;7:25-18.
74. Davies N, Diaz-Santana L, Lara-Saucedo D. Repeatability of ocular wavefront measurement. *Optom Vis Sci.* 2003;80:142-50.

75. de Gracia P, Dorronsoro C, Marin G, Hernandez M, Marcos S. Visual acuity under combined astigmatism and coma: optical and neural adaptation effects. *J Vis.* 2011;11:
76. de Monasterio FM, Gouras P. Functional properties of ganglion cells of the rhesus monkey retina. *J Physiol.* 1975;251:167-95.
77. De Valois RL, Albrecht DG, Thorell LG. Spatial frequency selectivity of cells in macaque visual cortex. *Vision Res.* 1982;22:545-59.
78. de Waard PW, Ijspeert JK, van den Berg TJ, de Jong PT. Intraocular light scattering in age-related cataracts. *Invest Ophthalmol Vis Sci.* 1992;33:618-25.
79. Deeley RJ, Drasdo N. The effect of optical degradation on the contrast sensitivity function measured at the fovea and in the periphery. *Vision Res.* 1987;27:1179-86.
80. DeYoe EA, Van ED. Concurrent processing streams in monkey visual cortex. *Trends Neurosci.* 1988;11:219-26.
81. Diaz Santana Haro, L. Wavefront Sensing in the Human Eye with a Shack-Hartmann Sensor. 2000. Imperial College of Science, Technology and Medicine, University of London. Ref Type: Thesis/Dissertation
82. Diaz SH, Dainty JC. Single-pass measurements of the wave-front aberrations of the human eye by use of retinal lipofuscin autofluorescence. *Opt Lett.* 1999;24:61-3.
83. Dietze HH, Cox MJ. Limitations of correcting spherical aberration with aspheric intraocular lenses. *J Refract Surg.* 2005;21:S541-S546
84. Donnelly WJ, Pesudovs K, Marsack JD, Sarver EJ, Applegate RA. Quantifying scatter in Shack-Hartmann images to evaluate nuclear cataract. *J Refract Surg.* 2004;20:S515-S522
85. Dow BM, Snyder AZ, Vautin RG, Bauer R. Magnification factor and receptive field size in foveal striate cortex of the monkey. *Exp Brain Res JID - 0043312.* 1981;44:213-28.
86. Drasdo N. The neural representation of visual space. *Nature JID - 0410462.* 1977;266:554-6.

87. Drasdo, N., Thompson, C. M., and Deeley, R. J. Psychophysical Evidence of Two Gradients of Neural Sampling in Peripheral Vision. Proc.NATO Advanced Research Workshop, Roros 1990 . 6-8-1990. NY, USA, Plenum Press.
88. Duffey, R. J. and Learning, D. U.S. Trends in Refractive Surgery: 2010 ISRS Survey. Internet . 2010. Ref Type: Electronic Citation Date Accessed February 2013
89. Durrie DS, Smith RT, Waring GO, Stahl JE, Schwendeman FJ. Comparing conventional and wavefront-optimized LASIK for the treatment of hyperopia. J Refract Surg. 2010;26:356-63.
90. Edgar DF, Barbur JL, Woodward EG. Pupil size measurements in relation to light scatter in the eye [abstract]. Invest Ophthalmol Vis Sci. 1995;36:σ938
91. Elliott DB, Hurst MA. Simple clinical techniques to evaluate visual function in patients with early cataract. Optom Vis Sci. 1990;67:822-5.
92. Elliott DB, Bullimore MA. Assessing the reliability, discriminative ability, and validity of disability glare tests. Invest Ophthalmol Vis Sci. 1993;34:108-19.
93. Ewbank A. Ten years of Trends in UK refractive surgery. Optician. 2010;
94. Famiglietti EVJ, Kolb H. Structural basis for ON-and OFF-center responses in retinal ganglion cells. Science. 1976;194:193-5.
95. Fang F, He S. Crowding alters the spatial distribution of attention modulation in human primary visual cortex. J Vis. 2008;8:6-9.
96. Fang L, Wang Y, He X. Evaluation of optical quality in white light from wavefront aberrations for a myopic population of human eyes. Clin Exp Optom. 2009;92:313-9.
97. Farah SG, Azar DT, Gurdal C, Wong J. Laser in situ keratomileusis: literature review of a developing technique. J Cataract Refract Surg. 1998;24:989-1006.
98. Felisbert FM, Solomon JA, Morgan MJ. The role of target salience in crowding. Perception. 1907;34:823-33.
99. Fernandez-Sanchez V, Ponce ME, Lara F, Montes-Mico R, Castejon-Mochon JF, Lopez-Gil N. Effect of 3rd-order aberrations on human vision. J Cataract Refract Surg. 2008;34:1339-44.

100. Fernandez, E. J, Unterhuber, A, Prieto, P. M., Hermann, B, Drexler, and Artal, P. Near infrared ocular wavefront sensing with femtosecond laser. *Invest Ophthalmol Vis Sci* 45. 2004. Ref Type: Abstract
101. Fick AE. Ueber Stabchensehschärfe und Zapfensehschärfe. *Arch f.Ophth.* 1898;45:336-56.
102. Fleming JF. Corneal asphericity and visual function after radial keratotomy. *Cornea.* 1993;12:233-40.
103. Franssen L, Tabernero J, Coppens JE, van den Berg TJ. Pupil size and retinal straylight in the normal eye. *Invest Ophthalmol Vis Sci.* 2007;48:2375-82.
104. Fuster JM, Jervey JP. Inferotemporal neurons distinguish and retain behaviorally relevant features of visual stimuli. *Science.* 1981;212:952-5.
105. Gallant JL, Braun J, Van ED. Selectivity for polar, hyperbolic, and Cartesian gratings in macaque visual cortex. *Science.* 1993;259:100-3.
106. Gamaly TO, El Danasoury A, El Maghraby A. A prospective, randomized, contralateral eye comparison of epithelial laser in situ keratomileusis and photorefractive keratectomy in eyes prone to haze. *J Refract Surg.* 2007;23:S1015-S1020
107. Gatinel D, Malet J, Hoang-Xuan T, Azar DT. Corneal asphericity change after excimer laser hyperopic surgery: theoretical effects on corneal profiles and corresponding Zernike expansions. *Invest Ophthalmol Vis Sci.* 2004;45:1349-59.
108. Gilaie-Dotan S, Bentin S, Harel M, Rees G, Saygin AP. Normal form from biological motion despite impaired ventral stream function. *Neuropsychologia.* 2011;49:1033-43.
109. Gilbert CD. Laminar differences in receptive field properties of cells in cat primary visual cortex. *J Physiol.* 1977;268:391-421.
110. Goldsberry DH, Epstein RJ, Majmudar PA, et al. Effect of mitomycin C on the corneal endothelium when used for corneal subepithelial haze prophylaxis following photorefractive keratectomy. *J Refract Surg.* 2007;23:724-7.

111. Gonzalez-Meijome JM, Villa-Collar C, Montes-Mico R, Gomes A. Asphericity of the anterior human cornea with different corneal diameters. *J Cataract Refract Surg.* 2007;33:465-73.
112. Green DG, Campbell F. Effect of focus on the visual response to a sinusoidally modulated spatial stimulus. *J Opt Soc Am.* 1965;55:1154-7.
113. Grill-Spector K, Kourtzi Z, Kanwisher N. The lateral occipital complex and its role in object recognition. *Vision Res.* 2001;41:1409-22.
114. Gross CG. Inferotemporal cortex and vision. *Prog Physiol Psychol.* 1973;5:77-115.
115. Grusser OJ. Migraine phosphenes and the retino-cortical magnification factor. *Vision Res.* 1995;35:1125-34.
116. Guillon M, Lydon DP, Wilson C. Corneal topography: a clinical model. *Ophthalmic Physiol Opt.* 1986;6:47-56.
117. Guirao A, Williams DR, Cox IG. Effect of rotation and translation on the expected benefit of an ideal method to correct the eye's higher-order aberrations. *J Opt Soc Am A Opt Image Sci Vis.* 2001;18:1003-15.
118. Guirao A, Williams DR. A method to predict refractive errors from wave aberration data. *Optom Vis Sci.* 2003;80:36-42.
119. Hadden OB, Ring CP, Morris AT, Elder MJ. Visual, refractive, and subjective outcomes after photorefractive keratectomy for myopia of 6 to 10 diopters using the Nidek laser. *J Cataract Refract Surg.* 1999;25:936-42.
120. Haegerstrom-Portnoy G, Brabyn J, Schneck ME, Jampolsky A. The SKILL Card. An acuity test of reduced luminance and contrast. Smith-Kettlewell Institute Low Luminance. *Invest Ophthalmol Vis Sci.* 1997;38:207-18.
121. Haegerstrom-Portnoy G. The Glenn A. Fry Award Lecture 2003: Vision in elders--summary of findings of the SKI study. *Optom Vis Sci.* 2005;82:87-93.
122. Han HS, Song JS, Kim HM. Long-term results of laser in situ keratomileusis for high myopia. *Korean J Ophthalmol.* 2000;14:1-6.
123. Harris MG, Brennan NA, Lowe R, Efron E. Hydration changes of Acuvue™ disposable contact lenses during disinfection. *Clin Exp Optom.* 1989;72:159-62.

124. He S, Cavanagh P, Intriligator J. Attentional resolution and the locus of visual awareness. *Nature*. 1996;383:334-7.
125. Helmholtz, H. *Handbuch der physiologischen Optik*. Voss. Helmholtz 's treatise on Physiological Optics, Vol II, the sensations of vision. 1911. Optical Society of America. Ref Type: Thesis/Dissertation
126. Hemenger RP. Sources of intraocular light scatter from inversion of an empirical glare function. *Appl Opt*. 1992;31:3687
127. Hendry SH, Yoshioka T. A neurochemically distinct third channel in the macaque dorsal lateral geniculate nucleus. *Science*. 1994;264:575-7.
128. Hennelly, M. The light scattering characteristics of the normal and contact lens-wearing eye. 2000. City University. Ref Type: Thesis/Dissertation
129. Hennelly ML, Barbur JL, Edgar DF, Woodward EG. The effect of age on the light scattering characteristics of the eye. *Ophthalmic Physiol Opt*. 1998;18:197-203.
130. Hernandez C, Domenech B, Segui MM, Illueca C. The effect of pupil and observation distance on the contrast sensitivity function. *Ophthalmic Physiol Opt*. 1996;16:336-41.
131. Hersh PS, Fry K, Blaker JW. Spherical aberration after laser in situ keratomileusis and photorefractive keratectomy. Clinical results and theoretical models of etiology. *J Cataract Refract Surg*. 2003;29:2096-104.
132. Hirsch J, Curcio CA. The spatial resolution capacity of human foveal retina. *Vision Res*. 1989;29:1095-101.
133. Ho A, Bilton SM. Low contrast charts effectively differentiate between types of blur. *Am J Optom Physiol Opt*. 1986;63:202-8.
134. Hoffman KP, Stone J. Conduction velocity of afferents to cat visual cortex: a correlation with cortical receptive field properties. *Brain Res*. 1971;32:460-6.
135. Holladay JT, Prager TC, Trujillo J, Ruiz RS. Brightness acuity test and outdoor visual acuity in cataract patients. *J Cataract Refract Surg*. 1987;13:67-9.
136. Holladay JT, Dudeja DR, Chang J. Functional vision and corneal changes after laser in situ keratomileusis determined by contrast sensitivity, glare testing, and corneal topography. *J Cataract Refract Surg*. 1999;25:663-9.

137. Holladay LL. The fundamentals of glare and visibility. *J Opt Soc Am.* 1926;12:271-319.
138. Howland B, Howland HC. Subjective measurement of high-order aberrations of the eye. *Science.* 1976;193:580-2.
139. Howland HC, Howland B. A subjective method for the measurement of monochromatic aberrations of the eye. *J Opt Soc Am.* 1977;67:1508-18.
140. Hubel DH, Wiesel TN. Receptive fields of single neurones in the cat's striate cortex. *J Physiol.* 1959;148:574-91.
141. Hubel DH, Wiesel TN. Receptive fields, binocular interaction and functional architecture in the cat's visual cortex. *J Physiol.* 1962;160:106-54.
142. Hubel DH, Wiesel TN. Binocular interaction in striate cortex of kittens reared with artificial squint. *J Neurophysiol.* 1965;28:1041-59.
143. Hubel DH, Wiesel TN. receptive fields and functional architecture in two nonstriate visual areas (18 and 19) of the cat. *J Neurophysiol.* 1965;28:229-89.
144. Hubel DH, Wiesel TN. Receptive fields and functional architecture of monkey striate cortex. *J Physiol.* 1968;195:215-43.
145. Hubel DH, Wiesel TN. Uniformity of monkey striate cortex: a parallel relationship between field size, scatter, and magnification factor. *J Comp Neurol JID - 0406041.* 1974;158:295-305.
146. Hubel DH, Wiesel TN, LeVay S. Plasticity of ocular dominance columns in monkey striate cortex. *Philos Trans R Soc Lond B Biol Sci.* 1977;278:377-409.
147. Hubel DH, Wiesel TN, Stryker MP. Anatomical demonstration of orientation columns in macaque monkey. *J Comp Neurol.* 1978;177:361-80.
148. Hull CC. Loss of resolution in a corneal topography system. *Graefes Arch Clin Exp Ophthalmol.* 1999;237:800-5.
149. Ijspeert JK, de Waard PW, van den Berg TJ, de Jong PT. The intraocular straylight function in 129 healthy volunteers; dependence on angle, age and pigmentation. *Vision Res.* 1990;30:699-707.

150. Irving EL, Woo GC, Charman WN. Notch in contrast sensitivity function of optical origin: diffraction effects of acrylic filters. *Ophthalmic Physiol Opt.* 1993;13:179-82.
151. Iskander D, Davis BA, Collins MJ, Franklin R. Objective refraction from monochromatic wavefront aberrations via Zernike power polynomials. *Ophthalmic Physiol Opt.* 2007;27:245-55.
152. Ivarsen A, Laurberg T, Moller-Pedersen T. Role of keratocyte loss on corneal wound repair after LASIK. *Invest Ophthalmol Vis Sci.* 2004;45:3499-506.
153. Jacobs JM, Taravella MJ. Incidence of intraoperative flap complications in laser in situ keratomileusis. *J Cataract Refract Surg.* 2002;28:23-8.
154. Jacobs RJ. Visual resolution and contour interaction in the fovea and periphery. *Vision Res JID - 0417402.* 1979;19:1187-95.
155. Jaeken B, Artal P. Optical quality of emmetropic and myopic eyes in the periphery measured with high-angular resolution. *Invest Ophthalmol Vis Sci.* 2012;53:3405-13.
156. Janoff LE. The exposure of various polymers to a 24-hour soak in Lensept: the effect on base curve. *J Am Optom Assoc.* 1985;56:222-5.
157. Jenkins TC. aberrations of the eye and their effects on vision. II. *Br J Physiol Opt.* 1963;20:161-201.
158. Jennings JA, Charman WN. Off-axis image quality in the human eye. *Vision Res JID - 0417402.* 1981;21:445-55.
159. Jimenez JR, Castro JJ, Jimenez R, Hita E. Interocular differences in higher-order aberrations on binocular visual performance. *Optom Vis Sci.* 2008;85:174-9.
160. Johnson ME. Refractive Surgery Part 4. *Developments in Refractive Management. Optician.* 7 A.D.;233:28-34.
161. Joslin CE, Wu SM, McMahon TT, Shahidi M. Higher-order wavefront aberrations in corneal refractive therapy. *Optom Vis Sci.* 2003;80:805-11.
162. Kamiya K, Shimizu K, Igarashi A, Kobashi H, Komatsu M. Comparison of visual acuity, higher-order aberrations and corneal asphericity after refractive

lenticule extraction and wavefront-guided laser-assisted in situ keratomileusis for myopia. *Br J Ophthalmol.* 2012;

163. Kanwisher N, Yovel G. The fusiform face area: a cortical region specialized for the perception of faces. *Philos Trans R Soc Lond B Biol Sci.* 2006;361:2109-28.

164. Kay CD, Morrison JD. The effects of pupil size and defocus on contrast sensitivity in man. *J Physiol.* 1985;367:15P

165. Kay CD, Morrison JD. A quantitative investigation into the effects of pupil diameter and defocus on contrast sensitivity for an extended range of spatial frequencies in natural and homotropinized eyes. *Ophthalmic Physiol Opt.* 1987;7:21-30.

166. Keir NJ, Simpson T, Hutchings N, Jones L, Fonn D. Outcomes of wavefront-guided laser in situ keratomileusis for hyperopia. *J Cataract Refract Surg.* 2011;37:886-93.

167. Kiely PM, Smith G, Carney L. The mean shape of the human cornea. *Optica Acta.* 1982;29:1027-40.

168. Kim ST, Koh JW, Yoon GJ, Yang SW. Clinical outcomes of epi-LASIK: 1-year results of on- and off-flap procedures with and without mitomycin-C. *Br J Ophthalmol.* 2010;94:592-6.

169. King JB. Dependence of the Strehl ratio on the magnitude of the variance of the wave aberration. *J Opt Soc Am.* 1968;58:655-61.

170. Koch DD, Liu JF. Survey of the clinical use of glare and contrast sensitivity testing. *J Cataract Refract Surg.* 1990;16:707-11.

171. Kolb H, Dekorver L. Midget ganglion cells of the parafovea of the human retina: a study by electron microscopy and serial section reconstructions. *J Comp Neurol.* 1991;303:617-36.

172. Koller T, Iseli HP, Hafezi F, Mrochen M, Seiler T. Q-factor customized ablation profile for the correction of myopic astigmatism. *J Cataract Refract Surg.* 2006;32:584-9.

173. Krauskopf J, Mollon JD. The independence of the temporal integration properties of individual chromatic mechanisms in the human eye. *J Physiol.* 1971;219:611-23.
174. Kuffler SW. Discharge patterns and functional organization of mammalian retina. *J Neurophysiol.* 1953;16:37-68.
175. Kulikowski JJ, Tolhurst DJ. Psychophysical evidence for sustained and transient detectors in human vision. *J Physiol JID - 0266262.* 1973;232:149-62.
176. Kvensakul, J. S. Z. The measurement of scattered light in the eye and its effects on visual performance. 2005. Ref Type: Thesis/Dissertation
177. Le Grand Y. *Optique physiologique.L'espace visuel.* Troisieme Edition ed. Paris: 1956:
178. Lee BB, Pokorny J, Smith VC, Martin PR, Valberg A. Luminance and chromatic modulation sensitivity of macaque ganglion cells and human observers. *J Opt Soc Am A.* 1990;7:2223-36.
179. Lee DK, Koch C, Braun J. Spatial vision thresholds in the near absence of attention. *Vision Res.* 1997;37:2409-18.
180. Legras R, Chateau N, Charman WN. Assessment of just-noticeable differences for refractive errors and spherical aberration using visual simulation. *Optom Vis Sci.* 2004;81:718-28.
181. Lennie P, Krauskopf J, Sclar G. Chromatic mechanisms in striate cortex of macaque. *J Neurosci.* 1990;10:649-69.
182. Lennie P, Trevarthen C, Van Essen D, Wassle H. Parallel processing of visual information. In: Spillman L, Werner JS, eds. *Visual Perception.. The Neurophysiological Foundations.* New York: Academic Press, 1990:103-28.
183. Levy Y, Segal O, Avni I, Zadok D. Ocular higher-order aberrations in eyes with supernormal vision. *Am J Ophthalmol.* 2005;139:225-8.
184. Li J, Xiong Y, Wang N, et al. Effects of spherical aberration on visual acuity at different contrasts. *J Cataract Refract Surg.* 2009;35:1389-95.

185. Liang J, Grimm B, Goelz S, Bille JF. Objective measurement of wave aberrations of the human eye with the use of a Hartmann-Shack wave-front sensor. *J Opt Soc Am A Opt Image Sci Vis.* 1994;11:1949-57.
186. Liang J, Williams DR. Aberrations and retinal image quality of the normal human eye. *J Opt Soc Am A Opt Image Sci Vis.* 1997;14:2873-83.
187. Liang J, Williams DR, Miller DT. Supernormal vision and high-resolution retinal imaging through adaptive optics. *J Opt Soc Am A Opt Image Sci Vis.* 1997;14:2884-92.
188. Liang J, Williams DR. Aberrations and retinal image quality of the normal human eye. *J Opt Soc Am A Opt Image Sci Vis.* 1997;14:2873-83.
189. Lihua F, Xingdao H, Fengying C. Theoretical analysis of wavefront aberration from treatment decentration with oblique incidence after conventional laser refractive surgery. *Opt Express.* 2010;18:22418-31.
190. Linberg KA, Fisher SK. An ultrastructural study of interplexiform cell synapses in the human retina. *J Comp Neurol.* 1986;243:561-76.
191. Livingstone M, Hubel D. Segregation of form, color, movement, and depth: anatomy, physiology, and perception. *Science.* 1988;240:740-9.
192. Livingstone MS, Hubel DH. Psychophysical evidence for separate channels for the perception of form, color, movement, and depth. *J Neurosci.* 1987;7:3416-68.
193. Livne T, Sagi D. Configuration influence on crowding. *Journal of Vision.* 2007;7 (2):1-12.
194. Llorente L, Diaz-Santana L, Lara-Saucedo D, Marcos S. Aberrations of the human eye in visible and near infrared illumination. *Optom Vis Sci.* 2003;80:26-35.
195. Llorente L, Barbero S, Merayo J, Marcos S. Total and corneal optical aberrations induced by laser in situ keratomileusis for hyperopia. *J Refract Surg.* 2004;20:203-16.
196. Lohmann C, Gartry DS, Muir MK. Haze in photorefractive keratectomy: its origins and consequences. *Lasers and Light in Ophthalmology.* 1991;4:15-34.
197. Lohmann CP, Fitzke F, O'Brart D, Muir MK, Timberlake G, Marshall J. Corneal light scattering and visual performance in myopic individuals with spectacles,

- contact lenses, or excimer laser photorefractive keratectomy. *Am J Ophthalmol.* 1993;115:444-53.
198. Lombardo M, Lombardo G. Wave aberration of human eyes and new descriptors of image optical quality and visual performance. *J Cataract Refract Surg.* 2010;36:313-31.
199. Lopez-Gil N, Howland HC. Measurement of the eye's near infrared wave-front aberration using the objective crossed-cylinder aberroscope technique. *Vision Res.* 1999;39:2031-7.
200. Ludvigh E. Extrafoveal visual acuity as measured by Snellen Test Letters. *Am.J.Ophthalmol.* 1941;24:303-10.
201. Lund JS, Henry GH, MacQueen CL, Harvey AR. Anatomical organization of the primary visual cortex (area 17) of the cat. A comparison with area 17 of the macaque monkey. *J Comp Neurol.* 1979;184:599-618.
202. Mahajan VN. *Aberration Theory Made Simple* (Vol. TT6) . Bellingham, WA: SPIE Optical Engineering Press., 1991:
203. Manche EE, Haw WW. Wavefront-guided laser in situ keratomileusis (Lasik) versus wavefront-guided photorefractive keratectomy (Prk): a prospective randomized eye-to-eye comparison (an American Ophthalmological Society thesis). *Trans Am Ophthalmol Soc.* 2011;109:201-20.
204. Mandelbaum J, Sloan LL. Peripheral visual acuity with special reference to scotopic illumination. *Am.J.Ophthalmol.* 1947;30:581-8.
205. Mandell RB, St Helen R. Mathematical models of the general corneal contour. *Br J Physiol Opt.* 1971;26:183-97.
206. Marcos S, Burns SA, Moreno-Barriusop E, Navarro R. A new approach to the study of ocular chromatic aberrations. *Vision Res.* 1999;39:4309-23.
207. Marcos S. Refractive surgery and optical aberrations. *Optics & Photonics News.* 2001;1:22-5.
208. Marsack JD, Thibos LN, Applegate RA. Metrics of optical quality derived from wave aberrations predict visual performance. *J Vis.* 2004;4:322-8.

209. Martin PR. Colour processing in the primate retina: recent progress. *J Physiol.* 1998;513 (Pt 3):631-8.
210. Masket S. Relationship between postoperative pupil size and disability glare. *J Cataract Refract Surg.* 1992;18:506-7.
211. Mastropasqua L, Toto L, Zuppari E, et al. Photorefractive keratectomy with aspheric profile of ablation versus conventional photorefractive keratectomy for myopia correction: six-month controlled clinical trial. *J Cataract Refract Surg.* 2006;32:109-16.
212. Matesanz BM, Issolio L, Arranz I, et al. Temporal retinal sensitivity in mesopic adaptation. *Ophthalmic Physiol Opt.* 2011;31:615-24.
213. Mathur A, Atchison DA, Scott DH. Ocular aberrations in the peripheral visual field. *Opt Lett.* 2008;33:863-5.
214. Mathur A, Atchison DA, Charman WN. Myopia and peripheral ocular aberrations. *J Vis.* 2009;9:15-2.
215. Maunsell JH, Newsome WT. Visual processing in monkey extrastriate cortex. *Annu Rev Neurosci.* 1987;10:363-401.
216. Maunsell JH, Nealey TA, DePriest DD. Magnocellular and parvocellular contributions to responses in the middle temporal visual area (MT) of the macaque monkey. *J Neurosci.* 1990;10:3323-34.
217. McGwin GJ, Scilley K, Brown J, Owsley C. Impact of cataract surgery on self-reported visual difficulties: comparison with a no-surgery reference group. *J Cataract Refract Surg.* 2003;29:941-8.
218. Melmoth DR, Rovamo JM. Scaling of letter size and contrast equalises perception across eccentricities and set sizes. *Vision Res.* 2003;43:769-77.
219. Merabet L, Desautels A, Minville K, Casanova C. Motion integration in a thalamic visual nucleus. *Nature.* 1998;396:265-8.
220. Merigan WH, Maunsell JH. Macaque vision after magnocellular lateral geniculate lesions. *Vis Neurosci.* 1990;5:347-52.
221. Merigan WH, Maunsell JH. How parallel are the primate visual pathways? *Annu Rev Neurosci.* 1993;16:369-402.

222. Miller KD. Understanding layer 4 of the cortical circuit: a model based on cat V1. *Cereb Cortex*. 2003;13:73-82.
223. Millodot M. Foveal and extra-foveal acuity with and without stabilized retinal images. *Br J Physiol Opt*. 1966;23:75-106.
224. Millodot M, Johnson CA, Lamont A, Leibowitz HW. Effect of dioptrics on peripheral visual acuity. *Vision Res*. 1975;15:1357-62.
225. Milner AD. Is visual processing in the dorsal stream accessible to consciousness? *Proc Biol Sci*. 2012;279:2289-98.
226. Miraftab M, Seyedian MA, Hashemi H. Wavefront-guided vs wavefront-optimized LASIK: a randomized clinical trial comparing contralateral eyes. *J Refract Surg*. 2011;27:245-50.
227. Mishkin M, Ungerleider LG, Macko KA. Object vision and spatial vision: Two cortical pathways. *Trends Neurosci*. 1983;6:414-7.
228. Mok KH, Lee VW. Effect of optical zone ablation diameter on LASIK-induced higher order optical aberrations. *J Refract Surg*. 2005;21:141-3.
229. Moller-Pedersen T, Cavanagh HD, Petroll WM, Jester JV. Neutralizing antibody to TGFbeta modulates stromal fibrosis but not regression of photoablative effect following PRK. *Curr Eye Res*. 1998;17:736-47.
230. Moller-Pedersen T, Cavanagh HD, Petroll WM, Jester JV. Stromal wound healing explains refractive instability and haze development after photorefractive keratectomy: a 1-year confocal microscopic study. *Ophthalmology*. 2000;107:1235-45.
231. Moller-Pedersen T. On the structural origin of refractive instability and corneal haze after excimer laser keratectomy for myopia. *Acta Ophthalmol Scand Suppl*. 2003;1-20.
232. Montes-Mico R, Charman WN. Choice of spatial frequency for contrast sensitivity evaluation after corneal refractive surgery. *J Refract Surg*. 2001;17:646-51.
233. Moran J, Desimone R. Selective attention gates visual processing in the extrastriate cortex. *Science*. 1985;229:782-4.

234. Moreno-Barriuso E, Lloves JM, Marcos S, Navarro R, Llorente L, Barbero S. Ocular aberrations before and after myopic corneal refractive surgery: LASIK-induced changes measured with laser ray tracing. *Invest Ophthalmol Vis Sci JID* - 7703701. 2001;42:1396-403.
235. Motter BC. Neural correlates of attentive selection for color or luminance in extrastriate area V4. *J Neurosci*. 1994;14:2178-89.
236. Movshon JA, Adelson EH, Gizzi MS, Newsome WT. The analysis of moving visual patterns. In: Chagas C, Gattass R, Gross, eds. *Pattern Recognition Mechanisms*. Vatican City: Pontifical Academy of Sciences, 1985:117-51.
237. Mutalib HA, Lee KC. Soft Contact Lens Parameter Changes After using the Lens2® Automated Lens Cleaner Machine. *Sains Malaysiana*. 2010;39:685-8.
238. Nakano EM, Bains HS, Hirai FE, Portellinha W, Oliveira M, Nakano K. Comparison of laser epithelial keratomileusis with and without mitomycin C for wavefront customized surface ablations. *J Refract Surg*. 2007;23:S1021-S1028
239. Nassaralla BA, McLeod SD, Nassaralla JJJ. Prophylactic mitomycin C to inhibit corneal haze after photorefractive keratectomy for residual myopia following radial keratotomy. *J Refract Surg*. 2007;23:226-32.
240. Nassiri N, Safi S, Aghazade AM, Sheibani K, Safi H, Panahi N. Visual outcome and contrast sensitivity after photorefractive keratectomy in low to moderate myopia: wavefront-optimized versus conventional methods. *J Cataract Refract Surg*. 2011;37:1858-64.
241. Nelson R, Famiglietti EVJ, Kolb H. Intracellular staining reveals different levels of stratification for on- and off-center ganglion cells in cat retina. *J Neurophysiol*. 1978;41:472-83.
242. Netto MV, Mohan RR, Medeiros FW, et al. Femtosecond laser and microkeratome corneal flaps: comparison of stromal wound healing and inflammation. *J Refract Surg*. 2007;23:667-76.
243. Neumann AC, McCarty GR, Locke J, Cobb B. Glare disability devices for cataractous eyes: a consumer's guide. *J Cataract Refract Surg*. 1988;14:212-6.

244. Nochez Y, Majzoub S, Pisella PJ. Effect of residual ocular spherical aberration on objective and subjective quality of vision in pseudophakic eyes. *J Cataract Refract Surg.* 2011;37:1076-81.
245. O'Brart DP, Corbett MC, Lohmann CP, Kerr MM, Marshall J. The effects of ablation diameter on the outcome of excimer laser photorefractive keratectomy. A prospective, randomized, double-blind study. *Arch Ophthalmol.* 1995;113:438-43.
246. Oliveira-Soto L, Charman WN. Some possible longer-term ocular changes following excimer laser refractive surgery. *Ophthalmic Physiol Opt.* 2002;22:274-88.
247. Ondategui JC, Vilaseca M, Arjona M, et al. Optical quality after myopic photorefractive keratectomy and laser in situ keratomileusis: comparison using a double-pass system. *J Cataract Refract Surg.* 2012;38:16-27.
248. Oshika T, Klyce SD, Applegate RA, Howland HC, El Danasoury MA. Comparison of corneal wavefront aberrations after photorefractive keratectomy and laser in situ keratomileusis. *Am J Ophthalmol JID - 0370500.* 1999;127:1-7.
249. Oshika T, Miyata K, Tokunaga T, et al. Higher order wavefront aberrations of cornea and magnitude of refractive correction in laser in situ keratomileusis. *Ophthalmology.* 2002;109:1154-8.
250. Oshika T, Okamoto C, Samejima T, Tokunaga T, Miyata K. Contrast sensitivity function and ocular higher-order wavefront aberrations in normal human eyes. *Ophthalmology.* 2006;113:1807-12.
251. Osterberg G. Topography of the layer of rods and cones in the human retina. *Acta Ophthal (Kbh.).* 1935;65:1-102.
252. Owsley C, Ball K, McGwin GJ, et al. Visual processing impairment and risk of motor vehicle crash among older adults. *JAMA.* 1998;279:1083-8.
253. Oyster C. Retina III: Regional Variation and Spatial Organization 649. In: Oyster C, ed. *The Human Eye: Structure and Function.* Massachusetts: Sinauer Associates, Inc., 1999:649-700.
254. Pallikaris IG, Kymionis GD, Panagopoulou SI, Siganos CS, Theodorakis MA, Pallikaris AI. Induced optical aberrations following formation of a laser in situ keratomileusis flap. *J Cataract Refract Surg.* 2002;28:1737-41.

255. Palomares M, Smith PR, Pitts CH, Carter BM. The effect of viewing eccentricity on enumeration. *PLoS One*. 2013;6:e20779-10.
256. Parker KE, Marsack JD, Elswick JD, Brunstetter TJ, Applegate RA. Controlled induction of spherical aberration with custom soft contact lenses. *Clin Exp Optom*. 2009;92:283-8.
257. Pascual-Leone A, Walsh V. Fast backprojections from the motion to the primary visual area necessary for visual awareness. *Science*. 2001;292:510-2.
258. Peichl L, Wässle H. Morphological identification of on- and off-centre brisk transient (Y) cells in the cat retina. *Proc R Soc Lond B Biol Sci*. 1981;212:139-53.
259. Pelli DG, Palomares M, Majaj NJ. Crowding is unlike ordinary masking: distinguishing feature integration from detection. *J Vis*. 2004;4:1136-69.
260. Periman LM, Ambrosio RJ, Harrison DA, Wilson SE. Correlation of pupil sizes measured with a mesopic infrared pupillometer and a photopic topographer. *J Refract Surg*. 2003;19:555-9.
261. Pesudovs K, Marsack JD, Donnelly WJ, Thibos LN, Applegate RA. Measuring visual acuity--mesopic or photopic conditions, and high or low contrast letters? *J Refract Surg*. 2004;20:S508-S514
262. Pietrasanta M, Restani L, Caleo M. The corpus callosum and the visual cortex: plasticity is a game for two. *Neural Plast*. 2012;2012:838672
263. Pipe D, Rapley L. *Ocular Anatomy & Histology*. 3rd ed. 2008:
264. Poirier FJ, Gurnsey R. Non-monotonic changes in performance with eccentricity modeled by multiple eccentricity-dependent limitations. *Vision Res*. 2005;45:2436-48.
265. Polyak SL. *The Retina*. Chicago: University of Chicago Press, 1941:425-8.
266. Pop M, Bains HS. Clinical outcomes of CATz versus OPDCAT. *J Refract Surg*. 2005;21:S636-S639
267. Popovic Z, Sjostrand J. Resolution, separation of retinal ganglion cells, and cortical magnification in humans. *Vision Res*. 2001;41:1313-9.

268. Prager TC, Urso RG, Holladay JT, Stewart RH. Glare testing in cataract patients: instrument evaluation and identification of sources of methodological error. *J Cataract Refract Surg.* 1989;15:149-57.
269. Puell MC, Palomo C, Sanchez-Ramos C, Villena C. Mesopic contrast sensitivity in the presence or absence of glare in a large driver population. *Graefes Arch Clin Exp Ophthalmol.* 2004;242:755-61.
270. Queiros A, Villa-Collar C, Gonzalez-Meijome JM, Jorge J, Gutierrez AR. Effect of pupil size on corneal aberrations before and after standard laser in situ keratomileusis, custom laser in situ keratomileusis, and corneal refractive therapy. *Am J Ophthalmol.* 2010;150:97-109.
271. Rae SM, Allen PM, Radhakrishnan H, et al. Increasing negative spherical aberration with soft contact lenses improves high and low contrast visual acuity in young adults. *Ophthalmic Physiol Opt.* 2009;29:593-601.
272. Randleman JB, Woodward M, Lynn MJ, Stulting RD. Risk assessment for ectasia after corneal refractive surgery. *Ophthalmology.* 2008;115:37-50.
273. Rao SC, Rainer G, Miller EK. Integration of what and where in the primate prefrontal cortex. *Science.* 1997;276:821-4.
274. Ravikumar S, Bradley A, Thibos L. Phase changes induced by optical aberrations degrade letter and face acuity. *J Vis.* 1912;10:18-0.
275. Regan D. The Charles F. Prentice Award Lecture 1990: specific tests and specific blindnesses: keys, locks, and parallel processing. *Optom Vis Sci.* 1991;68:489-512.
276. Robert ID, Davis BA, Collins MJ, Franklin R. Objective refraction from monochromatic wavefront aberrations via Zernike power polynomials. *Ophthalmic Physiol Opt.* 2007;27:245-55.
277. Rocha KM, Kagan R, Smith SD, Krueger RR. Thresholds for interface haze formation after thin-flap femtosecond laser in situ keratomileusis for myopia. *Am J Ophthalmol.* 2009;147:966-72, 972.
278. Rodiek RW. Which cells code for color? In: Valberg A, Lee BB, eds. *From Pigments to Perception: Advances in Understanding Visual Processes.* New York: Plenum, 1991:83-93.

279. Rodman HR, Albright TD. Single-unit analysis of pattern-motion selective properties in the middle temporal visual area (MT). *Exp Brain Res.* 1989;75:53-64.
280. Rolls ET, Cowey A. Topography of the retina and striate cortex and its relationship to visual acuity in rhesus monkeys and squirrel monkeys. *Exp Brain Res JID - 0043312.* 1970;10:298-310.
281. Rolls ET, Tovee MJ. Sparseness of the neuronal representation of stimuli in the primate temporal visual cortex. *J Neurophysiol.* 1995;73:713-26.
282. Rouger H, Benard Y, Legras R. Effect of monochromatic induced aberrations on visual performance measured by adaptive optics technology. *J Refract Surg.* 2010;26:578-87.
283. Rovamo J, Virsu V. An estimation and application of the human cortical magnification factor. *Exp Brain Res JID - 0043312.* 1979;37:495-510.
284. Royal College of Ophthalmologists. A Patients' Guide to Excimer Laser Refractive Surgery. 2011. 17 Cornwall Terrace, London, NW1 4QW, The Royal College of Ophthalmologists. Ref Type: Pamphlet
285. Rubin GS, Adamsons IA, Stark WJ. Comparison of acuity, contrast sensitivity, and disability glare before and after cataract surgery. *Arch Ophthalmol.* 1993;111:56-61.
286. Sachdev N, McGhee CN, Craig JP, Weed KH, McGhee JJ. Epithelial defect, diffuse lamellar keratitis, and epithelial ingrowth following post-LASIK epithelial toxicity. *J Cataract Refract Surg.* 2002;28:1463-6.
287. Santos VR, Waring GO, Lynn MJ, Holladay JT, Sperduto RD. Relationship between refractive error and visual acuity in the Prospective Evaluation of Radial Keratotomy (PERK) Study. *Arch Ophthalmol.* 1987;105:86-92.
288. Schiller PH, Finlay BL, Volman SF. Quantitative studies of single-cell properties in monkey striate cortex. I. Spatiotemporal organization of receptive fields. *J Neurophysiol.* 1976;39:1288-319.
289. Schiller PH, Malpeli JG. Functional specificity of lateral geniculate nucleus laminae of the rhesus monkey. *J Neurophysiol.* 1978;41:788-97.

290. Schiller PH, Logothetis NK, Charles ER. Functions of the colour-opponent and broad-band channels of the visual system. *Nature*. 1990;343:68-70.
291. Schiller PH, Logothetis NK, Charles ER. Role of the color-opponent and broad-band channels in vision. *Vis Neurosci*. 1990;5:321-46.
292. Schiller PH. The effects of V4 and middle temporal (MT) area lesions on visual performance in the rhesus monkey. *Vis Neurosci*. 1993;10:717-46.
293. Schmitz S, Krummenauer F, Henn S, Dick HB. Comparison of three different technologies for pupil diameter measurement. *Graefes Arch Clin Exp Ophthalmol*. 2003;241:472-7.
294. Schwartz SH. *Visual Perception: A Clinical Orientation*. 3rd ed. New York: McGraw-Hill, 2004:
295. Schwiegerling J, Snyder RW. Corneal ablation patterns to correct for spherical aberration in photorefractive keratectomy. *J Cataract Refract Surg JID* - 8604171. 2000;26:214-21.
296. Schwiegerling J. Scaling Zernike expansion coefficients to different pupil sizes. *J Opt Soc Am A Opt Image Sci Vis*. 2002;19:1937-45.
297. Seiler T, Mrochen M, Kaemmerer M. Operative correction of ocular aberrations to improve visual acuity. *J Refract Surg*. 2000;16:S619-S622
298. Serrao S, Lombardo G, Ducoli P, Lombardo M. Optical performance of the cornea six years following photorefractive keratectomy for myopia. *Invest Ophthalmol Vis Sci*. 2011;52:846-57.
299. Shah S, Laiquzzaman M, Naroo S. Refractive Surgery - an update. *Optometry Today*. 2007;47:40-5.
300. Sharma N, Ghate D, Agarwal T, Vajpayee RB. Refractive outcomes of laser in situ keratomileusis after flap complications. *J Cataract Refract Surg*. 2005;31:1334-7.
301. Slaughter MM, Miller R. The role of glutamate receptors in information processing in the distal retina. In: Gallego A, Gouras P, eds. *Neurocircuitry of the Retina, A Cajal Memorial*. New York: Elsevier, 1985:51-65.
302. Sloan LL. The photopic acuity-luminance function with special reference to parafoveal vision. *Vision Res*. 1968;8:901-11.

303. Smith AT, Singh KD, Williams AL, Greenlee MW. Estimating receptive field size from fMRI data in human striate and extrastriate visual cortex. *Cereb Cortex JID* - 9110718. 2001;11:1182-90.
304. Song H, Chui TY, Zhong Z, Elsner AE, Burns SA. Variation of cone photoreceptor packing density with retinal eccentricity and age. *Invest Ophthalmol Vis Sci*. 2011;52:7376-84.
305. Sperling HG, Joliffe CL. Intensity-time relationships at threshold for spectral stimuli in human vision. *J Opt Soc Am*. 1965. *J Opt Soc Am*. 1965;55:191-9.
306. Steinman BA, Steinman SB, Lehmkuhle S. Visual attention mechanisms show a center-surround organization. *Vision Res*. 1995;35:1859-69.
307. Steinman SB, Steinman BA. Vision and attention. I: Current models of visual attention. *Optom Vis Sci*. 1998;75:146-55.
308. Stell WK, Ishida AT, Lightfoot DO. Structural basis for on-and off-center responses in retinal bipolar cells. *Science*. 1977;198:1269-71.
309. Stiles, W. S. The effect of glare on the brightness difference threshold. *Proc Roy Soc* 1929. 104B, 322-355. 1929. Ref Type: Conference Proceeding
310. Stiles, W. S and Crawford, B. H. The effect of a glaring light source on extrafoveal vision. *Proc. Roy. Soc. London* 1937. 122B, 255-280. 1937. London. *Proc. Roy. Soc.* Ref Type: Conference Proceeding
311. Stockman A, Sharpe LT. Into the twilight zone: the complexities of mesopic vision and luminous efficiency. *Ophthalmic Physiol Opt*. 2006;26:225-39.
312. Stone J, Dreher B, Leventhal A. Hierarchical and parallel mechanisms in the organization of visual cortex. *Brain Res*. 1979;180:345-94.
313. Strasburger H, Rentschler I, Harvey LOJ. Cortical magnification theory fails to predict visual recognition. *Eur J Neurosci*. 1994;6:1583-7.
314. Strasburger H, Rentschler I, Jüttner M. Peripheral vision and pattern recognition: a review. *J Vis*. 2011;11:13-0.
315. Su PY, Hu FR. Intraindividual comparison of functional vision and higher order aberrations after implantation of aspheric and spherical intraocular lenses. *J Refract Surg*. 2009;25:265-72.

316. Sutton GL, Kim P. Laser in situ keratomileusis in 2010 - a review. *Clin Experiment Ophthalmol.* 2010;38:192-210.
317. Swanson WH, Ueno T, Smith VC, Pokorny J. Temporal modulation sensitivity and pulse-detection thresholds for chromatic and luminance perturbations. *J Opt Soc Am A.* 1987;4:1992-2005.
318. Tanabe T, Miyata K, Samejima T, Hirohara Y, Mihashi T, Oshika T. Influence of wavefront aberration and corneal subepithelial haze on low-contrast visual acuity after photorefractive keratectomy. *Am J Ophthalmol.* 2004;138:620-4.
319. Tanaka K, Saito H, Fukada Y, Moriya M. Coding visual images of objects in the inferotemporal cortex of the macaque monkey. *J Neurophysiol.* 1991;66:170-89.
320. Thibos LN, Hong X. Clinical applications of the Shack-Hartmann aberrometer. *Optom Vis Sci.* 1999;76:817-25.
321. Thibos LN, Applegate RA, Schwiegerling JT, Webb R. Report from the VSIA taskforce on standards for reporting optical aberrations of the eye. *J Refract Surg.* 2000;16:S654-S655
322. Thibos LN, Applegate RA, Schwiegerling JT, Webb R. Standards for reporting the optical aberrations of eyes. *J Refract Surg.* 2002;18:S652-S660
323. Thibos LN, Hong X, Bradley A, Cheng X. Statistical variation of aberration structure and image quality in a normal population of healthy eyes. *J Opt Soc Am A Opt Image Sci Vis.* 2002;19:2329-48.
324. Thibos LN, Hong X, Bradley A, Applegate RA. Accuracy and precision of objective refraction from wavefront aberrations. *J Vis.* 2004;4:329-51.
325. Tomidokoro A, Soya K, Miyata K, et al. Corneal irregular astigmatism and contrast sensitivity after photorefractive keratectomy. *Ophthalmology.* 2001;108:2209-12.
326. Tomita T. Electrical activity of vertebrate photoreceptors. *Q Rev Biophys.* 1970;3:179-222.
327. Tong F, Nakayama K, Vaughan JT, Kanwisher N. Binocular rivalry and visual awareness in human extrastriate cortex. *Neuron.* 1998;21:753-9.

328. Tovee MJ, Cohen-Tovee EM. The neural substrates of face-processing models: a review. . *Cognitive Neuropsychology*. 1993;10:505-28.
329. Ts'o DY, Gilbert CD. The organization of chromatic and spatial interactions in the primate striate cortex. *J Neurosci*. 1988;8:1712-27.
330. Ts'o DY, Roe AW, Gilbert CD. A hierarchy of the functional organization for color, form and disparity in primate visual area V2. *Vision Res*. 2001;41:1333-49.
331. Tsai YY, Lin JM. Ablation centration after active eye-tracker-assisted photorefractive keratectomy and laser in situ keratomileusis. *J Cataract Refract Surg*. 2000;26:28-34.
332. Tuan KM, Chernyak D. Corneal asphericity and visual function after wavefront-guided LASIK. *Optom Vis Sci*. 2006;83:605-10.
333. Van Buren KM. The retinal ganglion cell layer. Charles Thomas, 1963:
334. van den Berg TJ. Importance of pathological intraocular light scatter for visual disability. *Doc Ophthalmol*. 1986;61:327-33.
335. van den Berg TJ, Spekreijse H. Measurement of the straylight function of the eye in cataract and other optical media disturbances by means of a direct compensation method. *Invest Ophthalmol Vis Sci*. 1987;28:397
336. van den Berg TJ, Ijspeert JK, de Waard PW. Dependence of intraocular straylight on pigmentation and light transmission through the ocular wall. *Vision Res*. 1991;31:1361-7.
337. van den Berg TJ. Analysis of intraocular straylight, especially in relation to age. *Optom Vis Sci*. 1995;72:52-9.
338. van den Berg, T. J. Introduction to retinal straylight. Ocular Signal Transduction group Netherlands Institute for Neuroscience (NIN) Amsterdam, The Netherlands . 2008.
Ref Type: Internet Communication
339. van Meeteren A. Calculations on the optical modulation transfer function of the human eye for white light. *Optica Acta*. 1974;21:395-412.

340. Van ED, Newsome WT, Maunsell JH. The visual field representation in striate cortex of the macaque monkey: asymmetries, anisotropies, and individual variability. *Vision Res* JID - 0417402. 1984;24:429-48.
341. Van ED, Anderson CH, Felleman DJ. Information processing in the primate visual system: an integrated systems perspective. *Science*. 1992;255:419-23.
342. Veraart HG, van den Berg TJ, Ijspeert JK, Cardozo OL. Stray light in radial keratotomy and the influence of pupil size and straylight angle. *Am J Ophthalmol*. 1992;114:424-8.
343. Verdon W, Bullimore M, Maloney RK. Visual performance after photorefractive keratectomy. A prospective study. *Arch Ophthalmol*. 1996;114:1465-72.
344. Virsu V, Rovamo J. Visual resolution, contrast sensitivity, and the cortical magnification factor. *Exp Brain Res* JID - 0043312. 1979;37:475-94.
345. Virsu V, Nasanen R, Osmoviita K. Cortical magnification and peripheral vision. *J Opt Soc Am A* JID - 8402086. 1987;4:1568-78.
346. Vos, J. J and Bouman, M. A. Disability glare: theory. and practice. Proceedings of CIE 14th Session. Brussels. 298-308. 1959. Brussels. Ref Type: Conference Proceeding
347. Vos JJ. Disability glare-a state of the art report. *CIE-Journal*. 1984;3:39-53.
348. Vos JJ, Boogaard J. Contribution of the cornea to entoptic scatter. *J Opt Soc Am*. 1963;53:869-73.
349. Wald G. human vision and the spectrum. *Science*. 1945;101:653-8.
350. Wang L, Koch DD. Custom optimization of intraocular lens asphericity. *J Cataract Refract Surg*. 2007;33:1713-20.
351. Wassle H, Grunert U, Martin PR, Boycott BB. Immunocytochemical characterization and spatial distribution of midget bipolar cells in the macaque monkey retina. *Vision Res*. 1994;34:561-79.
352. Watson JD, Myers R, Frackowiak RS, et al. Area V5 of the human brain: evidence from a combined study using positron emission tomography and magnetic resonance imaging. *Cereb Cortex*. 1993;3:79-94.

353. Weale RA. Real light scatter in the human crystalline lens. *Graefes Arch Clin Exp Ophthalmol.* 1986;224:463-6.
354. Weiskrantz L, Cowey A. Striate cortex lesions and visual acuity of the rhesus monkey. *J Comp Physiol Psychol.* 1963;56:225-31.
355. Werblin FS, Dowling JE. Organization of the retina of the mudpuppy, *Necturus maculosus*. II. Intracellular recording. *J Neurophysiol.* 1969;32:339-55.
356. Wertheim T. Ueber die indirecte Sehscharfe. *Z.Psych.Physiol.Sinnesorg.* 1894;7:172-87.
357. Westheimer G. Pupil size and visual resolution. *Vision Res.* 1964;4:39-45.
358. Westheimer G. The spatial grain of the perifoveal visual field. *Vision Res JID* - 0417402. 1982;22:157-62.
359. Weymouth, F. W. Visual Sensory Units and the Minimal Angle of Resolution. *Am.J.Ophthalmol* 46, 102-112. 1958. Ref Type: Generic
360. Wong-Riley M. Changes in the visual system of monocularly sutured or enucleated cats demonstrable with cytochrome oxidase histochemistry. *Brain Res.* 1979;171:11-28.
361. Yamane N, Miyata K, Samejima T, et al. Ocular higher-order aberrations and contrast sensitivity after conventional laser in situ keratomileusis. *Invest Ophthalmol Vis Sci.* 2004;45:3986-90.
362. Yoon G, MacRae S, Williams DR, Cox IG. Causes of spherical aberration induced by laser refractive surgery. *J Cataract Refract Surg.* 2005;31:127-35.
363. Yoonessi A. Functional assessment of magno, parvo and konio-cellular pathways; current state and future clinical applications. *J Ophthalmic Vis Res.* 2011;6:119-26.
364. Young LK, Liversedge SP, Love GD, Myers RM, Smithson HE. Not all aberrations are equal: reading impairment depends on aberration type and magnitude. *J Vis.* 2011;11:20-10.
365. Young RW. The Renewal Of Rod And Cone Outer Segments In The Rhesus Monkey. *J.Cell Biol.* 1971;49:303-18.

366. Yue X, Cassidy BS, Devaney KJ, Holt DJ, Tootell RB. Lower-level stimulus features strongly influence responses in the fusiform face area. *Cereb Cortex*. 2011;21:35-47.
367. Yulish M, Beiran I, Miller B, Pikkell J. Ascorbate prophylaxis with mitomycin-C for corneal haze after laser-assisted sub-epithelial keratectomy. *Isr Med Assoc J*. 2012;14:382-5.
368. Zalentein WN, Tervo TM, Holopainen JM. Seven-year follow-up of LASIK for myopia. *J Refract Surg*. 2009;25:312-8.
369. Zeki S. The distribution of wavelength and orientation selective cells in different areas of monkey visual cortex. *Proc R Soc Lond B Biol Sci*. 1983;217:449-70.
370. Zele AJ, Cao D, Pokorny J. Rod-cone interactions and the temporal impulse response of the cone pathway. *Vision Res*. 2008;48:2593-8.
371. Zenger-Landolt B, Koch C. Flanker effects in peripheral contrast discrimination--psychophysics and modeling. *Vision Res*. 2001;41:3663-75.
372. Zhang J, Zhou YH, Wang NL, Li R. Comparison of visual performance between conventional LASIK and wavefront-guided LASIK with iris-registration. *Chin Med J (Engl)*. 2008;121:137-42.